INDC(CCP)- 426

IAEA
International Atomic Energy Agency

INDC International Nuclear Data Committee

Translations of Selected Papers published in

Jadernye Konstanty (Nuclear Constants) 2, 1999

Translated by the IAEA

February 2001

IAEA Nuclear Data Section, Vienna International Centre, A-1400 Vienna, Austria

Selected INDC documents may be downloaded in electronic form from
http://www-nds.iaea.org/reports-new/indc-reports/
or sent as an e-mail attachment.
Requests for hardcopy or e-mail transmittal should be directed to *services@iaeand.iaea.org*
or to:
Nuclear Data Section
International Atomic Energy Agency
Vienna International Centre
PO Box 100
A-1400 Vienna
Austria

Printed by the IAEA in Austria

February 2001

CONTENTS

1. Study of Delayed Neutron Decay Curves for ^{235}U and ^{239}Pu Fission due to Thermal Neutrons 7

2. Differential Cross-sections for the U(n,xn) Reaction at a Neutron Energy of 14.3 MeV 17

3. Evaluation of the Gamma-Ray Production Cross-sections for Nonelastic Interaction of Fast Neutrons with Al Nuclei 27

4. Evaluation of the Gamma-Ray Production Cross-sections for Nonelastic Interaction of Fast Neutrons with Lead Nuclei 53

5. Evaluation of Neutron Cross Sections for Cm-242, -243, -244 67

6. Evaluation of the Gamma-Ray Production Cross-sections for Nonelastic Interaction of Fast Neutrons with Iron Nuclei 75

7. Evaluation of Angular Distribution and Production Cross-sections for Discrete Gamma Lines in Iron 95

8. Resolved Resonance Parameters for ^{232}Pa 113

9. BOFOD-99: Present Status of the Evaluated Photonuclear Data File 119

10. WEB Server of the Centre for Photonuclear Experiments Data of the Scientific Research Institute for Nuclear Physics, Moscow State University: Hypertext Version of the Nuclear Physics Database 125

11. Library of Neutron Reaction Cross-sections in the ABBN-93 Constant System 141

12. A Library of Production Cross-sections for Displacements and Hydrogen, Helium and Tritium in the ABBN-93 Constant System 153

13. Discrete Processes Modelling and Geometry Description in RTS&T CODE 161

14. Verification Benchmark Calculations in Low and Medium Energy Regions using RTS&T Code 171

15. Notes on the CONSYST Code 189

00-30130 (116) [1]
Translated from Russian

NEUTRON CONSTANTS AND PARAMETERS

UDC 539.173.84

STUDY OF DELAYED NEUTRON DECAY CURVES FOR ^{235}U AND ^{239}Pu FISSION DUE TO THERMAL NEUTRONS

S.B. Borzakov, Yu.S. Zamyatnin, Ts. Panteleev, S.S. Pavlov, I. Ruskov
Joint Institute for Nuclear Research, Dubna

STUDY OF DELAYED NEUTRON DECAY CURVES FOR ^{235}U AND ^{239}Pu FISSION DUE TO THERMAL NEUTRONS. Experimental data and an analysis of delayed neutron decay curves in the time range 5-730 ms following irradiation of ^{235}U and ^{239}Pu are presented. The statistical accuracy is 0.3-0.4% for a time channel of 1 ms. Experimental data were compared with 6- and 8-group calculated data. The 7-group constant sets were proposed as most suitable for the description of the experimental curves.

It is well known that the time dependence of the number of delayed neutrons formed as a result of fission of nuclei and subsequent β-decay of the precursor fragments, $n_d(t)$, may be written as the sum of a large number of exponents with decay constants $\lambda = ln2/T_{1/2,i}$ and weights $a_i = Y_{ci} P_{ni}$:

$$n_d(t) = \sum_i a_i e^{-\lambda_i t} \qquad (1)$$

where $T_{1/2,i}$ is the half-life of the i-th precursor, Y_{ci} is its cumulative yield during fission of the nucleus, and P_{ni} is the probability of emission of a neutron in the process of β-decay. The summation is performed over all precursor isotopes.

Since the number of precursors is very high (currently over 270 of them are known), it is usual, for the practical application of Eq. (1), to divide the precursors into a number of separate groups with similar half-lives. The most commonly used is a 6-group system of constants first introduced by Keepin [1]. Some authors have proposed a more detailed grouping of the precursors [2, 3], but it has not gained wide acceptance. More recently Spriggs et al. have proposed an 8-group system [4, 5] which agrees better than the 6-group one with the results of experiments to measure the reactivity and rise time of critical systems. This system uses the same half-lives for all isotopes and different excitation energies. It proposes a more natural way of forming the long-lived groups corresponding to the precursors with the greatest yield. However, it is harder to highlight the dominant isotopes and neglect the contribution from the rest in the region of shorter-lived precursors, where the solution to such a problem becomes less unambiguous (see Fig. 1).

For this reason it was decided to analyse in greater detail the agreement between several systems of constants $\{\lambda_i; a_i\}$ proposed by various authors and the experimental data, and to enhance their accuracy by carrying out additional measurements in the region of short-lived delayed neutrons. This was necessary because the commonly used measurement method that involves moving the sample from the place of irradiation towards the neutron detector does not allow accurate determination of the characteristics of delayed neutrons emitted in the first second after irradiation. This explains the size of the errors and the spread in the data (15-35%) when determining the parameters of the 5th and 6th groups [6]. Thus it appeared desirable to measure the delayed neutron decay curves in the time interval from a few milliseconds to 1 second.

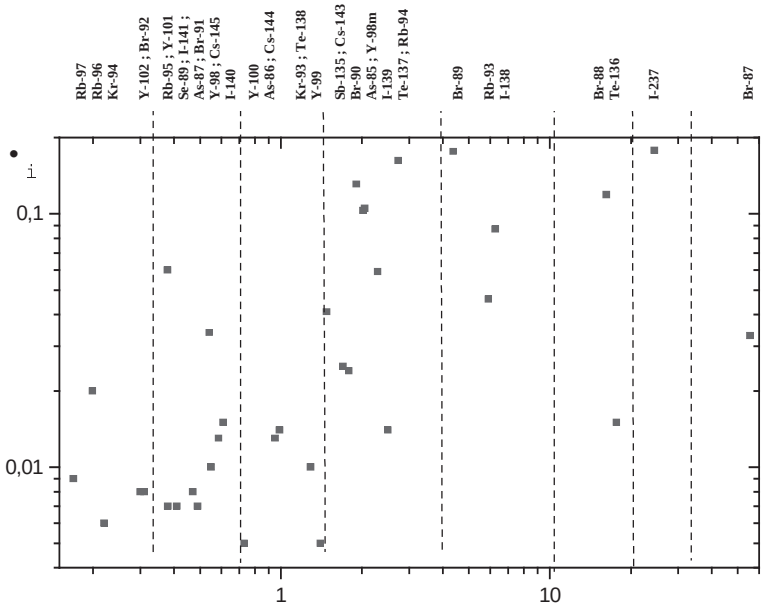

Fig. 1. Contribution of various isotopes to the delayed neutron yield (in per cent) for ^{235}U fission due to thermal neutrons.

The experiment

This was carried out at the Neutron Physics Laboratory of the Joint Institute for Nuclear Research using the "Izomer" device, which is designed for determining total delayed neutron yields from the fission of actinide nuclei by thermal neutrons and which uses the IBR-2 pulsed fast reactor as a neutron source [7-9]. This reactor, which has a mean power of 2 MW, a pulse repetition frequency of 5 Hz and a pulse power of 1350 MW, is a suitable neutron source for studying the decay curves of short-lived delayed neutron precursors. The principal components of the "Izomer" device are a thermal neutron chopper and a high-efficiency detector consisting of 12 ^{3}He counters in a moderator. The device is positioned at the outlet of a curved mirror neutron guide, which allows measurements to be made under adequately good background conditions.

This paper presents the results of repeated measurement and analysis of the decay curves for delayed neutrons formed as a result of fission of ^{235}U and ^{239}Pu due to thermal neutrons over a wider (by comparison with our earlier paper [9]) range of decay times from 5 to 730 ms after the end of irradiation. The measurements were carried out by periodic irradiation of the sample with an irradiation frequency of 1.25 Hz, which was achieved by reducing the rotation frequency of the chopper. Metallic ^{235}U and ^{239}Pu targets weighing 7 and 10 g, respectively, were used as samples.

The background, determined by measurements with a cadmium filter in the beam, amounted to no more than 1% of the total neutron count over the time interval investigated. The results of the measurements, with the background deducted, are shown in Fig. 2 for ^{235}U and Fig. 3 for ^{239}Pu. The data were accumulated over 40 hours for ^{235}U and 86 hours for ^{239}Pu. The statistical accuracy of the readings was 0.3-0.4% for ^{235}U and ^{239}Pu in each time channel equal to 1.024 ms.

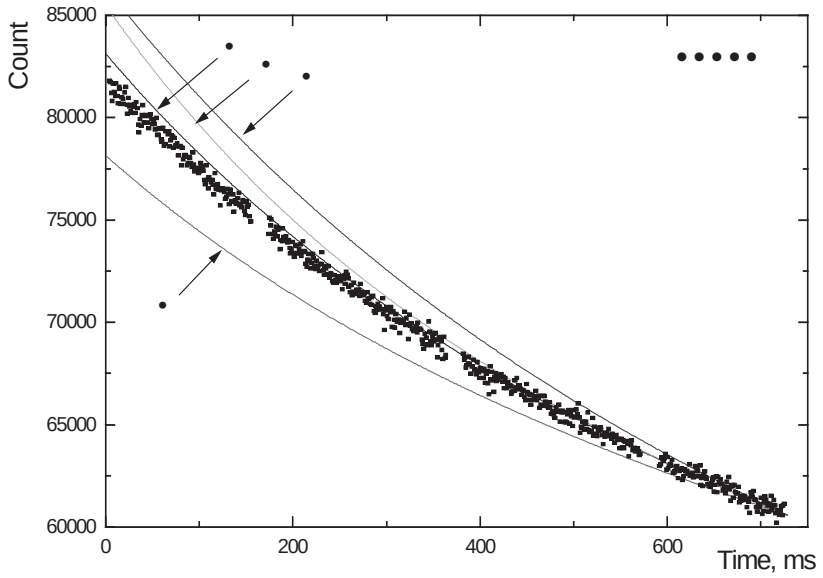

Fig. 2. Experimental curve obtained with a ^{235}U sample.
The decay curves shown were calculated using the following parameter sets:
1 - Keepin [10]; 2 - Waldo et al. [11]; 3 - Mills et al. [12]; 4 - Spriggs et al. [5].

Analysis and discussion of results

In order to compare the data obtained by us with the results of work published earlier, we plotted the decay curves using different sets of relative weights and half-lives for each group. The decay curves $\bar{n}_d(t)$ were calculated by the formula for taking into account the periodic nature of the irradiation which is given in Ref. [9]:

$$\bar{n}_d(t) = N_f \nu_d \varepsilon_d \sum_{i=1}^{6} \frac{a_i}{\Delta t} \cdot \frac{1-\exp(-\lambda_i \Delta t)}{1-\exp(-\lambda_i T)} \cdot \exp(-\lambda_i t). \qquad (2)$$

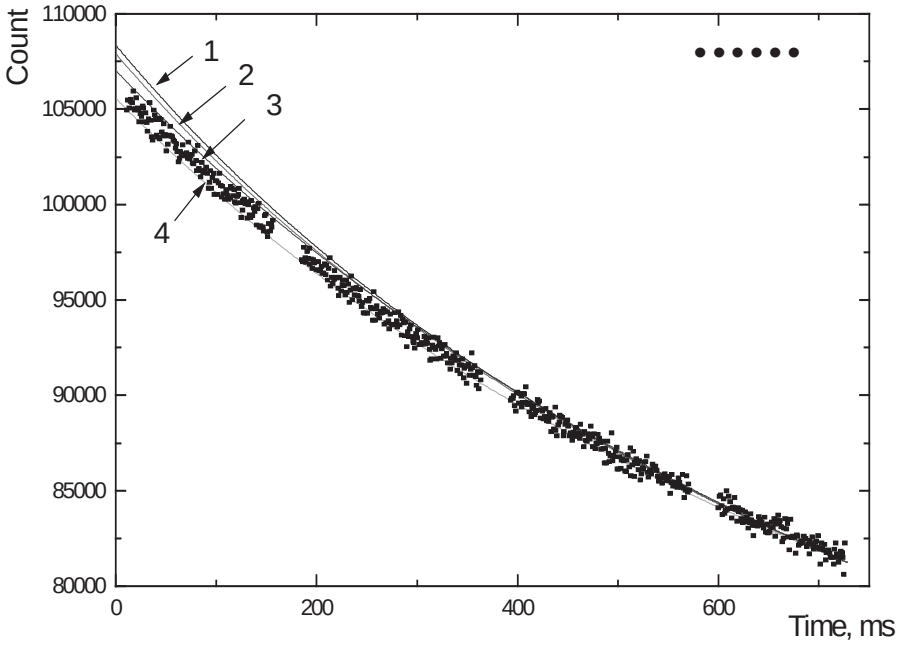

Fig. 3. Experimental curve obtained with a ^{239}Pu sample.
The decay curves shown were calculated using the following parameter sets: 1 - Tuttle [6]; 2 - Brady, England [13]; 3 - Wahl [14]; 4 - Waldo [11].

Here N_f is the number of fission events, ν_d is the delayed neutron yield, T is the irradiation period, Δt is the irradiation time within one period, ε_d is the detector efficiency, and a_i is the relative weight for the i-th group ($\Sigma a_i = 1$). Since it was necessary to use samples with large masses in order to achieve a high statistical accuracy of measurement of the number of delayed neutrons, the number of fission events was not determined in view of the counting error of the instrumentation. The normalization constant $C = N_f \nu_d \varepsilon_d$ was determined by fitting.

Fig. 2 shows experimental data for ^{235}U and decay curves calculated using the parameter sets given in Refs [10-12] and also [5] (Table V on p. 14). As may be seen from Fig. 2, the authors of Refs [11, 12] overestimate the contribution of short-lived precursors, whereas those of Ref. [5] underestimate it. The best description of the experimental data is achieved using the parameter sets from Ref. [10] and the expanded 8-group Keepin model proposed in Ref. [5]. The curves calculated with these parameter sets are practically identical. Experimental data for ^{239}Pu are given in Fig. 3 together with curves calculated using parameters obtained both experimentally [6, 11] and by calculation [13, 14].

The recent proposal by Spriggs et al. to use the 8-group system of constants from Ref. [5] with the parameters of the dominant precursors within the group as the group parameters is of great interest from our point of view. There is no doubt about the usefulness of such an approach, at least for the first four long-lived precursor groups (see Fig. 1). However, in view of the appreciable divergence of the curves in the short half-life region and the presence in the 5th and 7th groups of a large number of precursors with comparable yields,

we made an attempt to take into account the contribution of a larger number of delayed neutron precursors in these groups. In doing so we used half-life data from [15], P_n values from [16] and cumulative yields from [13]. In addition, the absence of precursors with an appreciable relative yield (>0.01%) in the range $T_{1/2} \approx 0.6\text{-}1.4$ and the correspondingly small total contribution a_6<0.02% means that it is helpful to eliminate it as a separate group and switch to a 7-group constant system (see Table 1).

Table 1

Breakdown into groups and parameter set for ^{235}U

Group number	Precursor nucleus	$T_{1/2,i}$, s	a_i (per 100 fission events)	Mean value of $T_{1/2,j}$, s	Group weight (per 100 fission events)
1	Br-87	55.60	0.054	55.6	0.054
2	I-137	24.50	0.233	24.5	0.233
3	Te-136	17.70	0.015	16.4	0.134
	Br-88	16.23	0.119		
4	I-138	6.27	0.087	4.99	0.309
	Rb-93	5.91	0.046		
	Br-89	4.37	0.176		
5	Rb-94	2.73	0.162	2.07	0.664
	Te-137	2.50	0.014		
	I-139	2.29	0.059		
	Y-98m	2.05	0.105		
	As-85	2.02	0.103		
	Br-90	1.91	0.131		
	Cs-143	1.79	0.024		
	Sb-135	1.70	0.025		
	Y-99	1.48	0.041		
	Kr-93	1.29	0.010		
6	Cs-144	0.99	0.014	0.494	0.159
	As-86	0.95	0.013		
	Y-100	0.73	0.005		
	I-140	0.61	0.015		
	Cs-145	0.586	0.013		
	Y-98	0.549	0.010		
	Br-91	0.542	0.034		
	As-87	0.49	0.007		
	I-141	0.470	0.008		
	Se-89	0.410	0.007		
	Y-101	0.380	0.007		
	Rb-95	0.379	0.060		
7	Br-92	0.31	0.008	0.218	0.045
	Y-102	0.30	0.008		
	Kr-94	0.22	0.006		
	Rb-96	0.199	0.020		
	Rb-97	0.169	0.009		

The mean half-life for each group is given by the formula

$$\langle T \rangle = \frac{\ln 2}{\langle \lambda \rangle},$$

where

$$\langle \lambda \rangle = \sum_i^j a_i \lambda_i \cdot \left(\sum_i^j a_i \right)^{-1}. \qquad (3)$$

Here *j* is the number of precursors included in the group.

A comparison of calculations using the proposed constant system with experimental results is given in Fig. 4 for ^{235}U. As may be seen from the figure, the agreement with experiment has improved significantly ($\chi^2 = 1.6$).

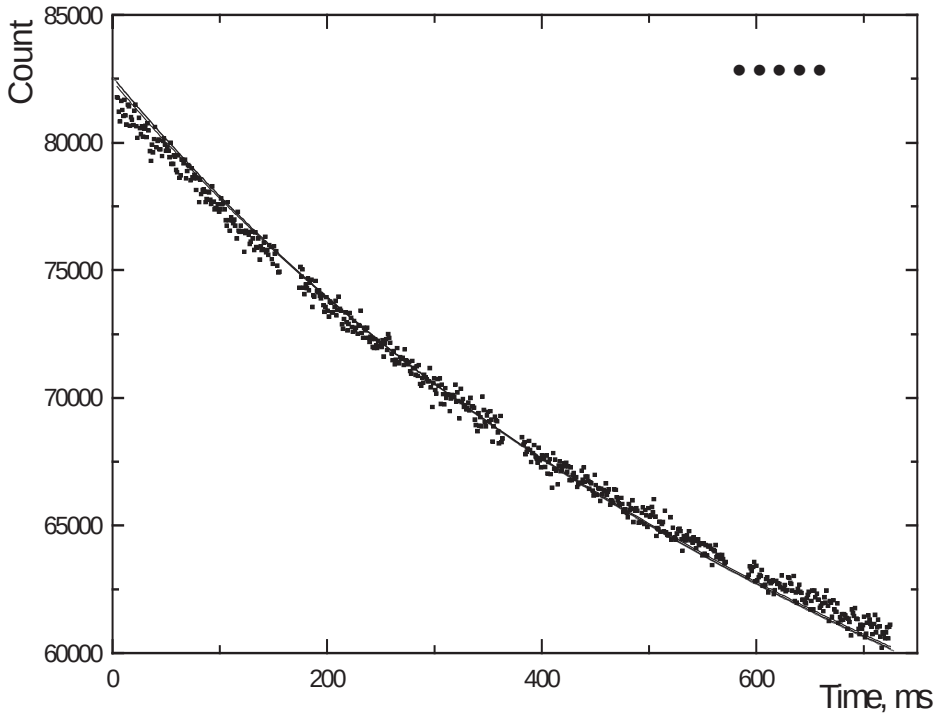

Fig. 4. Decay curve for ^{235}U calculated in a 7-group approximation.

Experimental data obtained with a ^{239}Pu sample were analysed in a 6- and a 7-group approximation in the same way as those for ^{235}U. The breakdown into groups for ^{239}Pu is given in Table 2. Fig. 5 shows the agreement between the calculated curve and the experimental data.

Table 2

Breakdown into groups for ^{239}Pu

Group number	Precursor nucleus	$T_{1/2,i}$, s	a_i (per 100 fission events)	Mean half-life, s	Group weight (per 100 fission events)
1	Br-87	55.6	0.017	55.6	0.017
2	I-137	24.5	0.157	24.5	0.157
3	Te-136	17.7	0.009	16.5	0.043
	Br-88	16.23	0.034		
4	I-138	6.27	0.061	5.40	0.123
	Rb-93	5.91	0.019		
	Br-82	4.37	0.043		
5	Nb-105	2.95	0.0117	2.097	0.248
	Rb-94	2.73	0.0635		
	I-139	2.29	0.0297		
	Y-98m	2.05	0.0440		
	As-85	2.02	0.0165		
	Br-90	1.91	0.0333		
	Cs-143	1.79	0.0103		
	Sb-135	1.70	0.0117		
	Y-99	1.48	0.0270		
6	Cs-144	0.99	0.0044	0.460	0.061
	Y-100	0.73	0.0034		
	I-140	0.61	0.0031		
	Cs-145	0.586	0.0032		
	Y-98	0.549	0.0085		
	Br-91	0.542	0.0046		
	Y-101	0.380	0.0027		
	Rb-95	0.379	0.0310		
7	Rb-96	0.199	0.0070	0.191	0.00915
	Rb-97	0.169	0.00215		

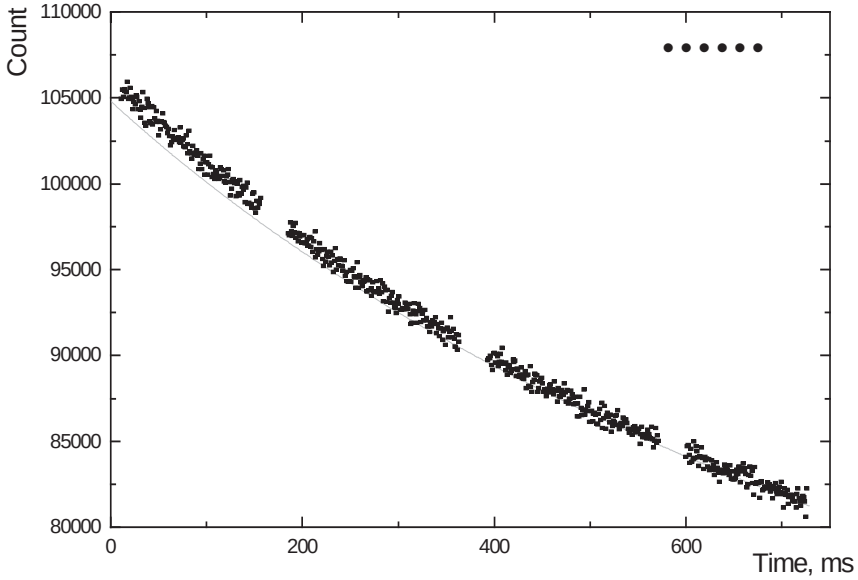

Fig. 5. Decay curve for ^{239}Pu calculated in a 7-group approximation.

Conclusion

The present paper gives the results of measurements and an analysis of decay curves for delayed neutrons in the time range 5-730 ms after the end of ^{235}U and ^{239}Pu irradiation carried out with high statistical accuracy (0.3-0.4% in a time channel of 1 ms).

The experimental data obtained are compared with results calculated for various sets of group constants in 6- and 8-group approximations.

For ^{235}U and ^{239}Pu a 7-group parameter set is proposed which is based on the characteristics of 30 precursors with a yield of 0.01% or higher that are known from the literature and which more accurately describes the experimental data in the time range considered.

The authors would like to thank Yu.V. Grigorev for providing the samples, V.I. Furman for supporting the work, and also G. Spriggs and V.M. Piksaikin for fruitful discussion of the data obtained.

References

[1] G.R. Keepin, Physics of Nuclear Kinetics, Addison Wesley, Reading. Mass., 1965.
[2] B.V. Maksyutenko, Yadernaya Fizika v. 13 No. 2, 1971.
[3] L.G. Manevich, P.Eh. Nemirovskij, M.S. Yudkevich, Voprosy atomnoj nauki i tekhniki, Ser. Yadernye konstanty, No. 2, 1988, p. 3.
[4] G.D Spriggs, Report at "Colloquy on Delayed Neutron Data", Obninsk, Russia, 9-10 April, 1997.
[5] G.D. Spriggs, J.M. Campbell, V.M. Piksaikin, LA-UR-98-1619, Los-Alamos, 1998.
[6] R.J. Tuttle, Nucl. Sci. Eng., v. 56, p. 37, 1975.
[7] S.B. Borzakov, E. Dermendjiev, Yu.S. Zamyatnin, V.M. Nazarov, S.S. Pavlov, A.D. Rogov, I. Ruskov, Preprint JINR P3-94-447, 1994.
[8] S.B. Borzakov, E. Dermendjiev, Yu.S. Zamyatnin, V.M. Nazarov, S.S. Pavlov, A.D. Rogov, I. Ruskov, Atomnaya Ehnergiya 79, 1955, p. 231.
[9] S.B. Borzakov, A.A. Andreev, E. Dermendjiev, A. Filip, V.I. Furman, Ts. Panteleev, I. Ruskov, Yu.S. Zamyatnin, Sh. Zejnalov. Joint Institute for Nuclear Research report E3-98-145, Dubna, 1998 (sent to Yadernaya Fizika).
[10] G. R. Keepin, T.F. Wimett, and R.K. Zeigler, Phys. Rev., v. 107, p. 1044, 1957.
[11] R.W. Waldo et al., Phys. Rev. C23, p. 1113, 1981.
[12] R.W. Mills et al., Nuclear Data for Science and Technology, Proceedings, FRG, Juelich, 13-17 May 1991, p. 86, Springler-Verlag, Berlin, 1992.
[13] M.C. Brady, T.R. England, Nucl. Sci. Eng., v. 103, p. 129, 1989.
[14] A.C. Wahl, Atomic Data and Nuclear Data Tables, v. 39, p. 1, 1988.
[15] G. Rudstam, IAEA Report INDC (SWD) 24/L+P, Vienna, 1993.
[16] G. Rudstam, At. Data and Nucl. Data Tables, v. 53, p. 1, 1993.

00-30130 (117) [2]
Translated from Russian

UDC 539.17

DIFFERENTIAL CROSS-SECTIONS FOR THE U(n,xn) REACTION AT A NEUTRON ENERGY OF 14.3 MeV

B.V. Devkin, M.G. Kobozev, A.A. Lychagin, S.P. Simakov, V.A. Talalaev
Institute for Physics and Power Engineering (IPPE), Obninsk

DIFFERENTIAL CROSS-SECTIONS FOR THE U(n,xn) REACTION AT A NEUTRON ENERGY OF 14.3 MeV. The results of measurements of double-differential neutron emission cross-sections for the U(n,xn) reaction at 14.3 ± 0.1 MeV incident neutron energy are given. The measurements were made using the time-of-flight technique with the IPPE's KG-0.3 pulsed neutron generator. The paper describes the experimental set-up and the results of the measurements and contains comparisons with data from other experiments and the ENDF-B6 and ENDL-85 evaluated data libraries.

Uranium is one of the main elements in thermal and fast reactor cores. Its use has also been proposed in blankets for thermonuclear devices, where it can serve to multiply neutrons and breed plutonium. To predict the main parameters of such devices correctly it is very important to have a precise knowledge of the energy-angular distributions of secondary neutrons from inelastic interaction processes between neutrons and uranium nuclei. The accuracy required for these practical applications is about 10-15% [1] over a wide range of initial neutron energies. Such accuracy levels have not yet been achieved because the experimental data measured by various authors have a much greater spread. On a fundamental level, this type of data is of undoubted interest for research into the mechanism of interaction of fast neutrons with nuclei and induced fission processes [2].

Taking the above into account, we measured double-differential neutron emission cross-sections for the U(n,xn) reaction at an incident neutron energy 14.3 MeV. The present paper contains a short description of the experimental apparatus, measurement results, and a comparison with other authors' data and with widely used evaluated nuclear data libraries.

The experiment

Measurements of double-differential neutron emission cross-sections for the U(n,xn) reaction were carried out using the time-of-flight method with a fast neutron spectrometer and the KG-0.3 pulsed neutron generator [3]. The experimental set-up is shown schematically in Fig. 1. A short (2.5 ns) pulse of 14 MeV neutrons was generated through T(d,n) reactions produced by bombarding a solid tritium target with a pulsed beam of 280 keV deuterons. The target assembly (target-holder) was made from a thin steel tube 0.5 mm thick. The solid titanium tritium target on a copper support had a diameter of 11 mm and a thickness of 0.8 mm. The deuteron beam was passed through a diaphragm with an aperture 8 mm in diameter. At a distance of about 50 cm from the target a cylindrical pick-up electrode was

mounted from which an electrical signal was taken to obtain stop pulses.

The uranium sample used came in the shape of a hollow cylinder with external and internal diameters of 4.52 cm and 3.98 cm, respectively, and a height of 4.87 cm. The sample was made from depleted ^{238}U (^{235}U content 0.2%) and weighed 326.8 g. The sample was placed at a distance of 14 cm from the TiT target at an angle of 78° to the direction of the deuteron beam striking the target. The energy of the neutrons striking the sample was 14.3 ± 0.1 MeV.

The neutron detector consisted of an NE-218 liquid scintillator in a glass vial (diameter 10 cm, thickness 5 cm) viewed by an XP-2041 photomultiplier. The anode pulses from the photomultiplier reached the discriminator with a tracking threshold which generated start pulses for time-of-flight analysis. At the same time, the discriminator separated neutron and gamma counts according to the shape of the signal from the detector. The detector had a time resolution of 3 ns, a neutron detection threshold of $\approx$ 0.3 MeV and a gamma ray suppression factor of ≈ 5.

The scintillation detector was positioned at a time-of-flight distance of 215 cm from the centre of the sample. It was placed in a lead housing 10 cm thick inside a massive shield made from a mixture of paraffin wax and lithium hydride. An iron and a copper cone were placed in front of this shield to reduce the probability of neutrons from the source striking the detector directly. The whole shield together with the detector was moved around the centre of the scatterer so that neutron spectra could be measured at angles from 30° to 150° in 30° steps.

The efficiency of the detector was determined by two experimental methods. First, the neutron spectrum of spontaneous ^{252}Cf fission was measured, which is known for the 0.1-10 MeV energy range to within 3% [4]. A fast-response fission ionization chamber with a layer of ^{252}Cf was used as a neutron source. This method enabled us to measure the efficiency up to an energy of $\approx$ 6 MeV, since at higher energies the number of fission neutrons becomes very small. To determine the efficiency in the high-energy region, a second method was used which relates to the cross-section for neutron scattering by hydrogen, which is known to within less than 1% [5]. A stilbene crystal (10 mm in diameter, 40 mm high) was used as a scatterer. The crystal was mounted on the photo cathode of an FEU-30 photomultiplier the signals from which were used to obtain stop pulses and generate recoil protons of the necessary energy [6].

To measure the background due to neutron scattering by walls and apparatus in the experiment room, measurements were made without the sample. The measurement procedure (data accumulation) involved repeating measurements a number of times at different angles alternately with and without the sample. This provided the necessary read-out statistics and enabled us to average the possible variation in spectrum parameters for the whole of the experiment.

The pulses supplied by the neutron generator were monitored by the time-of-flight method using a detector consisting of a stilbene crystal (Ø 20 x 20 mm) and an FEU-30 photomultiplier. A long counter was used to monitor the neutrons flux from the target.

Initial processing of experimental data and calculation of corrections

The individual experimental spectra collected were summed with progression along the time axis to compensate for the time drift of the apparatus. For this, the positions of the centres of mass of the 14 MeV neutron peaks in each individual spectrum were calculated and the degree of displacement was determined. This processing produced total "effect + background" and "background" time spectra for each scattering angle. After normalizing the "background" spectrum to the same number of monitor readings and subtracting it from the "effect + background" spectrum, the resulting time distribution was converted into an energy spectrum. Absolute normalization of the energy spectra for secondary neutrons was carried out with respect to the neutron scattering cross-section for hydrogen from Ref. [5].

A correction for multiple scattering and neutron attenuation in the sample calculated using the Monte Carlo method was included in the experimental data. These calculations involved detailed modelling of the experiment, in particular the energy-angular distribution of the source neutrons and the dimensions and position of the scatterer and neutron detector. The calculations were carried out using the MCNP-4B program [7] with the ENDF-B6 and ENDL-85 evaluated nuclear data libraries. The correction was derived from the ratio of $\sigma_{sample}(E,\Theta)$, the spectrum of neutrons scattered by the sample at a given angle Θ, to $\sigma(E,\Theta)$, the differential cross-section for the U(n,xn) reaction. The value of the correction $\sigma_{sample}(E,\Theta)/\sigma(E,\Theta)$ for an angle of 90° is shown in Fig. 2. It can be seen that with a sample of finite dimensions, the neutron spectrum is lower in the energy range above 1 MeV and higher at lower energies. It is also clear that the general trend is practically independent of the evaluated data library used. The resultant correction function was therefore derived by averaging the calculation results with data from ENDF-B6 and ENDL-85.

The full neutron emission spectrum includes neutrons from inelastic processes and elastic neutron scattering. Because of the energy resolution of the spectrometer, the peak for the elastically scattered neutrons has an appreciable width (FWHM $\approx$ 2 MeV), which leads to the mixing of neutrons from elastic and inelastic processes in the high-energy region of the measured emission spectra. The shape of the elastic scattering peak was determined using the source neutron spectrum, measured with the detector positioned at an angle of 0°. This spectrum was normalized to the elastic scattering peak in the neutron emission spectrum for the angle in question and subtracted. What remained was the spectrum of inelastically scattered neutrons.

The error in the experimental data consists of the statistical error (3-30%); the uncertainty in the determination of the detector efficiency (5-10%) and in the absolute normalization of the cross-sections (5%); and the inaccuracy in calculating the corrections for multiple neutron interactions with the sample (2%). The overall error varies between 8 and 30% depending on the energy and angle of the scattered neutrons.

A more detailed description of the experimental apparatus, the measurement method and the initial processing of the data can be found in earlier papers [3, 8].

Experimental results

The experimental data measured in this study are compared with known and available results from other authors [9, 10, 11, 12, 13, 14, 15, 16] in Figs 3-5. The main parameters of these experiments are given in the table: initial neutron energy, sample composition and dimensions, path length, range of secondary neutron energies and scattering angles, EXFOR number and original study reference. The table shows that the various experiments were carried out under different experimental conditions.

Table

Main parameters of the experiments to measure differential cross-sections for the U(n,xn) reaction at ≈ 14 MeV incident neutron energy

Energy (MeV)	Sample dimensions (cm)	Path length (cm)	Range		EXFOR number	Reference
			of energies (MeV)	of angles (degrees)		
14.1	U ∅22 × ∅12 × 1	200	0.2-14	92	40332	[9]
14.1 ± 0.1	U (8% ^{235}U) ∅5.0 × 1.0	40	0.1-8.75	30-130	20578	[10]
14	U ∅10 × ∅12 × 1	≈ 740	0.5-14	45-145	-	[11]
14.36	U ∅4.6 × 10.0	200	0.1-5	33-153	-	[12]
14.3 ± 0.12	U (2% ^{235}U) ∅4.5 × ∅4.0 × 4.9 ∅4.5 × ∅3.5 × 4.9 ∅4.5 × ∅3.0 × 4.9	205	0.6-10	90	40335	[13]
14.6 ± 0.3	U (8% ^{235}U)	300	2-12	5-175	40620	[14]
14.1 ± 0.3	U (8% ^{235}U) ∅2.0 × 5.0	500	0.4-14	30-135	22158	[15]
14.1	U ∅12 × ∅8 × 0.6	≈ 500	1-6	15-165	-	[16]

Figure 3 compares energy differential neutron emission cross-sections for the U(n,xn) reaction, i.e. double-differential cross-sections integrated with respect to the scattering angle. Results from those studies in which the energy spectra were measured at only one angle were multiplied by 4π. Fig. 3 shows a considerable spread in the experimental data.

In Ref. [9], neutron emission cross-sections were measured in ring geometry with a solid sample; moreover, they are given in relative units (Fig. 3 shows numerical data from this study as they appear in EXFOR 40332). These measurements were subsequently repeated by

the authors [12] but in a cylindrical geometry; however, the numerical data for the emission spectra are not available.

In Ref. [10], the reaction cross-sections were measured over a relatively short path length of 40 cm and the sample was thick, but corrections were made for multiple scattering. It would appear that all these factors were the reason for the elevated cross-section in the energy region below 1 MeV. In Ref. [11], the neutron spectra were measured in ring geometry with a solid sample. The numerical data for this experiment are not available.

In Ref. [13], the emission cross-sections were measured only at a 90° angle and, as Fig. 3 shows, they have a considerable spread in the high energy region. Moreover, they stop suddenly at neutron energies above 10 MeV. In Ref. [14], the neutron spectra were measured with a high detector threshold, and in addition numerical data in the EXFOR library are presented in the form of an average over broad energy groups (at 1-2 MeV intervals). Reference [15] involved the most detailed measurements of double-differential neutron emission cross-sections in terms of both secondary neutron energy and scattering angles. In this study, however, the peak for the elastically scattered neutrons was not separated out. In Ref. [16] the secondary neutron spectra were measured in a relatively narrow energy range (1-6 MeV) and the numerical data are not available via EXFOR.

Experimental data obtained in this study are also shown in Fig. 3. The comparison shows that, taking into account the specific features of earlier measurements mentioned above and the experimental errors, there is satisfactory agreement among the results of this experiment and the last three experiments [13, 14, 15]. For example, the spread in the data from the present study and Refs. [13] and [15] does not exceed 10% in the 0.8-10 MeV energy range, although it increases beyond this range.

Figure 4 compares the experimental data obtained in the present study with evaluated data from the ENDF-B6 and ENDL-85 libraries. It can be seen that significant differences (up to 30%) occur only in the energy region above 6 MeV, with the evaluated data fluctuating around the experimental data.

Figure 5 gives a comparative analysis of angular differential cross-sections (i.e. cross-sections integrated with respect to secondary neutron energy in the energy groups indicated). In addition to our experimental data, it gives measurement results from Refs. [14] and [15]. It can be seen that the spread in the data on the angular distributions of the neutrons is greatest (≈ 2) at forward angles and in the hard part of the spectrum. However, if the measurement error is taken into account the results of the different experiments can be considered consistent.

With regard to the evaluated data, Fig. 5 shows that the ENDL-85 library assumes an isotropic distribution of secondary neutrons. In library ENDF-B6, the angular anisotropy adopted for the 4-10 MeV energy range is clearly too low in comparison with that observed in the overall results of the three experimental studies.

The double-differential cross-sections for the U(n,xn) reaction obtained in the present study have been transmitted to the EXFOR experimental data library.

Conclusion

Double-differential neutron emission cross-sections for the U(n,xn) reaction at an incident neutron energy of 14.3 ± 0.1 MeV were measured.

Analysis of available numerical data from other authors showed considerable variation between them; moreover, many measurements were taken at particular angles or within a narrow range of secondary neutron energies. The results of the present study agree most closely with those of Ref. [15], and together they provide the most comprehensive information on double-differential cross-sections for the U(n,xn) reaction at 14 MeV.

Comparison with the evaluated data of ENDF-B6 and ENDL-85 revealed discrepancies (up to 30%) in the high-energy region of secondary neutron energy distributions; moreover, angular anisotropy was ignored (ENDL-85) or underestimated (ENDF-B6).

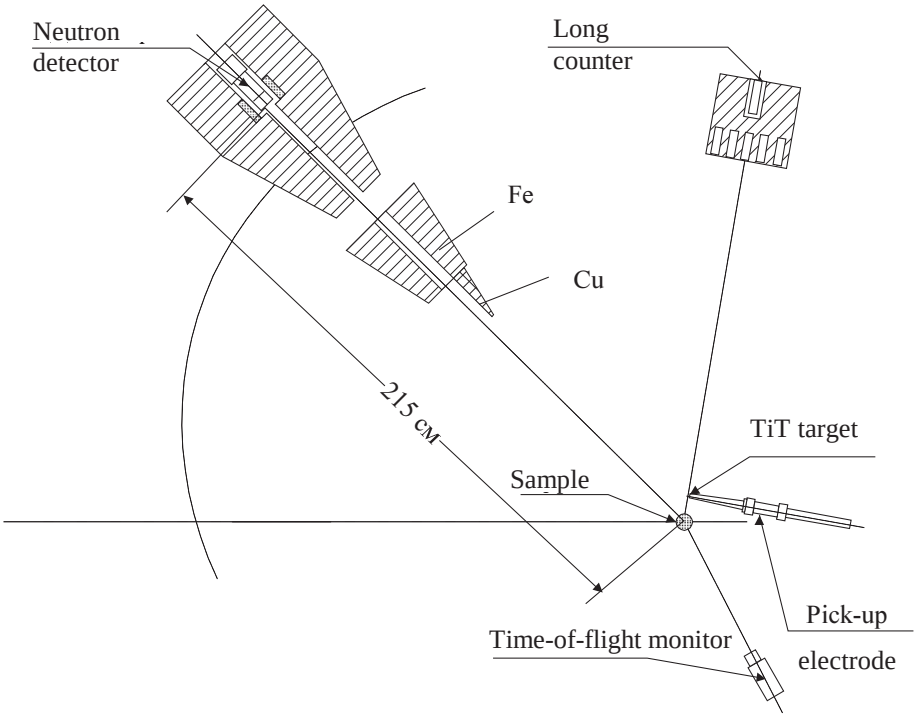

Fig. 1. Geometry of the experimental set-up for measuring neutron spectra for the U(n,xn) reaction.

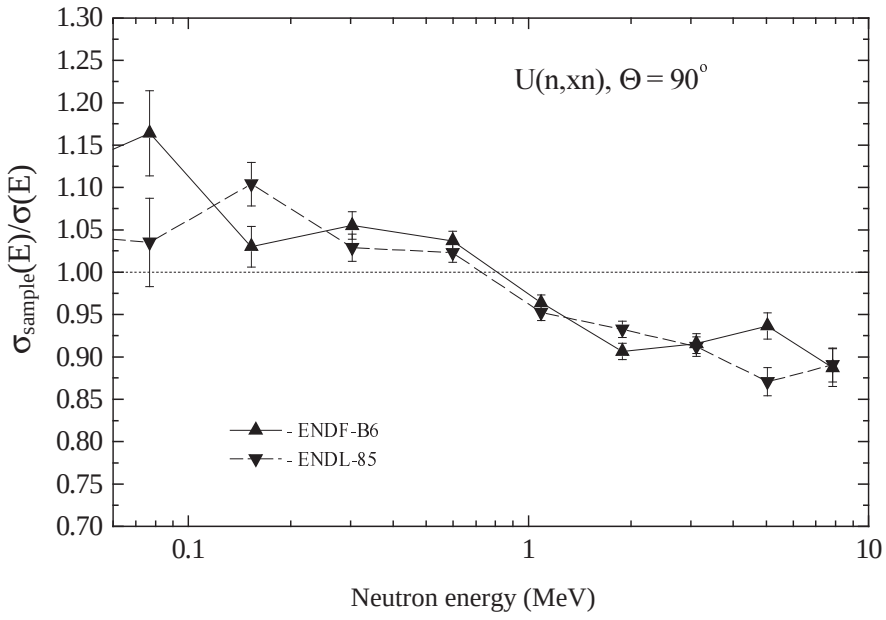

Fig. 2. Dependence of the correction for multiple scattering and neutron attenuation in a depleted uranium sample (∅4.52 × ∅3.98 × 4.87 см) on secondary neutron energy. Results of calculations with the ENDF-B6 (5) and ENDL-85 (6) libraries are shown with the statistical error in the calculation.

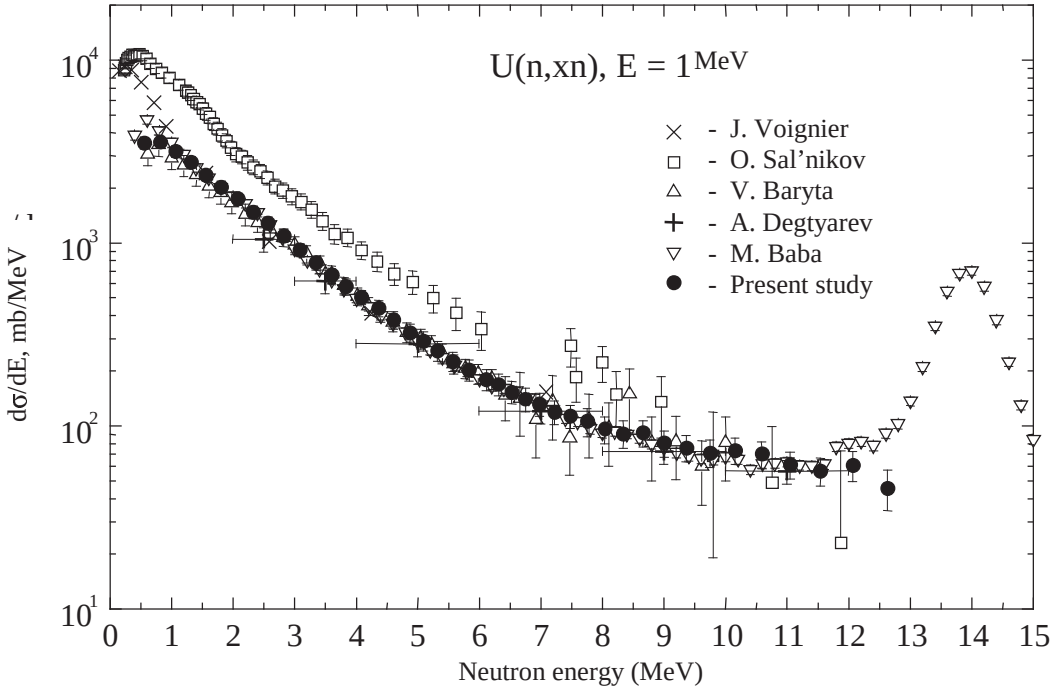

Fig. 3. Comparison of experimental data on differential cross-sections for the U(n,xn) reaction: • - present study, × - [10], □ - [9], Δ - [13], + - [14], ∇ - [15].

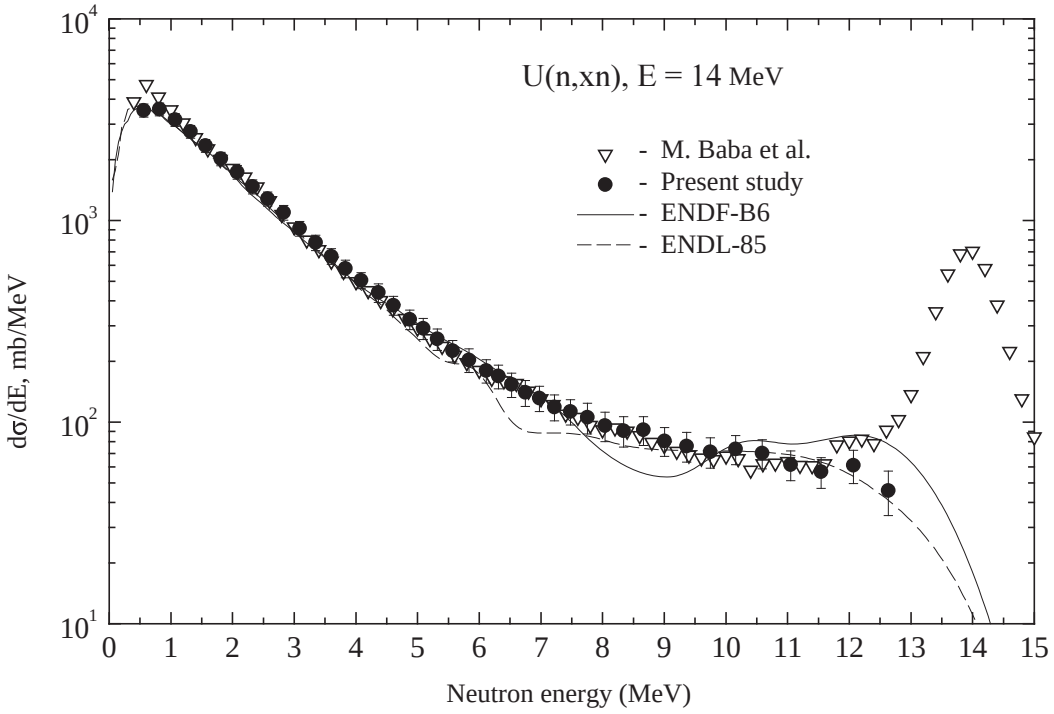

Fig. 4. Comparison of experimental and evaluated differential cross-sections for the U(n,xn) reaction. Experimental data: • - present study, ∇ - [15]. Evaluated data: ——— ENDF-B6, - - - - - ENDL-85.

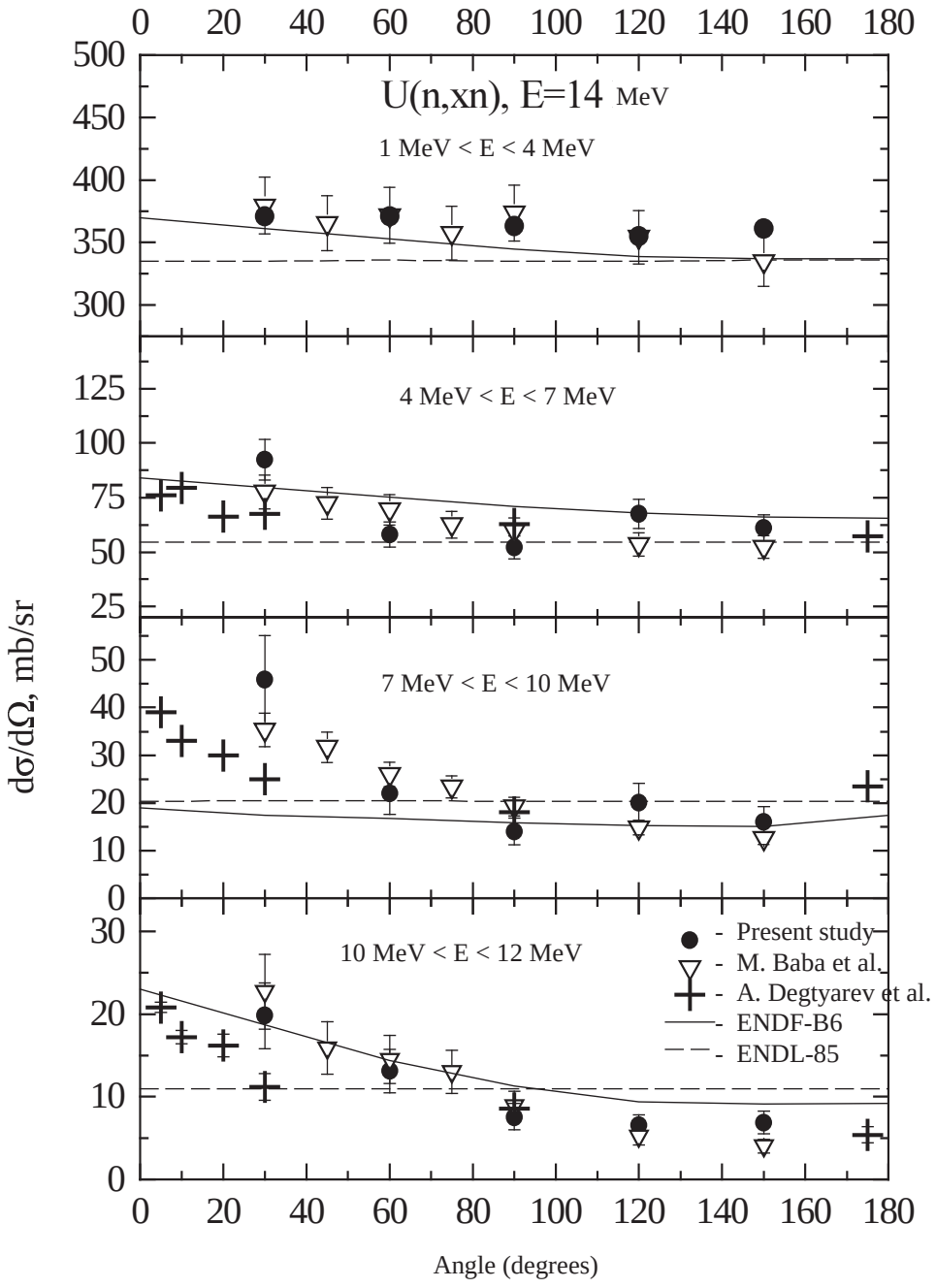

Fig. 5. Differential cross-sections (angular distributions of neutrons) for the U(n,xn) reaction. Experimental data: • - present study, + - [14], ∇ - [15]. Evaluated data: ——— ENDF-B6, - - - - - ENDL-85.

References

[1] World Request List for Nuclear Data. Report INDC(SEC)-104, Vienna, 1993.

[2] G.N. Smirenkin, G.N. Lovchikova, et al. Measurement of energy spectra of neutrons from emission fission of ^{238}U nuclei,Yadernaya Fizika, 1996, vol. 59, No. 11, p. 1934 (in Russian).

[3] A.B. Anufrienko, B.V. Devkin, et al. Multi-purpose fast-neutron time-of-flight spectrometer,Voprosy atomnoj nauki i tekhniki. Seriya Reaktorostroenie, 1997, issue 5, p. 34 (in Russian).

[4] W. Manhart. Evaluation of the Cf-252 fission neutron spectrum between 0 and 20 MeV. Report IAEA-TECDOC-410, IAEA, Vienna, 1987, p. 158.

[5] G.M. Hale and P.G. Young. The H(n,n)H Cross Section below 20 MeV. Report NEANDC-311 "U", Paris, 1992, p. 10.

[6] N.V. Kornilov, V.I. Plyaskin. Preprint FEhI-496, Obninsk, 1974 (in Russian).

[7] J.F. Briesmeister (ed.). MCNP- A General Monte Carlo N-Particle Transport Code. Version 4B, Los Alamos, 1997.

[8] S.P. Simakov, B.V. Devkin, et al. 14 MeV facilities and research in IPPE. Report INDC(CCP)-351, IAEA, Vienna, 1993,Voprosy atomnoj nauki i tekhniki. Seria Yadernye Konstanty, 1993, issue 3-4, p. 93.

[9] O.A. Sal'nikov, N.I. Fetisov, et al. Neutron inelastic scattering spectrum for ^{232}Th, ^{238}U and ^{235}U nuclei, Izvestiya AN SSSR, Ser. fizich., 1968, vol. 32, No. 4, p. 653 (in Russian).

[10] J. Voignier, G. Clayeux, F. Bertrand. Inelastic neutron scattering in several elements with 14.1 MeV neutrons. Proc. Int. Conf. Knoxvill, 1971, p. 196.

[11] J.L. Kammerdiener. Neutron spectra emitted by ^{239}Pu, ^{238}U, ^{235}U, Pb, Nb, Al, and C irradiated by 14 MeV neutrons. Report UCRL-51232, Lawrence Livermore Laboratory, 1972.

[12] O.A. Sal'nikov, G.N. Lovchikova, et al. Interaction of 14.36 MeV neutrons with ^{232}Th and ^{238}U nuclei. Preprint FEhI-441, Obninsk, 1973 (in Russian).

[13] V.Ya. Baryba, B.V. Zhuravlev, N.V. Kornilov, O.A. Sal'nikov. Secondary neutron spectrum from bombardment of U-238 nuclei with 14.3 MeV neutrons: Preprint FEhI-671, Obninsk, 1976 (in Russian).

[14] A.P. Degtyarev, B.E. Leshchenko, et al. Angular distributions of neutrons from the (n,xn) reaction for ^{56}Fe, ^{59}Co, ^{56}Fe, ^{93}Nb, ^{115}In, ^{56}Fe, ^{209}Bi, ^{238}U nuclei and 14.6 MeV initial energy,Yadernaya Fizika, 1981, vol. 34, issue 2, p. 299 (in Russian).

[15] M. Baba. Wakabayshi et al. Measurements of prompt fission neutron spectra and double-differential neutron inelastic scattering cross sections for 238-U and 232-Th. Report INDC(JPN)-129, IAEA, Vienna, 1989.

[16] T. Elfruth, K. Seidel, S. Unholzer. Measurement, Evaluation and Analysis of 14.1 MeV Neutron Induced Cross Sections of ^{238}U. Report INDC(NDS)-272, IAEA, Vienna, 1993, p. 59.

00-30130 [3]
Translated from Russian

UDC 171.017

EVALUATION OF THE GAMMA-RAY PRODUCTION CROSS-SECTIONS FOR NONELASTIC INTERACTION OF FAST NEUTRONS WITH Al NUCLEI

A.G. Zvenigorodskij, M.S. Shvetsov, A.M. Shvetsov, M.V. Savin,
Yu.A. Nefedov, V.A. Zherebtsov
Russian Federal Nuclear Centre - All-Russia Scientific Research
Institute for Experimental Physics, Sarov

EVALUATION OF THE GAMMA-RAY PRODUCTION CROSS-SECTIONS FOR NONELASTIC INTERACTION OF FAST NEUTRONS WITH Al NUCLEI. The total gamma-ray production cross-sections in the 0.5-10 MeV energy range and discrete gamma line production cross-sections for E = 791, 843, 952, 984, 1013, 1692, 1719, 1809, 2210, 2980 + 3001 keV were evaluated. The total cross-sections were evaluated for neutron energies of 1-18.8 MeV, and the cross-sections for discrete lines for neutron energies of 1-16 MeV. The evaluations were performed using cubic spline approximation curves. The curve parameters were determined by the maximum likelihood method.

The situation as regards gamma-ray production constants is currently unsatisfactory [1]. The experimental data and the evaluated data based on them which are given in the various libraries disagree with one another. Moreover, the need for reliable and accurate data has grown in many branches of science and technology, in particular for the development and design of the TOKAMAK-type fusion reactor.

One possible way of improving the situation could be to measure the differential gamma-ray production cross-sections for the most important structural materials at an incident neutron energy of E_n = 14 MeV. The results could then be used to perform a critical analysis and re-evaluation of the available data.

In this paper we present the results obtained by compiling the data in the literature, and we make a preliminary evaluation of the total gamma-ray production cross-sections and discrete gamma line production cross-sections for Al nuclei in the E_n = 1.0-18.8 MeV and E_n = 1-16 MeV energy range respectively.

Cubic spline approximation curves were used for this evaluation. The parameters for these were determined by the maximum likelihood method, taking into account systematic and random error [2].

1. Review of experimental work

Discrete gamma line production cross-sections, and total gamma-ray production cross-sections comprising the sum of discrete gamma line production cross-sections and continuous distribution gamma-ray production cross-sections are given in Refs. [3-7, 9, 11, 12, 14-27].

In Ref. [3], the production cross-sections and angular distributions for discrete gamma lines with an energy of E_γ = 0.840, 1.010, 1.720, 2.210, 2.730 and for doublet of 2.976 and 3.001 MeV lines are measured for the three neutron energy values E_n = 3.57, 4.07 and 4.57 MeV. The time-of-flight method and a double-crystal NaI(Tl) total absorption spectrometer were used for the measurements. The Al sample was a hollow cylinder 5.1 cm long with an external diameter of 2.54 cm and an internal diameter of 1.25 cm. The uncertainties of the cross-section measurements lay in the 17-20% range in the main.

In Ref. [4], measurement results are given for the production cross-sections and angular distributions for discrete gamma lines with an energy of E_γ = 1.013, 1.717, 2.213, 2.980 and 3.002 MeV for neutron energies of E_n = 3.5 MeV. The time-of-flight method and a Ge(Li) gamma detector with a volume of V = 15 cm^3 were used for the measurements. The Al sample, which was a cylinder 4.7 cm long and 3.08 cm in diameter, was positioned 57 cm from the Ge(Li) gamma detector and 9 cm from the accelerator target. The measurement results had an uncertainty level of ±4%. In addition, there was a ±8% error due to the normalization of the measurement results relative to the cross-section of the $^{56}Fe(n,n'\gamma)$ reaction.

In Ref. [5], the production cross-sections for discrete gamma lines in the $0.79 \le E_\gamma \le 4.5$ MeV range are measured at an angle of $\theta = 125°$ for neutron energies of E_n = 5.3, 5.9, 6.4 and 7.0 MeV. The time-of-flight method and a Ge(Li) gamma detector with a volume of V = 70 cm^3 positioned 165 cm from the sample were used for the measurements. The Al sample was a hollow cylinder 3 cm long with an external diameter of 4 cm and an internal diameter of 2 cm positioned 10.5 cm from the accelerator target. The uncertainty level for determination of the cross-sections lay in the 9-15% range in the majority of cases.

In Ref. [6], measurement results are given for the production cross-sections for discrete gamma lines in the $0.794 \le E_\gamma \le 3.212$ MeV range for a neutron energy of E_n = 4.21 MeV. A Van de Graaff accelerator, the time-of-flight method and an anti-Compton gamma spectrometer with a central Ge(Li) gamma detector were used for the measurements which were performed at an angle of $\theta = 55°$. The Al sample was a cylinder 2.54 cm in diameter and 5 cm long. The uncertainty level for determination of the cross-sections was 15-20%.

In Ref. [7], measurement results are given for the total gamma-ray production cross-sections in the $0.47 \le E_\gamma \le 8.0$ MeV range and the discrete gamma line production cross-sections in the $0.79 \le E_\gamma \le 6.5$ MeV range in the neutron energy intervals ΔE_n = 0.89-1.32-2.14-3.06-4.10-5.15-6.15-7.71-9.78-12.56-16.74 MeV. The measurements were carried out at an angle of $\theta = 125°$ using a Ge(Li) gamma detector with a volume of V = 80 cm^3, a linear electron accelerator, the time-of-flight method, a multichannel analyser and a computer. The scattering sample was ring-shaped. The discrete gamma line production cross-sections were

determined with an uncertainty of 10-20%. The random error in the total cross-sections lay in the 4-15% range. The systematic error lay in the 10-12% range.

In Ref. [9], the total production cross-section for gamma rays with an energy of $0.69 \le E_\gamma \le 10.0$ MeV was measured at an angle of $\theta = 90$ and 125° for individual groups of neutrons in the $E_n = 0.85$-20.0 MeV energy range. A gamma spectrometer based on an NaI crystal, the time-of-flight method and a linear electron accelerator were used for the measurements. In the EXFOR system these results are presented as a file containing 2875 points. The statistical error is, in the main, 10-25%. The systematic error is ≈ 10%. In this paper, we give measurement results for discrete gamma lines with an energy of $E_\gamma = 1.013$ and 2.210 MeV for $E_n \le 4$ MeV neutrons. The measurement methodology is described in detail in Ref. [10].

In Ref. [11], measurement results are given for the discrete gamma line production cross-sections for nonelastic interaction of neutrons with an energy of $E_n = 5.35$, 5.85, 6.40, 6.90, 7.45, 7.95, 8.50 and 9.00 MeV with Al nuclei. The measurements were carried out at angles of $\theta = 55$, 75 and 90° using a pulsed Van de Graaff accelerator, the time-of-flight method, a Ge(Li) gamma detector with a volume of $V = 30$ cm^3 and a 2048-channel pulse analyser. The sample weighed 24 g and was positioned at a distance of R = 10 cm from the neutron source and at a distance of R = 75-90 cm from the Ge(Li) gamma detector. The spectrum comprised a series of discrete gamma lines corresponding to the direct and cascade transitions from excitation levels with an energy of $E_{lev} \le 8.0$ MeV. The uncertainty level for determination of the production cross-sections for the various gamma lines lies, in the main, in the 10-50% range.

The authors of Ref. [12] measured the total gamma-ray production cross-sections in Al using a linear electron accelerator and the time-of-flight method. The sample was ring-shaped with an external diameter of 25 cm, an internal diameter of 15 cm, 1.3 cm thick, and positioned 47.7 m from the neutron source. Gamma rays in the $E_\gamma = 0.7$-10.0 MeV range were registered using an NE-213 scintillation detector positioned coaxially relative to the ring, so that the average gamma ray scattering angle was 127 degrees. The front surface of the detector was 5.48 cm from the surface of the ring. The differential cross-sections measured in the $E_n = 1$-20 MeV range were obtained with an uncertainty of 5-10% in the majority of cases. The systematic error was ≈ 10%. The measurement methodology is described in detail in Ref. [13].

In Ref. [14], measurement results are given for the yield of discrete gamma lines with an energy of $E_\gamma = 0.843$, 1.013, 1.719, 2.210 and for doublet of 2.976 and 3.001 MeV lines. The measurements were performed on an isochronous cyclotron at an angle of $\theta = 125°$ in the $E_n = 0.8$-13.0 MeV range using the time-of-flight method and a Ge(Li) gamma detector with a volume of $V = 40$ cm^3. The Al sample was positioned at a time base of 57.92 m; it was ring-shaped with an external diameter of 24 cm, an internal diameter of 12 cm, and 1 cm thick. The total uncertainty level, excluding statistical error, was around 12%.

Refs. [15-18] give measurement results for the total gamma-ray production cross-sections for nonelastic interaction of neutrons with Al at an energy of 14 MeV.

Ref. [15] gives measurement results for the gamma-ray production group cross-sections for a neutron energy of E_n = 14 MeV. The measurements were performed at an angle of $\theta = 85°$ using Compton and pair spectrometers in ring geometry in the E_γ = 0.5-10 MeV range. The uncertainty level of the results is not indicated.

In Ref. [16], the total gamma-ray production cross-sections for nonelastic interaction of neutrons at an energy of E_n = 14.2 MeV with nuclei of Al and other elements were measured at angles of θ = 90, 110 and 130° using an anti-Compton gamma spectrometer based on a large NaI(Tl) crystal, and the time-of-flight method. The samples used were either disks with a diameter of 44 mm and 6 mm high, or hollow cylinders with an external diameter of 25 mm, a wall thickness of 3 mm, and 32 mm long. The uncertainty level for the differential cross-sections in the $0.5 \le E_\gamma \le 4.0$ MeV range is 10-12%, and for $E_\gamma \ge 4.0$ MeV it is 15-20%.

In Ref. [17], the gamma-ray production group cross-sections for nonelastic interaction of 14 MeV neutrons with Al nuclei in the $E\gamma$ = 0.5-10.0 MeV range were measured using the time-of-flight method, a gamma detector based on a large 200 × 100 mm NaI(Tl) crystal and spherical samples (4π geometry). The uncertainty level of the measured cross-sections is in the 13-20% range.

In Ref. [18], the gamma-ray production cross-sections for nonelastic interaction of 14 MeV neutrons with Al nuclei were measured at an angle of θ = 125° using the time-of-flight method and a gamma detector based on a large 200 × 100 mm NaI(Tl) crystal. 14 MeV neutrons were obtained from the $T(d,n)^4He$ reaction in a titanium-tritium target irradiated with 120 keV deuterons. The Al sample was 150 mm in diameter and 12 mm thick, and was positioned 185 mm from the target and 8 m from the front surface of the gamma detector. The uncertainty levels of the measured differential cross-sections lay mainly in the 8-15% range, P = 0.68.

In Ref. [19], measurement results are given for the discrete gamma line production cross-sections and the total gamma-ray production cross-sections for nuclei of Al, Fe etc. The measurements were performed on an anti-Compton spectrometer with a central NaI(Tl) crystal measuring 5.8 × 15.2 cm using the time-of-flight method and a Van de Graaff accelerator. The samples were hollow cylinders 3.8 cm long with an external diameter of 2 cm and an internal diameter of 1.6 cm and were positioned 8.7 cm from the centre of the accelerator's gas target. The measurements were performed at angles of θ = 39, 55, 72 and 90° for the three neutron energy values E_n = 4.0, 6.0 and 7.5 MeV. The uncertainty level for the majority of the data was ≈ 10%.

In Ref. [20], measurement results are given for the discrete gamma line production cross-sections for nonelastic interaction of 2.5 MeV neutrons with nuclei of Al, Fe, Cu and Pb. The measurements were performed on spherical samples (4π geometry) using a Ge(Li) gamma detector. The production cross-sections for individual gamma lines were determined relative to the E_γ = 0.847 MeV gamma line yield from the (n, n'γ) reaction in Fe. The uncertainty level for determination of the cross-sections was ≈ 16%.

In Ref. [21], measurement results are given for the discrete gamma line production cross-sections for nonelastic scattering of 3 MeV neutrons on nuclei of Na, Si, Al, Cr, Zr, Nb,

Mo, Cd, W, Pb and Bi. Electrostatic and cascade accelerators were used as the neutron source. Disk and ring scatterer geometry was used in the experiments. The gamma spectra were measured using a gamma detector based on an NaI(Tl) crystal. The uncertainty level for determination of the discrete gamma line production cross-sections for Al was ≈ 13%.

In Refs. [22-26], measurement results are given for the production cross-sections for discrete gamma lines only for nonelastic interaction of neutrons with an energy of E_n = 14-15 MeV with nuclei of Al, Fe, Cu and Pb. In Ref. [22], measurements were performed at E_n = 14.7 MeV at an angle of $\theta = 90°$ using a spectrometer based on an NaI(Tl) crystal measuring 4×4 inches. The samples were made of Al, Fe and Pb and were cylinders 1.5 inches in diameter and 3 inches long. The uncertainty level for determination of the production cross-sections for strong gamma lines was ≈ 10%, and for weak gamma lines it was 20-35%.

In Ref. [23], the discrete gamma line production cross-sections for the $^{27}Al(n, x\gamma)$ reaction were measured at an average angle of $\theta = 80 \pm 30°$ using a Ge(Li) gamma detector S = 70 mm^2 in area and 7 mm thick in the E_γ = 0.472-6.481 MeV range. Neutrons with an energy of 15.1 ± 0.4 MeV were obtained using a Van de Graaff accelerator via the $T(d, n)^4He$ reaction. The Al sample, which was a disk 14 cm in diameter and 4.5 cm thick, was positioned 10 cm from the neutron source and 50 cm from the detector. The discrete gamma line production cross-sections were determined relative to the production cross-section for the E_γ = 4.44 MeV gamma line from the $^{12}C(n, n'\gamma)^{12}C$ reaction. The uncertainty level for determination of the cross-sections was in the 16-30% range.

In Ref. [24], measurement results are given for discrete gamma lines for nonelastic interaction of neutrons with an energy of E_n = 14 MeV with nuclei of Al, Fe and Pb. The measurements were performed with a pulsed 14 MeV neutron source on spherical samples (4π geometry) using the time-of-flight method and a gamma detector based on a 200×100 mm NaI(Tl) crystal. The uncertainty level for determination of the cross-section for strong lines was ≈ 10%, and for weak lines it was 20-30%.

Very recently, discrete gamma line production cross-section measurement results were published in Refs. [25] and [26] for the Al(n, xγ) reaction.

In Ref. [25], the prompt and delayed discrete gamma line production cross-sections were measured with a pulsed E_n = 14.9 ± 0.5 MeV neutron source using the time-of-flight method and a Ge(Li) gamma detector with a volume of V = 110.7 cm^3 placed 139.4 cm from the centre of the target. The cylindrical sample weighed 60.48 g and was positioned 13.4 cm from the neutron source. The measurements were performed for angles of θ = 55, 90 and 140°. The uncertainty level for determination of the cross-sections was in the 3-5% range in the main.

In Ref. [26], measurement results are given for the discrete gamma line production cross-sections for nonelastic interaction of neutrons with Al nuclei at an energy of E_n = 14.58 ± 0.03 MeV. The time-of-flight method was used in the measurements, taking the point when the pulse from associated α-radiation is registered as the zero time point. The gamma radiation was registered using a high-purity Ge gamma detector. The detector, which

had a volume of V = 244 cm^3, was positioned 21 cm from the Al sample, which was an 8 × 8 cm plate weighing 86.2 g. The gamma-ray production cross-section values for the Al(n, xγ) reaction were determined relative to the E_γ = 0.8468 MeV gamma line yield from the (n, n'γ) reaction in ^{56}Fe. The uncertainty level for determination of the cross-sections lay in the 7-11% range.

In Ref. [27], measurement results are given for the integrated (with respect to E_γ) gamma-ray production cross-sections ($E_\gamma \geq 0.7$ MeV) for nonelastic interaction of neutrons with an energy of E_n = 7.8, 10.0, 11.5 and 13.0 MeV with nuclei of Al, Si, Fe, Ni, Cu, Pb and Bi. The measurements were carried out at an angle of $\theta = 90°$ for all the above-mentioned energies, and at an angle of $\theta = 125°$ for E_n = 7.8 and 11.5 MeV. The measurements were performed using an anti-Compton gamma spectrometer with a central NaI(Tl) crystal 7.6 cm in diameter and 15.2 cm long, and the time-of-flight method. The samples, which were cylindrical, 2 or 3 cm in diameter and 3 cm high, were positioned 10 cm from the neutron source and 80 cm from the gamma detector. The integrated cross-sections were determined with an uncertainty of $\approx$ 13-15%.

In concluding this section we would note that, in the main, corrections for attenuation and multiple scattering of neutrons and gamma rays in the sample were introduced in all works when determining the gamma-ray production cross-sections. The total cross-sections with respect to angle given in this paper were determined by multiplying the differential cross-sections by 4π.

2. Evaluation of the total gamma-ray production cross-sections

By total cross-section we usually understand the sum of the continuous distribution gamma-ray and discrete gamma line production cross-sections. In nonelastic interaction of fast neutrons with Al nuclei, gamma rays are produced by the (n, n'γ), (n, pγ), (n, αγ), (n, dγ), (n, npγ), (n, nαγ) and (n, 2nγ) reactions with values of Q = 0, -1.83, -3.13, -6.05, -8.27, -10.09 and -13.06 MeV respectively. At a neutron energy of $E_n \leq$ (3-4) MeV, the gamma-ray spectrum is mainly discrete in nature. At higher neutron energy values, the proportion of continuous distribution gamma radiation becomes significant.

The difficulty of obtaining reliable evaluated data for Al is due generally to the paucity of the experimental data required for the evaluation, and in particular to the lack of sufficient correlated data. At present, the results from only three sources, Refs. [7], [9] and [12], can be used to obtain evaluated cross-sections over a wide neutron energy range: E_n = 1-20 MeV. The results of our latest measurements (see Table 1) may be used to evaluate cross-sections in the E_n = 14 MeV region. The measurement methodology is described in Ref. [1].

At the first stage of the evaluation, it is useful to compare the results given in these papers with others, e.g. Refs. [3], [15-20] and [24, 27], as regards the cross-section value integrated with respect to Eγ for a fixed neutron energy value. This comparison is a useful guide to the level of correlation of the experimental data. Fig. 1, which plots the results from the above-mentioned sources, reveals a certain polarization in the data. Some data are closer to the data from Ref. [7], and others to the data from Refs. [9, 12]; but they mostly lie within the boundaries drawn by the experimental results from these two sources. On the basis of the

above, it should be possible to make an evaluation for the whole set of data cited, giving pride of place however to the data from Refs. [7] and [9, 12].

Here, the following should be noted:

(a) The source data taken from Refs. [7] and [9, 12] are presented in the EXFOR experimental data library as an array consisting of 188, 2875 and 1009 points respectively. The neutron energy intervals in which the gamma spectrum measurements were performed, and the gamma-ray energy scale are not the same in these sources;

(b) The complex instrumental spectra were processed using the continuous distribution processing method, which means that information on discrete gamma lines whose energy coincides with the boundaries of the intervals we selected is split up between neighbouring energy groups. The discrete gamma lines for Al to which this applies are those with energies of E_γ = 1.013, 2.210 and 3.001 MeV. In the evaluation, the data from the literature were used in the form in which they are given in the original sources;

(c) The type of the uncertainties given in EXFOR 10219009 [7] is not indicated for the total gamma-ray production cross-sections, but it is so small - 4-15%, in the main - that we may assume it is statistical. The systematic error, which is 10-12%, is given in the other paper by the same authors [8].

In view of the above, the results from Refs. [7, 9, 12] were reduced to a common energy scale with respect to gamma-ray energy to facilitate the evaluation. The data in the literature obtained with monoenergetic neutron sources were also reduced to a common energy scale with respect to gamma-ray energy and divided into the energy groups ΔE_γ = 0.50-0.75-1.0-1.5-2.0-2.5-3.0-4.0-5.0-6.0-7.0-8.0-10.0 MeV, like the data in Refs. [7, 9, 12].

Cubic spline approximation curves were used to evaluate the cross-sections. The parameters for these were determined by the maximum likelihood method, taking into account systematic and random error. The approximation curves in the $E_n \leq 14.0$ MeV neutron energy range were determined using the set of total gamma-ray production cross-sections and individual discrete gamma line production cross-sections. At a neutron energy of $E_n > 14.0$ MeV, the approximation curves for some gamma-ray groups were determined using the data from Refs. [7] and [9] normalized relative to the evaluated cross-section value at the E_n = 14.0 MeV point. In a series of cases, the uncertainty level of data which were noticeably divergent had to be increased in the evaluation in order to decrease their weighting, i.e. reduce their effect on the cross-section value to be evaluated.

The results of the evaluation are shown in Figs 2-13. The evaluated cross-section may be determined using the following formula:

$$\sigma_{n,x\gamma}(E) = A^i_0 + A^i_1(E - E_i) + A^i_2(E - E_i)^2 + A^i_3(E - E_i)^3 , \qquad (1)$$

where i is the spline node number, E is the current neutron energy value and E_i is the node energy. $E_i<E<E_{i+1,}$ A^i_0, A^i_1, A^i_2, A^i_3 are the spline coefficients.

The spline coefficient values are given in Table 2.

All the above transformations and evaluations were performed on a personal computer using specially developed software.

3. Evaluation of the discrete gamma line production cross-sections

In nonelastic interaction of fast neutrons with Al nuclei, discrete gamma lines are produced by the (n, n'γ), (n, pγ), (n, dγ) and (n, npγ) reactions in the main. The thresholds of the reactions involving emission of charged particles are 1.90, 6.27 and 8.58 MeV respectively.

The discrete gamma line production cross-sections were evaluated using the experimental results from Refs. [3-7, 11, 14, 20-23, 25, 26]. In the majority of the above sources, the cross-sections were measured using a Ge(Li) gamma detector. We find the data from Ref. [7] to be the most informative. In this paper, we give measurement results for the production cross-sections for nine gamma lines from the (n, n'γ) reaction and 22 gamma lines from the (n, pγ) reaction. The measurements were performed for 20 neutron groups in the E_n = 0.885-16.738 MeV neutron energy range.

Cubic spline approximation curves were used to evaluate the discrete gamma line production cross-sections. The parameters for these were determined by the maximum likelihood method, taking into account systematic and statistical error. The procedure used to evaluate the discrete gamma line production cross-sections is similar to the procedure used to evaluate the total cross-sections. The results of the evaluation are shown in Figs 14-24.

The evaluated discrete gamma line production cross-section may be determined using equation (1) with the spline coefficients given in Table 3.

Table 1

Total gamma-ray production cross-sections for the (n,xγ) reaction in Al, $\sigma_\gamma \pm \Delta\sigma_\gamma$, mb, P = 0.68

Energy interval Eγ, MeV	Data from this paper E_n = 14.0 MeV at $\theta=125^o$ multiplied by 4π	[15] E_n = 14 MeV at $\theta=85^o$ multiplied by 4π	[16] E_n = 14.2 MeV at $\theta=130^o$ multiplied by 4π	[17] E_n = 14 MeV 4π-measurement
0.50 - 0.75	52 ± 8	57	43 ± 6	59 ± 12
0.75 - 1.00	142 ± 14	171	141 ± 14	177 ± 35
1.00 - 1.50	199 ± 21	132	143 ± 15	292 ± 48
1.50 - 2.00	294 ± 30	235	276 ± 28	285 ± 40
2.00 - 2.50	293 ± 30	206	226 ± 23	281 ± 37
2.50 - 3.00	183 ± 20	122	136 ± 16	232 ± 31
3.00 - 4.00	200 ± 25	127	147 ± 17	122 ± 25
4.00 - 5.00	128 ± 19	88	105 ± 13	124 ± 25
5.00 - 6.00	90 ± 15	54	76 ± 11	97 ± 19
6.00 - 7.00	64 ± 13	40	70 ± 11	87 ± 18
7.00 - 8.00	40 ± 9	28	49 ± 9	72 ± 16
8.00 - 10.0	34 ± 12	19	17 ± 4	78 ± 23
0.50 - 10.0	1720	1279	1429	1906

Table 2

Coefficients of the spline curves describing the evaluated values of the gamma-ray production cross-sections in the ΔE_γ energy groups relative to neutron energy for nonelastic interaction of neutrons with aluminium nuclei

ΔE_γ,MeV	Node number	Energy of node, MeV	A_0, mb	A_1, mb/MeV	A_2, mb/MeV^2	A_3, mb/MeV^3	$\Delta\sigma_{n,x\gamma}$, mb
0.75-1.0	1	1.105	70.54084	148.098	592.5531	-980.4001	9.275974
	2	1.8108	125.5453	56.51405	-10.02066	0.5357746	24.12311
	3	7.1043	223.3833	-4.535681	-1.512296	0.05272213	13.64606
	4	14.30015	132.0826	-18.1103	-0.3741546	0.6546707	6.05035
1.0-1.5	1	1.105	37.36366	72.30383	-7.83413	0.2580128	4.878466
	2	8.794489	247.4345	-2.409546	-1.882169	-0.03296928	12.11585
	3	14.30166	171.5738	-26.14016	-2.426871	1.893871	8.5458
1.5-2.0	1	1.73	0.7037287	-1.791641	-15.07842	27.66624	0.7746546
	2	2.906109	22.74791	77.5471	82.5371	-86.11962	1.312125
	3	4.227984	70.55925	45.83413	-12.55672	1.145484	5.592879
	4	10.07462	138.2386	16.47369	7.534958	-0.8188055	8.063758
2.0-2.5	1	1.73	1.118066	-107.949	309.1931	-79.1271	0.5087464
	2	2.9214	177.574	291.8493	-547.3726	250.4432	9.974748
	3	4.1128	171.8519	54.03267	9.025676	-3.898033	9.339524
	4	7.3466	309.1473	-9.883467	9.339634	-1.51022	13.49546
	5	10.7506	324.1569	1.203017	-6.082735	0.2490398	24.44844
	6	14.1546	267.5928	-31.55121	-3.539541	1.233235	11.79085
2.5-3.0	1	2.6	2.250825	-20.24043	168.7128	-68.43934	0.4892585
	2	4.106571	120.6623	22.09314	-2.600705	0.06494859	4.456381
	3	14.30126	144.4157	-10.68296	-0.6143129	0.4781565	5.084888
3.0-4.0	1	3.25	19.69589	94.04345	1.934419	-33.30333	1.723385
	2	4.18	82.04161	11.22932	33.4998	-7.846424	6.57736
	3	7.125	205.2427	4.386439	1.069673	-0.259925	9.055371
	4	14.255	196.6826	-20.00136	-4.490122	1.069554	8.179253
4.0-5.0	1	4.245	1.988	-77.82594	529.2528	-746.8517	0.857943
	2	4.680154	6.799669	119.1246	-67.29909	15.02091	2.360952
	3	6.130654	83.83639	18.69961	-1.93561	0.01538762	3.852897
	4	14.25345	116.2652	-9.699706	-1.560638	0.2525623	5.386101
5.0-6.0	1	5.26	1.351186	15.2261	34.371	-11.37637	1.102266
	2	7.158151	76.28762	22.7424	-3.997372	0.1397388	4.12155
	3	14.29995	85.72474	-12.9722	-1.003415	0.3590131	3.950489
6.0-7.0	1	6.51	2.51986	35.58362	-3.997574	0.00904778	1.588408
	2	11.0388	82.52102	-0.0680906	-3.874647	0.5253981	6.356327
	3	14.30535	59.26764	-8.563004	1.27407	-0.187601	3.390112
7.0-8.0	1	7.79	4.715164	30.38712	-4.711767	0.1451778	1.711701
	2	12.0644	59.85329	-1.935416	-2.850122	0.389581	5.308947
	3	14.30092	45.62657	-8.838051	-0.236199	0.1873357	2.560417
8.0-10.0	1	8.27	1.659587	-0.5784749	11.43226	-2.789511	1.09025
	2	10.0516	21.1415	13.59442	-3.477114	0.2056236	2.307442

Table 3

Coefficients of the spline curves describing the evaluated values of the discrete gamma line production cross-sections relative to neutron energy for nonelastic interaction of neutrons with aluminium nuclei

ΔE_γ.MeV	Node number	Energy of node. MeV	A_0. mb	A_1. mb/MeV	A_2. mb/MeV^2	A_3. mb/MeV^3	$\Delta\sigma_{n.x\gamma}$. mb
0.7910	1	31150	0.0099309	23.221	-7.0475	0.63154	0.011175
	2	7.2780	20.106	-2.6217	0.83969	-0.080668	1.0660
	3	11.567	17.944	0.12942	-0.19828	-0.019313	1.7418
	4	15.730	-	-	-	-	5.3788
0.8430	1	0.95000	2.0000	487.09	-326.57	-127.10	0.99995
	2	1.6646	136.93	-174.34	149.28	-34.815	11.813
	3	3.7109	106.95	-0.74574	-1.4037	0.074660	5.2067
	4	-	-	-	-	-	2.4135
0.9520	1	3.9000	0.0099935	1.0167	1.0046	-0.11081	0.011179
	2	9.4500	17.652	1.9275	-0.84044	0.072678	1.5222
	3	15.000	-	-	-	-	2.2971
0.9840	1	2.921	0.010048	4.7485	0.23241	-0.026792	0.011204
	2	8.4313	28.750	4.8693	-0.21049	-0.098685	1.6417
	3	14.900	-	-	-	-	1.6216
1.013	1	1.0500	0.0099458	1105.4	-4858.8	6433.3	0.0099178
	2	1.5000	99.777	287.06	-371.93	156.36	1.7800
	3	3.1445	261.36	-348.33	434.60	-153.99	2.4767
	4	4.4492	204.69	-0.68731	-1.9017	0.063166	1.5210
	5	15.730	-	-	-	-	3.6222
1.692	1	3.6610	0.0099247	7.3364	-0.65533	0.019079	0.011043
	2	14.900	-	-	-	-	2.5720
1.719	1	2.8350	0.0099835	143.32	-68.900	15.898	0.010654
	2	3.7377	84.936	57.799	-392.26	374.74	5.6907
	3	4.3824	59.577	19.318	-12.483	2.2479	3.1885
	4	6.1877	66.996	-3.7730	-0.30812	0.023430	1.0874
	5	15.730	-	-	-	-	1.8843
1.809	1	10.456	0.010006	8.3447	4.8923	1.5498	0.0081837
	2	13.093	84.454	66.478	17.153	-11.400	13.309
	3	15.730	-	-	-	-	17.867
2.210	1	2.2940	0.010048	543.91	-517.53	175.90	0.017864
	2	3.5346	214.11	-28.233	-82.738	98.031	20.274
	3	4.2669	187.57	8.3066	-0.88389	-0.042155	11.130
	4	15.730	-	-	-	-	6.1525
2.300	1	4.6760	0.0099850	38.283	-17.249	2.5577	0.011138
	2	6.9148	27.962	-0.49298	-0.070445	0.69892	1.6561
	3	8.6144	30.351	5.3239	3.4931	-2.1428	2.1329
	4	10.847	35.804	-11.119	4.1067	-0.49502	3.0032
	5	15.000	-	-	-	-	7.4994
2.9800+ 3.0010	1	2.9500	0.013282	71.372	259.84	-168.95	0.1201
	2	4.0345	167.53	38.850	-100.57	41.228	1.9100
	3	5.7215	144.79	51.525	-53.107	14.817	2.4116
	4	6.9265	155.69	-11.918	0.45755	0.011871	2.1353
	5	15.000	-	-	-	-	6.0253

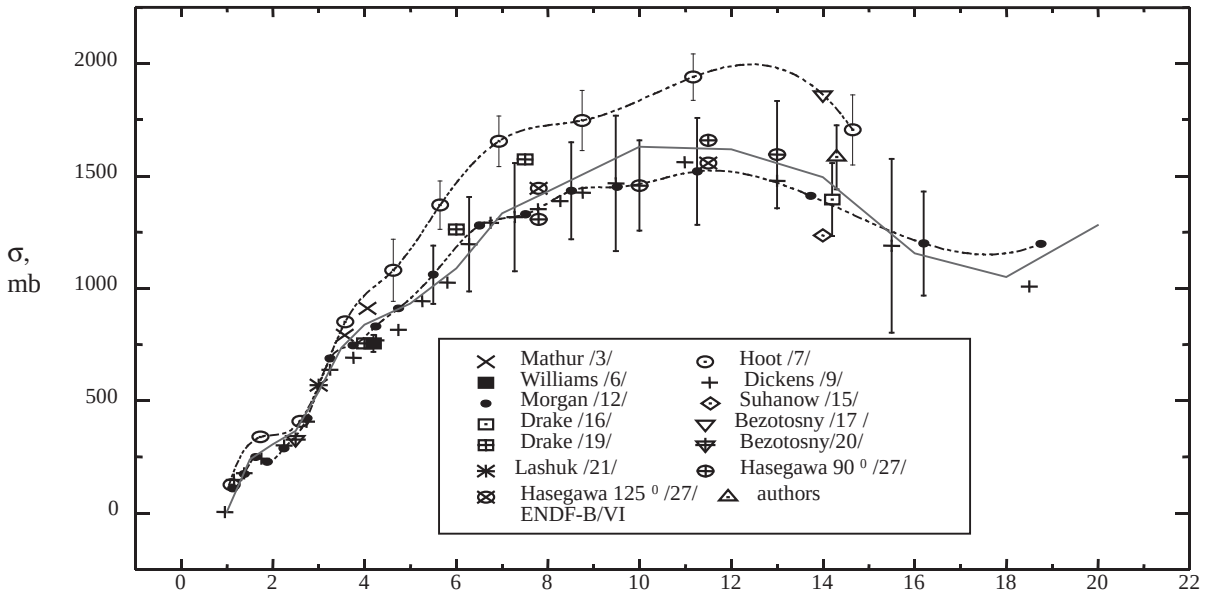

Fig. 1. Total γ-ray production cross-section for the Al(n,xγ) reaction, E_γ>0.7 MeV.

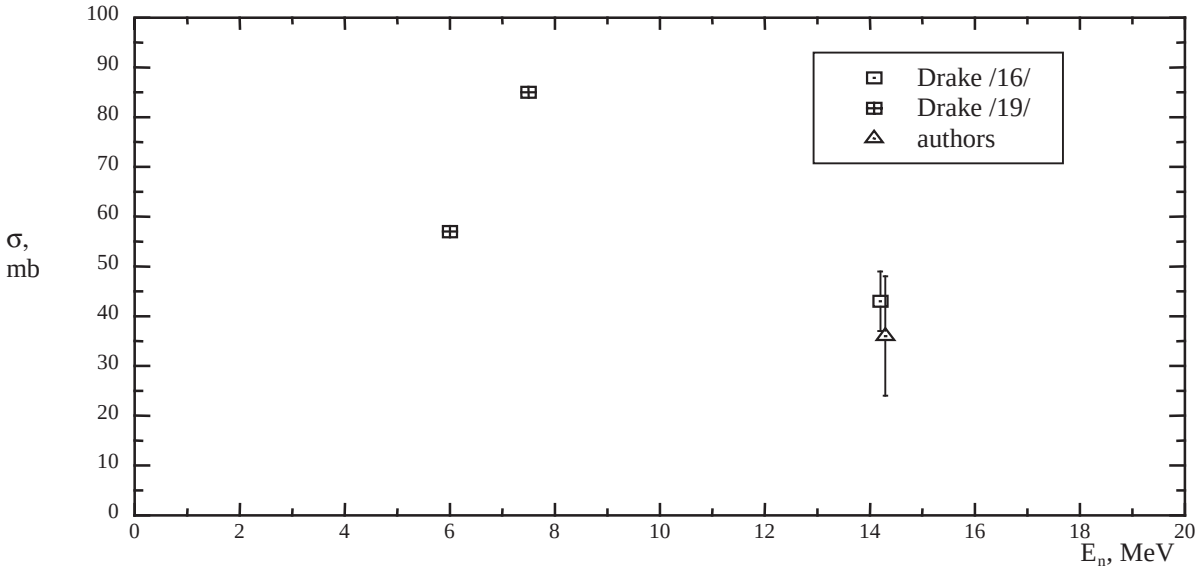

Fig. 2. Total γ-ray production cross-section for the Al(n,xγ) reaction, E_γ=0.5-0.75 MeV.

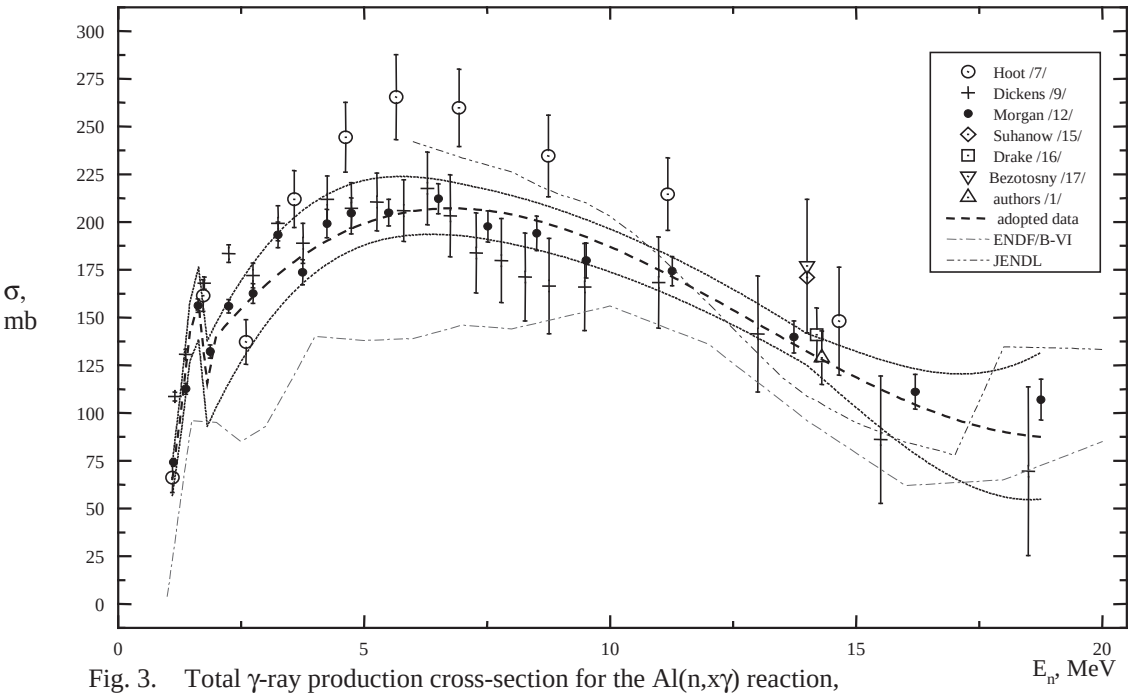

Fig. 3. Total γ-ray production cross-section for the Al(n,xγ) reaction, E_γ=0.75-1.0-MeV.

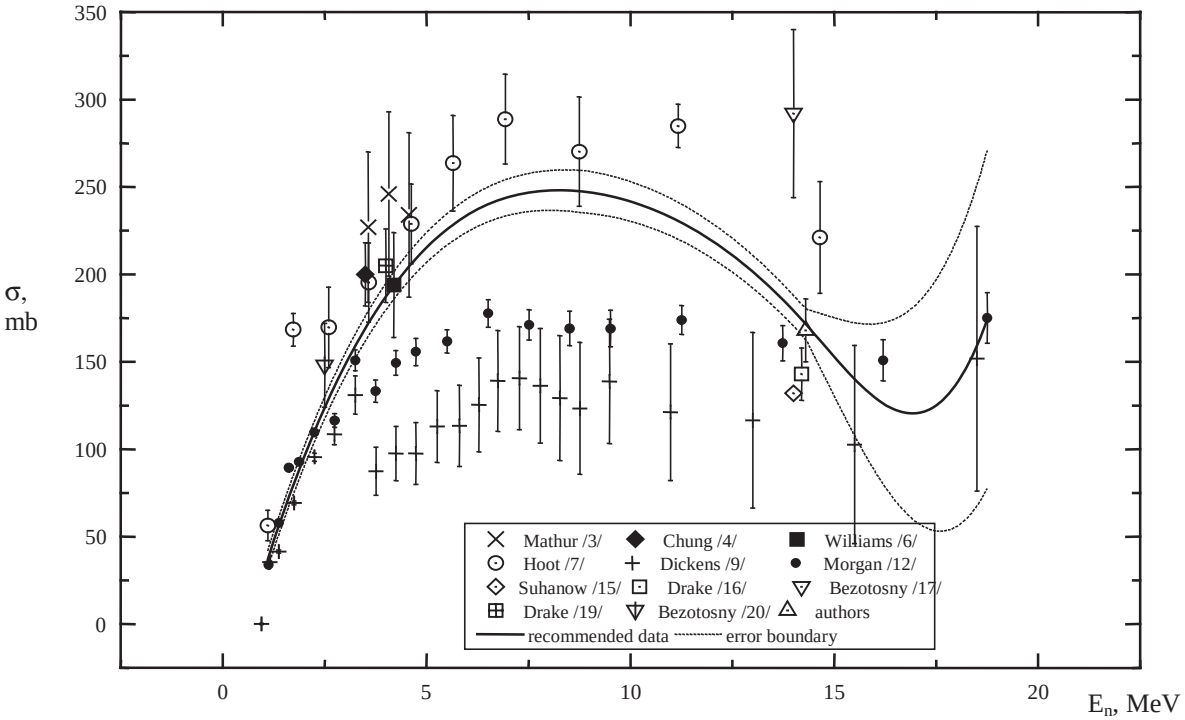

Fig. 4. Total γ-ray production cross-section for the Al(n,xγ) reaction, E_γ=1.0-1.5 MeV.

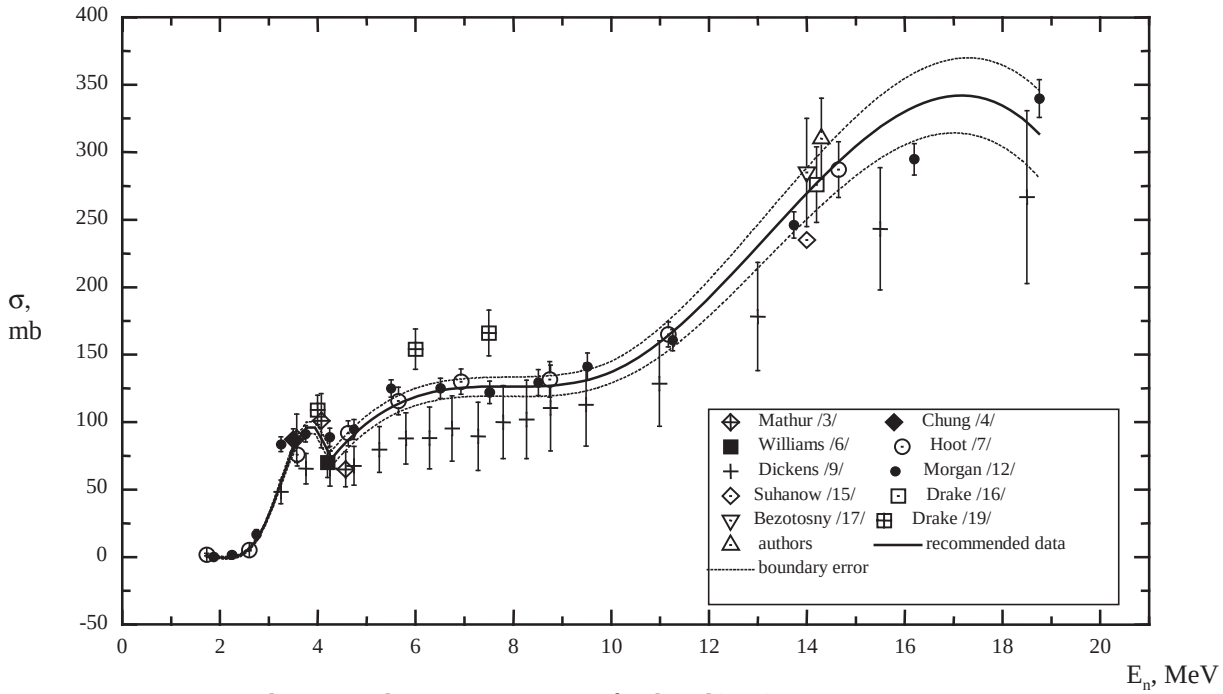

Fig. 5. Total γ-ray production cross-section for the Al(n,xγ) reaction, E_γ=1.5-2.0 MeV.

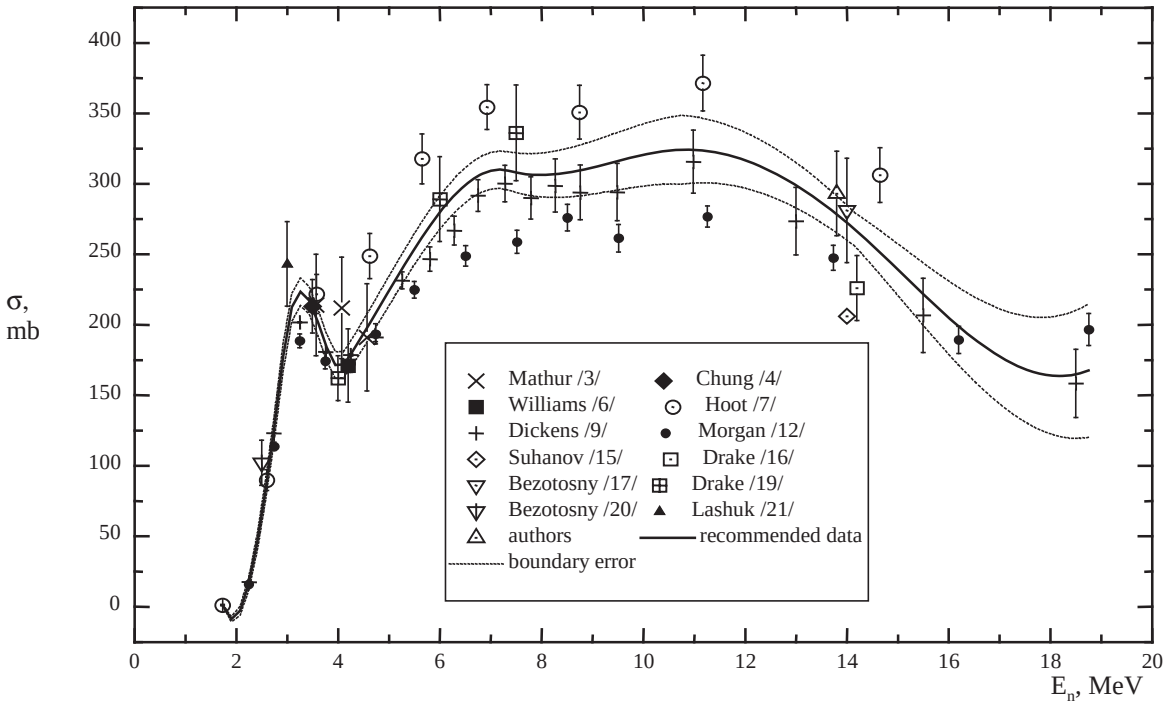

Fig. 6. Total γ-ray production cross-section for the Al(n,xγ) reaction, E_γ=2.0-2.5 MeV.

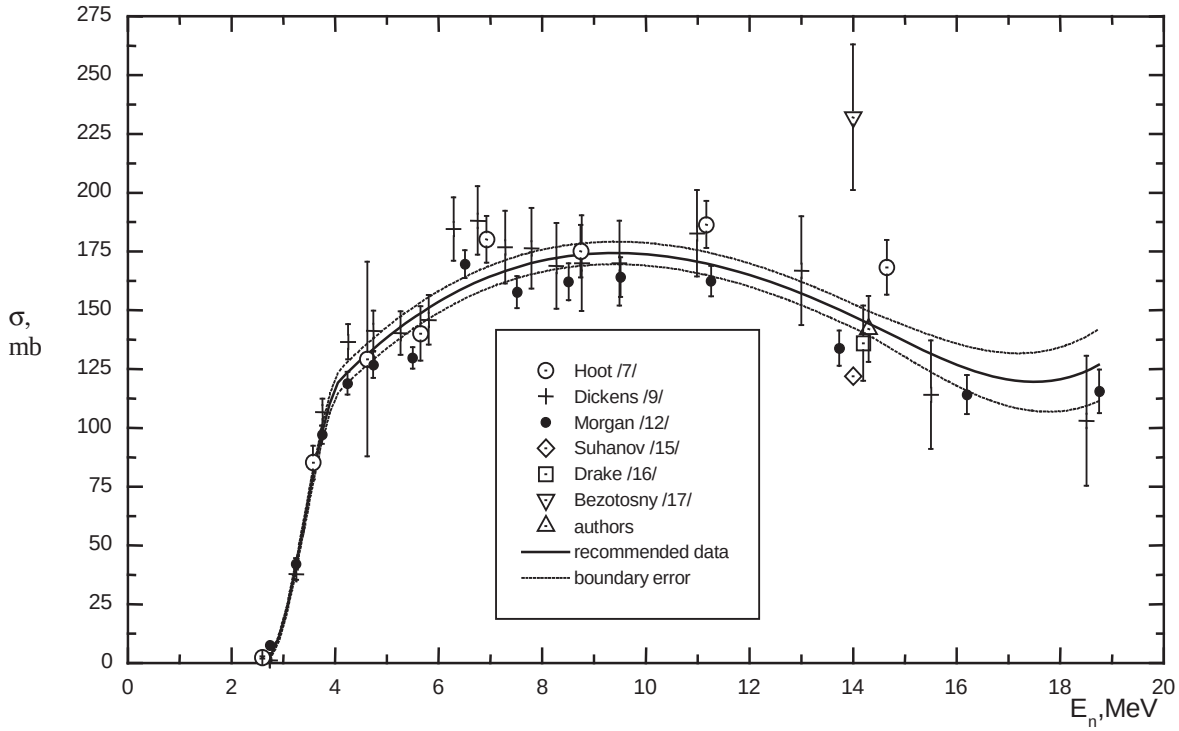

Fig. 7. Total γ-ray production cross-section for the Al(n,xγ) reaction, E_γ=2.5-3.0 MeV.

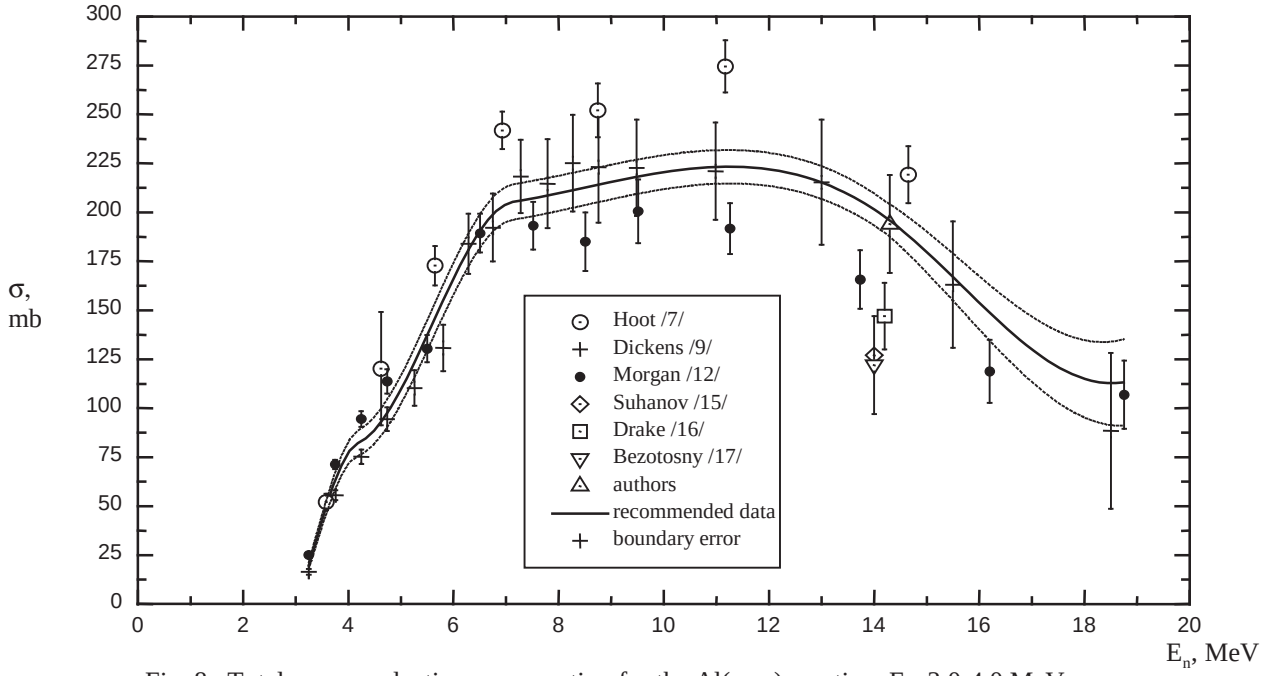

Fig. 8. Total γ-ray production cross-section for the Al(n,xγ) reaction, E_γ=3.0-4.0 MeV.

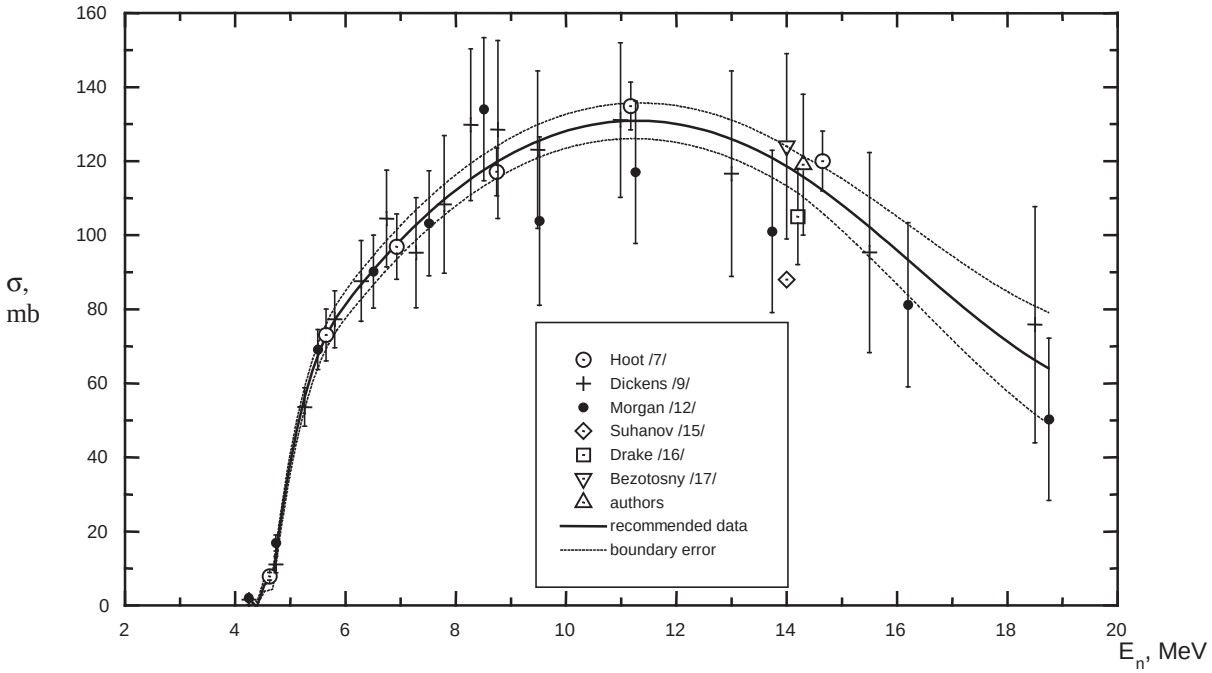

Fig. 9. Total γ-ray production cross-section for the Al(n,xγ) reaction, E_γ=4.0-5.0 MeV.

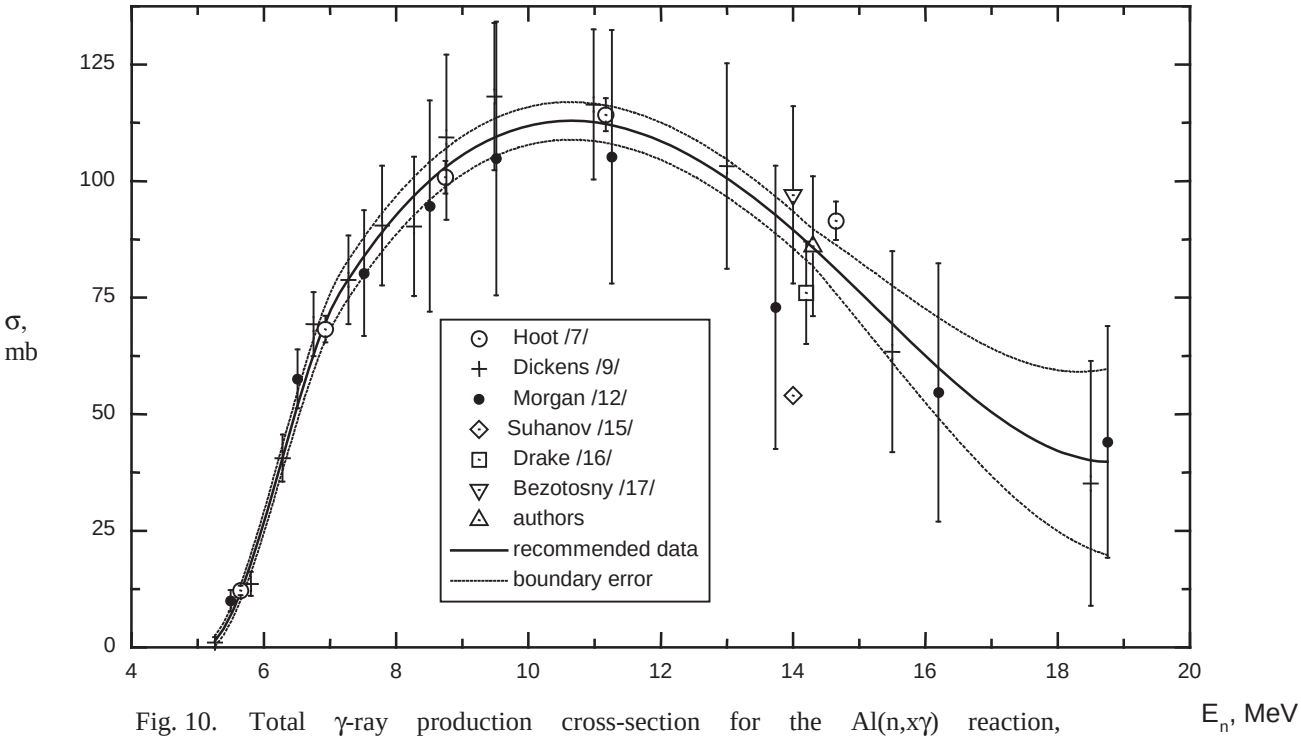

Fig. 10. Total γ-ray production cross-section for the Al(n,xγ) reaction, E_γ=5.0-6.0 MeV.

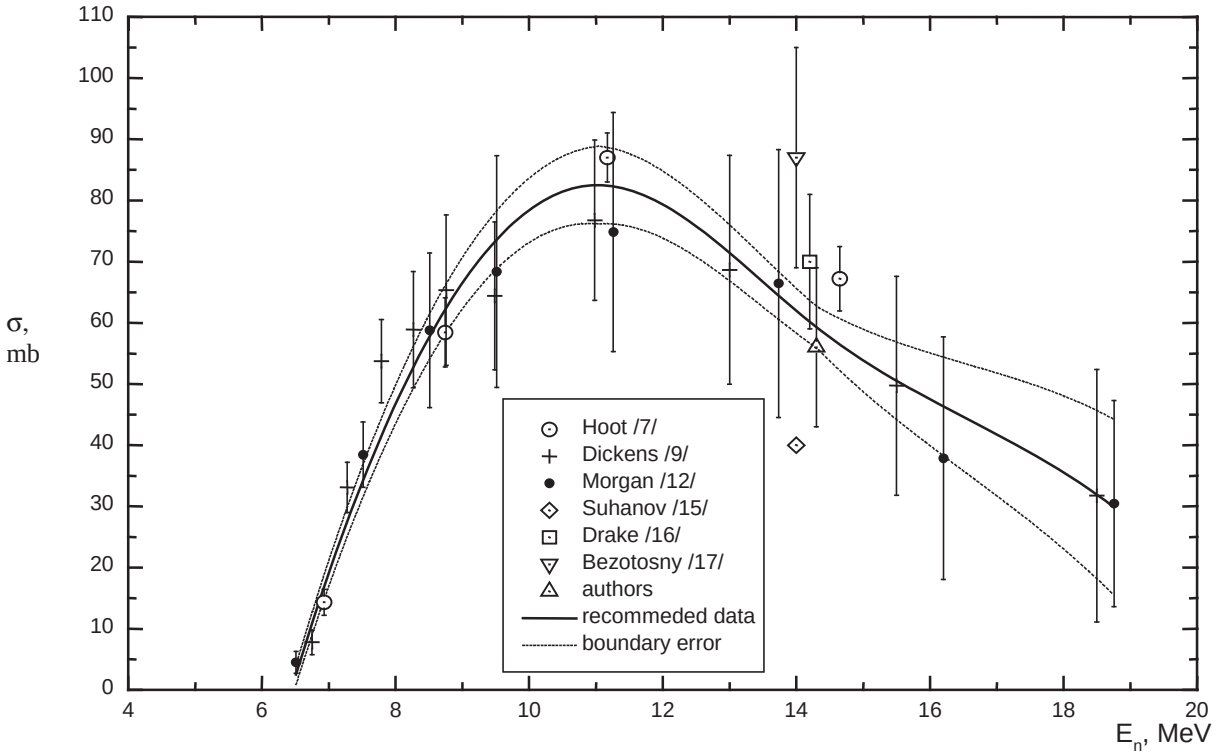

Fig. 11. Total γ-ray production cross-section for the Al(n,xγ) reaction, E_γ=6.0-7.0 MeV.

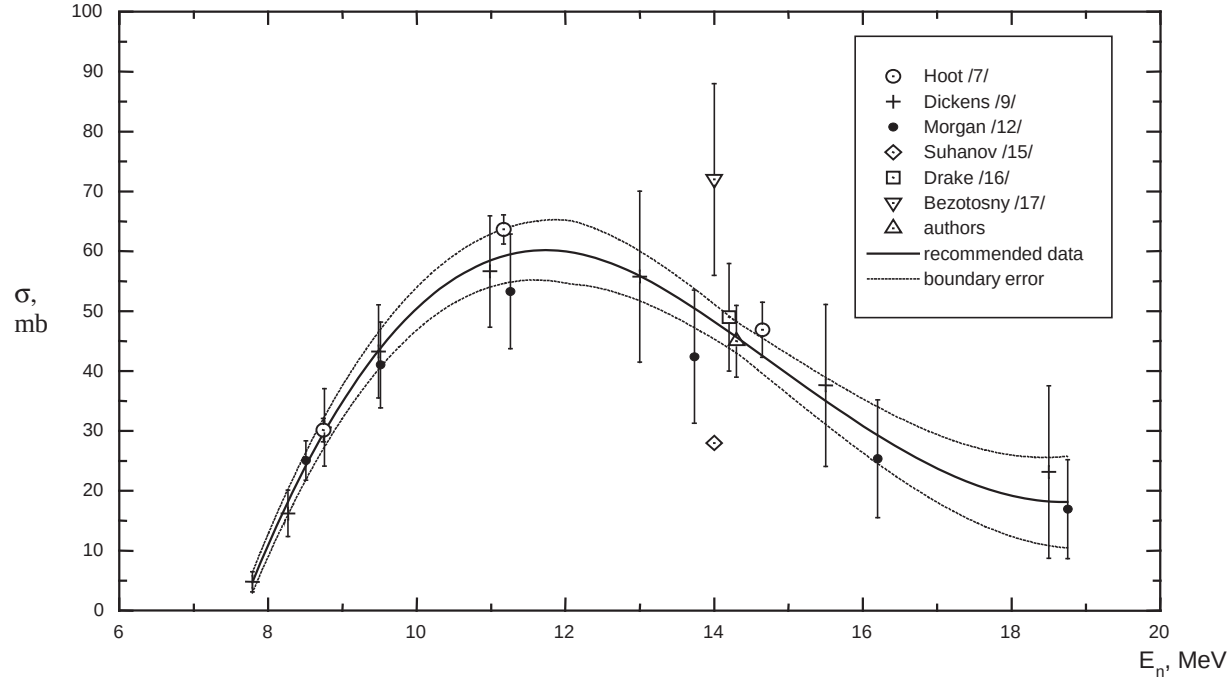

Fig. 12. Total γ-ray production cross-section for the Al(n,xγ) reaction, E_γ=7.0-8.0 MeV.

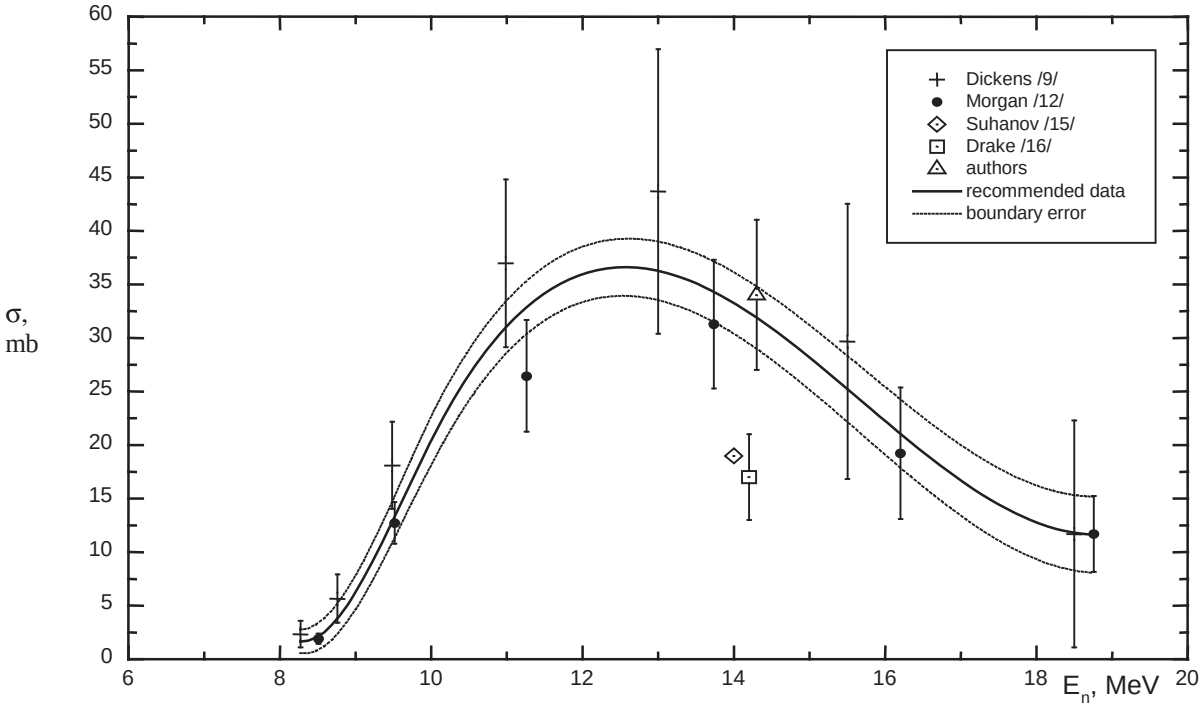

Fig. 13. Total γ-ray production cross-section for the Al(n,xγ) reaction, E_γ=8.0-10.0 MeV.

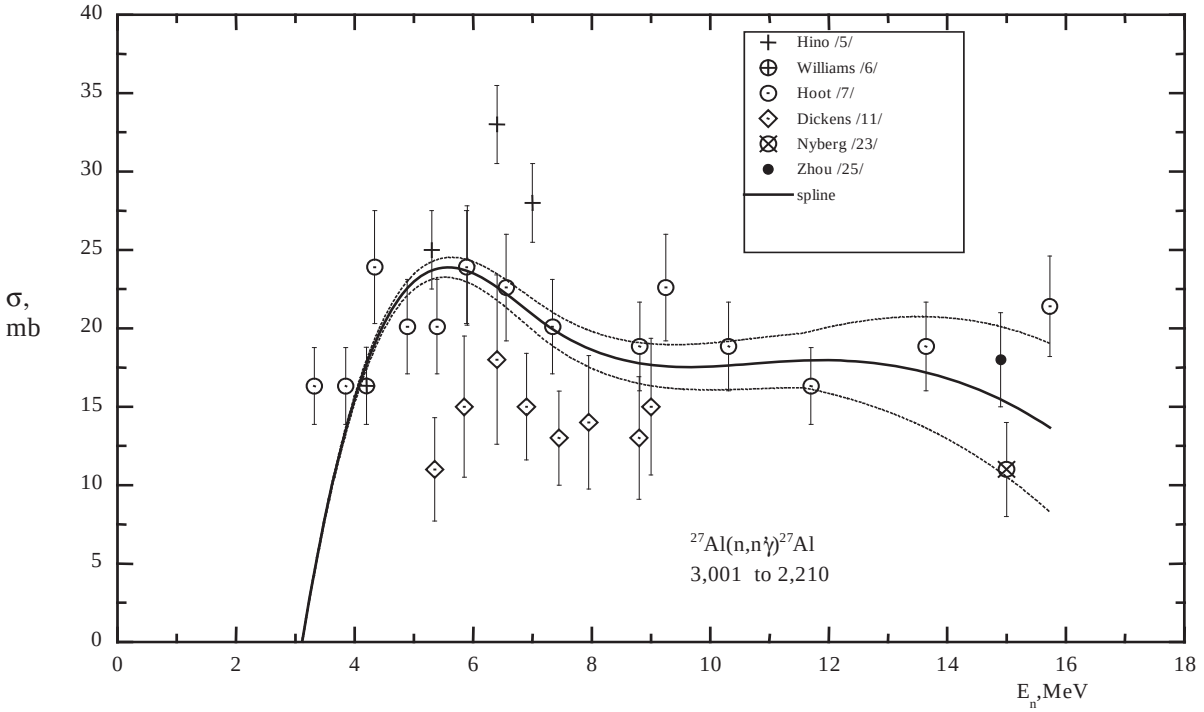

Fig. 14. Total γ-ray production cross-section for E_γ=0.791 MeV.

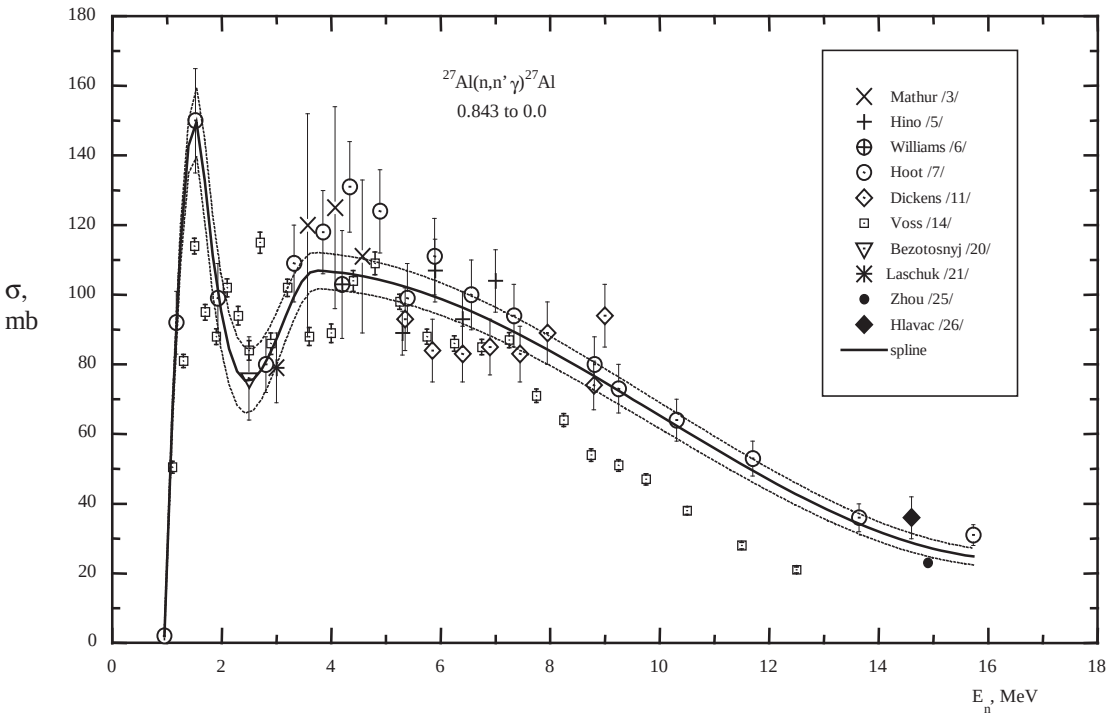

Fig. 15. Total γ-ray production cross-section for E_γ=0.843 MeV.

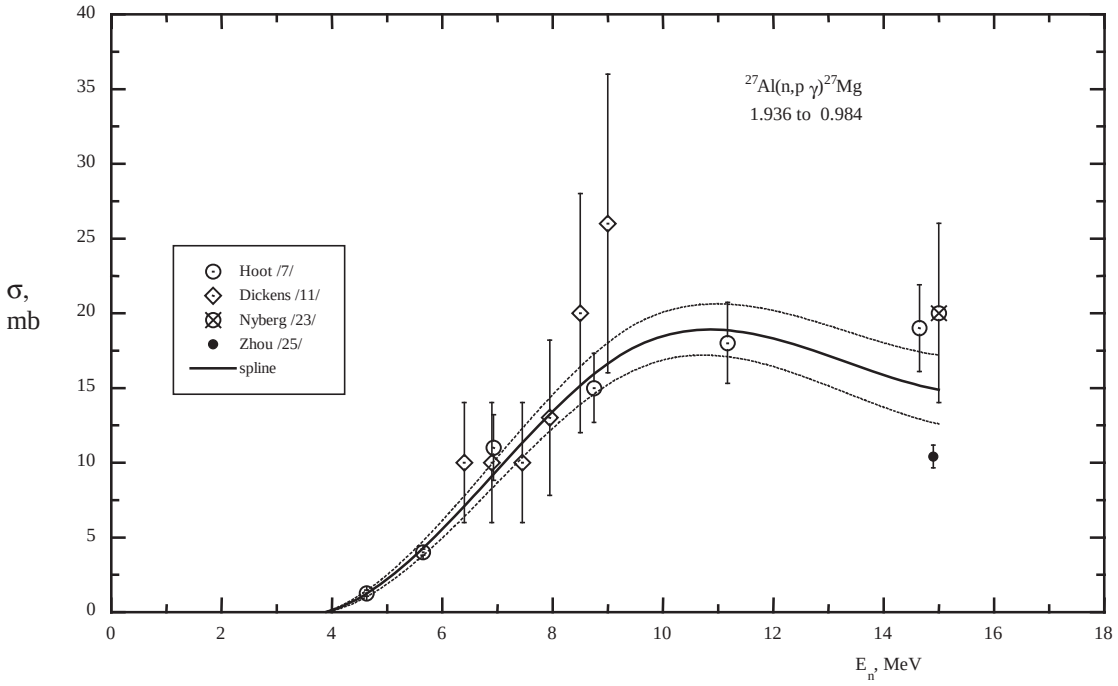

Fig. 16. Total γ-ray production cross-section for E_γ=0.952 MeV.

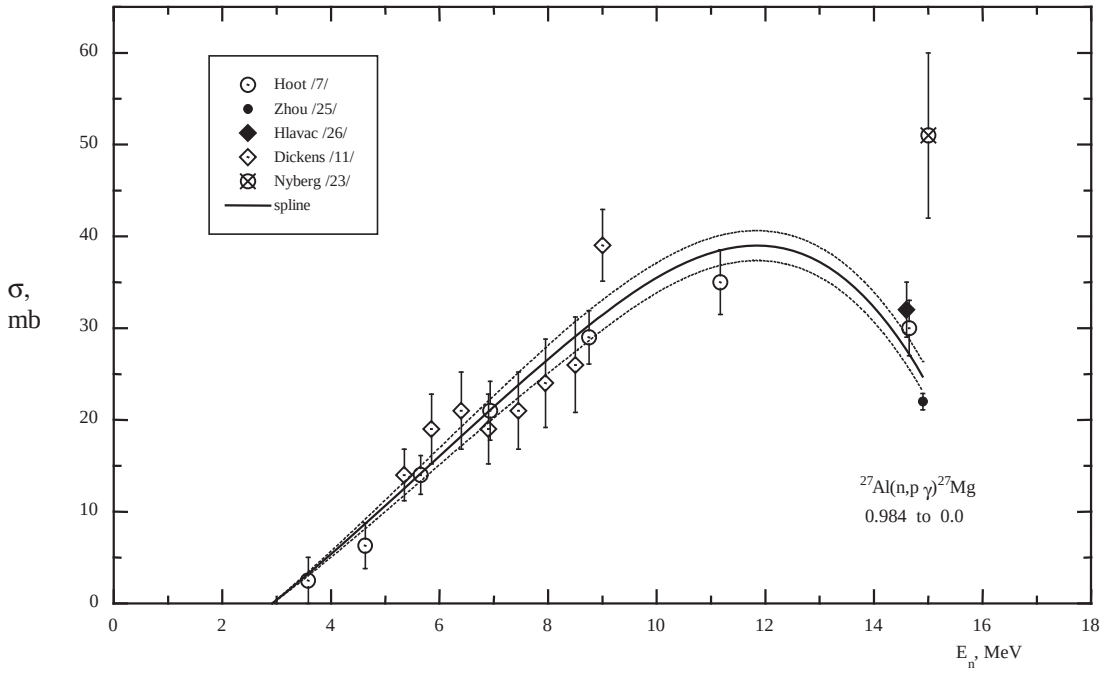

Fig. 17. Total γ-ray production cross-section for E_γ= 0.984 MeV.

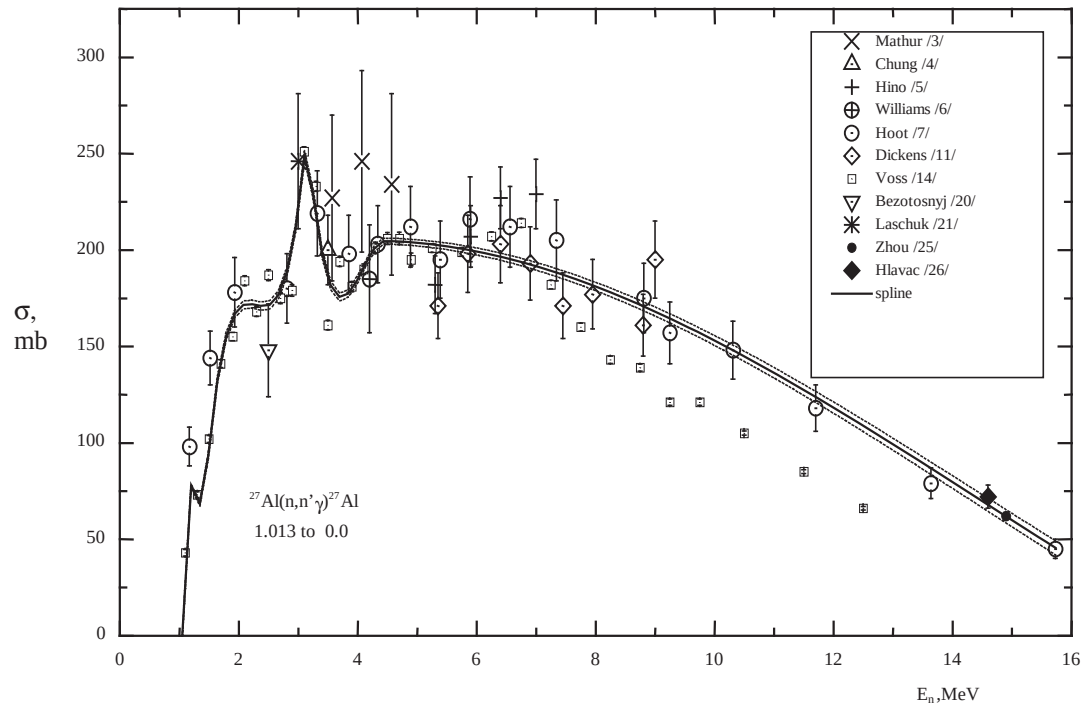

Fig. 18. Total γ-ray production cross-section for E_γ=1.013 MeV.

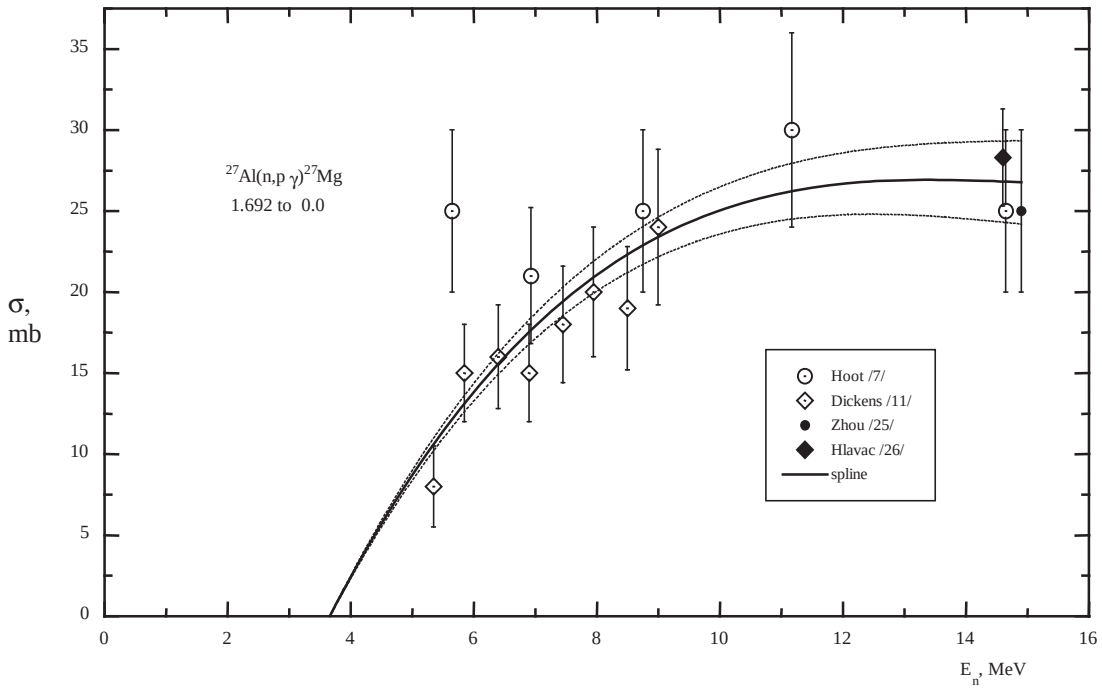

Fig. 19. Total γ-ray production cross-section for E_γ=1.692 MeV.

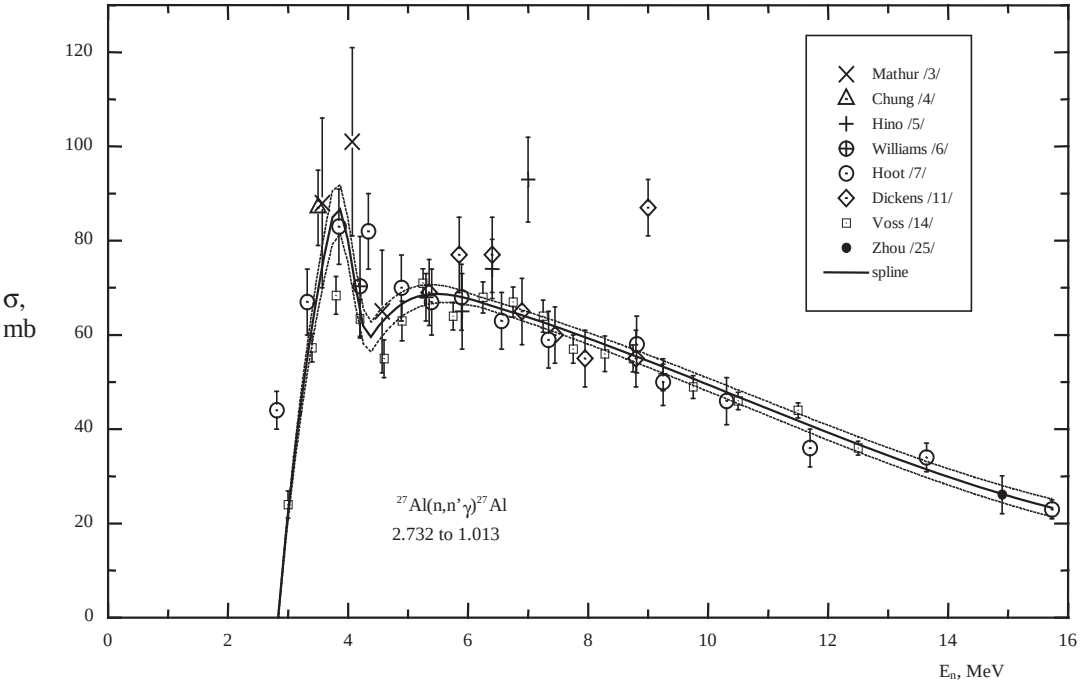

Fig. 20. Total γ-ray production cross-section for E_γ=1.719 MeV.

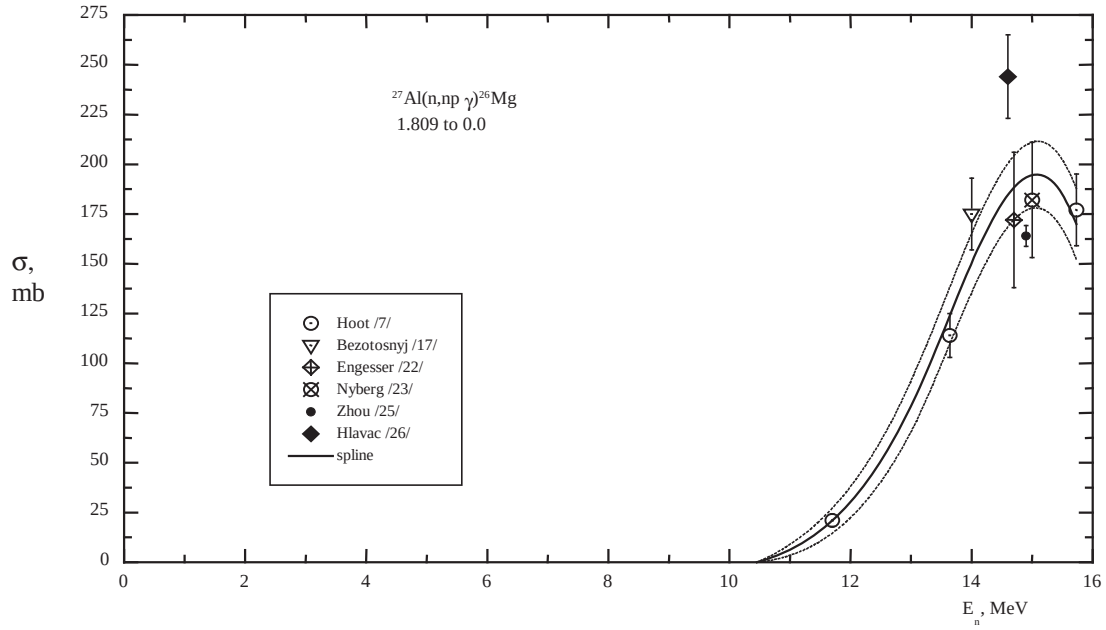

Fig. 21. Total γ-ray production cross-section for E_γ=1.809 MeV.

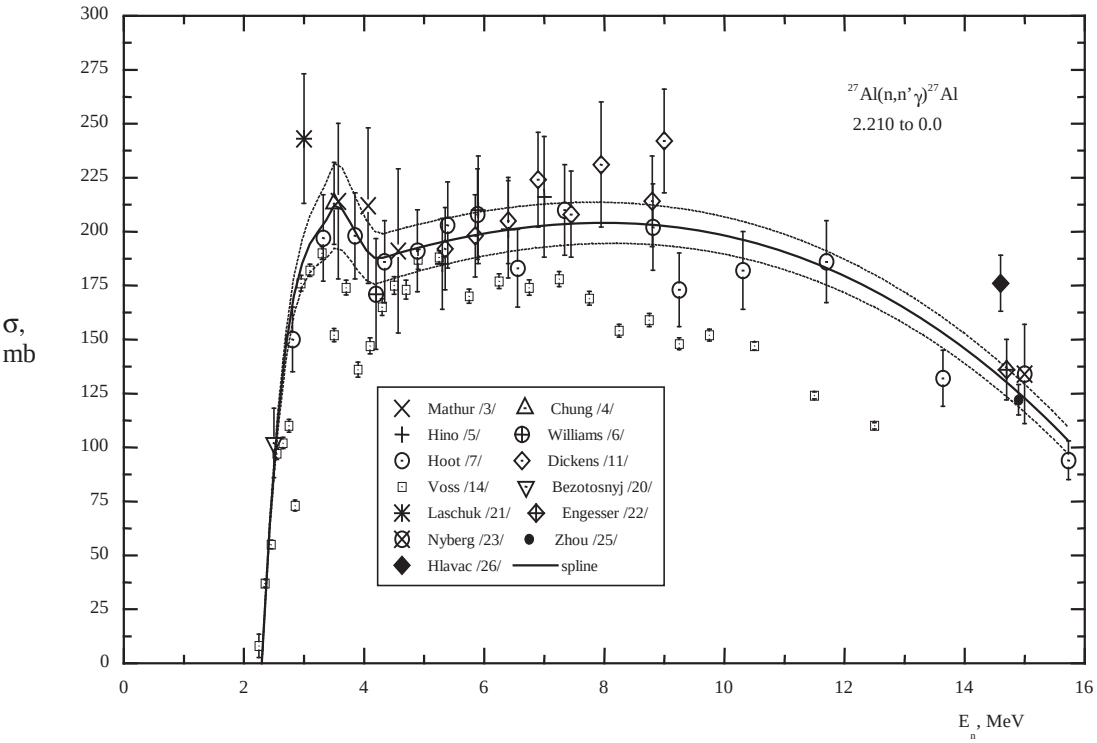

Fig. 22. Total γ-ray production cross-section for E_γ=2.210 MeV.

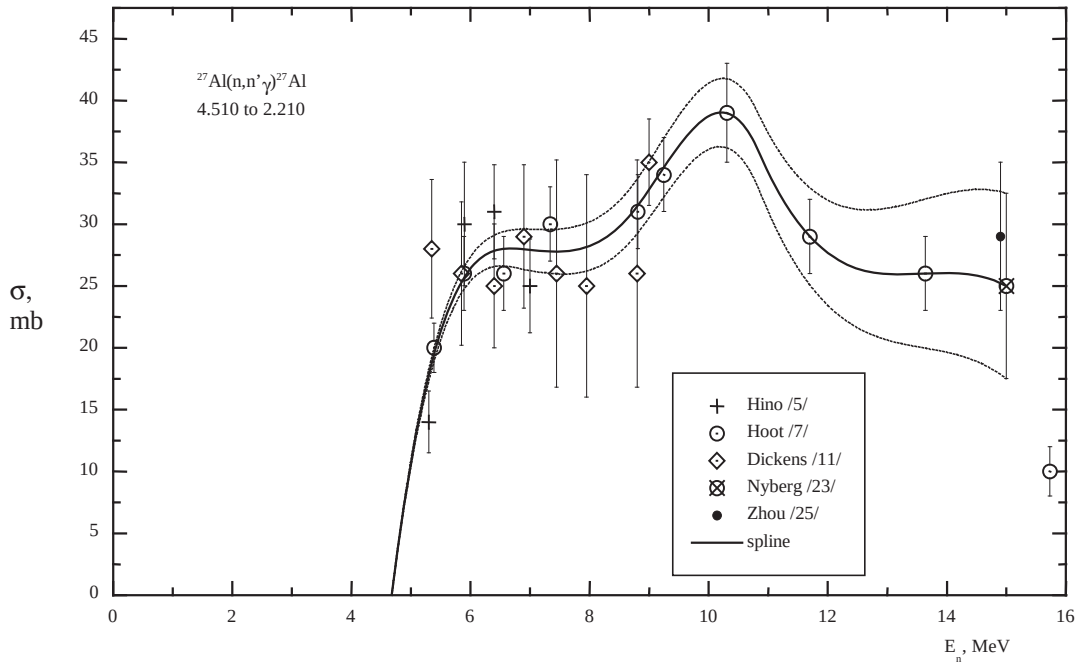

Fig. 23. Total γ-ray production cross-section for E_γ=2.300 MeV.

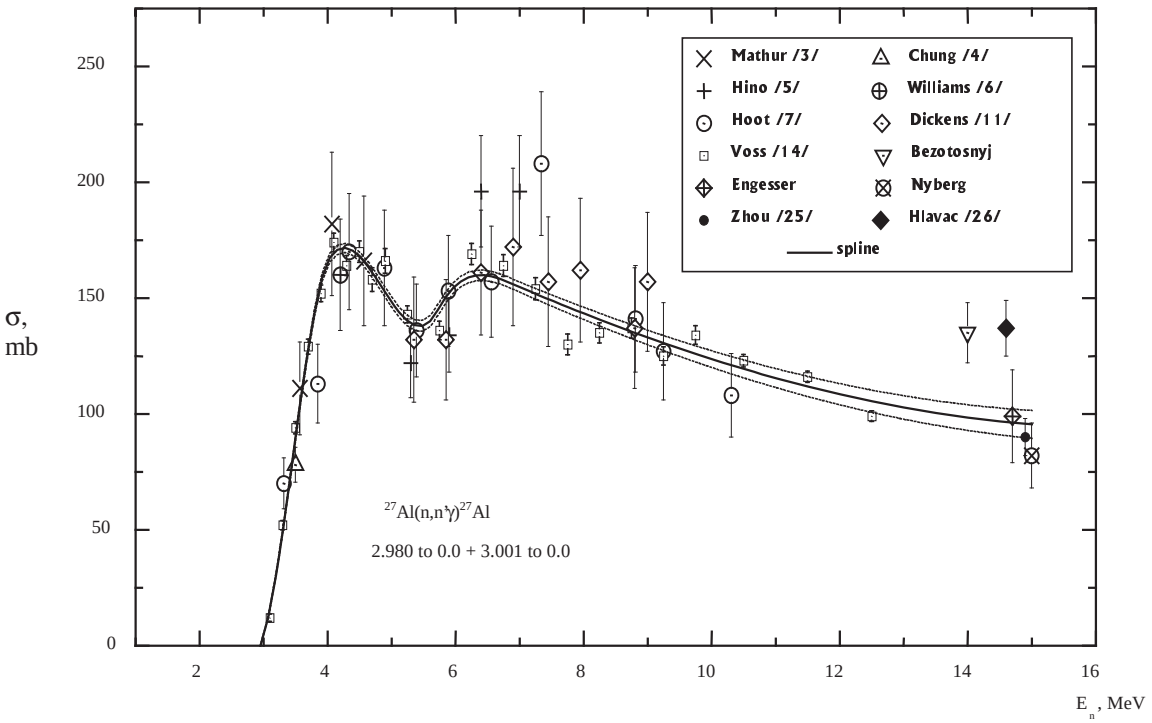

Fig. 24. Total γ-ray production cross-section for E_γ=2.980-3.001 MeV.

References

[1] V.M. Gorbachev, V.I. Nagornyj, Yu.Ya. Nefedov, A.M. Shvetsov, M.S. Shvetsov, Gamma-ray production cross-sections for interaction of 13.8 MeV neutrons with nuclei of Cu, W and ^{235}U, Voprosy atomnoj nauki i tekhniki, Ser. Yadernye konstanty, 1996, N2, P.47.

[2] A. Horsley, J.B. Parker, K. Parker, J.A. Price, Curve Fitting Statistical Techniques for Use in the Mechanised Evaluation of Neutron Cross Sections, N.I.M.-1968, V.62, N1, P.29-42.

[3] S.C. Mathur, W.E. Tucker, R.W. Benjamin, I.L. Morgan, Angular distributions of Gamma Rays Produced by Neutron Bombardment of Al, Mg and Si, Nucl. Phys., 1965, V.73, N3, P.561, EXFOR 11466.

[4] K.C. Chung, D.E. Velkley, J.D. Brandenberger, M.T. McEllistrem, ^{27}Al(n, n'γ) reactions and the 3002 keV level, Nucl. Phys. A, 1968, V.115, N2, P.476.

[5] Y. Hino, T. Yamamoto, S. Itagaki, K. Sugiyama, Gamma-Ray Production Cross Sections for Fast Neutron Interactions with Al, Ni, Cu and Nb, C. 79 KNOX, 45, 1979, EXFOR 21681.

[6] G.H. Williams, W.E. Tucker, J.B. Ashe, A High Resolution (n, n'γ) Gamma-Ray Spectrometer System, P.ORO-2791-32, 1 7, 7102, EXFOR 12690.

[7] C.G. Hoot, V.J. Orphan, J. John, Gamma-Ray Production Cross Sections for Iron and Aluminum, Report GULF-RT-A10743, 1971, EXFOR 10219009.

[8] V.C. Rogers, D.R. Dixon, C.G. Hoot, D. Costello, V.J. Orphan, Gamma-Ray Production Cross Sections for Copper from 0.67 to 19.6 MeV, Nucl. Sci. Eng., 1977, V.62, P.716.

[9] J.K. Dickens, T.A. Love, G.L. Morgan, Gamma-Ray Production due to Neutron Interactions with Aluminum for Incident Neutron Energies between 0.85 and 20 MeV, Tabulated Differential Cross Sections, Report ORNL-TM-4232, 1973, EXFOR 10352.

[10] J.K. Dickens, G.L. Morgan, F.G. Perey, Neutron-Induced Gamma-Ray Production in Iron for the Energy Range $0.85 \leq E_n \leq 20$ MeV, Nucl. Sci. Eng., 1973, V.50, P.311.

[11] J.K. Dickens, Al(n, n'γ) Reactions for $5.3 \leq E_n \leq 9$ MeV, Phys. Rev./C, 1972, V.5, P.100.

[12] G.L. Morgan, F.G. Perey, Cross Sections for the Al(n,xn) and Al(n, xγ) Reactions between 1 and 20 MeV, Report ORNL-TM-5241, 1976, EXFOR 10976003.

[13] G.L. Morgan, F.G. Perey, Cross Sections for the Al(n,xn) and Al(n, xγ) Reactions between 1 and 20 MeV, Nucl. Sci. Eng., 1976, V.61, P.337.

[14] F. Voss, S. Cierjacks, L. Kropp, Measurement of High Resolution Gamma-Ray Production Cross Sections in Inelastic Neutron Scattering on Al and Fe between 0.8 to 13 MeV, Report KFK-1494, 1971, EXFOR 20371.

[15] B.I. Sukhanov, P.D. Smotrin, Measurement of the gamma-ray production group cross-sections for interaction of 14 MeV neutrons with nuclei of N, O, Al, Fe and Pb and checking of the system of gamma production constants in an integrated experiment, Voprosy atomnoj nauki i tekhniki, Ser. Yadernye konstanty, 1976, N23, P.134.

[16] D.M. Drake, E.D. Arthur, M.G. Silbert, Cross Sections for Gamma-Ray Production by 14 MeV Neutrons., Nucl. Sci. Eng., 1978, V.65, P.49.

[17] V.M. Bezotosnyj, V.M. Gorbachev, M.S. Shvetsov, A.M. Surov, Group and total gamma-ray production cross-sections for nonelastic interaction of 14 MeV neutrons with various nuclei, Atomnaya ehnergiya, 1980, V.49, N4, P.239.

[18] V.M. Gorbachev, V.I. Nagornyj, Yu.Ya. Nefedov, A.M. Shvetsov, M.S. Shvetsov, A.L. Shmarova, G.G. Farafontov, "Measurement of gamma-ray production cross-sections for the (n, xγ) reaction in Al and Fe in order to test the evaluated data files for E_n = 14 MeV", Proc. XI International Seminar on "Exact measurements in nuclear spectroscopy" (TIYaS-XI), 2-5 September 1996, Sarov, Voprosy atomnoj nauki i tekhniki, Ser. Fizika yadernykh reaktorov, TIYaS-XI, 1997, Special issue, P.101.

[19] D.M. Drake, J.C. Hopkins, C.S. Young, H. Conde, Gamma-Ray Production Cross Sections for Fast Neutron Interactions with Several Elements, Nucl. Sci. Eng., 1970, V.40, P.294.

[20] V.M. Bezotosnyj, V.M. Gorbachev, M.S. Shvetsov et al., Gamma-ray production cross-sections for inelastic interaction of 2.5 MeV neutrons with various nuclei, Voprosy atomnoj nauki i tekhniki, Ser. Yadernye konstanty, 1976, N22, P.21.

[21] A.I. Lashuk, I.P. Sadokhin, Gamma-ray production cross-sections for inelastic scattering of 3 MeV neutrons, Voprosy atomnoj nauki i tekhniki, Ser. Yadernye konstanty, 1996, N2, P.59.

[22] F.C. Engesser, W.E. Thompson, Gamma Rays Resulting from Interactions of 14.7 MeV Neutrons with Various Elements, J. Nucl. Energy, 1967, V.21, P.487.

[23] K. Nyberg-Ponnert, B. Jonsson, I. Bergvist, Gamma Rays Produced by the Interaction of 15 MeV Neutrons in N, O, Mg and Al, Phys. Scripta, 1971, V.4, P.165.

[24] V.M. Bezotosnyj, V.M. Gorbachev, L.M. Surov, M.S. Shvetsov, Gamma-ray production cross-sections for nonelastic interaction of 14 MeV neutrons with various nuclei, Voprosy atomnoj nauki i tekhniki, Seriya Yadernye konstanty, 1975, N19, P.77.

[25] H. Zhou, G. Haung, Study of Total Discrete Gamma Radiation from Aluminum Under 14.9-MeV Neutron Bombardment, Nucl. Sci. Eng., 1997, V.125, P.61.

[26] S. Hlavac, L. Dostal, I. Turzo, Study of Gamma Radiation from the Interaction of 14.6-MeV Neutrons with ^{27}Al, Nucl. Sci. Eng., 1997, V.125, P.196.

[27] K. Hasegawa, M. Mizumoto, S. Chiba, M. Sugimoto, Y. Yamanouti, M. Igashira, H. Kibazawa, Gamma-Ray Production Cross Section Measurements of some Structural Materials between 7.8 and 13 MeV, Nuclear Data for Science and Technology, Proc. of an Int. Conf., Juelich, Germany, 3-17 May 1991, Editor S.M. Quim, Springer-Verlag, P.329.

00-30130 [4]
Translated from Russian

UDC 171.017

EVALUATION OF THE GAMMA-RAY PRODUCTION CROSS-SECTIONS FOR NONELASTIC INTERACTION OF FAST NEUTRONS WITH LEAD NUCLEI

A.G. Zvenigorodskij, M.S. Shvetsov, A.M. Shvetsov, M.V. Savin, Yu.Ya. Nefedov, V.A. Zherebtsov
Russian Federal Nuclear Centre-All-Russia Scientific Research Institute for Experimental Physics, Sarov

EVALUATION OF THE GAMMA-RAY PRODUCTION CROSS-SECTIONS FOR NONELASTIC INTERACTION OF FAST NEUTRONS WITH LEAD NUCLEI. The total gamma-ray production cross-sections in the energy range E_γ=0.5-10 MeV were evaluated for neutron energies from 0.8 to 18.8 MeV. The evaluations were performed using cubic spline approximation curves. The curve parameters were determined by the maximum likelihood method.

Recently, there has been an increasing need for reliable and accurate data for testing production programs, for selecting effective gamma-producing elements for fusion power facility designs and for solving a number of applied experimental nuclear physics tasks. All these requirements are fully applicable to lead, an important structural element. One possible way of resolving this issue could be to measure the differential gamma-ray production cross-sections for nonelastic interaction of E_n = 14 MeV neutrons with nuclei of this element. The results could then be used to perform a critical analysis and re-evaluation of the available data.

In this paper we present the results of our measurements on E_n = 14 MeV neutrons and a compilation of the data in the literature, which are then used to evaluate the total prompt gamma-ray production cross-sections for Pb nuclei in the energy range E_n = 0.8-18.8 MeV.

The evaluation was carried out using cubic spline approximation curves whose parameters were determined by the maximum likelihood method with allowance made for systematic and random errors assuming a Gaussian distribution of the latter.

1. Review of experimental work

Analysis showed that the measurement results which can be used to evaluate the total gamma-ray production cross-sections diverge noticeably and are to be found in only a few papers. There is only one paper [1] where the total gamma-ray production cross-sections with an energy E_γ = 0.3-10 MeV have been measured in detail in the neutron energy range E_n = 0.6-20.0 MeV. The entire range was broken down into 18 neutron groups with widths ranging from 0.4 to 2.5 MeV. The measurements were carried out on an electron linear

accelerator at an angle of 125º using the time-of-flight method and an NaI crystal based gamma detector measuring 12.7 cm in diameter and 12.7 cm in height. The lead sample under investigation, of a natural isotopic composition and in the form of a plate measuring 30 × 30 cm with a thickness of 0.011 atoms/barn, was placed at a distance of 47 m from the accelerator target and 1.4 m from the gamma-ray detector.

The uncertainty levels in the cross-sections are mainly in the 10-70% range. These errors do not include the neutron flux normalization error of 10%.

In reference [2], total gamma-ray production cross-sections with an energy E_γ = 1-5 MeV were measured in the neutron energy range E_n = 1-10 MeV. The entire range was broken down into 22 neutron groups with widths ranging from 0.12 to 1.41 MeV. The measurements were performed using an electron linear accelerator at an angle of 125º and the time-of-flight method. The sample under investigation, made of lead of a natural isotopic composition, was in the form of a hollow truncated cone with a wall thickness of 4 mm. The gamma-rays were detected using a hydrogen-free liquid scintillation detector (∅ 54 mm, h = 38 mm). The total error is mainly in the 20-40% range.

Reference [3] gives the results of measurements of the production cross-sections of a sum of discrete gamma lines with the energies (538, 570, 563), (763, 803, 860), (1357, 1462) keV and the gamma line production cross-section with an energy of 2615 keV. The measurements were carried out on an electron linear accelerator at an angle of 125º in the neutron energy range E_n = 1-10 MeV using the time-of-flight method and gamma detector based on an NaI(Tl) crystal measuring 40 mm in diameter and 40 mm in height. The sample under investigation, made of lead of a natural isotopic composition, was in the form of a hollow truncated cone. Measurements were carried out on two samples with wall thicknesses of 8 and 4 mm, respectively. The measurement methodology is described in Ref. [4]. The total uncertainty level in the cross-sections lies mainly in the range 10-30%, and the systematic error in the range 6-8%.

Reference [5] gives the measurement results of gamma-ray production group cross-sections for nonelastic neutron interaction at E_n = 14 MeV with the nuclei of lead of natural isotopic composition. The measurements were performed at an angle of 85º using Compton and pair spectrometers in ring geometry in the gamma-ray energy range E_γ = 0.5-8.0 MeV. The uncertainty level of the measurement results is not indicated.

In Ref. [6], gamma-ray production group cross-sections of nonelastic interaction of 14.0 MeV neutrons with Pb nuclei were measured in the energy range E_γ = 0.5-8.0 MeV. The measurements were carried out on a pulsed neutron generator using the time-of-flight method, a gamma detector based on a large NaI(Tl) crystal (200 mm in diameter, 100 mm in height) and a spherical sample (4π geometry) made of Pb of a natural isotopic composition. The uncertainty level of the cross-sections measured is mainly in the 15-20% range.

In Ref. [7], measurements were made of discrete gamma line production cross-sections on monoenergetic neutrons with an energy of 2.577 ± 0.010 MeV, obtained by irradiating a

tritium gas target with protons in an electrostatic generator. The sample, in the shape of a ring, was made of natural lead. The total cross-section measurement error is 12-15%.

Reference [8] gives the measurement results of the discrete gamma line production cross-sections for nonelastic interaction of neutrons with an energy E_n = 2.5 MeV with nuclei of, inter alia, Pb. The measurements were performed on spherical samples made of Pb of a natural isotopic composition using a Ge(Li) gamma detector. The production cross-sections of the individual gamma lines were determined relative to the E_γ = 0.847 MeV gamma line yield from the (n, n'γ) reaction in Fe. The uncertainty level for determination of the cross-sections is ≈16%.

Reference [9] gives the measurement results of the discrete gamma line production cross-sections for nonelastic scattering of neutrons with an energy E_n = 3.0 MeV on nuclei of, inter alia, Pb of a natural isotopic composition.

The neutron source used was the $^2H(d,n)^3He$ reaction on a KG-1.2 cascade generator. Disk and ring scatterer geometry and an NaI(Tl) crystal based gamma detector were used in the experiments. The uncertainty level for determination of the discrete gamma line production cross-sections is 11-20%.

In Ref. [10], measurement results are given for the integral gamma-ray production cross-sections ($E_\gamma \geq 0.7$ MeV) for nonelastic interaction of neutrons with an energy E_n = 7.8, 10.0, 11.5 and 13.0 eV with nuclei of Al, Si, Fe, Ni, Cu, Pb and Bi. The measurements were carried out at an angle of 90º for all the above-mentioned neutron energies and, for E_n = 7.8 and 11.5 MeV, also at an angle of 125º. The measurements were performed using an anti-Compton gamma spectrometer with a central NaI(Tl) crystal, measuring 7.6 cm in diameter and 15.2 cm in length, and the time-of-flight method. The samples, which were cylindrical, 2 or 3 cm in diameter and 3 cm high, were positioned 10 cm from the neutron source and 80 cm from the gamma detector.

The uncertainty level of the integral cross-sections is in the 14-20% range.

In conclusion, it should be noted that the total cross-sections with respect to angle given in this paper were determined by multiplying the differential cross-sections by 4π.

2. Evaluation of the total gamma-ray production cross-sections

The total gamma-ray production cross-sections were evaluated mainly on the basis of the measurement results given in Refs [1] and [2], and our latest measurement results. Our measurements were carried out on a pulsed 14 MeV neutron source at an angle of 125º using the time-of-flight method and a gamma detector based on an NaI(Tl) crystal measuring 150 mm in diameter and 100 mm in height. The measurement methodology is described in detail in Ref. [12]. The measurement results are given in Table 1. For comparison, this Table also gives the measurement results from Refs [1] ($\overline{E}_n$ = 13.8 MeV), [5] and [6]. However, the results of the two latter papers and the results of Ref. [8] were not used when evaluating the cross-sections because in Ref. [5] the measurement uncertainty levels are not indicated and in

Refs [6] and [8] the corrections for repeated scattering of neutrons and gamma-rays in the sample are not properly taken into account. In Table 1 and the figures, the results of these papers are shown for illustration purposes. Thus, it is useful to compare the results only with the data in Ref. [1], from which it is clear that the values of the differential cross-sections generally show satisfactory internal agreement. However, the high values of the total measurement errors in Ref. [1] are worthy of mention, being 3-5 times higher than ours. Clearly, it follows that the evaluated values of the cross-section and its uncertainty level for the neutron energy E_n = 14 MeV will be fully determined by our measurement results.

Table 1

Total gamma-ray production cross-sections for the (n,xγ) reaction in Pb, $\sigma_\gamma \pm \Delta\sigma_\gamma$, mb

Energy range ΔE_γ,(MeV)	Data from this paper E_n = 14.3 MeV $\theta=125^o$	[1] E_n=12.53-15.06 MeV; $\theta=125^o$	[5] E_n = 14.0 MeV $\theta=85^o$	[6] E_n = 14.0 MeV 4π-geometry
0.50-0.75	1368±27	1608±487	1844	1717±235
0.75-1.00	935±91	933±247	1336	1243±170
1.00-1.50	640±68	525±321	1040	1215±200
1.50-2.00	634±60	640±256	648	653±115
2.00-2.50	357±35	306±185	407	485±80
2.50-3.00	504±43	479±131	450	322±76
3.00-4.00	242±42	206±177	271	300±60
4.00-5.00	180±41	96±128	145	178±36
5.00-6.00	40±17	36±93	84	101±22
6.00-7.00	13±12	29±49	40	55±17
7.00-8.00	6±10	23±21	26	47±14
8.00-10.0	3±6	4±10		
Total ($E_\gamma \geq 0.5$ MeV)	4922±443	4885	6291	6316

When evaluating cross-sections in the $E_n \leq 5.12$ MeV region, use was made not only of the results of the aforementioned papers but also of the measurement results of the discrete gamma line production cross-sections given in Refs [3], [7] and [9]. Thus, the total gamma line production cross-section with energies E_γ = 0.538, 0.570 and 0.583 MeV [3] was used when evaluating cross-sections in the group E_γ = 0.5-0.75 MeV, and the gamma line production cross-section with energy E_γ = 2.615 MeV in the group E_γ = 2.5-3 MeV. As can be seen from Figs 1 and 9, the cross-section values used for evaluation [3] are in good agreement with the total cross-section measurement results [1] in the region $E_n \leq 5.12$ MeV.

To evaluate the cross-sections correctly using the data of the aforementioned papers some preparatory work was necessary:

a) the initial data for the cross-sections [1], contained in the EXFOR experimental data library as a file comprising 396 points, were put, like the results in Ref. [2], into the gamma-ray energy groups $\Delta E\gamma$ = 0.50-0.75-1.0-1.5-2.0-2.5-3.0-4.0-5.0-6.0-7.0-8.0-10.0 MeV;

(b) the total discrete gamma line production cross-sections in any gamma-ray energy group were based on the measurement results in Refs [7] and [9];

(c) in the $E_n \geq 14$ MeV region for the $E\gamma$ = 1.0-1.5 MeV group, the data from Ref. [1] were normalized relative to our measurement results at the point where E_n = 14 MeV.

Taking the above into account, the evaluation of the total gamma-ray production cross-sections was carried out using cubic spline approximation curves whose parameters were determined by the maximum likelihood method with allowance made for systematic and random errors [11] assuming a Gaussian distribution of the latter.

The evaluation results are given in Figs 1-12. The evaluated cross-sections may also be determined using the following formula:

$$\sigma_{n,x\gamma} = A_0^i + A_1^i \cdot (E - E_i) + A_2^i \cdot (E - E_i)^2 + A_3^i \cdot (E - E_i)^3 ,$$

where: *i* is the spline node number,
E is the instantaneous neutron energy value,
E_i is the node energy, $E_i < E < E_{i+1}$, and
A_0^i, A_1^i, A_2^i, A_3^i are the spline coefficients.

The spline coefficient values are given in Table 2.

Table 2

Coefficients of the spline curves describing the evaluated values of the gamma-ray production cross-sections in the ΔE_γ energy groups as a function of neutron energy

ΔE_γ,MeV	Node number	Energy of node, MeV	A_0, mb	A_1, mb/MeV	A_2, mb/MeV^2	A_3, mb/MeV^3	$\Delta\sigma_{n,x\gamma}$, mb
0.5-0.75	1	0.8	63.07941	-194.7813	363.4424	-80.05972	7.261451
	2	3.14	571.5588	191.0042	329.9477	-86.67431	26.48954
	3	4.94	1478.912	536.3416	-138.0936	8.57516	73.90182
	4	11.6	1458.897	-161.9958	33.23811	5.527131	198.2779
	5	14.3	1372.605	138.3684	78.00787	-20.66864	63.358
0.75-1.0	1	0.8	21.00257	325.1531	-51.21148	15.61688	2.899992
	2	1.52	234.3937	275.696	-17.47903	-1.225848	14.8741
	3	6.02	1009.37	43.91443	-45.10124	5.677883	81.81417
	4	9.62	847.8569	-60.05845	16.21989	0.1567728	116.2412
	5	14.3	938.1076	102.0608	18.42098	-7.550602	45.44958
1.0-1.5	1	1.12	-3.260987	41.48945	-50.69332	33.81639	7.799817
	2	2.3576	34.54323	71.39833	74.86016	-27.34221	10.06348
	3	3.772	207.9228	119.0663	-41.15828	34.83935	36.45736
	4	5.0096	358.2796	177.2768	88.19327	-41.45579	90.05789
	5	6.9544	731.6792	49.92523	-153.6764	33.25732	145.1408
	6	9.076	463.4726	-153.0621	57.99982	-4.266371	138.569
	7	14.2999	638.459	103.6319	-8.861314	-2.338431	33.63916

ΔE_{γ}, MeV	Node number	Energy of node, MeV	A_0, mb	A_1, mb/MeV	A_2, mb/MeV^2	A_3, mb/MeV^3	$\Delta\sigma_{n,x\gamma}$, mb
1.5-2.0	1	1.61	7.479239	12.60769	107.8639	-32.47968	3.735003
	2	2.38355	66.74139	121.1784	32.48995	-7.019529	5.70504
	3	6.4232	623.7135	40.02415	30.59636	-13.95343	56.13884
	4	9.94715	534.0903	-264.1661	115.7971	-11.44068	102.2334
	5	14.30105	634.789	93.54774	-33.6378	2.932427	30.66937
2.0-2.5	1	2.13	6.401106	-8.826794	43.65766	3.919844	7.002888
	2	3.88035	145.7267	83.20603	25.82107	-5.983447	35.56344
	3	9.495975	367.645	-192.8595	67.36778	-5.765723	63.18036
	4	14.30032	356.6707	55.20806	-15.7338	1.603341	19.87078
2.5-3.0	1	2.75	63.51957	-48.05785	691.5082	-236.3448	8.975517
	2	3.8735	547.2142	610.7809	-135.4024	7.425454	30.33721
	3	12.059	546.9526	-113.3216	46.94076	-2.392984	80.73181
	4	14.306	502.1745	61.38358	30.80966	-9.773098	24.5744
3.0-4.0	1	3.08	5.456516	-15.56308	70.44065	-7.241693	5.992113
	2	4.9664	178.1499	172.8866	-17.48783	-1.049617	24.68585
	3	11.2544	312.8537	-171.5426	64.73216	-5.271205	125.1126
	4	14.30015	241.938	76.07687	16.56785	-4.169433	29.65141
4.0-5.0	1	4.18	5.236191	28.68988	25.57908	3.081072	3.89513
	2	6.5192	251.7496	198.9366	-68.44701	5.49897	26.06924
	3	11.9286	195.4273	-58.8518	20.79137	0.4994683	78.66585
	4	14.30435	179.658	48.39567	24.35121	-5.752507	11.95615
5.0-6.0	1	5.5	10	46.4029	46.39569	-12.79858	13.04004
	2	7.628	195.5106	69.99226	-35.31046	14.07972	54.72455
	3	8.559	241.4293	40.85544	-52.60676	7.890463	80.3944
	4	11.352	117.0768	-68.34902	13.50742	0.2746417	79.23695
	5	14.30294	40.0635	18.54482	15.93877	-1.39321	7.981056
6.0-7.0	1	6.5	16.50931	68.6862	-18.06738	1.180742	10.97629
	2	14.30281	13.37235	2.39789	9.571943	-1.522723	6.901029
7.0-8.0	1	7.5	6.00684	20.7613	-2.829854	-0.5107502	5.035916
	2	9.082	29.74665	7.97284	-5.253874	0.5542531	8.672459
	3	14.30119	7.04159	-1.575645	3.424377	-0.6188966	3.854948
8.0-10.0	1	8.5	2	0.2337239	0.07715326	-0.0108772	3.006998
	2	11.93333	3.271701	0.3788547	-0.0348822	0.02193135	5.124293
	3	15.36667	5.048844	0.9148961	0.1910107	-0.0850374	11.27041

Conclusion

Available data in the literature on the total prompt gamma-ray production cross-sections of nonelastic fast neutron interaction with the nuclei of lead of natural isotopic composition were selected and analysed. Considerable divergence is seen between the results obtained by various authors. Evaluation using cubic spline approximation curves whose parameters were determined by the maximum likelihood method enabled more valid gamma-ray production cross-sections to be obtained.

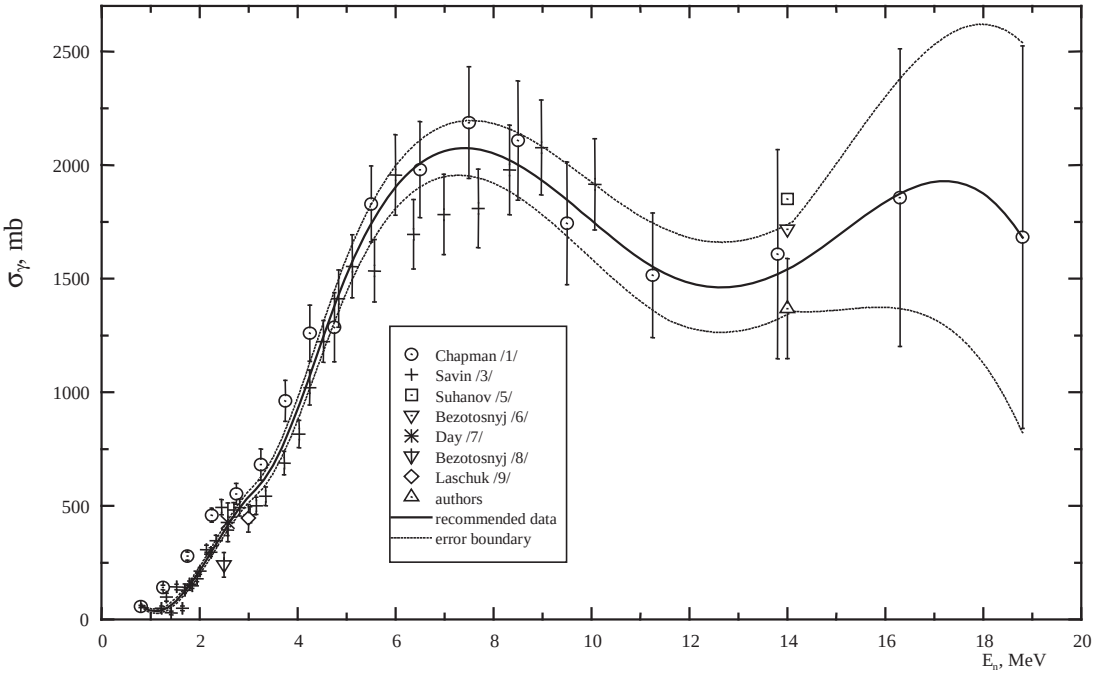

Fig. 1. Total gamma-production cross-section for energy E_γ=0.5-0.75 MeV for nonelastic neutron interaction with Pb nuclei.

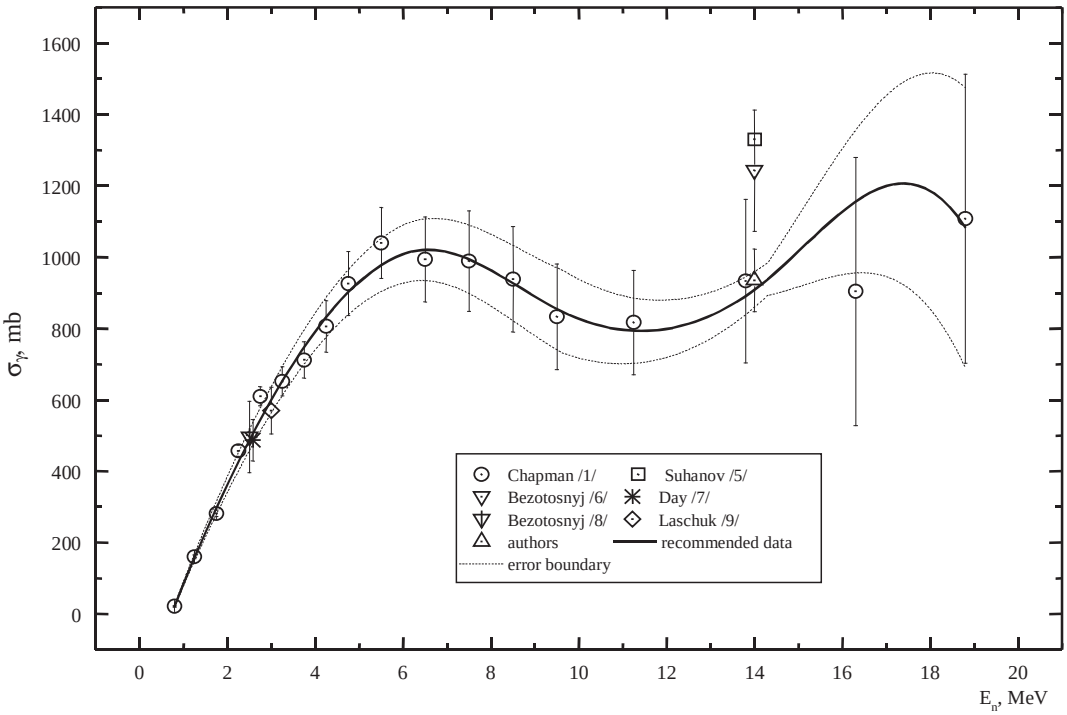

Fig. 2. Total gamma-production cross-section for energy E_γ=0.75-1.0 MeV for nonelastic neutron interaction with Pb nuclei.

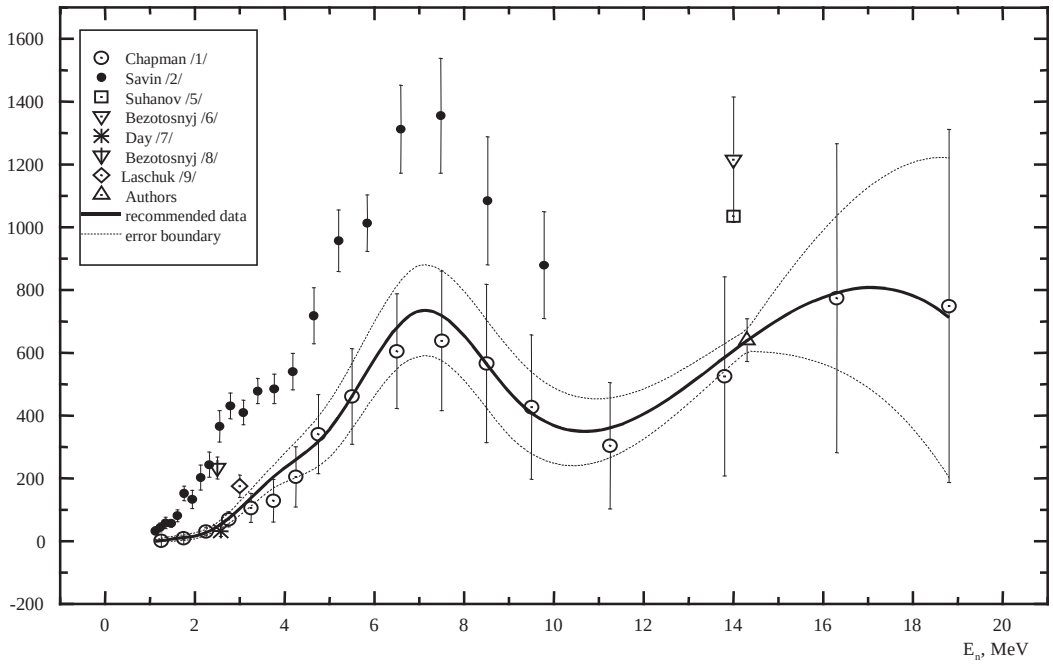

Fig. 3. Total gamma-production cross-section for energy E_γ=1.0-1.5 MeV for nonelastic neutron interaction with Pb nuclei.

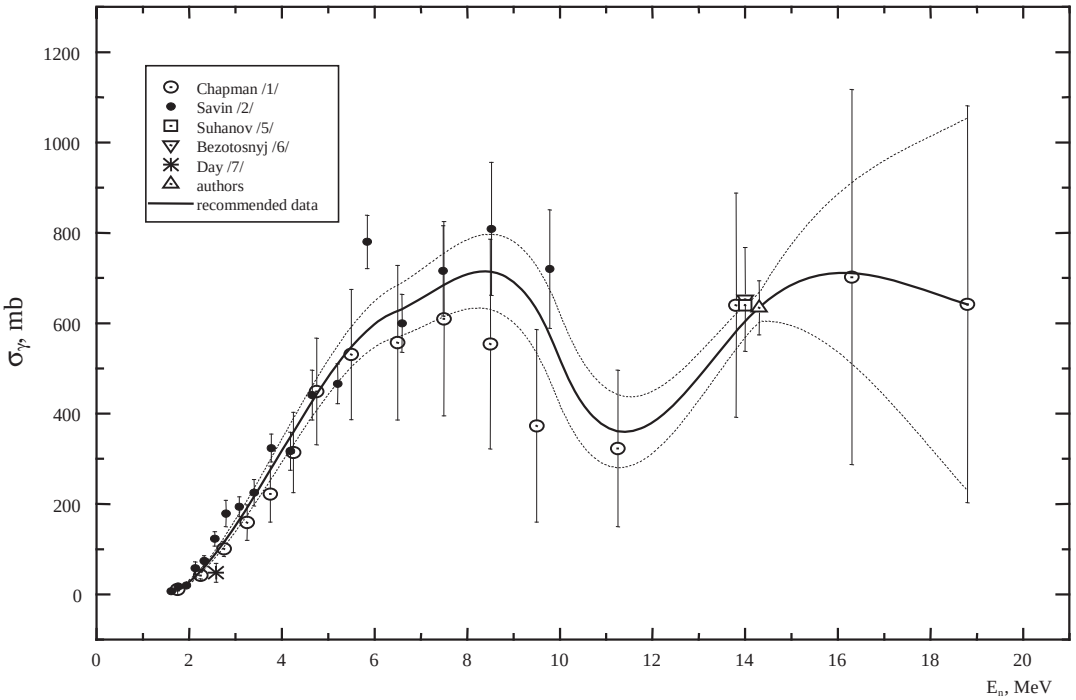

Fig. 4. Total gamma-production cross-section for energy E_γ=1.5-2.0 MeV for nonelastic neutron interaction with Pb nuclei.

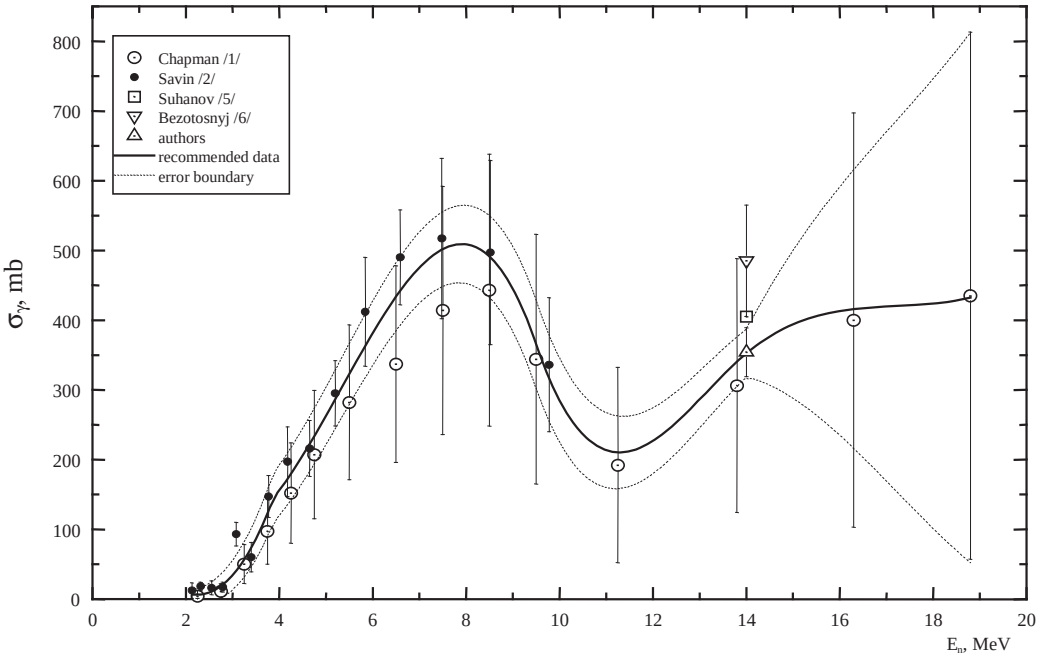

Fig. 5. Total gamma-production cross-section for energy E_γ=2.0-2.5 MeV for nonelastic neutron interaction with Pb nuclei.

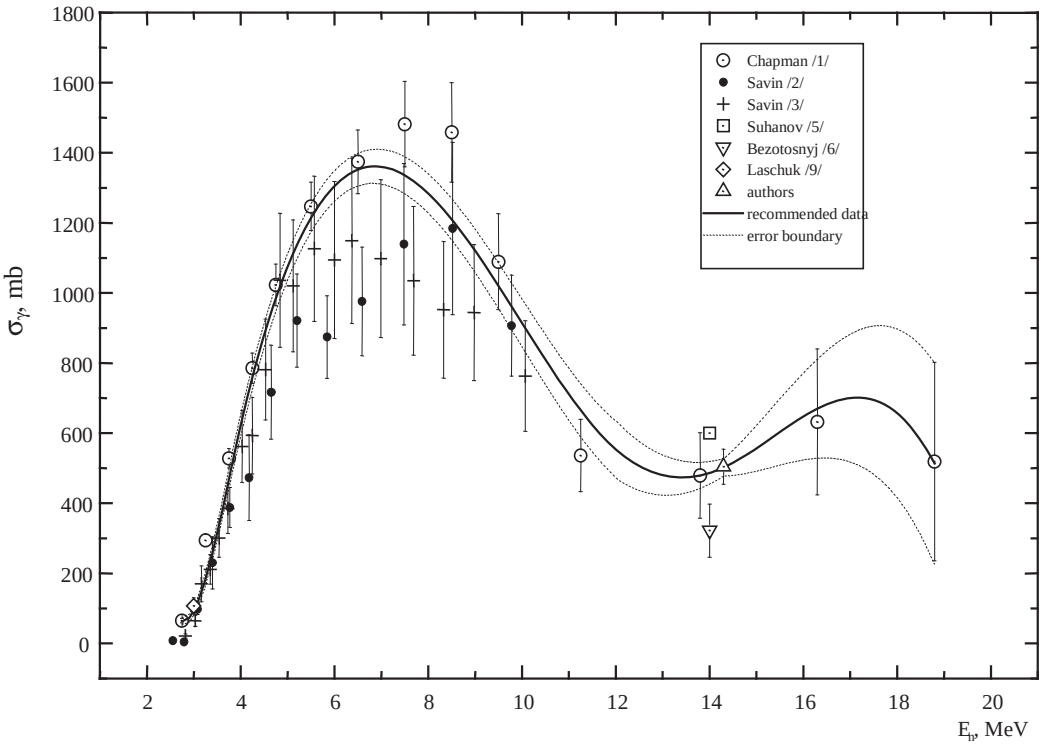

Fig. 6. Total gamma-production cross-section for energy E_γ=2.5-3.0 MeV for nonelastic neutron interaction with Pb nuclei.

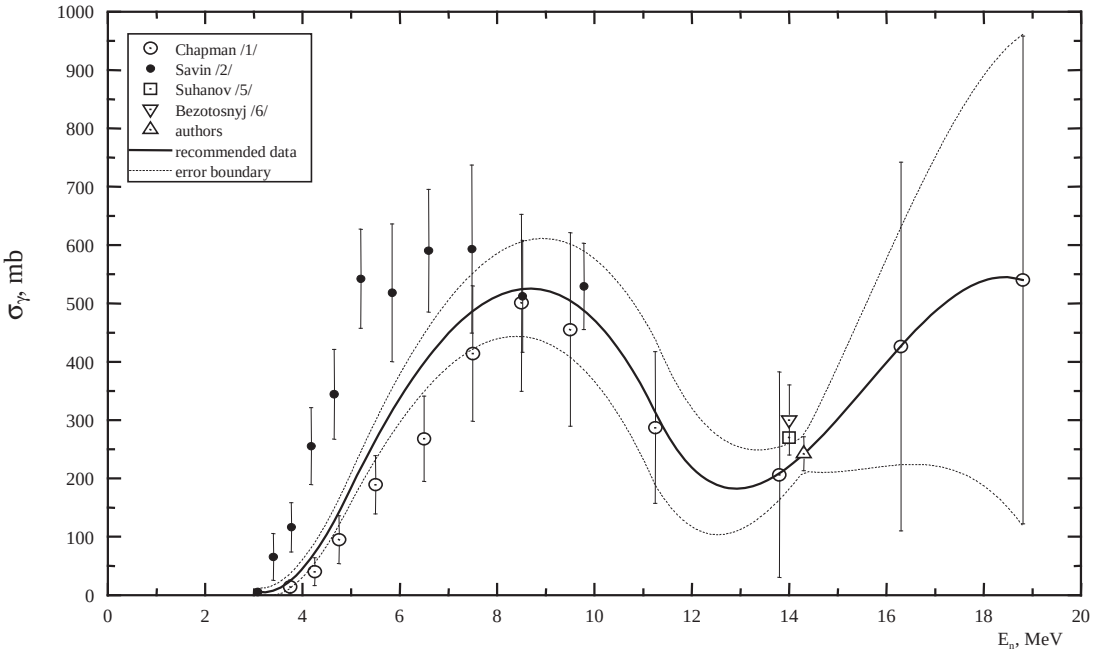

Fig. 7. Total gamma-production cross-section for energy E_γ=0.3.0-4.0 MeV for nonelastic neutron interaction with Pb nuclei.

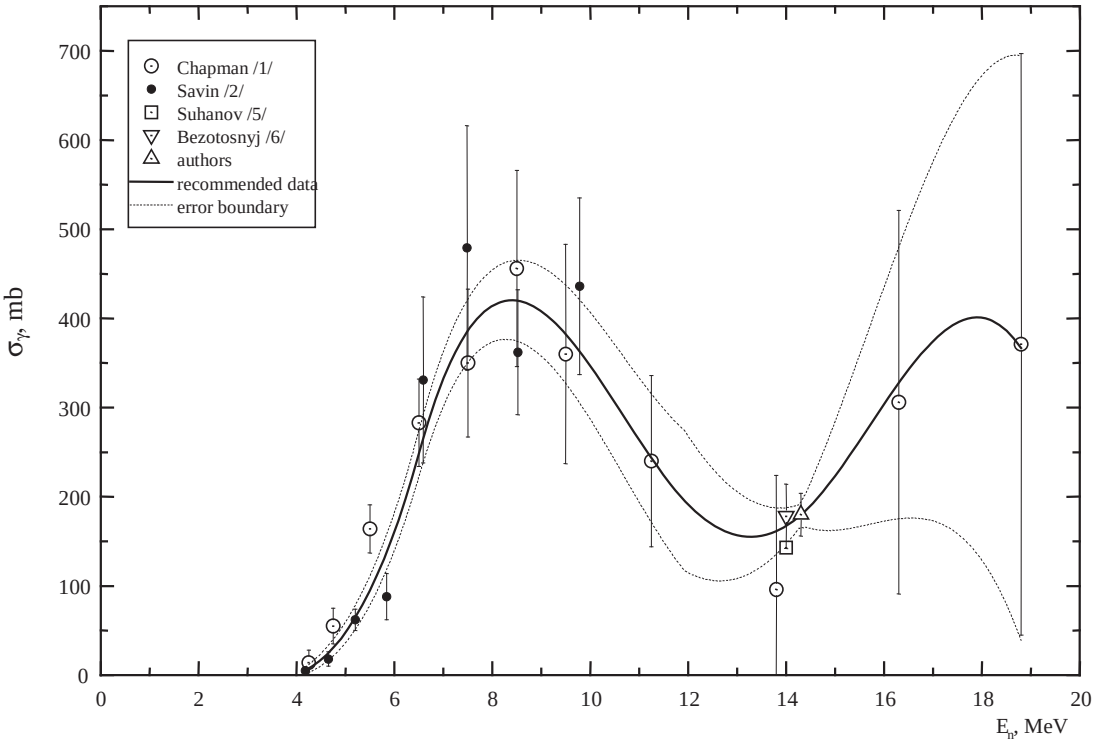

Fig. 8. Total gamma-production cross-section for energy E_γ=4.0-5.0 MeV for nonelastic neutron interaction with Pb nuclei.

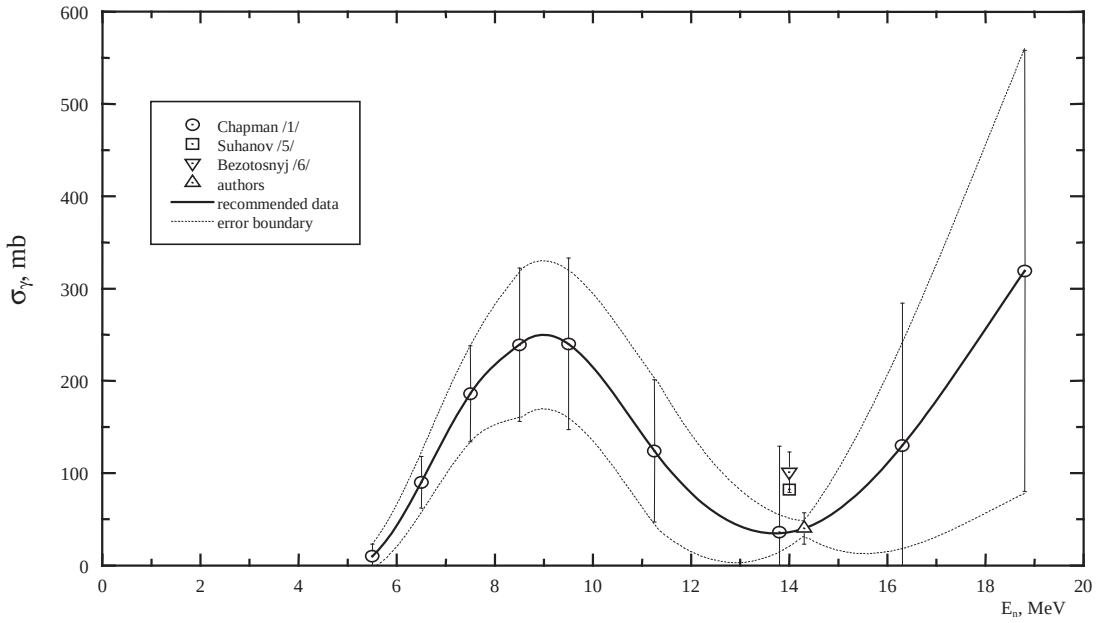

Fig. 9. Total gamma-production cross-section for energy E_γ=5.0-6.0 MeV for nonelastic neutron interaction with Pb nuclei.

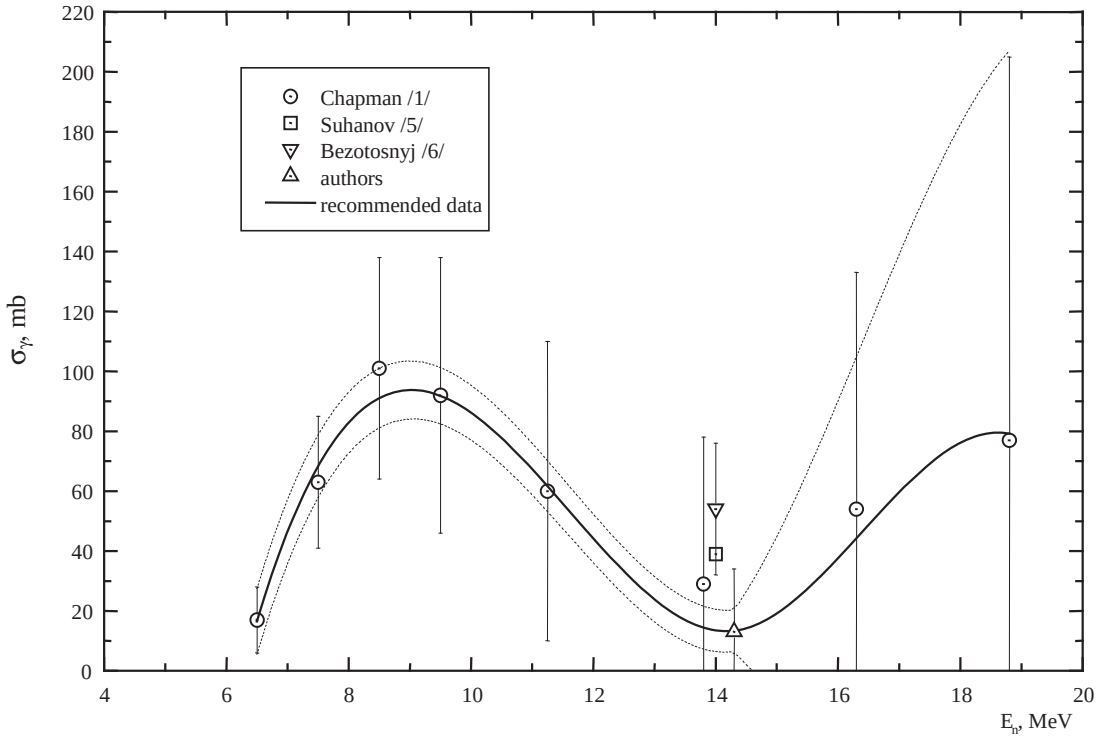

Fig. 10. Total gamma-production cross-section for energy E_γ=0.6.0-7.0 MeV for nonelastic neutron interaction with Pb nuclei.

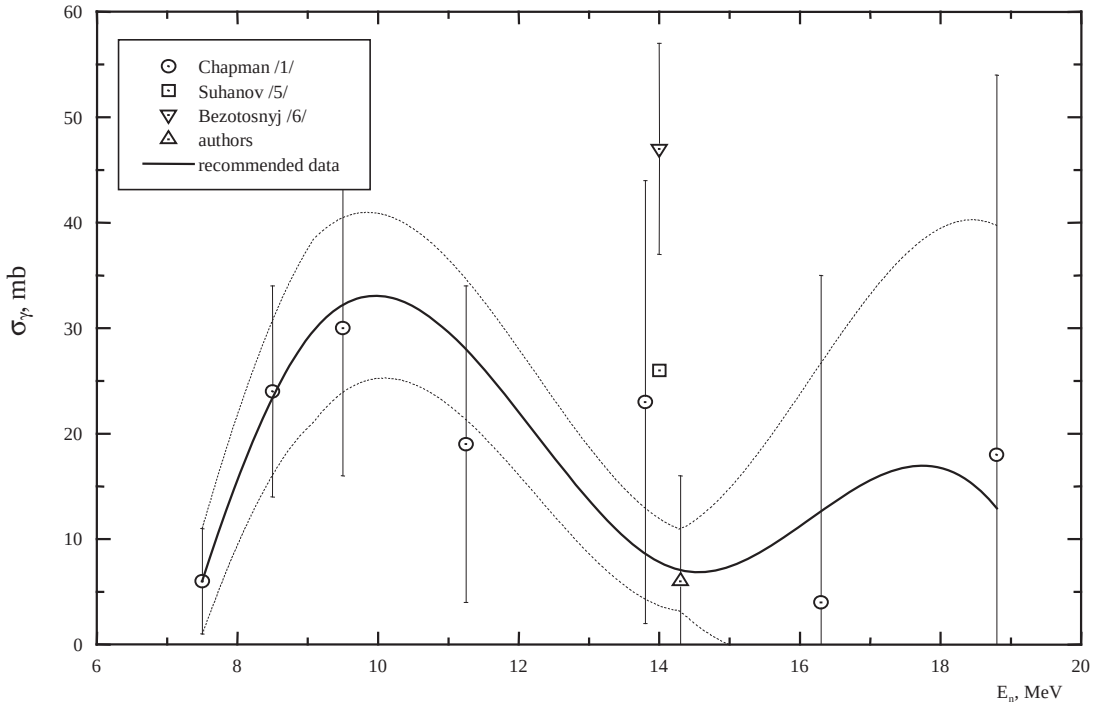

Fig. 11. Total gamma-production cross-section for energy E_γ=7.0-8.0 MeV for nonelastic neutron interaction with Pb nuclei.

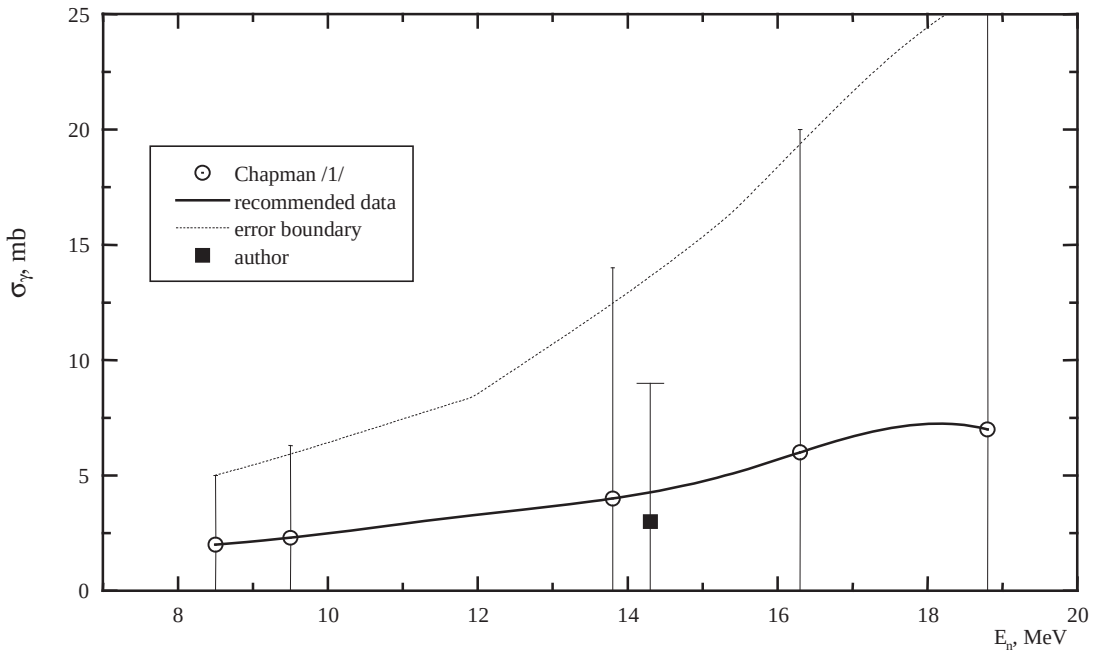

Fig. 12. Total gamma-production cross-section for energy E_γ=8.0-10.0 MeV for nonelastic neutron interaction with Pb nuclei.

References

[1] G.T. Chapman, G.L. Morgan, Pb(n,xγ) reaction cross-section for incident neutron energies between 0.6 and 20.0 MeV. R. ORNL-TM-4822. 1975. EXFOR 10586003.

[2] M.V. Savin, Yu.A. Khokhlov, I.N. Paramonova et al., Gamma-ray production cross-sections for fast neutron interaction with carbon, lead and rhenium nuclei, Atomnaya ehnergiya, Vol. 49, No. 4 (1980) p. 236. EXFOR 40508008.

[3] M.V. Savin, Yu.A. Khokhlov, I.N. Paramonova et al., Discrete gamma line production cross-sections in the (n,x) reaction in lead for E_n = 1-10 MeV. Nuclear physics research in the USSR. Collection of abstracts, Nuclear Data Centre, Atomizdat, No. 24 (1977) p. 11. EXFOR 40542002.

[4] M.V. Savin, Yu.A. Khokhlov, I.N. Paramonova et al., Nucl. Phys. Vol. 33, No. 3 (1976) p. 512.

[5] B.I. Sukhanov, P.D. Smotrin, Measurement of the gamma-ray production group cross-sections for interaction of 14 MeV neutrons with nuclei of N, O, Al, Fe and Pb and checking of the system of gamma production data in an integral experiment, Voprosy atomnoj nauki i tekhniki, Ser. Yadernye konstanty, No. 23 (1976) p. 134.

[6] V.M. Bezotosnyj, V.M. Gorbachev, M.S. Shvetsov, L.M. Surov, Group and total gamma-ray production cross-sections for nonelastic interaction of 14 MeV neutrons with various nuclei, Atomnaya ehnergiya, Vol. 49 (1980) No. 4, p. 239.

[7] R.B. Day, Gamma-ray from neutron inelastic scattering, Phys. Rev. Vol. 102 (1956) p. 767.

[8] V.M. Bezotosnyj, V.M. Gorbachev, M.S. Shvetsov et al., Gamma-ray production cross-sections for inelastic interaction of 2.5 MeV neutrons with various nuclei, Voprosy atomnoj nauki i tekhniki, Ser. Yadernye konstanty, No. 22 (1976) p. 21.

[9] A.I. Lashuk, I.P. Sadokhin, Gamma-ray production sections for inelastic scattering of neutrons with an energy of 3 MeV, Voprosy atomnoj nauki i tekhniki, Ser. Yadernye konstanty, No. 2 (1996) p. 59.

[10] K. Hasegawa, M. Mizumoto, S. Chiba, M. Sugimoto, Y. Yamanouti, M. Igashira, H. Kibazawa, Gamma-ray production cross section measurements of some structural materials between 7.8 and 13.0 MeV, Nuclear Data for Science and Technology. Proc. of an Int. Conf. Jülich, Germany, 3-17 May 1991. Editor S.M. Qaim. Springer-Verlag. p. 329.

[11] A. Horsley, J.B. Parker, K. Parker, J.A. Price, Curve fitting and statistical techniques for use in the mechanised evaluation of neutron cross sections, Nucl. Instr. and Methods, Vol. 62 (1968) No. 1. pp 29-42.

[12] V.M. Gorbachev, V.I. Nagornyj, Yu.Ya. Nefedov., A.M. Shvetsov, M.S. Shvetsov, Gamma-ray production cross-sections for interaction of 13.8 MeV neutrons with nuclei of Cu, W and ^{235}U, Voprosy atomnoj nauki i tekhniki, Ser. Yadernye konstanty, No. 2 (1996).

UDC 539.172

EVALUATION OF NEUTRON CROSS SECTIONS FOR Cm-242, -243, -244

A.I. Blokhin, A.S. Badikov, A.V. Ignatyuk, V.P. Lunev,
V.N. Manokhin, G.Ya. Tertychny, K.I. Zolotarev
Institute of Physics and Power Engineering, Obninsk, Russia

EVALUATION OF NEUTRON CROSS SECTIONS FOR Cm-242, -243, -244. The work is devoted to the analysis of available experimental and evaluated data on the neutron cross sections for Cm-242, Cm-243, Cm-244. A comparison of experimental data with the results of theoretical calculations and the evaluations of the most important cross sections were performed. As a result the new version of complete files of evaluated neutron cross sections for Cm-242, Cm-243, Cm-244 were performed. These files were included into the BROND-3 library the formations of which is under development in Russian Nuclear Data Center.

For curium isotopes there are considerably less experimental data than for americium isotopes. The measurements of the total and radiative capture cross sections are restricted to the neutron resonance region and only the fission cross sections were measured in the fast neutron energy region. That is why all the neutron cross section evaluations are mainly based on the analysis of the available measured fission cross sections and on the statistical calculations of other cross sections. For Cm-245 and Cm-246 the new experimental fission cross sections, obtained in the framework of the Project [18] agree good enough with the available experimental data and the new cross section evaluations made by Minsk's group in 1996 [1, 2]. For Cm-243 the discrepancies of the measured fission cross sections with the new evaluation of Minsk's group are considerable for all neutron energies. For Cm-244 the new experimental data call for the re-examination of the previous evaluations [3]. In this paper the changes in the evaluated neutron cross sections of Cm-242, Cm-243 and Cm-244, due to the new experimental data, are considered.

Evaluation of neutron cross sections for Cm-243 and Cm-244

The available experimental fission cross section data for Cm-243 [4-11] are shown in Fig. 1 together with different cross section evaluations. The approximation curves were obtained by statistical analysis of the correlated experimental data on the basis of nonlinear regression model using rational functions.

The recommended fission cross sections in the group form are given in Table 1 together with the corresponding uncertainties. In the precise measurements of the fission cross section on the fast critical assembly with the mean neutron energy of 300 keV the integral cross section of 2.651±0.090 barn [12] was obtained, which is in good agreement with our fission cross section evaluation and disagrees considerably with the calculations for other fission cross section evaluations. So our recommended evaluation in the energy region above 1 MeV may be considered as supported by the integral measurement results.

The results of the optical-statistical calculation of the inelastic scattering and (n,2n) reaction cross sections consistent with the evaluated fission cross section are shown in Fig. 2. These results are strongly differ from the cross sections adopted in other evaluations. For high neutron energies

these differences are due to not only the differences in the fission cross sections but to the discrepancies in the neutron absorption cross sections as well. The Minsk's group used for curium isotopes as well as for americium ones the optical potential resulting in lower absorption cross sections than the observed fission cross section for the light curium isotopes at the neutron energy of 14 MeV.

The experimental data available for the Cm-244 fission cross sections are shown in Fig. 3 together with different evaluations. Our fission cross section evaluation in the group form is given in Table 2 together with the corresponding uncertainties.

The discrepancies of the experimental data for Cm-244 are not so considerable as for the Cm-243 however the integral fission cross section of 1.35 barn, calculated for the fast critical assembly with our evaluated data, is noticeably above the measured integral cross section equal to 1.232±0.039 barn [12]. The calculated integral fission cross section remains approximately the same at the use of the ENDF/B-VI and Minsk's group evaluations. At present we do not see any explanation of this contradiction between the microscopic and integral data and the problem of fission cross section validation in the energy region below 1 MeV for Cm-244 remains open.

The results of the optical-statistical calculations of the inelastic scattering and (n,3n) reaction cross sections consistent with our Cm-244 fission cross section evaluation are shown in Fig. 4. The discrepancies in the (n,2n) reaction cross sections are very considerable and obviously due to the discrepancies in the neutron fission and absorption cross section evaluations.

Evaluation of neutron cross section for Cm-242

For Cm-242 there is only one measurement of the fission cross sections in the subthreshold region [13], which is not sufficient to evaluate reliably the fission cross section in the region of the first "plateau". Because in the Cm-242 previous evaluations the empirical fission cross section systematics [16] were used combined with the theoretical calculations [14, 15] and results of the fissility analysis of curium isotopes in the charged particle induced reactions [17]. The results of such data systematics are given in Fig. 5 together with the experimental data, obtained in the framework of the Project [18], and the results of fission cross section measurements at the neutron energy of 14.5 MeV [11].

Extrapolating the corresponding data we obtain for Cm-242 the evaluation of the fission cross section of 2.80±0.15 barn in the neutron energy region of 14 MeV. The evaluation of cross sections in the region of the first plateau is more problematic. For the neutron energy of ~5.5 MeV the extrapolation of experimental dependence gives the evaluated cross sections value equal to 2.25 barn. If assumed plateau slope for Cm-242 is the same as for Cm-244, then at the energy about 2 MeV one should expect the fission cross section value to be equal to 2.45 barn. No doubts that the uncertainty of this evaluation is above 10-15%. The great concern is caused however by the contradiction of the experimental data on cross sections of the curium isotope fission by neutrons with the results of the analysis of the same isotopes fissility in direct reactions induced by charged particles (Fig. 5). This contradiction in the data was noted early in [16], and we have no explanation of it up to now.

The results of the optical-statistical calculations of the fission, inelastic scattering and (n,2n) reaction cross sections consistent with the evaluations made above for fission cross sections of Cm-

242 at the first plateau and 14 MeV are given in Fig. 6 together with previous evaluations of these cross sections. The discrepancies of the evaluations are considerable and the task of the testing of evaluated data remains.

On the base of the evaluations considered above the modified files of evaluated neutron cross sections were formed for the BROND-3 library. For Cm-242 and Cm-244 the neutron cross sections for the resolved and unresolved resonance regions as well as the neutron angular distributions and neutron spectra were taken from the previous BROND-2 evaluations [15]. For Cm-243 the relevant evaluations of Minsk's group [3] were used for this purpose.

Table 1
Group cross section for ^{243}Cm(n,f) reaction

Energy range, MeV		Cross section, mb	Error, mb	Error, %
0.10	0.15	3258.	128.	3.94
0.15	0.20	2866.	119.	4.15
0.20	0.25	2645.	112.	4.24
0.25	0.30	2503.	106.	4.23
0.30	0.40	2369.	99.8	4.21
0.40	0.50	2259.	94.8	4.20
0.50	0.70	2181.	90.5	4.15
0.70	0.90	2161.	89.9	4.16
0.90	1.00	2193.	91.8	4.19
1.00	1.25	2272.	96.1	4.23
1.25	1.50	2404.	105.	4.38
1.50	2.00	2527.	108.	4.30
2.00	2.50	2540.	110.	4.33
2.50	3.00	2476.	107.	4.35
3.00	3.25	2417.	105.	4.36
3.25	3.50	2375.	103.	4.33
3.50	3.75	2332.	100.	4.29
3.75	4.00	2288.	97.1	4.24
4.00	4.25	2241.	94.6	4.22
4.25	4.50	2191.	93.0	4.25
4.50	4.75	2139.	92.1	4.31
4.75	5.00	2087.	91.1	4.37
5.00	5.25	2040.	89.6	4.39
5.25	5.50	2011.	88.5	4.40
5.50	5.75	2016.	89.9	4.46
5.75	6.00	2074.	93.8	4.52
6.00	6.25	2191.	102.	4.65
6.25	6.50	2343.	111.	4.74
6.50	6.75	2494.	116.	4.65
6.75	7.00	2615.	131.	5.01
7.00	7.50	2724.	182.	6.68
7.50	8.00	2785.	243.	8.72
8.00	8.50	2799.	269.	9.61
8.50	9.00	2794.	271.	9.71
9.00	10.00	2780.	255.	9.16
10.00	12.00	2758.	202.	7.32
12.00	14.00	2748.	137.	5.00
14.00	17.00	2759.	123.	4.46
17.00	20.00	2789.	224.	8.02

Table 2

Group cross section for $^{244}Cm(n,f)$ reaction

Energy range, MeV		Cross section, mb	Error, mb	Error, %
0.10	0.20	45.34	11.1	24.5
0.20	0.30	77.25	10.6	13.7
0.30	0.40	162.9	13.1	8.0
0.40	0.50	303.6	18.5	6.1
0.50	0.60	593.5	31.3	5.3
0.60	0.70	1020.	48.1	4.7
0.70	0.80	1504.	65.3	4.3
0.80	0.90	1913.	76.1	3.9
0.90	1.00	2169.	83.5	3.8
1.00	1.30	2287.	90.4	3.9
1.30	1.60	2189.	97.9	4.5
1.60	2.00	2081.	98.4	4.7
2.00	2.50	2118.	104.	4.9
2.50	3.00	2161.	118.	5.5
3.00	3.50	2082.	160.	7.7
3.50	4.00	2021.	143.	7.1
4.00	4.50	1983.	117.	5.9
4.50	5.00	1958.	100.	5.1
5.00	5.50	1949.	97.6	5.0
5.50	5.75	1965.	99.7	5.1
5.75	6.00	1998.	102.	5.1
6.00	6.20	2048.	107.	5.2
6.20	6.40	2113.	113.	5.3
6.40	6.60	2194.	123.	5.6
6.60	6.80	2287.	140.	6.1
6.80	7.00	2383.	160.	6.7
7.00	7.25	2482.	177.	7.1
7.25	7.50	2571.	188.	7.3
7.50	7.75	2635.	196.	7.4
7.75	8.00	2677.	209.	7.8
8.00	10.00	2717.	245.	9.0
10.00	12.00	2709.	205.	7.6
12.00	14.00	2712.	148.	5.5
14.00	16.00	2726.	151.	5.5
16.00	18.00	2743.	194.	7.1
18.00	20.00	2760.	244.	8.8

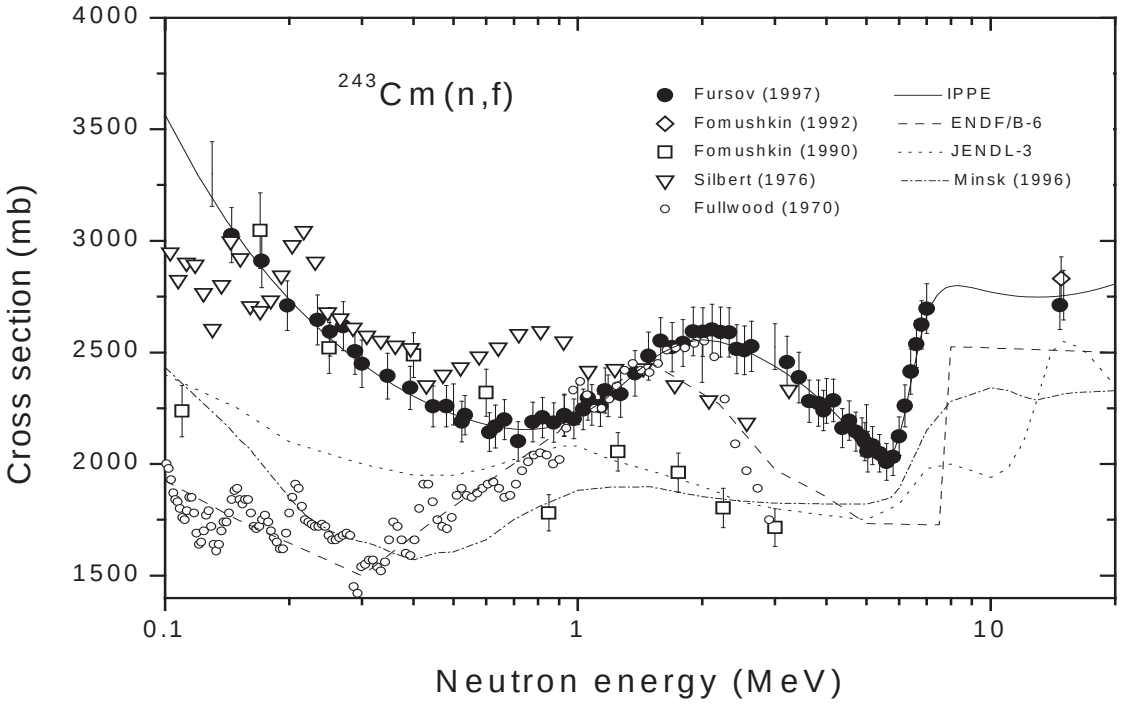

Fig. 1. Comparison of the evaluated fission cross sections for ^{243}Cm with experimental data.

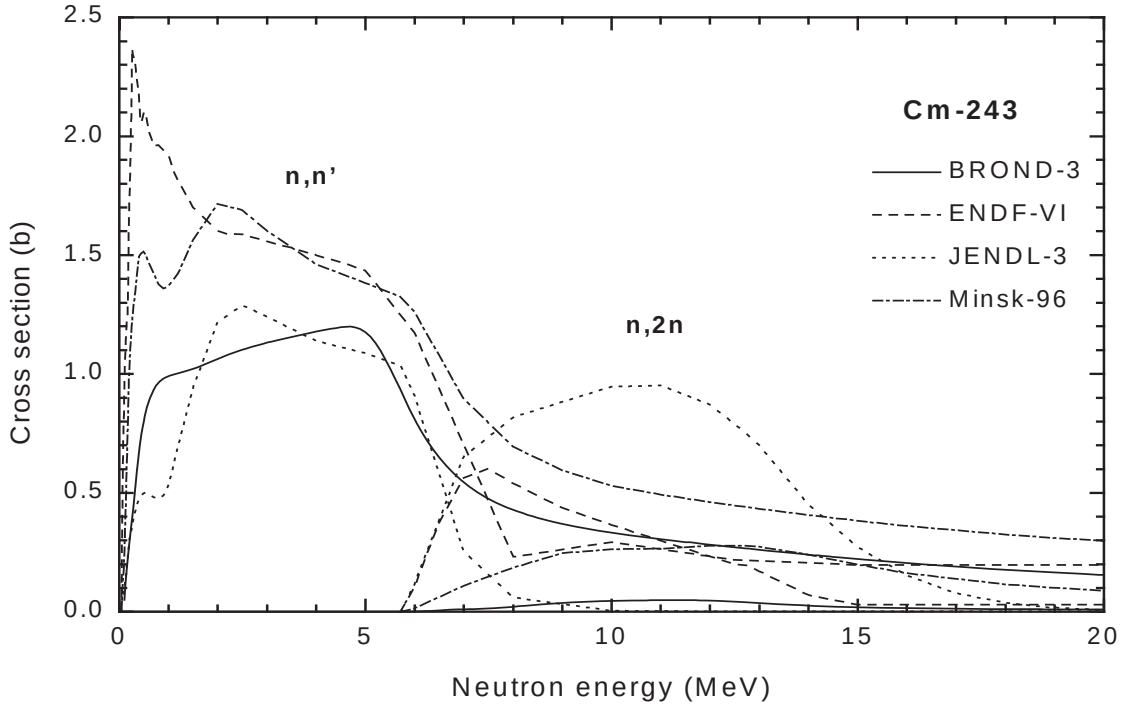

Fig. 2. Comparison of the evaluated inelastic and (n,2n) reaction cross sections for ^{243}Cm.

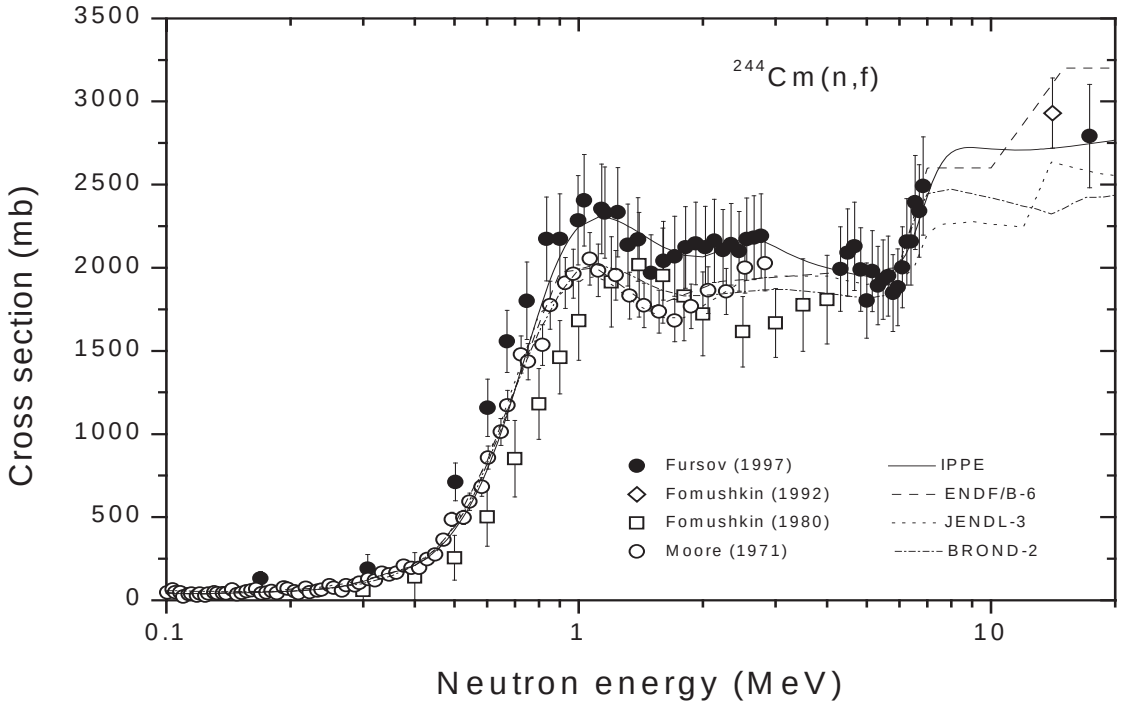

Fig. 3. Comparison of the evaluated fission cross sections for ^{244}Cm with experimental data.

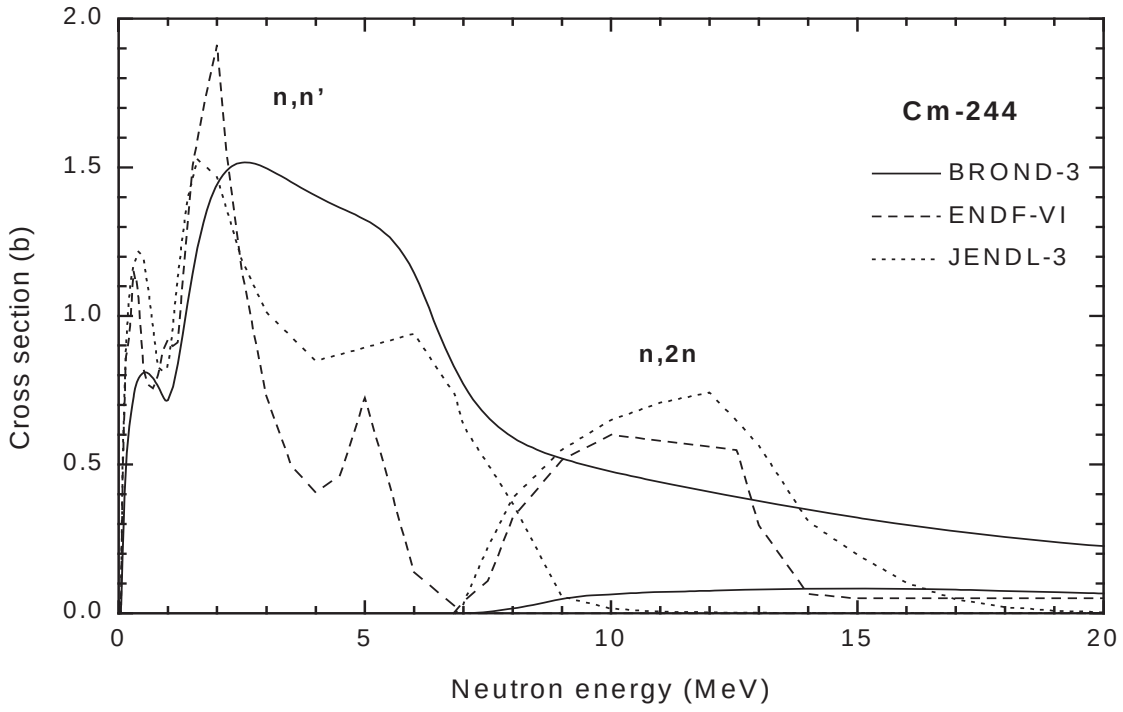

Fig. 4. Comparison of the evaluated inelastic and (n,2n) reaction cross sections for ^{244}Cm.

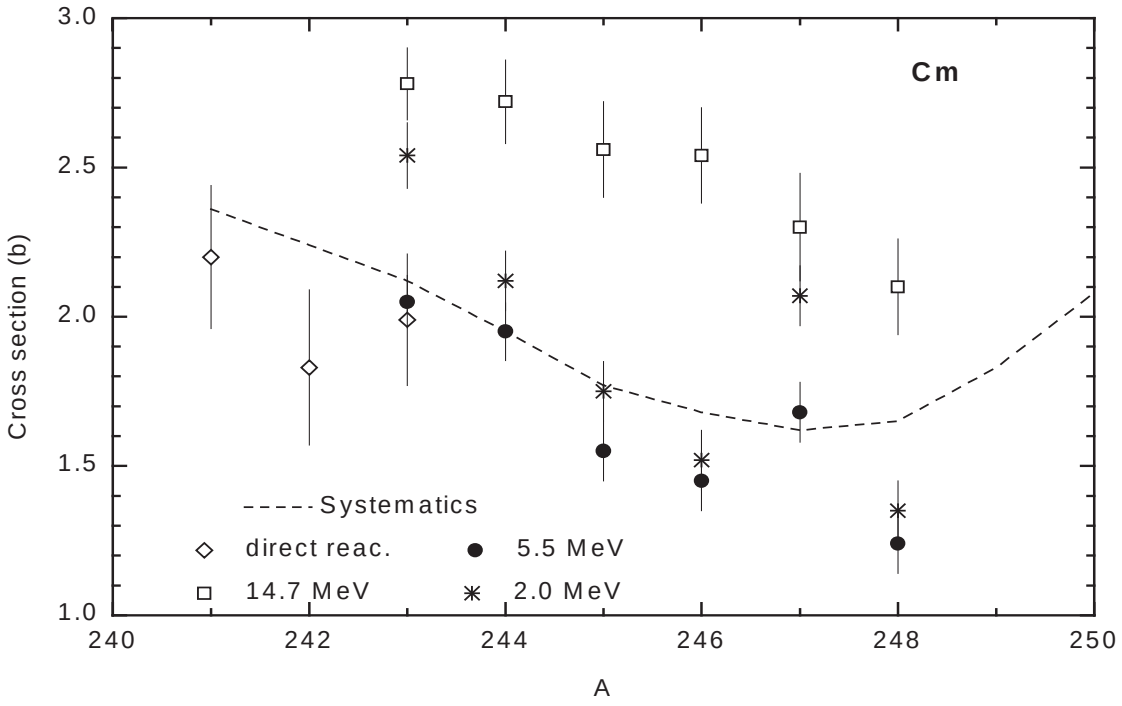

Fig. 5. Experimental data sets on the fission cross sections for curium isotopes at the neutron energies 2.0 (∗), 5.5 (•) and 14.7 (□) MeV. Dashed line corresponds to the systematics of the first plateau proposed in Ref. [125].

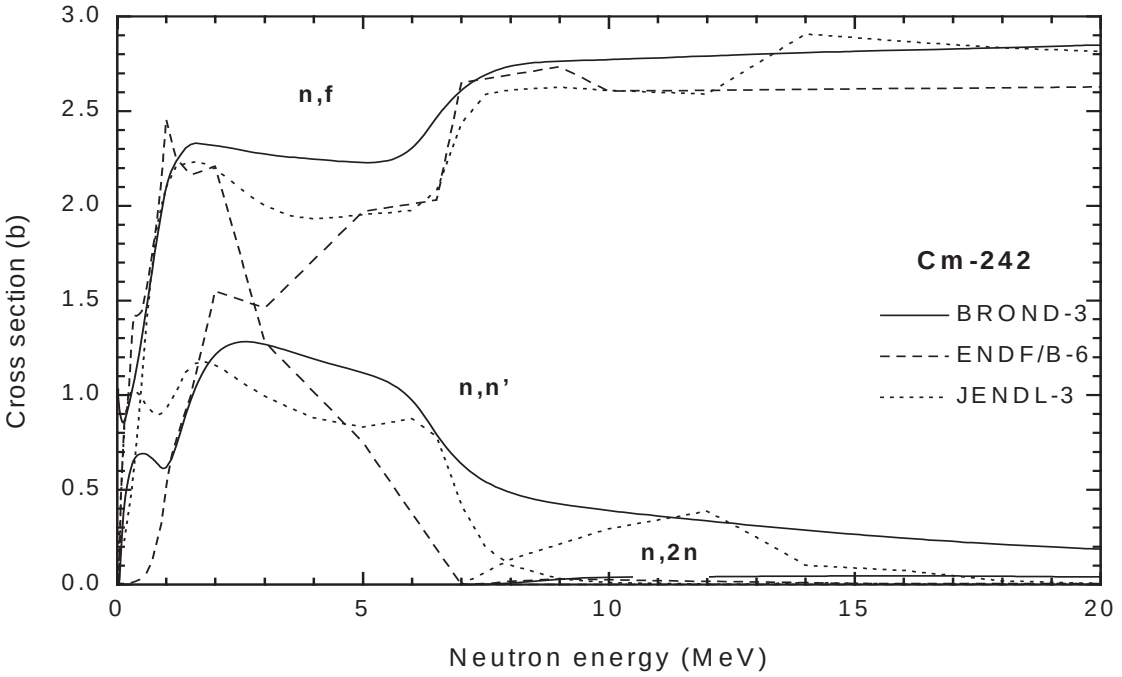

Fig. 6. Comparison of the evaluated fission, inelastic and (n,2n) reaction cross sections for ^{242}Cm.

References

[1] V.M. Maslov et al. Report INDC(BLR)-003, IAEA, Vienna, 1995.
[2] V.M. Maslov et al. Report INDC(BLR)-004, IAEA, Vienna, 1996.
[3] V.M. Maslov et al. Report INDC(BLR)-002, IAEA, Vienna, 1995.
[4] E.F. Fomushkin et al. Yadernaya Fizika (Sov.), 1967, v.5, p.966.
[5] R.R. Fullwood, D.R. Dixon. Report LA-4420, 1970.
[6] M.S. Moore, G.A. Keyworth. Phys.Rev., 1971, v.C3 (4), p.1656.
[7] M.G. Silbert Report LA-6239-MS, 1976.
[8] E.F. Fomushkin et al. Yadernaya Fizika (Sov.), 1980, v.31 (1), p.39.
[9] P.D. Knootz, D.M. Barton. In: Proc. Conf. on Neutron Cross Sections and Technology (Washington, 1968), v.1, p.597.
[10] P.E. Vorotnikov et al. Atomnaya Energiya, 1984, v.57 (1), p.61.
[11] E.F. Fomushkin et al. VANT, Ser. Nuclear Constants, 1992, is.1, p.5.
[12] E.F. Fomushkin et al. In: Proc. Conf. Nucl.Data for Science and Technology (Trieste, 1997), v. 1, p. 462.
[13] P.E. Vorotnikov et al. Yadernaya Fizika, 1984, v.40, p.1141.
[14] A.V. Ignatyuk, V.M. Maslov. VANT, Ser. Nuclear Constants, 1986, is.4, p.43.
[15] L.A. Bakhanovich et al. VANT, Ser. Nuclear Constants, 1989, is.1, p.36.
[16] V.M. Kupriyanov et al. Yadernaya Fizika, 1984, v.39, p.281.
[17] H. Britt, J. Wilhelmy. Report LA-UR79-614, 1981.
[18] Final Technical Report on Project ISTC 304-95, Obninsk, 1997.

00-30130 [6]
Translated from Russian

UDC 539.171.017

EVALUATION OF THE TOTAL GAMMA-RAY PRODUCTION CROSS-SECTIONS FOR NONELASTIC INTERACTION OF FAST NEUTRONS WITH IRON NUCLEI

M.V. Savin, Yu.Ya. Nefedov, A.V. Livke, A.G. Zvenigorodskij
Russian Federal Nuclear Centre - All-Russia Scientific Research Institute for Experimental Physics, Sarov

EVALUATION OF THE TOTAL GAMMA-RAY PRODUCTION CROSS-SECTIONS FOR NONELASTIC INTERACTION OF FAST NEUTRONS WITH IRON NUCLEI. Experimental data on the total gamma-ray production cross-sections for inelastic interaction of fast neutrons with iron nuclei were analysed. The total gamma-ray production cross-sections, grouped according to Eγ, were evaluated in the neutron energy range 0.5-19 MeV. The statistical spline approximation method was used to evaluate the experimental data. Evaluated data stored in the ENDF, JENDL, BROND, and other, libraries on gamma-ray production spectra and cross-sections for inelastic interaction of fast neutrons with iron nuclei were analysed.

As will be shown below, the evaluated data on γ-ray production cross-sections in various libraries (ENDF, JENDL, BROND and others) differ considerably. Possible reasons for this are that the experimental data available at the time the evaluations for the various libraries were made were insufficient and also the results obtained by the different authors diverged by amounts greater than the measurement errors given. Recently, more experimental work has been done improving earlier results. Several authors (C.G. Hoot, V.J. Orphan et al. [1-2], J.K. Dickens et al. [3], G.T. Chapman et al. [4]) have, in their later papers, published data for iron which differ from the data they published earlier by ~(20-50)%. Under the circumstances, there is a need to try and obtain more reliable γ-ray production spectral distributions and cross-sections. The present paper analyses the evaluated data for γ-ray production spectra and cross-sections for inelastic interaction of neutrons with iron nuclei contained in the various libraries and compiles the available experimental data.

The numerical experimental material is derived mainly from the EXFOR library and from tables published in the original papers.

Brief summary and analysis of the experimental data

There is a large body of experimental work on investigation of the γ-rays produced during inelastic interaction of neutrons with iron nuclei. The aim here is not to give a complete bibliography of the investigations carried out. Our attention is focused mainly on recent papers in which the total γ-ray production cross-sections have been measured (sum of the γ-lines and continuum).

Total γ-ray production cross-sections were first measured by Perkin [5], who studied continuous distribution gamma-ray spectra for a number of nuclei, including iron at the neutron energies 3.5, 5.5, 6.5, 7.5 and 8.5 MeV. The work was done on a Van de Graaff accelerator using a gas target to obtain (p,T) and (d,D) reaction neutrons. The γ radiation was recorded using a three crystal pair spectrometer based on NaI(Tl) scintillators at an angle of 90º to the charged particle beam axis. The sample, made of natural iron in the form of a hollow cylinder 2 cm high and with external and internal diameters of 2 and 1 cm, respectively, was placed near the neutron target. An all-wave counter was used to monitor the neutron flux. The γ-ray spectra were normalized with respect to the 2.62 MeV and 4.43 MeV γ-line production cross-section of lead and carbon, respectively. Corrections for in-sample neutron and γ-ray attenuation and multiple scattering were calculated using the Monte Carlo method. The correction for the γ-rays formed in the crystal through the interaction of neutrons scattered in the sample, was determined by recording γ-ray spectra at 90º and 0º to the axis of the charged particles with subsequent correction of the spectra using the angular dependence of elastic and inelastic neutron scattering cross-sections. It should be noted that this method can lead to large uncertainties in the γ-ray spectrum, particularly in the low energy region.

C.G. Hoot, V.J. Orphan et al. [1-2] performed measurements on the linear electron accelerator at the IRT (Intelcom Radiation Technology, San Diego, California) laboratory in the neutron energy range 0.86-16.74 MeV using the time-of-flight method for selecting the neutron energy. The sample, which was ring-shaped ($\varnothing_{ext}$ = 48.3 cm, $\varnothing_{int}$ = 27.9 cm) was placed at a distance of 51.85 m from the accelerator target. The γ-rays were recorded on a Ge(Li) detector (V = 80 cm^3), placed on the axis of the neutron beam such that the average γ-ray detection angle was 125º. The neutron beam incident on the sample at $E_n > 1$ MeV was measured by the time-of-flight method using a calibrated NE-211 scintillation detector (∅ = 5.08 cm, h = 5.08 cm) and with a calibrated lithium scintillation glass detector in the $E_n < 3$ MeV region. The uncertainties in determination of the neutron flux and its shape were < 3%. The curve for the γ-ray detector efficiency was measured with an uncertainty of ± 5% for $E\gamma \leq 2.754$ MeV and ~ 8% for higher energies. A beryllium sample was used to determine the background. Corrections were made for system "dead time", and for neutron and γ-flux attenuation and scattering in the sample. The error introduced by the correction for γ-ray attenuation was approximately ± 2%, and for neutron attenuation and multiple scattering ± 3%. The data published in Ref. [1] and contained in the EXFOR-10219 experimental data library differ by up to 25% from the results published by the same authors later in Ref. [2]. We could not find any explanation in this regard. We took the results given in the later paper [2] as the main ones. The tables of results in Ref. [2] give no indication of the measurement uncertainties. In our evaluation we used the uncertainties indicated in Ref. [1].

In the paper by J.K. Dickens et al. [3] the γ-ray production cross-sections for neutron interaction with iron nuclei were measured on the continuous neutron spectrum of the ORELA accelerator in the energy range E_n = 0.8-20 MeV using the time-of-flight method with a resolution < 5 ns. Gamma-rays with an energy of 0.7-10 MeV were detected by means of an NaI(Tl) crystal (∅ = 12.7 cm, h = 12.7 cm) in lead shielding placed 140 cm away from the sample at an angle of 125º to the neutron beam. The crystal was shielded against neutrons scattered from the sample by a 25 cm thick LiH slab. The response function of the gamma-spectrometer in the $E\gamma$ = 0.66-6.13 MeV range was measured in real geometry using calibrated γ-sources instead of the sample. At energies $E\gamma$ = 6.13-10.6 MeV the response

function was determined by measuring the neutron capture γ-ray spectrum. The sample, made of natural iron in the form of a 30 x 30 x 0.64 cm slab, was placed at a distance of 47 m from the accelerator target. The neutron flux to the sample was measured by the time-of-flight method using a calibrated scintillation counter based on an NE-213 detector (∅ = 4.65 cm, h = 4.2 cm).

G.T. Chapman et al. [4], using the same method with minor changes, repeated the measurements on iron and obtained γ-ray production cross sections which, for the entire neutron energy range, were about 1.5 times lower than those obtained by Dickens [3]. The authors of Ref. [4] made a detailed analysis of the experimental set-up used in both cases and performed additional calibrating measurements. However, the authors of Ref. [4] were not able to give a fully satisfactory explanation for the variance between the data for iron and suggested that Ref. [3] apparently indicated no "dead time" for neutron detection.

In our evaluation we used Chapman's results [4] (EXFOR-10580) since they were obtained later than those in Ref. [3]. The error indicated in the tables includes statistical errors and inaccuracies in calculation of the corrections for γ-ray and neutron absorption in the sample and detection of annihilation γ-rays. This error does not include the 10% systematic error associated mainly with determination of the neutron flux.

E. Tanabe et al. [6] performed measurements at neutron energies of 6-33 MeV on the Tohoku University cyclotron (Japan) using the (p,n) reaction on a beryllium target at a proton energy of 35 MeV. The iron sample, in the form of a slab measuring 20 x 20 x 2 cm, was placed at a distance of 12.09 m from the cyclotron target. Gamma-radiation from the sample in the energy interval Eγ = (1.575-10.5) MeV was measured with a BGO scintillator (∅ = 5.08 cm, h = 2.54 cm) placed at a distance of 55 cm from the sample at an angle of 144º to the neutron beam axis. The response function of the BGO scintillator was calculated by the Monte Carlo method. The neutron flux to the sample was measured by the time-of-flight method using an NE-213 scintillator (∅ = 7.62 cm, h = 7.62 cm). According to the evaluations of the authors of Ref. [6], the measurement errors comprise: determination of the neutron flux - 10%, the detector response matrix - (1-3)%, counting statistics ~ 1%; the error levels of corrections for neutron and γ-ray interaction in the sample are negligible. The total error was evaluated automatically when reconstructing the γ-ray spectrum.

In a number of papers total γ-ray production cross-sections were measured on monoenergetic neutrons. D.M. Drake et al. [7-8] (EXFOR 10025, EXFOR 10684) measured the total production cross-sections of γ-rays with an energy of 0.5-6.75 MeV at neutron energies of 4, 5.74, 7.2, 7.67 and 14.2 MeV at a γ-ray angle of emission from the sample of 55º in relation to the neutron beam axis. In addition, at neutron energies 6.0 and 7.5 MeV the differential cross-sections dσ/dΩ/dE were measured at angles of 39º, 55º, 72º and 90º. The measurements were carried out on the 8.0 MeV pulsed Van de Graaff accelerator at Los Alamos. The duration of the charged particle beam pulse was < 1 ns. The gamma radiation was detected using an NaI(Tl) crystal (∅ = 5.8 cm, h = 15.2 cm). To reduce the Compton scattering contribution to the spectrometer response function, the crystal was placed in an NaI(Tl) annulus (∅ = 20.3 cm, h = 30.5 cm). The background from neutrons scattered on the sample was excluded by the time-of-flight method with a resolution of ~ 3 ns. The neutron flux on the sample was measured using a (ΔE-E) proton recoil telescope. An

NE-102A plastic scintillator was used to monitor the neutron flux. The gamma detector response function at all energies in the range under investigation (response matrix) was in the form of an analytical expression for each γ-ray energy with 10 parameters, which were determined by applying the least squares method to the experimental response functions obtained on isotope sources. No measurement errors are given in the tabular data in the paper.

From analysis of Fig. 2 in Ref. [7] it can be assumed that there was insufficient γ-ray and neutron separation in the experiment and this might have led to an additional systematic error.

Sukhanov et al. [9] measured total γ-ray production cross-sections at a neutron energy of 14 MeV. The measurements were performed in a ring geometry and the γ -rays were detected at an average angle of 85º to the neutron beam axis. To measure the γ-ray spectra in the 0.5-2.5 MeV energy region, a dual detector Compton spectrometer based on stilbene crystals with n-γ separation was used, and for γ-rays - (1.5-10) MeV - a pair spectrometer based on three NaI(Tl) crystals was used. The paper does not analyse the corrections and errors. Account was taken of the contribution of neutrons scattered on the sample by taking measurements on a carbon sample. This method contains many uncertainties.

S. Hlavac and P. Oblozinsky [10-11] measured γ-ray production cross-sections of iron on neutrons with an energy of 14.6 MeV, applying the time-of-flight method based on (α-n-γ) coincidences to separate the neutrons and γ-rays from the sample. The neutron generator was operated in static mode. For the measurements, five detectors were used simultaneously: a $T(d,n)^4He$ reaction α-particle detector - a 0.1 mm thick scintillation film with a photomultiplier; Ge(Li) (70 cm^3) and NaI(Tl) (∅ = 160 mm, h = 100 mm) γ-ray detectors in a coincidence arrangement; a detector of secondary reaction neutrons - an NE-213 liquid scintillator; and a primary neutron detector - a stilbene crystal. The neutron flux on the sample was measured in two ways: by counting the associated α-particles and using a calibrated stilbene crystal. The error level for determination of the neutron flux was 4%. The detector combination used enabled discrete γ-line production cross-sections, γ-ray production cross-sections of the continuous spectrum and γ-ray multiplicity depending on the neutron energy escaping from the composite nucleus to be obtained. The sample weighed 232 g. The γ-rays were detected at an angle of 90º to the neutron flux direction. There was a ± 5% error in determining the γ-ray detector efficiency. The total measurement error, without taking into account the error introduced by the spectrum reconstruction procedure, was 7-12%. The time-of-flight method is used to separate the neutrons and γ-rays from the sample. There is, however, some doubt that, with the detector-sample distance of 30 cm and temporal resolution of 7.5 ns indicated in the paper, separation is adequate and there would be no additional uncertainties in the cross-section value.

Yu.Ya. Nefedov et al. [12] measured the total γ-ray production cross-sections of natural iron. The measurements were made using the time-of-flight technique on an OI-G-18 reference neutron source [13], based on an NG-150M high-current neutron generator. The 14.31 MeV neutron flux on the sample disc (150 mm in diameter, 4.1 mm thick) was measured using an enhanced efficiency proton telescope, calibrated in accordance with a reference telescope. The error for determination of the neutron fluence at the sample location was ± 3% (P = 0.95). The γ-rays from the sample were detected using an NaI(Tl) crystal scintillation detector (∅ = 15 mm, h = 100 mm), positioned at an angle of 125º to the neutron

beam axis at a distance of 8 m from the sample behind a concrete wall with a collimator. The spectrometer response function was determined by means of Monte Carlo calculations and tested against the experimental response functions, measured on isotopic sources in real geometry. The neutron generator was operating in pulsed mode. The duration of the neutron pulse was 30 ns which, for a flight basis of 8 m, ensured reliable separation of the neutron and γ-radiation detected by the γ-spectrometer. The total measurement error comprised the error in determining the neutron fluence, the spectrometer calibration (response function), corrections for multiple scattering and absorption of neutron and γ-rays in the sample, and statistical errors.

I. Murata et al. [14] measured γ-ray production cross-sections for a number of elements on the OKTAVIAN pulsed neutron source at Osaka University, Japan, at the neutron energy E_n = 14.6 MeV. The measurements were made using the time-of-flight technique on an NaI(Tl) crystal (∅ = 12.7 cm, h = 12.7 cm) placed at a distance of 316 cm from the sample at an angle of 125º to the direction of the neutron flux. The neutron pulse duration was 3 ns. The neutron flux on the sample was measured using an NE-213 liquid scintillator placed 4 m away by means of the time-of-flight method and separation of neutron and γ-radiation according to the pulse shape.

K. Hasegawa et al. [15] have reported the results of measurements of total γ-ray production cross-sections for iron on neutrons with energies of 7.8, 10.0, 11.5 and 13.0 MeV with a γ-ray emission angle of 90º, and also at an angle of 125º at E_n = 11.5. MeV. The measurements were performed on a 14 MeV pulsed neutron generator (JAERI, Japan). The γ radiation was detected using an NaI(Tl) crystal, (∅ = 7.6 cm, h = 15.2 cm), which was surrounded with an NaI(Tl) crystal annulus to suppress Compton scattering in the background (∅ = 25.4 cm, h = 25.4 cm). The gamma detector was placed 80 cm from the sample. The neutron pulse duration was ~ 4-9 ns. The neutron flux on the cylindrical sample (∅ = 3 cm, h = 3 cm) was measured by the time-of-flight method using an NE-213 liquid scintillator .

At our request, Drs Murata and Hasegawa kindly provided us with numerical material obtained from their measurements.

Evaluation

Since our main comments on the experimental data were made in the description of the experimental set-up, in this section we will include only additional procedures and assumptions made during the evaluations.

Statistical approximation of the data files was carried out using splines. Given satisfactory data, the spline approximation program developed by V.A. Zherebtsov [16] produces reliable smoothed curves with automatic selection of spline knots. In addition, when making an evaluation, a set of experimental data can be described more accurately by changing the weight of certain data and/or additional selection of knots and boundary conditions. The results of the spline approximations are presented in the form of tables of knot and coefficient values of spline polynomials from which the value of the function $S_i(h)$ can be calculated at any point using the expression:

$$S_i(h) = A_o + A_1h + \ldots..A_nh^n, \quad (1)$$

where $h = X - X_i$, and X_i is the left boundary (knot) of the corresponding interval. The last column of the table gives the errors of the results in the knot (interpolation between knots is linear).

All the experimental data were brought into a single energy grid: $E\gamma$ = 0.5-0.75-1.0-1.5-2.0-2.5-3.0-4.0-5.0-6.0-7.0-8.0-10.0 MeV. The spectral distribution in most experimental work is presented in the form of a histogram with even or uneven spacing and so transformation into another grid was done by simple summing the data within the new spacing (grid). At interval boundaries which did not coincide with the boundaries of the original intervals, a linear approximation of the initial data was performed at three points located in the middle of each interval with integration in the new boundaries with retention of the areas. The statistical errors of the results in the new grid were determined as the square root of the sum of the squares of the errors of the summed intervals. The systematic errors were used as weighting factors in spline approximation of the data. The tables in Ref. [2] give experimental results without indicating the errors; we assumed that the errors were the same as in Ref. [1] published previously by the same authors.

The experimental data obtained for (d,T) neutrons in the E_n = 14-15 MeV region in all the γ-ray energy intervals are systematically lower than the results obtained for the white neutron source of a linear electron accelerator using the time-of-flight technique. The reason for this may be either that the γ-ray background from nonelastic interaction of neutrons with the elements of the γ-spectrometer has not been taken fully into account in the white neutron source measurements, or inaccuracy in determining the integral neutron flux on the sample and, no less important, the uniformity of its distribution on the sample surface in experiments on (d,T)-neutrons because of the "solid" measurement geometry. In our view, the most accurate results in this regard are Nefedov's [12], who determined the neutron flux using a metrologically certified proton telescope, and for this reason we assigned the greatest weight to these data for statistical approximation.

The total γ-ray production cross-sections are made up of the discrete γ-line and continuum production cross-sections. Discrete radiation has a specific angular anisotropy, whereas the continuum is basically isotropically irradiated. The γ- rays in the experiments were detected at various angles with respect to the direction of the neutron flux on the sample. Since the γ spectrum is averaged over many lines in the neutron energy region $E_n \geq 3$ MeV, all the results were, for comparison, multiplied by 4π without making allowance for angular dependency except for the energy range ΔE_γ = 0.75-1.0 MeV, where the 846.8 keV γ-line angular dependency was used.

The evaluated total γ-ray production cross-sections for inelastic interaction of neutrons with iron nuclei are given in Figs 1-13 and in Table 1, and the spline coefficient values are given in Table 2.

The main features of the data in the ΔE_γ intervals, and their evaluation, are:

In the Eγ = 0.5-0.75 MeV interval (Fig. 1) there are very few data. As can be seen from Fig. 1, there is considerable scatter of the data, particularly at neutron energies near 15 MeV. For E_n > 15 MeV there are no data whatsoever;

In the Eγ = 0.75-1.0 MeV interval (Fig. 2) at neutron energies ≤ 3 MeV the total γ-ray production cross-section should, basically, coincide with the 846.8 keV γ-line production cross-section, since for even iron isotopes the continuous excitation spectrum region is high. The small contribution of ^{57}Fe in this energy region is barely noticeable. Clearly, in this γ-ray energy range it would have been possible to take as the total cross-sections for E_n ≤3 MeV the evaluated data for the 846.8 keV γ-line with all its irregularities and angular dependences;

In the Eγ = 1.0-1.5 MeV interval (Fig. 3) the experimental data show good agreement with each other except for the results in Refs [11] and [14], which are considerably lower than the other sets of data at neutron energies near 15 MeV;

In the Eγ = 1.5-2.0 MeV interval (Fig. 4) the experimental data show reasonable agreement with each other except for Perkin's results [5], which are considerably higher than the overall data set. In the spline approximation, little weight was given to Perkin's data;

In the E_γ = 2.0-2.5 MeV interval (Fig. 5) the data taken from Tanabe et al. [6] are 1.3-1.5 times higher that the other authors' results. At the same time, in the 2.5-3.0 MeV interval these authors' data is 1.5-2 times lower than the others. Clearly, in processing the measurement results a redistribution of events with respect to the intervals occurred;

In the E_γ = 2.5-3.0 MeV interval (Fig. 6) Chapman's data [4] are considerably higher than the data of Orphan [2], Hasegawa [15] and the set of measurement results for 14 MeV neutrons. The energy trend of the approximating curve is mainly determined by Chapman's detailed data [4], but at neutron energies of E_n > 8 MeV the evaluated curve is considerably lower than the results in [4], owing to the great weight of data near $E_n \cong 15$ MeV and the good agreement of the data produced by Orphan [2] and Hasegawa [15] with the E_n = 15 MeV results. The same is true of the results in the γ-ray energy ranges Eγ = 3-4 MeV (Fig. 7), Eγ = 4-5 MeV (Fig. 8), Eγ = 5-6 MeV (Fig. 9) and Eγ = 6-7 MeV (Fig. 10);

In the E_γ = 7-8 MeV interval (Fig. 11) the data show considerable scatter. The approximating curve was based on Nefedov's results [12] and less weight was given to Hlavac's data [11];

In the E_γ = 8-10 MeV interval (Fig. 12) there are very few data. Nevertheless, the approximating curve looks plausible.

Figure 13 shows the total γ-ray production cross-sections integrated with respect to Eγ in the 0.5-10.0 MeV range (the γ-ray detection thresholds in keV are given in parentheses). As well as the experimental data, the figure shows the total γ-ray production cross-section

contained in the following libraries: BROND-2 (2601 material), ENDF/B-V (1326 material), JENDL-3.2 (2600 material), JEF-2 (2631 material) - photon production cross-section averaged for iron isotopes with the weights ^{54}Fe-0.0581, ^{56}Fe-0.9164, ^{57}Fe-0.0221. As can be seen from Fig. 13, there is very great disparity between the total γ-ray production cross-sections given in the libraries, particularly in the neutron energy regions near and above the inelastic (n,2n) and (n,p) reaction channels. The data in the JENDL-3.2 library are much too high compared with the experimental results.

Conclusion

The present paper collects and analyses experimental results for differential and integral γ-ray production cross-sections of iron with energies of 0.5-10.0 MeV in the 0.5-20.0 MeV neutron energy range. An evaluation is made of total γ-ray production cross-sections in the 0.5-19.0 MeV neutron energy range and presented in Eγ groups. From the results of the analyses performed the following conclusions may be drawn:

- The evaluated data for the total γ-ray production cross-sections on iron given in the ENDF, BROND, JENDL, and other, libraries, show considerable scatter, particularly in neutron energy regions near and above the inelastic (n,2n) and (n,p) reaction channels. For example, the data in the JENDL-3 library are ~1.5 times higher than the overall set of experimental results. In our view, the γ-ray production multiplicity values in the JENDL library are far too high. The data in the JEF-2 library are obtained from Hauser-Feschbach model calculations and relate only to inelastic neutron scattering. Even taking this into account, the JEF-2 library data are particularly low. This is especially true of the neutron energy region below 10 MeV, where inelastic scattering is the main neutron interaction process with γ-ray production;

- The data in the BROND-2 and ENDF/B-V libraries correspond more closely than the rest to the experimental data;

- Taken as a whole, the experimental data show satisfactory agreement amongst themselves except for isolated results. There is a large scatter of data for total γ-ray production cross-sections near E_n = 14 MeV. The measurements on (d,T) neutrons clearly contained some inaccuracies in determination of the neutron fluxes on the sample; this is perfectly possible considering the small distances from the source to the sample for the measurements. The most correct results appear to be those obtained by Nefedov's group [12], where total neutron emission was determined with high accuracy, and where Monte Carlo type calculations were used to establish with greater accuracy the actual number of interactions in the sample (neutron flux on the sample).

Table 1

Total γ-ray production cross-sections for inelastic interaction of neutrons with nuclei of natural iron [mb]

E_n, MeV	E_γ, MeV												
	0.5-0.75	0.75 -1.0	1.0 -1.5	1.5 -2.0	2.0 -2.5	2.5 -3.0	3.0 -4.0	4.0 -5.0	5.0 -6.0	6.0 -7.0	7.0 -8.0	8.0-10.0	Sum
0.80		119.19											119.19
1.00		238.31	2.88										241.19
1.20		363.49	3.69										367.19
1.40		490.85	8.90										499.75
1.60		616.38	18.35										634.72
1.80		736.09	31.71										767.80
2.00		846.00	48.71	0.00									894.70
2.20		942.10	69.02	3.38									1014.50
2.40		1020.42	92.35	18.99									1131.76
2.60		1076.95	118.38	39.98	9.54								1244.86
2.80		1110.48	146.83	64.69	29.87								1351.87
3.00		1137.79	177.38	91.45	56.79								1463.41
3.20		1162.51	209.73	118.62	86.43	10.03							1587.31
3.40		1184.76	243.57	144.71	115.19	34.21	12.18						1734.62
3.60		1204.67	278.61	169.34	141.90	61.12	41.82						1897.45
3.80		1222.36	314.53	192.55	166.60	86.13	73.14						2055.32
4.00	31.62	1237.97	351.04	214.38	189.38	108.82	103.82						2237.02
4.20	40.39	1251.60	387.83	234.88	210.31	129.30	132.91						2387.22
4.40	49.81	1263.40	424.59	254.08	229.45	147.73	160.42	0.81					2530.29
4.60	59.82	1273.47	461.03	272.03	246.89	164.23	186.38	2.25					2666.11
4.80	69.15	1281.96	496.84	288.77	262.69	178.95	210.86	6.61					2795.83
5.00	78.74	1288.99	531.71	304.34	276.93	192.01	233.89	13.38					2919.99
5.20	89.07	1294.67	565.34	318.79	289.69	203.57	255.51	22.04					3038.67
5.40	100.04	1299.14	597.43	332.15	301.03	213.76	275.77	32.07	4.53				3155.92
5.60	111.59	1302.52	627.67	344.46	311.03	222.70	294.72	42.96	10.22				3267.87
5.80	123.62	1304.93	655.82	355.77	319.76	230.55	312.41	54.20	16.12				3373.18
6.00	136.06	1306.50	681.90	366.12	327.30	237.43	328.86	65.27	22.23				3471.69
6.20	148.82	1307.37	706.02	375.56	333.71	243.49	344.14	75.91	28.51				3563.52
6.40	161.83	1307.64	728.26	384.11	339.08	248.87	358.28	86.10	34.93				3649.09
6.60	175.00	1307.44	748.73	391.83	343.47	253.69	371.33	95.85	41.47				3728.81
6.80	188.25	1306.91	767.52	398.76	346.96	258.09	383.33	105.15	48.10	3.01			3806.10
7.00	201.50	1306.17	784.73	404.94	349.62	262.17	394.34	114.02	54.80	8.98			3881.26
7.20	214.67	1305.34	800.46	410.40	351.53	265.92	404.38	122.45	61.53	16.66			3953.34
7.40	227.68	1304.54	814.80	415.19	352.75	269.36	413.52	130.45	68.28	25.40	4.04		4026.00
7.60	240.44	1303.91	827.85	419.36	353.36	272.47	421.78	138.02	75.02	34.55	8.84		4095.61
7.80	252.88	1303.47	839.71	422.94	353.44	275.27	429.22	145.16	81.72	43.49	13.54		4160.84
8.00	264.91	1303.12	850.48	425.98	353.05	277.75	435.84	151.87	88.35	51.91	18.14		4221.40
8.20	276.45	1302.75	860.25	428.68	352.28	279.92	441.65	158.16	94.88	59.80	22.63		4277.45
8.40	287.42	1302.25	869.11	431.30	351.19	281.77	446.67	164.04	101.30	67.18	26.99	1.05	4330.26
8.60	297.74	1301.50	877.18	433.80	349.85	283.31	450.88	169.49	107.57	74.05	31.23	1.66	4378.27
8.80	307.33	1300.38	884.54	436.14	348.35	284.54	454.31	174.53	113.68	80.44	35.33	3.68	4423.24
9.00	316.10	1298.79	891.29	438.27	346.74	285.46	456.97	179.16	119.58	86.34	39.28	6.88	4464.86

$E_{n,}$ MeV	E_{γ}, MeV												
	0.5-0.75	0.75 -1.0	1.0 -1.5	1.5 -2.0	2.0 -2.5	2.5 -3.0	3.0 -4.0	4.0 -5.0	5.0 -6.0	6.0 -7.0	7.0 -8.0	8.0-10.0	Sum
9.20	323.98	1296.60	897.53	440.13	345.12	286.07	458.84	183.38	125.26	91.78	43.07	11.04	4502.82
9.40	330.89	1293.72	903.35	441.68	343.42	286.38	459.96	187.20	130.69	96.76	46.70	15.95	4536.68
9.60	336.73	1290.02	908.77	442.86	341.26	286.38	460.31	190.61	135.84	101.30	50.16	21.38	4565.62
9.80	341.44	1285.38	913.74	443.64	338.65	286.07	459.92	193.62	140.68	105.40	53.44	27.12	4589.09
10.00	344.92	1279.70	918.19	443.95	335.59	285.46	458.78	196.23	145.20	109.07	56.53	32.95	4606.58
10.20	347.11	1272.87	922.08	443.75	332.13	284.56	456.90	198.45	149.36	112.34	59.42	38.64	4617.60
10.40	347.91	1264.76	925.35	442.99	328.28	283.35	454.30	200.27	153.13	115.20	62.11	43.98	4621.63
10.60	347.25	1255.27	927.93	441.63	324.08	281.84	450.97	201.70	156.50	117.67	64.58	48.90	4618.31
10.80	345.04	1244.28	929.77	439.60	319.53	280.03	446.93	202.75	159.43	119.76	66.83	53.40	4607.36
11.00	341.20	1231.67	930.82	436.87	314.67	277.93	442.18	203.41	161.90	121.49	68.85	57.49	4588.49
11.20	335.66	1217.34	931.02	433.38	309.53	275.54	436.73	203.69	163.88	122.86	70.63	61.17	4561.41
11.40	328.33	1201.17	930.30	429.08	304.13	272.85	430.58	203.59	165.35	123.88	72.17	64.44	4525.86
11.60	319.27	1183.05	928.62	423.93	298.49	269.86	423.75	203.11	166.28	124.57	73.44	67.31	4481.69
11.80	308.73	1162.85	925.92	417.87	292.63	266.59	416.25	202.26	166.64	124.94	74.46	69.80	4428.94
12.00	296.94	1140.48	922.14	410.86	286.59	263.03	408.07	201.04	166.46	124.99	75.20	71.90	4367.69
12.20	284.14	1117.34	917.22	402.85	280.39	259.19	399.22	199.44	165.76	124.75	75.65	73.62	4299.58
12.40	270.58	1094.85	911.10	393.79	274.06	255.10	389.72	197.49	164.58	124.21	75.82	74.97	4226.26
12.60	256.49	1073.04	903.74	383.62	267.61	250.77	379.57	195.16	162.94	123.40	75.70	75.95	4147.99
12.80	242.12	1051.91	895.06	372.55	261.07	246.24	368.77	192.48	160.88	122.31	75.30	76.58	4065.28
13.00	227.71	1031.47	885.03	361.27	254.47	241.52	357.34	189.44	158.42	120.98	74.63	76.85	3979.12
13.20	213.50	1011.73	874.39	349.84	247.83	236.64	345.28	186.05	155.59	119.40	73.72	76.77	3890.75
13.40	199.74	992.70	863.84	338.32	241.19	231.62	332.84	182.30	152.42	117.58	72.58	76.35	3801.47
13.60	186.66	974.38	853.41	326.76	234.55	226.49	320.78	178.20	148.94	115.54	71.23	75.59	3712.52
13.80	174.51	956.79	843.15	315.19	227.95	221.26	309.16	173.76	145.18	113.29	69.67	74.50	3624.41
14.00	163.52	939.94	833.11	303.68	221.42	215.96	297.99	168.97	141.16	110.84	67.94	73.09	3537.61
14.20	153.95	923.83	823.33	292.25	214.97	210.61	287.26	163.87	136.93	108.20	66.03	71.39	3452.64
14.40	146.03	908.48	813.87	280.96	208.64	205.25	277.00	158.59	132.50	105.39	63.98	69.42	3370.10
14.60	140.00	893.89	804.76	269.86	202.44	199.88	267.21	153.16	127.92	102.41	61.80	67.21	3290.51
14.80	136.03	880.07	796.07	258.99	196.40	194.53	257.89	147.62	123.19	99.27	59.49	64.79	3214.34
15.00	133.96	867.04	787.83	248.40	190.55	189.23	249.04	142.01	118.36	95.99	57.08	62.20	3141.69
15.20	133.56	854.79	780.09	238.13	184.92	184.00	240.69	136.37	113.46	92.58	54.59	59.47	3072.64
15.40		843.35	772.90	228.23	179.52	178.86	232.83	130.74	108.51	89.08	52.03	56.62	2872.65
15.60		832.72	766.31	218.75	174.38	173.83	225.47	125.15	103.54	85.52	49.41	53.69	2808.76
15.80		822.90	760.36	209.73	169.53	168.94	218.61	119.66	98.59	81.93	46.75	50.70	2747.71
16.00		813.92	755.10	201.23	164.99	164.22	212.27	114.28	93.68	78.34	44.08	47.70	2689.80
16.20		805.77	750.58	193.27	160.79	159.68	206.45	109.07	88.84	74.79	41.39	44.70	2635.34
16.40		798.47	746.85	185.92	156.95	155.34	201.16	104.07	84.10	71.31	38.72	41.74	2584.63
16.60		792.02	743.95	179.22	153.49	151.24	196.41	99.30	79.48	67.93	36.07	38.85	2537.99
16.80		786.44	741.94	173.22	150.45	147.39	192.19	94.82	75.03	64.69	33.47	36.06	2495.70
17.00		781.74	740.85	167.95	147.84	143.82	188.53	90.66	70.77	61.62	30.92	33.41	2458.09
17.20		777.91	740.73	163.48	145.70	140.54	185.41	86.85	66.72	58.74	28.45	30.91	2425.45
17.40		774.98	741.64	159.83	144.04	137.59	182.86	83.45	62.92	56.10	26.07	28.61	2398.09
17.60		772.96	743.62	157.07	142.89	134.99	180.88	80.47	59.40	53.72	23.79	26.53	2376.32
17.80		771.84	746.72	155.23	142.28	132.75	179.47	77.98	56.18	51.64	21.64	24.70	2360.44
18.00		771.64	750.98	154.37	142.23	130.91	178.65	76.00	53.30	49.89	19.63	23.16	2350.75
18.20		772.38	756.45	154.53	142.76	129.48	178.41	74.57	50.78	48.51	17.77	21.93	2347.56
140		774.05	763.18	155.75	143.91	128.49	178.77	73.73	48.66	47.52	16.08	21.05	2351.18
18.60		776.67	771.22	158.08	145.69	127.96	179.74	73.53	46.96	46.96	14.57	20.54	2361.91

E_n, MeV	E_γ, MeV												
	0.5-0.75	0.75 -1.0	1.0 -1.5	1.5 -2.0	2.0 -2.5	2.5 -3.0	3.0 -4.0	4.0 -5.0	5.0 -6.0	6.0 -7.0	7.0 -8.0	8.0-10.0	Sum
18.80		780.25	780.61	161.58	148.13	127.92	181.31	73.99	45.71	46.86	13.27	20.44	2380.06
19.00		784.77	791.37	166.27	151.26	128.38	183.50	75.16	44.94	47.25	12.19	20.78	2405.88

Table 2

Spline coefficients for describing total gamma-ray production cross-sections

Gamma-ray energy E_γ, MeV	Knot energy MeV	A_0. mb	A_1. mb/MeV	A_2. mb/MeV^2	A_3. mb/MeV^3	Error $\Delta\sigma_{n.x\gamma}$. mb in knot
0.5-0.75	4	39.72426	26.48169	14.23219	-1.694671	28.89904
	11.314	11.314	-37.29713	-22.95229	5.036199	32.12741
0.75-1.0	0.920434	190	600	96.87354	-83.17192	20
	2.70717	1096.889	149.6147	-34.69323	2.608416	50.20095
	7.531356	1304.103	-3.003366	3.057218	-2.367373	34.40215
	11.9982	1140.694	-117.3972	8.16264	0.1920175	30.6283
1.0-1.5	1.21225	3.883379	16.35994	56.45171	-6.33124	0.6047695
	5.60613	628.5609	145.7478	-27.00442	2.024082	11.11997
	9.297	900.3976	29.12752	-4.592544	-1.186779	19.82357
	12.9879	885.6698	-53.27529	0.3263598	0.9858602	26.25624
1.5-2.0	1.62875	3.101717	-72.20927	146.9519	-34.49811	1.421201
	3.22936	122.5407	133.0686	-18.70214	0.8681675	3.479485
	8.03121	426.4102	13.51291	-0.3173846	-1.026607	10.82905
	12.65523	380.6084	-55.27378	-2.73802	0.9654304	12.27029
2.0-2.5	2.21903	2.994673	-56.03705	222.9062	-80.61551	0.8709263
	3.25069	93.91022	146.4871	-26.59718	1.524892	2.655494
	9.26872	344.5676	-7.958471	-6.275572	0.5191551	7.477077
2.5-3.0	2.72721	1.027713	-95.3419	305.545	-134.548	1.108404
	3.56152	56.02717	133.5309	-31.2191	2.857305	1.689299
	6.73189	256.63	21.73712	-4.04296	0.027978	6.98354
	11.9046	264.7651	-17.8432	-3.60879	0.481236	9.403133
3.0-4.0	3.23111	-9.9223	120.6987	69.90084	-46.0514	4.55719
	3.8784	85.00281	153.3065	-19.525	0.740886	3.397029
	7.60033	423.3229	38.75502	-11.2524	0.310877	9.88796
	13.2641	338.3452	-58.7901	5.769414	0.060246	15.01314
4.0-5.0	4.238964	2.12887	-15.64161	48.15544	-10.74102	1.214867
	5.90815	60.23712	55.33983	-5.630853	0.05591577	3.101402
	14.05175	167.6728	-25.24631	-2.686676	0.8104964	4.514674
5.0-6.0	5.245716	0.3197872	26.8063	3.385416	-0.5498463	0.8053819
	11.62116	166.3403	2.925671	-7.131134	0.6105156	2.464091
6.0-7.0	6.2472	0.75506	-20.444	51.82917	-13.4862	0.8811301
	7.695482	38.89055	44.81941	-6.7665	0.232879	1.934633
	14.9369	97.05405	-16.5436	-1.70739	0.680031	3.567489
7.0-8.0	7.273477	0.9534719	24.50198	-1.03348	-0.175011	3.45245
	12.37224	75.81696	0.3135805	-3.710497	0.3341635	3.343712
8.0-10.0	8.264331	1.539119	-6.555459	22.13929	-4.572944	1.380069
	10.27116	40.58681	27.05338	-5.392056	0.1273021	3.965319
	13.83886	74.25343	-6.559979	-4.029531	0.6380777	3.405728

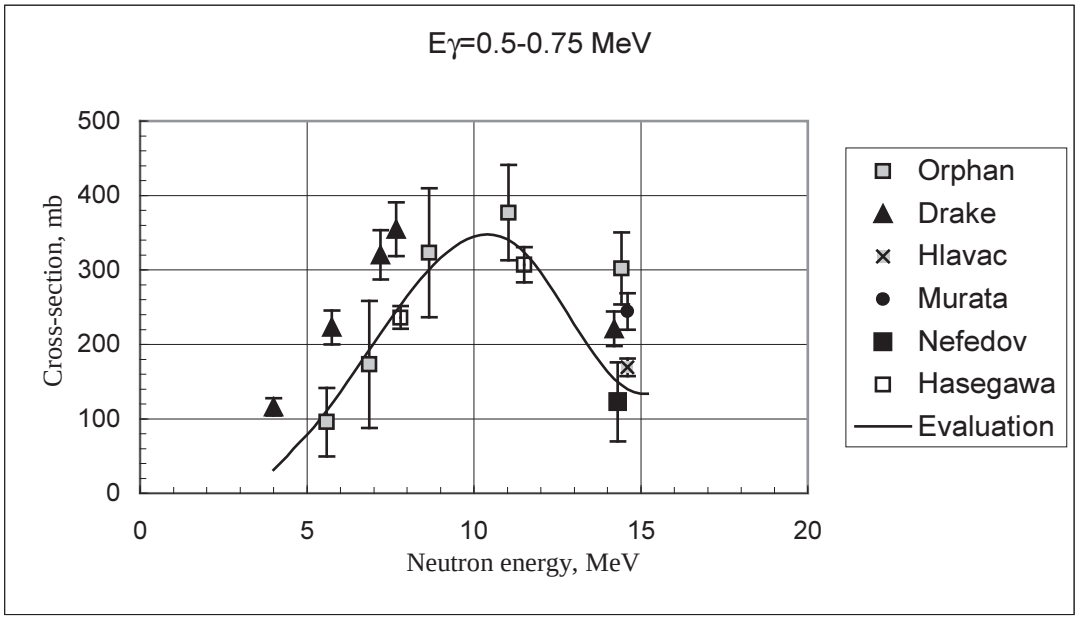

Fig. 1. Total γ-ray production cross-sections with energy 0.5-0.75 MeV.

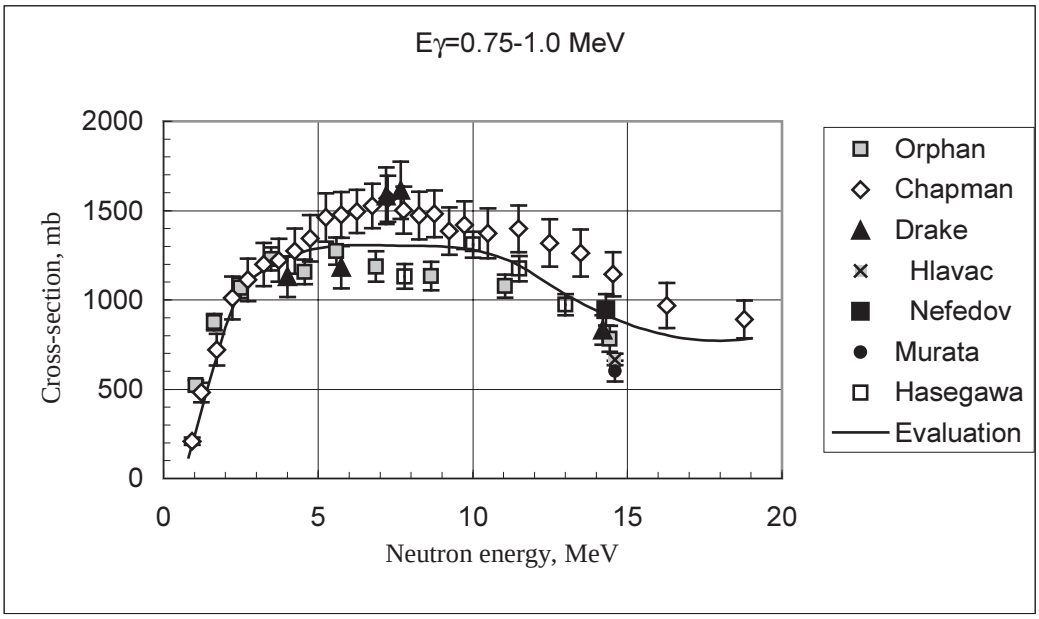

Fig. 2. Total γ-ray production cross-sections with energy 0.75-1.0 MeV.

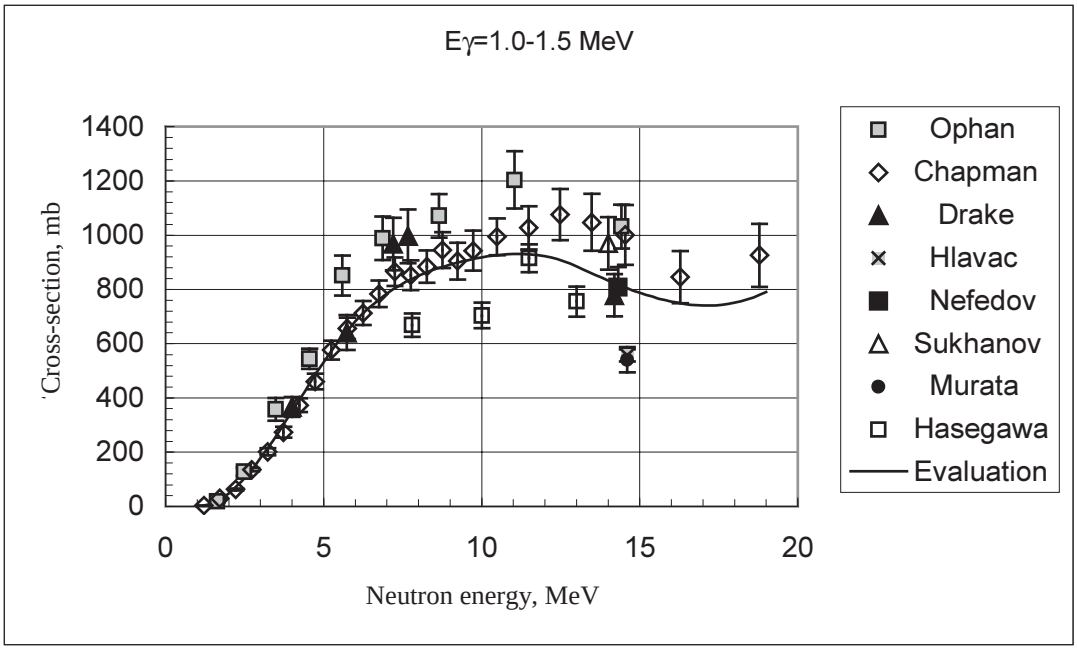

Fig. 3. Total γ-ray production cross-sections with energy 1.0-1.5 MeV.

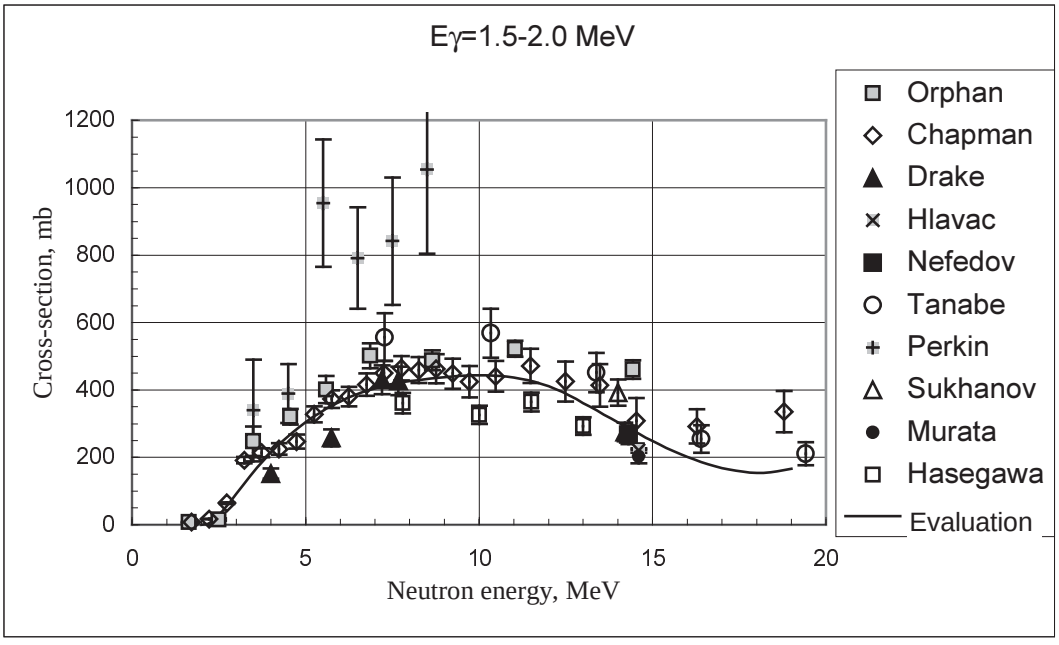

Fig. 4. Total γ-ray production cross-sections with energy 1.5-2.0 MeV.

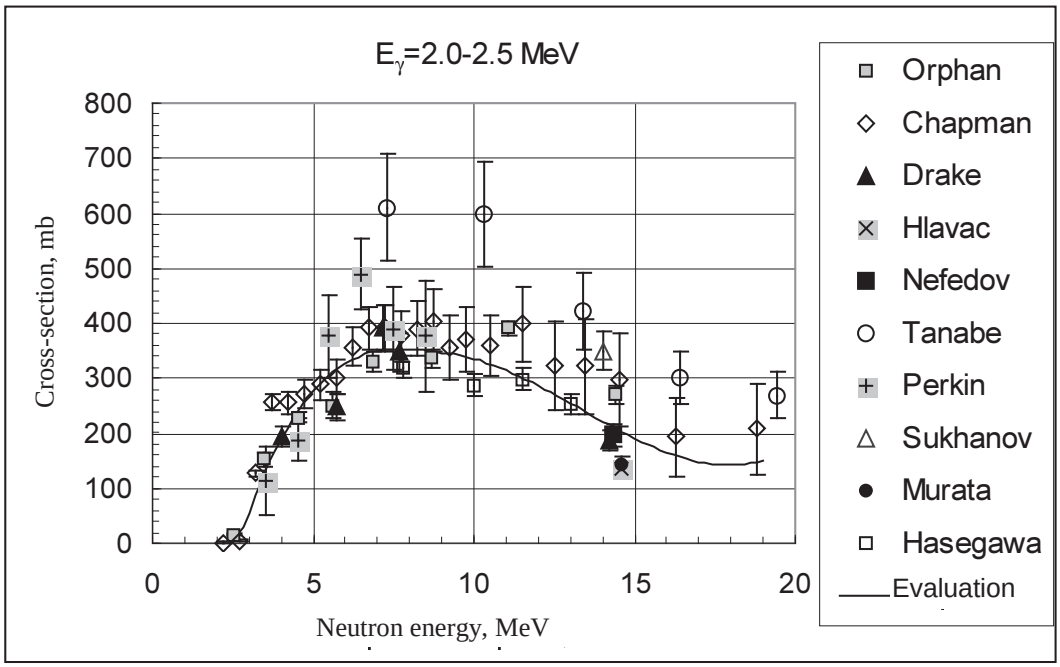

Fig. 5. Total γ-ray production cross-sections with energy 2.0-2.5 MeV.

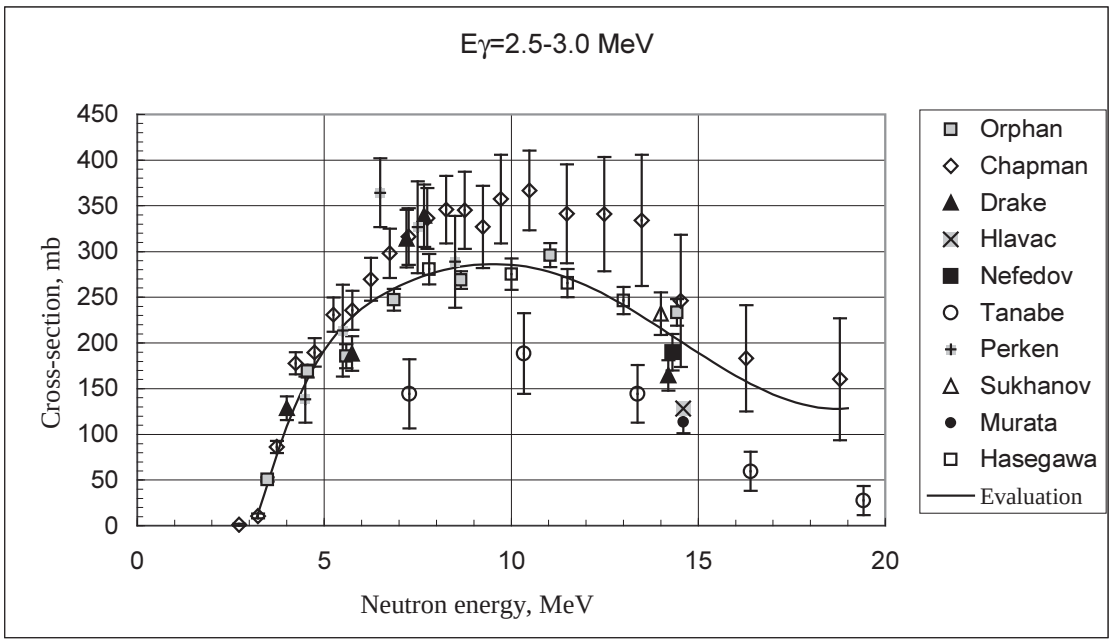

Fig. 6. Total γ-ray production cross-sections with energy 2.5-3.0 MeV.

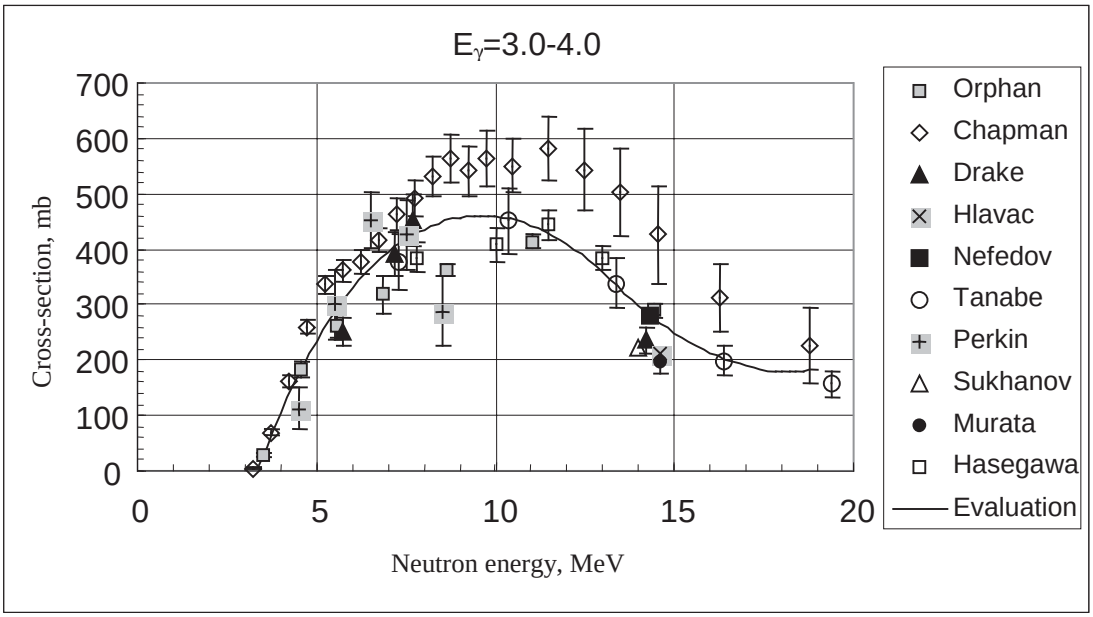

Fig. 7. Total γ-ray production cross-sections with energy 3.0-4.0 MeV.

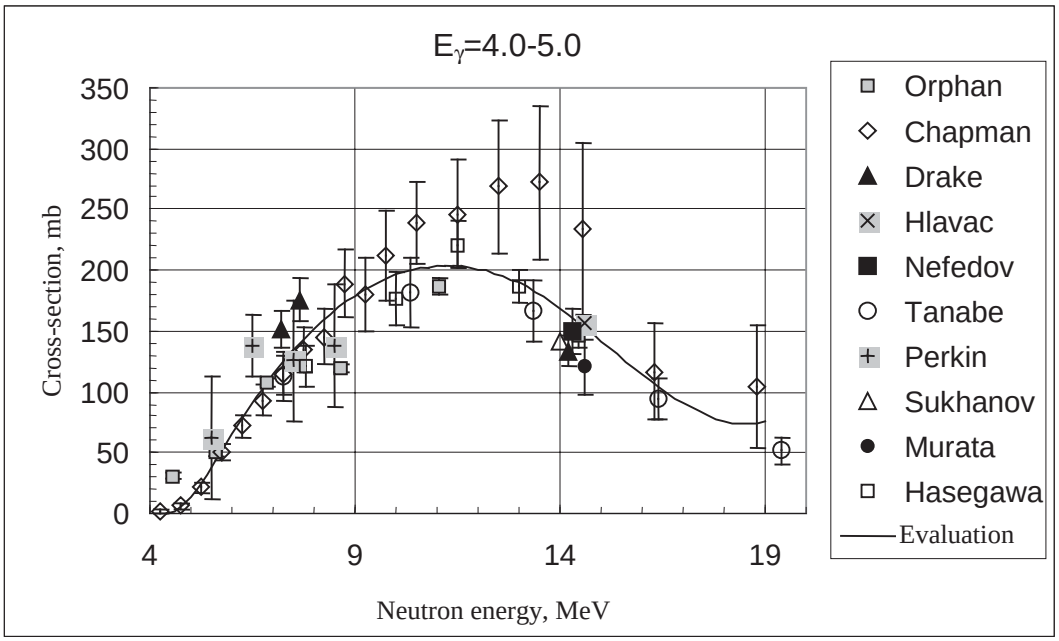

Fig. 8. Total γ-ray production cross-sections with energy 4.0-5.0 MeV.

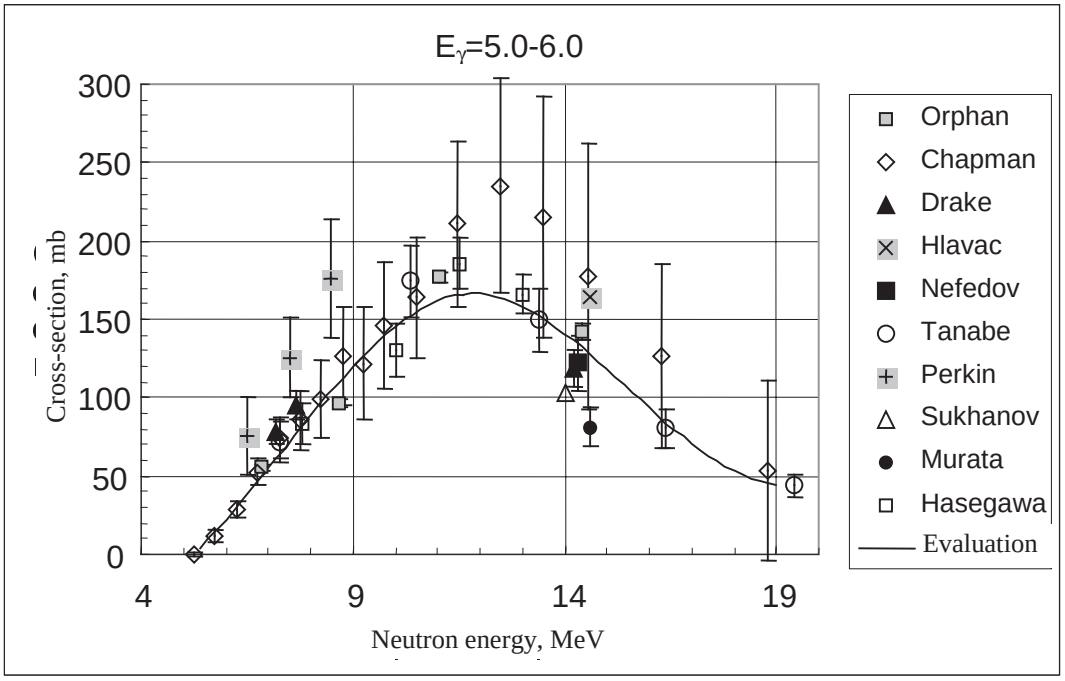

Fig. 9. Total γ-ray production cross-sections with energy 5.0-6.0 MeV.

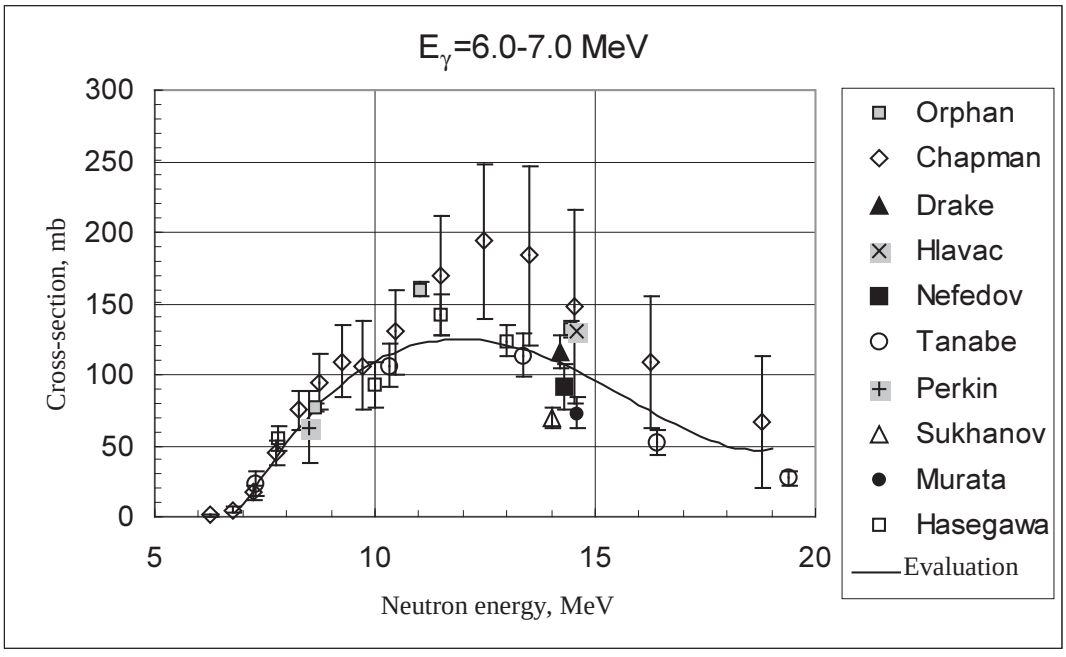

Fig. 10. Total γ-ray production cross-sections with energy 6.0-7.0 MeV.

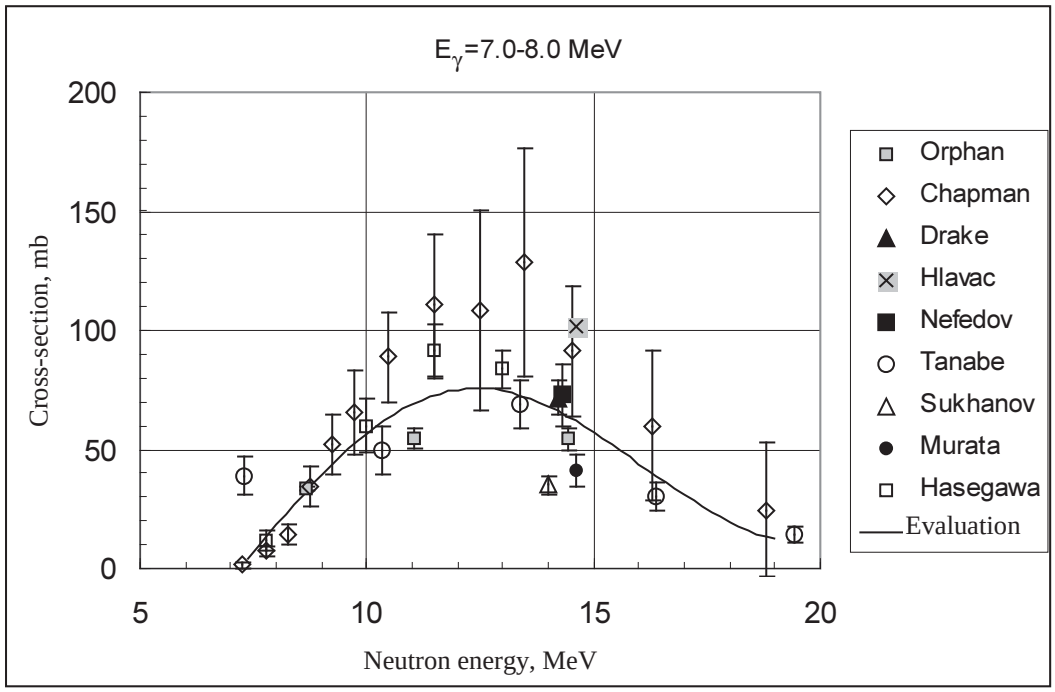

Fig. 11. Total γ-ray production cross-sections with energy 7.0-8.0 MeV.

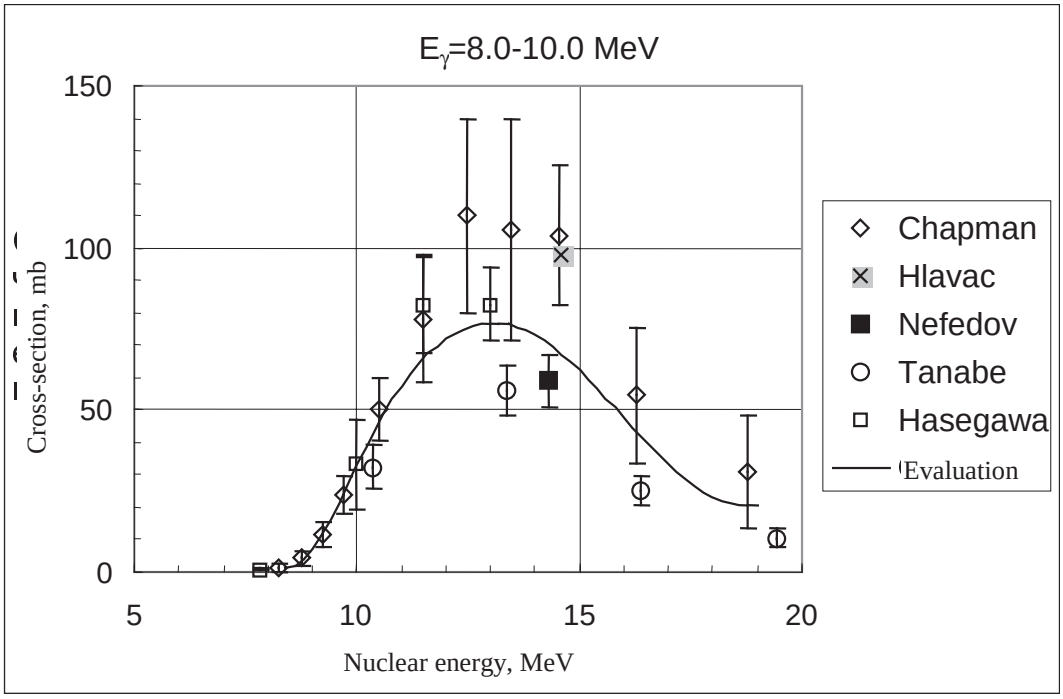

Fig. 12. Total γ-ray production cross-sections with energy 8.0-10.0 MeV.

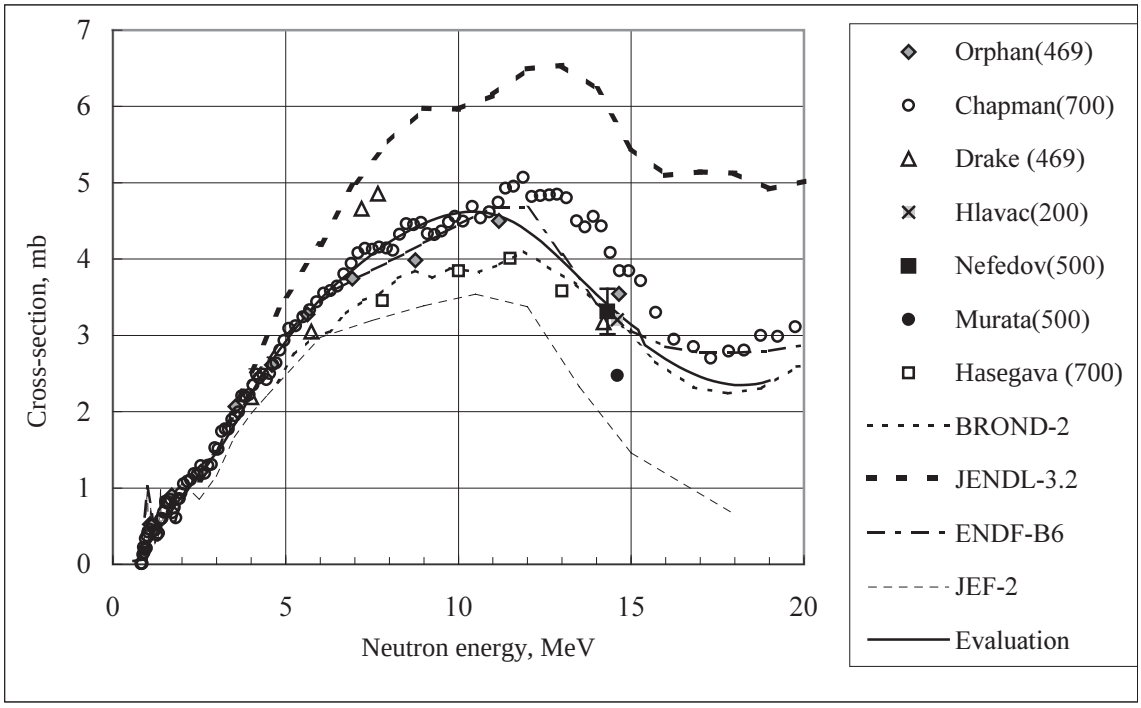

Fig. 13. Total γ-ray production cross-sections with energy 0.5-10.0 MeV for inelastic interaction of neutrons with nuclei of iron of a natural isotopic composition.

References

[1] C.G. Hoot, V.J. Orphan, J. John, GULF-RT-A-10743 (1971); EXFOR-10219.
[2] V.J. Orphan, C.G. Hoot, V.C. Rogers, Nucl. Sci. Eng., vol. 57 (1975) pp 309-327.
[3] a) J.K. Dickens, G.L. Morgan and F.G. Perey, ORNL-TM-4798 (1972);
b) J.K. Dickens, G.L. Morgan and F.G. Perey, Nucl. Sci. Eng., vol. 50 (1973) pp 311-336.
[4] G.T Chapman, G.L. Morgan, ORNL-TM-5416, (1976); EXFOR-10580.
[5] J.L. Perkin, Nuclear Physics, vol. 60 (1964) pp 561-580.
[6] E. Tanabe, K. Shin, T. Nakamura, J. Nucl. Scie. Techn., vol. 31 (11) (1994) pp 1133-1142.
[7] D.M. Drake, E.D. Arthur, M.G. Silbert, J. Nucl. Sci. Eng., vol. 65 (1978) pp 49-64, EXFOR-10684.
[8] D.M. Drake, J.C. Hopkins, C.S. Young, H. Conde, J. Nucl. Sci. Eng., vol. 40 (1970) pp 294-305, EXFOR-10025.
[9] B.I. Sukhanov, M.D. Smotrin, Voprosy atomnoj nauki i tekhniki, Ser. Yadernye konstanty, No. 23 (1976) pp 134-135, EXFOR-40496.
[10] S. Hlavac, P. Oblozinsky, Nucl. Instr. Meth., vol. 206 (1983) pp 127-134.
[11] S. Hlavac, P. Oblozinsky, IAEA report INDC (CSR) - 5/GI - Vienna - 1983 - EXFOR-30801.
[12] V.M. Gorbachev, V.I. Nagornyj, Yu.Ya. Nefedov, et al., Voprosy atomnoj nauki i tekhniki, Ser. Fizika yadernykh reaktorov, TIYaS-XI, Special issue, 1997, Proc.

11th International Seminar on accurate measurements in nuclear spectroscopy, Sarov, 2-5 September 1996.

[13] G.A. Borisov, V.D. Sevast'yanov, Yu.Ya. Nefedov, et al., 5th All-Soviet meeting on neutron measurement metrology on reactors and accelerators, Report abstracts, All-Union Scientific Research Institute of Physical and Radiation Measurements, Moscow (1990) p. 3.

[14] I. Murata, J. Yamamoto, A. Takahashi, in Proc. of Internal Conference on Nuclear Data for Science and Technology, Mito, Japan, 30 May-3 June 1988, p. 275, EXFOR-22096.

[15] K. Hasegawa, M. Mizumoto, S. Chiba et. al., in Proc. of International Conference on Nuclear Data for Science and Technology, Jülich, 13-17 May 1991, pp 329-331.

[16] S.N. Abramovich, B.Ya. Guzhovskij, V.A. Zherebtsov, A.G. Zvenigorodskij Spravochnoe posobie, GKAEh (USSR State Committee on the Utilization of Atomic Energy), Moscow, 1989 pp 27-34.

00-30130 [7]
Translated from Russian

UDC 539.171.017

EVALUATION OF ANGULAR DISTRIBUTIONS AND PRODUCTION CROSS-SECTIONS FOR DISCRETE GAMMA LINES IN IRON

M.V. Savin, A.V. Livke, A.G. Zvenigorodskij
Russian Federal Nuclear Centre - All-Russia Scientific Research Institute for Experimental Physics, Sarov

EVALUATION OF ANGULAR DISTRIBUTIONS AND PRODUCTION CROSS-SECTIONS FOR DISCRETE GAMMA-LINES IN IRON. The experimental data were compiled and the angular distributions and production cross-sections for the E_γ = 846.8, 1238.3 and 1810.8 keV discrete gamma-lines evaluated. The Legendre polynomial coefficients describing the angular distributions in the energy range up to E_n = 14.0 MeV and cross-section values in the E_n = 0.85-19.0 MeV range were evaluated.

Discrete gamma line production cross-sections are of interest because they can be used in a number of practical applications as basic information on the phenomena under investigation. In addition, discrete gamma lines can be used as reference (standard) cross-sections when carrying out measurements and evaluations.

In this paper, we have compiled the experimental data and evaluated the angular distributions and production cross-sections for the following main gamma lines of ^{56}Fe: E_γ = 846.8 keV (transition from the first level E_{lev} = 846.8(2^+) to the ground state (0^+)); E_γ = 1238.3 keV (transition from the second level E_{lev} = 2085.1 keV (4^+) to the first level); and E_γ = 1810.8 keV (transition from the third level E_{lev} = 2657.6 keV (2^+) to the first level).

A statistical approximation of the data files was produced using splines. With adequate data, the spline approximation program developed by V.A. Zherebtsov [1] produces reliable averaged curves automatically selecting the spline knots. Furthermore, the possibility is provided of intervening in the evaluator's approximation process, changing the weighting of certain data and/or selecting additional knots and boundary conditions in order to improve the statistical description of the data files.

The spline approximation results are presented in the form of tables of knot values and spline polynomial coefficients from which the value of the function Si(h) can be calculated at any point using the following expression:

$$S_i(h) = A_o + A_1 h + A_n h^n, \quad (1)$$

where $h = X - X_i$, X_i being the left boundary (knot) of the corresponding interval.

In the experiments, the discrete gamma line production cross-sections were measured at different angles to the neutron beam axis by the various authors. It would therefore be wrong to make a direct comparison of results, particularly in the neutron energy region close to the gamma production excitation energy in the nucleus. Therefore, the angular distributions of the discrete gamma rays were first of all evaluated.

1. Angular distributions

The angular distributions of discrete gamma rays $\sigma(\theta)$ produced by inelastic interaction of neutrons are described with adequate accuracy by the even terms of the Legendre polynomial. In most cases, a good description of the angular distributions can be achieved using only three terms: P_0, P_2 and P_4.

$$\sigma(\theta)=\frac{\sigma_0}{4\pi}(1+\alpha_2 P_2(\theta)+\alpha_4 P_4(\theta)) \qquad (2)$$

In the evaluation process, the coefficients α_2 and α_4 (2) were found using the method of least squares and all the available experimental data [2-6] on angular distributions for the main 847, 1240 and 1810 keV gamma lines. The results obtained are given in Tables 1-3. These tables also give references to sources whose results were used to obtain the coefficients α_2 and α_4. In a number of cases, values for α_2 and α_4 given by the authors of experimental papers were used. The values of the coefficients are given in Figs 1-3.

The figures show that very few experimental data are available for reliable determination of the energy dependences of the expansion coefficient $\alpha_{2,4}(E_n)$, and the available results show a poor level of integral agreement. We therefore used calculated results for the angular distributions produced using the Hauser-Feshbach statistical model of the nucleus, taking into account competition from electromagnetic transitions in cascade decay of excited states [7]. These results are also given in Tables 1-3 and in the figures.

As the figures show, any form of statistical approximation of the data is unlikely to yield sensible results. Therefore, first of all, we performed a spline approximation of the energy dependences $\alpha_2(E_n)$ and $\alpha_4(E_n)$ selecting spline knots and changing the weightings of experimental data. The results obtained were then corrected slightly to take account of the general pattern of the dependence of the angular distributions on the extent to which the neutron energy exceeds the energy of the level from which gamma rays are emitted.

The values of the α_4 coefficients for the E_γ = 1240 and 1810 keV gamma lines have a wide spread. Since the α_4 coefficients for these gamma lines are low, we assumed $\alpha_4 = 0$ for these gamma lines. The error in the description of angular distributions for this kind of approximation relative to the ratio of the coefficients α_2 and α_4 may be 0.5-2%.

The evaluated values of the coefficients α_2 and α_4 are shown in Figs 1-3 as a continuous line.

Table 1

Experimental and calculated values of the coefficients in the expansion of the angular distributions using the Legendre polynomial for the E_γ = 846.8 keV gamma line

Experimental data								Calculated data [7]		
E_n (MeV)	α_2	α_4	Ref.	E_n (MeV)	α_2	α_4	Ref.	E_n (MeV)	α_2	α_4
0.95	0.464	-0.484	[5]	0.98	0.5395	-0.303	[4]	2.8	0.172	-0.0449
1.05	0.504	-0.247	[5]	1.08	0.4355	-0.142	[4]	3.1	0.174	-0.0432
1.5	0.223	-0.169	[5]	1.18	0.3996	-0.3323	[4]	3.5	0.175	-0.0473
2.5	0.178	-0.050	[3]	1.28	0.305	0	[4]	4	0.169	-0.0549
2.8	0.3335	0.117	[6]	1.38	0.3852	0	[4]	6	0.129	-0.0701
3.1	0.152	-0.077	[5]	1.59	0.323	-0.1531	[4]	7.5	0.115	-0.0656
3.5	0.193	-0.005	[5]	1.68	0.2226	-0.1547	[4]	7.95	0.112	-0.0632
4	0.149	-0.033	[5]	1.79	0.2167	-0.0840	[4]	8.5	0.108	-0.0004
6	0.231	0.024	[2]	1.85	0.2409	-0.0974	[4]	9	0.104	-0.058
7.5	0.19	-0.084	[2]	2.03	0.1842	-0.0238	[4]	14.1	0.0756	-0.0384
8.8	0.1887	0.028	[3]							
14.1	0.09	-0.1	[3]							

Table 2

Experimental and calculated values of the coefficients in the expansion of the angular distributions using the Legendre polynomial for the E_γ = 1238.3 keV gamma line

Experimental data				Calculated data [7]		
E_n (MeV)	α_2	α_4	Ref.	E_n (MeV)	α_2	α_4
2.5	0.302	0.0239	[3]	2.8	0.34	-0.0772
2.8	0.635	0.0146	[6]	3.1	0.341	-0.0781
3.1	0.243	0.0627	[5]	3.5	0.34	-0.0798
3.5	0.387	-0.0705	[5]	4	0.337	-0.0829
4	0.289	-0.0514	[5]	6	0.268	-0.0537
6	0.263	-0.0103	[2]	7.5	0.228	-0.0319
7.5	0.633	0.127	[2]	7.95	0.219	-0.028
8.8	0.22	-0.045	[3]	8.5	0.21	-0.0246
14.1	0.14	-0.1	[3]	9	0.203	-0.0225
				14.1	0.157	-0.0179

Table 3

Experimental and calculated values of the coefficients in the expansion of the angular distributions using the Legendre polynomial for the E_γ = 1810.8 keV gamma line

Experimental data				Calculated data [7]		
E_n (MeV)	α_2	α_4	Ref.	E_n (MeV)	α_2	α_4
2.8	0.491	0.29	[6]	2.8	0.444	-0.00214
3.1	0.236	0.0604	[5]	3.1	0.405	-0.00188
3.5	0.273	0.067	[5]	3.5	0.301	-0.00129
4	0.1075	-0.0146	[5]	4	0.245	-0.00081
6	-0.0003	0.027	[2]	6	0.194	-0.00061
7.5	0.0026	-0.1235	[2]	7.5	0.158	-0.00063
8.8	0.067	0.021	[3]	7.95	0.15	-0.00061
				8.5	0.142	-0.00058
				9	0.135	-0.00056
				14.1	0.092	-0.00036

2. Discrete gamma-ray production cross-sections

A large number of measurements were made at the early stage of research, mostly using gamma-ray scintillation spectrometers. However attractive these spectrometers may be, their energy resolution is insufficient for a detailed study of the line structure of spectra. A set of closely grouped gamma lines is registered by these detectors as one line, which introduces an uncertainty into the discrete line production cross-section being measured. Therefore, in the main, we only looked at data obtained using detectors with a high energy resolution. Moreover, we did not use results obtained via relative measurements (mainly for the E_γ = 847 keV gamma line in iron). The whole set of studies may be divided into three groups: studies carried out using 14-15 MeV (d,T) neutrons [2, 8-14]; measurements performed using monochromatic neutrons over a wide energy range [15-18]; and studies carried out for a continuous spectrum using the time-of-flight method [19-23].

A few comments on some of the experiments.- In Ref. [8], the measurement results were normalized to the production cross-section value for the E_γ = 4.43 MeV gamma line in carbon at a neutron energy of E_n = 14.8 MeV. The iron sample, which was a disk 15 cm in diameter and about 3 cm thick, was positioned 10 cm from the neutron source. The measurement geometry, sample dimensions and data normalization are not optimal. The measurement error given by the authors of 1%, 3% and 10% for the 847, 1240 and 1810 keV lines respectively is improbable. In Ref. [13], the authors do not indicate the error for determination of the distance between the neutron source and the sample, which could be considerable in the "compact" geometry used for the measurements. In Ref. [14], the time-of-flight method is used to separate out neutrons and gamma rays from the sample. However, since the distance between the detector and the sample was 30 cm and the time resolution 7.5 ns, as the paper indicates, it is doubtful the separation would be adequate and that there would not be additional uncertainty in the cross-section value.

Although Refs [20, 21] used an NaI(Tl) detector, we did take the results of this study for the E_γ = 846.8 keV gamma line into consideration, because the work was carried out sufficiently correctly for a wide neutron energy range and the contribution of adjacent gamma lines to the 847 keV gamma line peak (787.8 and 869 keV lines at E_n > 3.5 MeV) is negligible.

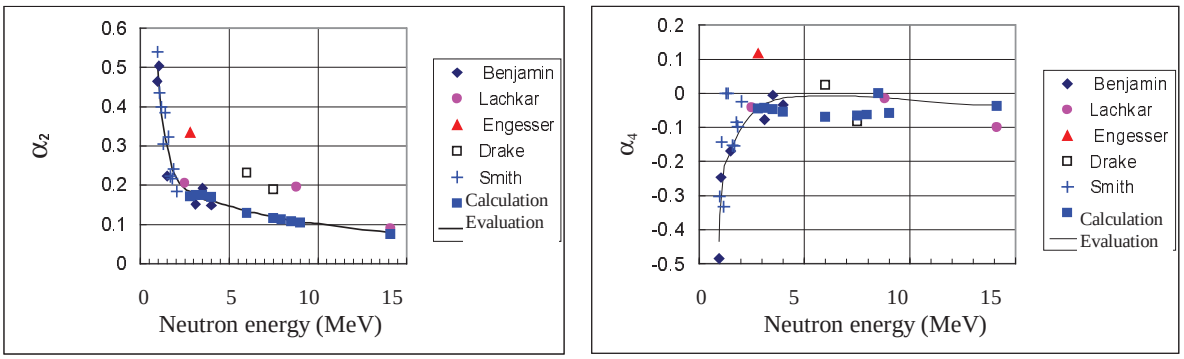

Fig. 1. Values of the coefficients α_2 and α_4 of the Legendre polynomials used to describe the angular distributions of the E_γ = 846.8 keV gamma line.

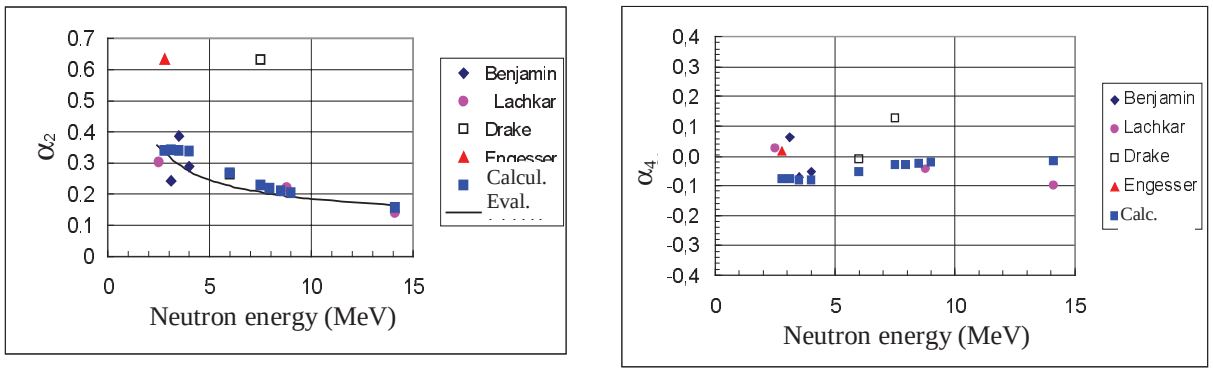

Fig. 2. Values of the coefficients α_2 and α_4 of the Legendre polynomials used to describe the angular distributions of the E_γ = 1238.3 keV gamma line.

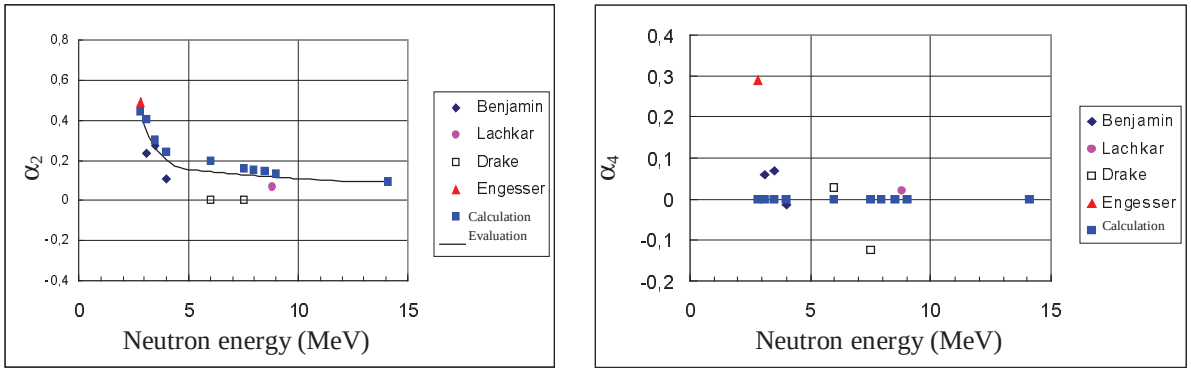

Fig. 3. Values of the coefficients α_2 and α_4 of the Legendre polynomials used to describe the angular distributions of the E_γ = 1810.8 keV gamma line.

As mentioned earlier, in the various studies the gamma-ray detectors were positioned at different angles when measuring the discrete gamma line production cross-sections. Furthermore, some authors give data for ^{56}Fe and others for the natural isotopic composition, even though the 847, 1240 and 1810 lines are formed as a result of excitation and decay of the ^{56}Fe nucleus. With a view to presenting the results of different authors on the same scale, all the available experimental data were normalized to the natural isotope mixture (^{56}Fe content - 0.91754) and reduced to the angle-integrated production cross-section σ_0 for the specific gamma line using the formula

$$\sigma_0 = \frac{4\pi\sigma(\theta)}{1+\alpha_2 P_2(\theta)+\alpha_4 P_4(\theta)}\ , \qquad (3)$$

where θ is the angle at which the differential cross-section was measured.

In formula (2), the Legendre polynomial coefficients α_2 and α_4 from our evaluation were used.

Where the data were obtained using a continuous spectrum neutron source and the time-of-flight method, the average neutron energy for each interval ΔE_n was determined on the basis that, in the experiment, events are registered at evenly distributed intervals of times of flight Δt. Here, the average energy corresponding to the average interval time will be:

$$\overline{E}_{avi} = \frac{4}{\left(\frac{1}{\sqrt{E_{1i}}}+\frac{1}{\sqrt{E_{2i}}}\right)^2}, \qquad (4)$$

where E_{1i} and E_{2i} are the lower and upper limits of the ith interval given in the tabulated data. For low neutron energies, determining the average interval energy in this way yields a result which hardly differs from the simple average: $E_{av} = (E_1 + E_2)/2$. At high energies, the difference becomes significant, which is particularly important in the $E_n \geq 10$ MeV region where there is a sharp dip in the cross-sections owing to decay channel competition.

846.8 keV gamma line

The experimental values for the angle-integrated 846.8 keV gamma line production cross-sections are shown in Figs 4-5. In order not to clutter the diagrams, the measurement errors are not shown, since they differ but little in the various studies, lying in the 10-15% range. All measurement errors were taken into account when performing the approximation of the data.

The experimental results of the different authors show a fair level of agreement in the main, apart from some of Drake's values [2] which are noticeably higher than the overall data. The considerable spread of the data obtained using 14-16 MeV monoenergetic neutrons is somewhat surprising; here, one could expect a better level of agreement. This broad spread may be due to the fact that these measurements were performed in a "compact" geometry, resulting in a high level of uncertainty in the magnitude of the neutron flux onto the sample.

Near the excitation threshold of the level ($E_{thr} \leq E_n \leq 3$ MeV), the energy dependence of the production cross-section for the 846.8 keV line, resulting from a dipole ($2^+ \rightarrow 0^+$) transition, has a complex structure. This structure is delineated particularly well in Ref. [22] by Voss. Voss's data, which are averaged over the $\Delta E_n \cong 50$ keV interval are shown in Figs 4-5 as a continuous line.

In the $E_n < 3$ MeV neutron energy region, to obtain an "averaged" curve when performing the spline approximation a higher number of spline knots was specified. In the $E_n \geq$ 2.8 MeV neutron energy region where the structure may be ignored, only two knots were specified. The overall evaluated cross-section curve for the 846.8 keV line is shown in Figs 4-5 as a continuous line.

1238.3 keV line

The experimental data and the results of the evaluation for the 1238.3 keV gamma line production cross-section are shown in Fig. 6. Voss's results [22] were averaged over broad energy intervals - at the beginning of the scale $\Delta E = 0.2$ MeV, and subsequently $\Delta E \cong 0.5$ MeV. Drake's [2], Yamamoto's [10] and Broder's [14] data differ significantly from the results of other authors. These results were given as low weighting when performing the spline approximation.

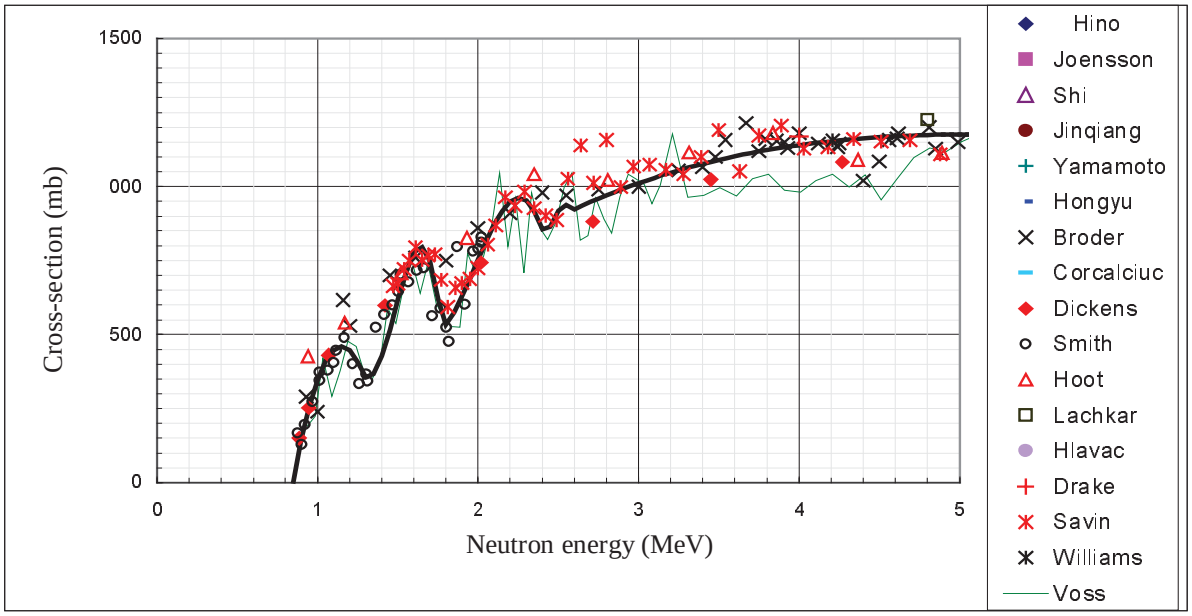

Fig. 4. Production cross-section for the E_γ = 846.8 keV gamma line (thick line - evaluation).

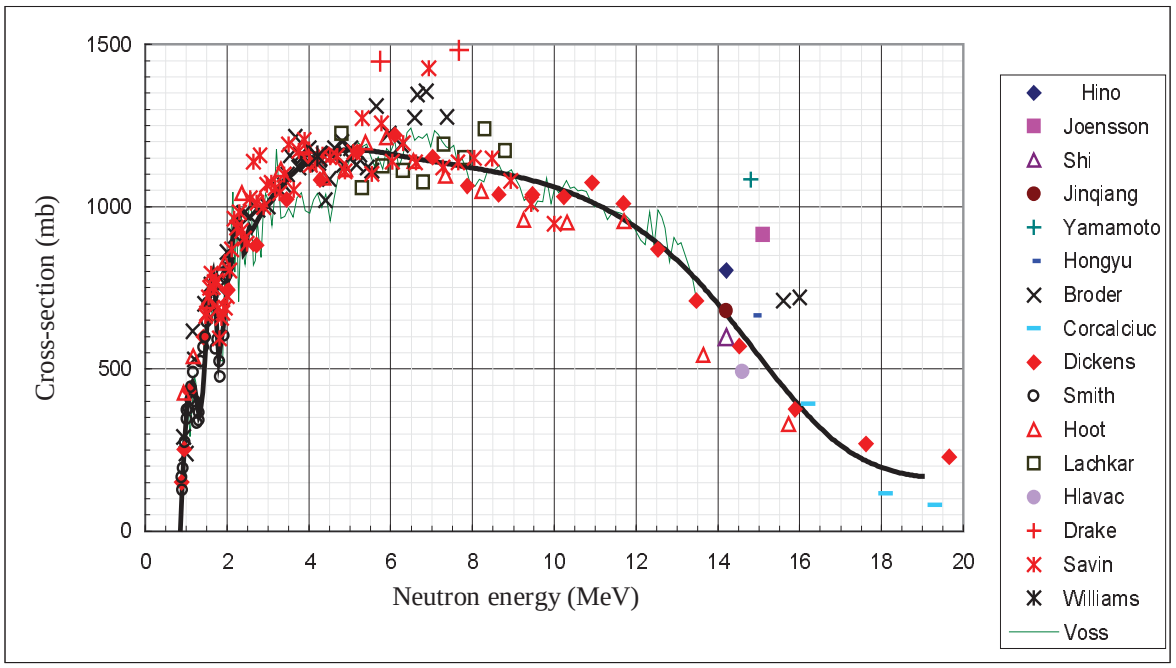

Fig. 5. Production cross-section for the E_γ = 846.8 keV gamma line (thick line - evaluation).

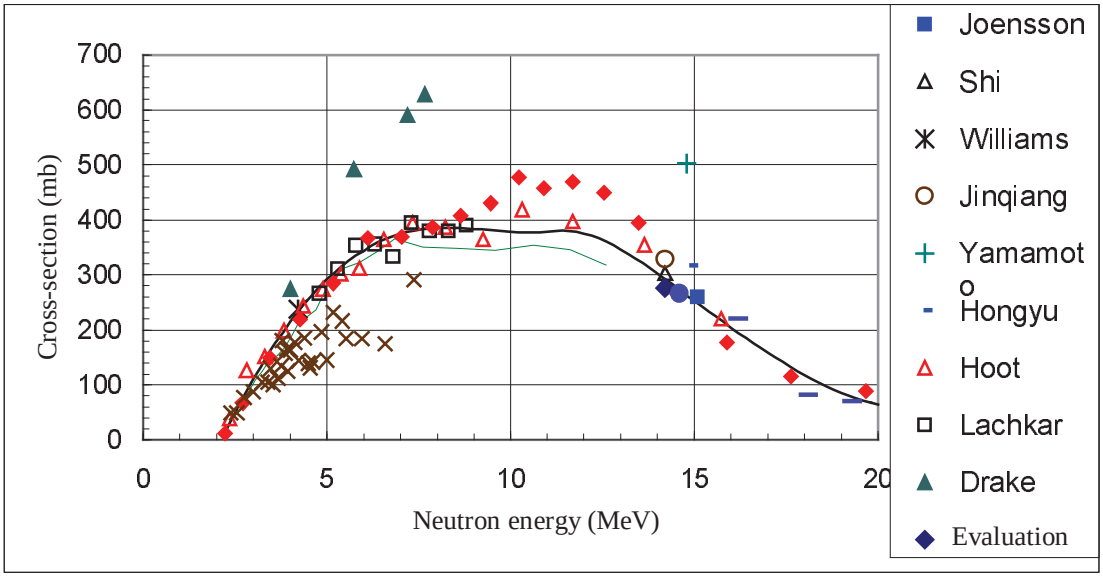

Fig. 6. Production cross-section for the E_γ = 1238.3 keV gamma line.

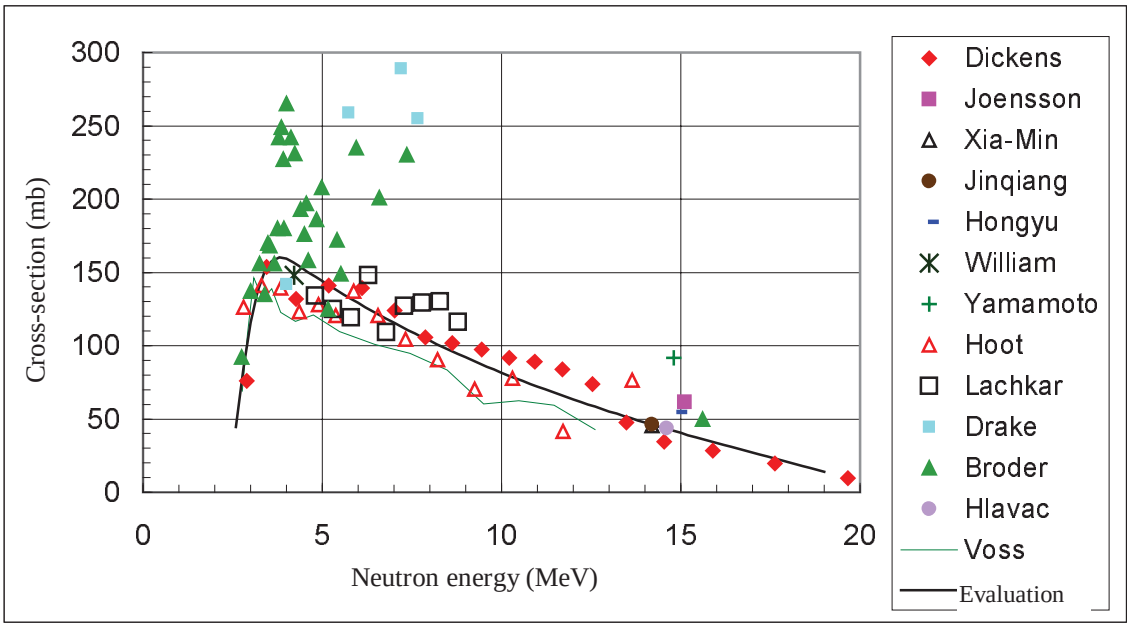

Fig. 7. Production cross-section for the E_γ = 1810.3 keV gamma line.

1810.8 keV line

The experimental results and the evaluated data for the 1810.8 keV gamma line are shown in Fig. 7. Voss's data in Ref. [22] are averaged over broad energy intervals - $\Delta E \cong 0.2$ MeV.

The figure shows that the results obtained for monoenergetic neutrons (Drake [2], Broder [14]) differ greatly from the cross-sections measured using the time-of-flight method and a continuous neutron spectrum (Hoot [19], Voss [22], Dickens [23]). At the same time, the results for a continuous spectrum show a not unsatisfactory level of agreement with Lachkar's data [3] and, in the E_n = 14-15 MeV interval, with the results in Refs [8, 11, 12, 14].

Conclusion

In conclusion, with regard to the discrete gamma line production cross-sections, the error of the evaluated 847.8 keV gamma line production cross-section is 5-10% over the whole energy range; for the 1238.3 keV gamma line, the error is generally 10-15%. With regard to the 1810.8 keV line there is a high level of uncertainty, owing to the spread of data; further experimental and theoretical research is needed here.

The angular distributions are most significant in the neutron energy region close to the excitation threshold of the production level. At high energies, there is averaging with respect to momenta when many transitions merge.

There is considerable divergence in the data obtained via measurements using (d,T) neutrons, which, it would seem, is due to error in the determination of the neutron flux onto the sample.

The evaluated values of the coefficients α_2 and α_4 and the gamma-ray production cross-sections are given in Tables 4-8. The data are given for iron of natural isotopic composition.

Table 4

Evaluated values of the coefficients α_2 and α_4 of the Legendre polynomials used to describe the angular distributions of the discrete gamma lines

E_γ = 846.8 keV			E_γ =1238.3 keV		E_γ = 1810.8 keV	
E_n (MeV)	α_2	α_4	E_n (MeV)	α_2	E_n (MeV)	α_2
0.95	0.510	-0.4333				
1	0.480	-0.3562				
1.2	0.380	-0.2134				
1.4	0.320	-0.1850				
1.6	0.280	-0.1534				
1.8	0.240	-0.1264				
2	0.220	-0.1035				
2.2	0.205	-0.0843				
2.4	0.195	-0.0683	2.4	0.358		
2.6	0.188	-0.0552	2.6	0.345		
2.8	0.184	-0.0445	2.8	0.334	2.8	0.506
3	0.178	-0.0359	3	0.322	3	0.377
3.2	0.170	-0.0291	3.2	0.307	3.2	0.316
3.4	0.169	-0.0238	3.4	0.300	3.4	0.278
3.6	0.164	-0.0198	3.6	0.292	3.6	0.246
3.8	0.162	-0.0167	3.8	0.281	3.8	0.220
4	0.160	-0.0144	4	0.276	4	0.200
4.2	0.158	-0.0128	4.2	0.265	4.2	0.184
4.4	0.155	-0.0115	4.4	0.260	4.4	0.172
4.6	0.152	-0.0106	4.6	0.254	4.6	0.164
4.8	0.150	-0.0099	4.8	0.250	4.8	0.158
5	0.147	-0.0093	5	0.246	5	0.154
5.2	0.145	-0.0088	5.2	0.241	5.2	0.151
5.4	0.141	-0.0084	5.4	0.237	5.4	0.149
5.6	0.138	-0.0081	5.6	0.233	5.6	0.147
5.8	0.136	-0.0079	5.8	0.230	5.8	0.145
6	0.132	-0.0077	6	0.228	6	0.143
6.2	0.131	-0.0076	6.2	0.223	6.2	0.140
6.4	0.130	-0.0076	6.4	0.219	6.4	0.138
6.6	0.128	-0.0077	6.6	0.216	6.6	0.136
6.8	0.126	-0.0078	6.8	0.214	6.8	0.134
7	0.124	-0.0081	7	0.212	7	0.132
7.2	0.122	-0.0084	7.2	0.212	7.2	0.130
7.4	0.121	-0.0088	7.4	0.209	7.4	0.129
7.6	0.120	-0.0092	7.6	0.205	7.6	0.127
7.8	0.118	-0.0098	7.8	0.201	7.8	0.125
8	0.115	-0.0104	8	0.200	8	0.123

E_γ = 846.8 keV			E_γ =1238.3 keV		E_γ = 1810.8 keV	
E_n (MeV)	α_2	α_4	E_n (MeV)	α_2	E_n (MeV)	α_2
8.2	0.113	-0.0111	8.2	0.198	8.2	0.121
8.4	0.111	-0.0118	8.4	0.196	8.4	0.119
8.6	0.108	-0.0127	8.6	0.196	8.6	0.118
8.8	0.107	-0.0135	8.8	0.191	8.8	0.116
9	0.106	-0.0144	9	0.191	9	0.114
9.2	0.105	-0.0154	9.2	0.190	9.2	0.113
9.4	0.104	-0.0164	9.4	0.189	9.4	0.111
9.6	0.104	-0.0175	9.6	0.187	9.6	0.110
9.8	0.103	-0.0186	9.8	0.186	9.8	0.108
10	0.102	-0.0197	10	0.185	10	0.107
10.5	0.100	-0.0225	10.5	0.182	10.5	0.103
11	0.096	-0.0254	11	0.179	11	0.100
11.5	0.093	-0.0281	11.5	0.177	11.5	0.098
12	0.090	-0.0305	12	0.175	12	0.096
12.5	0.087	-0.0325	12.5	0.172	12.5	0.094
13	0.085	-0.0339	13	0.170	13	0.093
13.5	0.083	-0.0344	13.5	0.167	13.5	0.092
14	0.080	-0.0339	14	0.164	14	0.091

Table 5

Production cross-sections for discrete gamma rays with an energy of E_γ = 846.8 keV

E_n (MeV)	Cross-section (mb)	E_n (MeV)	Cross-section (mb)	E_n (MeV)	Cross-section (mb)	E_n (MeV)	Cross-section (mb)
0.85	5.01	2.45	863.70	6.60	1148.22	13.00	834.90
0.90	144.85	2.50	917.55	6.80	1143.99	13.20	810.74
0.95	258.83	2.55	936.71	7.00	1139.89	13.40	785.17
1.00	347.08	2.60	924.00	7.20	1135.86	13.60	758.13
1.05	409.78	2.65	936.20	7.40	1131.85	13.80	729.62
1.10	447.07	2.70	948.02	7.60	1127.82	14.00	699.82
1.15	459.11	2.75	959.47	7.80	1123.72	14.20	668.98
1.20	446.05	2.80	970.55	8.00	1119.50	14.40	637.33
1.25	408.05	2.85	981.26	8.20	1115.11	14.60	605.13
1.30	356.49	2.90	991.62	8.40	1110.51	14.80	572.61
1.35	366.86	2.95	1001.62	8.60	1105.64	15.00	540.03
1.40	426.63	3.00	1011.28	8.80	1100.46	15.20	507.63
1.45	516.67	3.05	1020.59	9.00	1094.93	15.40	475.65
1.50	617.80	3.10	1029.57	9.20	1088.98	15.60	444.34
1.55	710.89	3.15	1038.21	9.40	1082.59	15.80	413.94
1.60	776.79	3.20	1046.53	9.60	1075.68	16.00	384.70
1.65	796.33	3.40	1076.67	9.80	1068.23	16.20	356.87
1.70	750.37	3.60	1102.03	10.00	1060.18	16.40	330.68
1.75	619.76	3.80	1122.97	10.20	1051.48	16.60	306.38
1.80	533.98	4.00	1139.84	10.40	1042.09	16.80	284.21
1.85	575.54	4.20	1152.99	10.60	1031.95	17.00	264.38
1.90	628.57	4.40	1162.78	10.80	1021.03	17.20	246.80
1.95	688.79	4.60	1169.55	11.00	1009.26	17.40	231.36
2.00	751.94	4.80	1173.65	11.20	996.61	17.60	217.90
2.05	813.73	5.00	1175.44	11.40	983.02	17.80	206.30
2.10	869.90	5.20	1175.26	11.60	968.45	18.00	196.43
2.15	916.17	5.40	1173.48	11.80	952.85	18.20	188.14
2.20	948.27	5.60	1170.43	12.00	936.17	18.40	181.30
2.25	961.93	5.80	1166.47	12.20	918.36	18.60	175.78
2.30	952.88	6.00	1161.95	12.40	899.38	18.80	171.45
2.35	916.83	6.20	1157.22	12.60	879.17	19.00	168.16
2.40	855.18	6.40	1152.61	12.80	857.70		

Table 6

Production cross-sections for discrete gamma rays with an energy of E_γ = 1238.8 keV

E_n (MeV)	Cross-section (mb)	E_n (MeV)	Cross-section (mb)	E_n (MeV)	Cross-section (mb)	E_n (MeV)	Cross-section (mb)
2.20	8.39	6.80	370.11	11.40	380.17	16.00	204.39
2.40	35.85	7.00	374.39	11.60	379.84	16.20	194.91
2.60	62.15	7.20	377.87	11.80	378.22	16.40	185.56
2.80	87.28	7.40	380.60	12.00	375.41	16.60	176.36
3.00	111.28	7.60	382.65	12.20	371.48	16.80	167.35
3.20	134.15	7.80	384.09	12.40	366.55	17.00	158.52
3.40	155.91	8.00	384.98	12.60	360.71	17.20	149.92
3.60	176.57	8.20	385.39	12.80	354.04	17.40	141.55
3.80	196.15	8.40	385.39	13.00	346.66	17.60	133.44
4.00	214.66	8.60	385.04	13.20	338.65	17.80	125.60
4.20	232.13	8.80	384.41	13.40	330.10	18.00	118.07
4.40	248.55	9.00	383.57	13.60	321.12	18.20	110.85
4.60	263.95	9.20	382.58	13.80	311.80	18.40	103.96
4.80	278.35	9.40	381.50	14.00	302.23	18.60	97.44
5.00	291.75	9.60	380.41	14.20	292.51	18.80	91.30
5.20	304.17	9.80	379.38	14.40	282.72	19.00	85.55
5.40	315.63	10.00	378.46	14.60	272.88	19.20	80.22
5.60	326.14	10.20	377.72	14.80	263.02	19.40	75.34
5.80	335.72	10.40	377.24	15.00	253.14	19.60	70.91
6.00	344.38	10.60	377.07	15.20	243.28	19.80	66.96
6.20	352.13	10.80	377.28	15.40	233.46	20.00	63.51
6.40	358.99	11.00	377.95	15.60	223.69		
6.60	364.98	11.20	379.13	15.80	213.99		

Table 7

Production cross-sections for discrete gamma rays with an energy of E_γ = 1810.8 keV

E_n (MeV)	Cross-section (mb)	E_n (MeV)	Cross-section (mb)	E_n (MeV)	Cross-section (mb)	E_n (MeV)	Cross-section (mb)
2.60	44.70	6.80	118.31	11.00	72.13	15.20	39.04
2.80	85.29	7.00	115.70	11.20	70.32	15.40	37.66
3.00	115.67	7.20	113.14	11.40	68.54	15.60	36.29
3.20	136.92	7.40	110.62	11.60	66.78	15.80	34.94
3.40	150.48	7.60	108.15	11.80	65.05	16.00	33.59
3.60	157.81	7.80	105.72	12.00	63.35	16.20	32.26
3.80	160.33	8.00	103.34	12.20	61.67	16.40	30.93
4.00	159.50	8.20	101.00	12.40	60.02	16.60	29.61
4.20	156.76	8.40	98.69	12.60	58.40	16.80	28.29
4.40	153.49	8.60	96.43	12.80	56.79	17.00	26.98
4.60	150.27	8.80	94.21	13.00	55.21	17.20	25.68
4.80	147.10	9.00	92.02	13.20	53.65	17.40	24.38
5.00	143.99	9.20	89.88	13.40	52.11	17.60	23.08
5.20	140.93	9.40	87.77	13.60	50.59	17.80	21.79
5.40	137.92	9.60	85.70	13.80	49.09	18.00	20.50
5.60	134.97	9.80	83.66	14.00	47.60	18.20	19.21
5.80	132.07	10.00	81.66	14.20	46.14	18.40	17.92
6.00	129.22	10.20	79.69	14.40	44.69	18.60	16.63
6.20	126.42	10.40	77.75	14.60	43.25	18.80	15.34
6.40	123.67	10.60	75.85	14.80	41.84	19.00	14.04
6.60	120.96	10.80	73.97	15.00	40.43		

Table 8

Spline approximation coefficients for discrete gamma line production cross-sections

amma ray energy E_γ (MeV)	Knot energy (MeV)	A_0 (mb)	A_1 (mb/MeV)	A_2 (mb/MeV^2)	A_3 (mb/MeV^3)	Error $\Delta\sigma_{n,x\gamma}$ (mb) at the knot
0.847	0.85	5.00673	3056.678	-5205.465	206.9289	0.5034176
	1.25853	399.0849	-1683.515	16889.24	-25536.03	61.98173
	1.77459	518.6271	517.0054	3582.455	-5697.28	69.99478
	2.38724	869.9078	-1508.664	29158.96	-106710.4	75.95874
	2.57013	916.5241	252.5369	-77.84503	7.311781	47.50709
	6.261371	1155.78	-23.27785	3.123605	-0.9995274	46.84921
	13.6167	755.8115	-139.5534	-18.93195	5.099319	32.27791
	16.8083	283.3481	-104.5702	29.893	-2.811044	19.6597
1.240	2.23	12.58569	139.3748	-14.78536	0.3077466	1.324959
	6.9268	372.9234	20.85369	-10.44909	1.382759	5.428989
	11.2322	379.3714	7.773093	-18.37684	1.986758	5.016663
	14.1677	294.0896	-48.75668	-0.8804508	0.4220889	4.267272
1.810	2.75	76.09608	190.5655	-136.6633	30.07322	4.349928
	4.272715	155.5753	-16.44436	0.7155358	-0.01707704	2.339919

References

[1] S.N. Abramovich, B.Ya. Guzhovskij, V.A. Zherebtsov, A.G. Zvenigorodskij, Reference Handbook, GKAEh (USSR State Committee on the Utilization of Atomic Energy), Moscow (1989) pp. 27-34.

[2] D.M. Drake, J.C. Hopkins, C.S. Young, H. Conde, J. Nucl. Sci. Eng. v.40 (1970) pp. 294-305, EXFOR-10025.

[3] J. Lachkar, J. Sigand, Y. Patin, G. Haonat, Nucl. Scie. Eng. v.55 (1974) p. 168-187.

[4] D. L. Smith, Report ANL - NDM - 20 -1976 - EXFOR-10613.

[5] R.W. Benjamin, P.S. Buchanan, J.L. Morgan, Nucl. Phys. v.79 (1966) p. 241.

[6] F.C. Engesser, W.E. Thompson, WASH-1124 (1968) p. 134.

[7] B.M. Dzyuba, L.M. Lazarev, I.N. Paramonova, M.V. Savin, Voprosy Atomnoj Nauki i Tekhniki, Seriya: Yadernye konstanty, N1 (1985), pp 72-76.

[8] B. Joensson, K. Nyberg, I Bergqvist, J. Arkiv for Fisik v.39 (1969) p. 295, EXFOR-20164.

[9] Y. Hino, T. Yamamoto, T. Saito, Y. Arai, S. Itagaki, K. Sugiyama, J. Nucl. Sci. Techn. v. 15(2) (1978) p. 85, EXFOR-20626.

[10] T. Yamamoto, Y. Hino, S. Itagaki, K. Sugiyama, J. Nucl. Sci. Techn. v. 15(11) (1978) p. 797, EXFOR-21304.

[11] Shi Xia-Min, Shen Rong-Lin, Xing Jin Qiang, Shen Rong-Lin, Ding Da-Zhao, Chinese J. of Nuclear Physics (in Chinese) v. 4(2) (1982) p. 120, EXFOR-30656.

[12] Zhou Hongyu, Tang Lin, Yan Yiming et al., IAEA Report INDC (CPR)-10 (1986), EXFOR-30904, Chinese J. of Nuclear Physics v. 10 (1988) p. 166.

[13] Xing Jinqiang, Cao Zhong, Wu Yongshun, Chen Qun, Chinese J. of Nucl. Phys. (in Chinese) v. 10(3) (1988) p. 282, EXFOR-32513.

[14] S. Hlavac, P. Oblozinsky, IAEA report INDC (CSR) - 5[GI, Vienna (1983), EXFOR-30801.

[15] D.L. Broder, A.F. Gamamit, A.I. Lashuk, I.P. Sadokhin, Nuclear Data for Reactors, IAEA, Vienna (1970), v. II, pp 295-300, Proceedings of the Second International Conf., Helsinki, 15-19 June (1970).

[16] J. Lachkar, J. Sigand, Y. Patin, G. Haonat, Nucl. Scie. Eng. v. 55 (1974) p.168-187.

[17] V. Korkal'chuk, G.A. Prokopets, B. Kholmkvist, Yadernaya Fizika v. 20 N6 (1979) pp 1096-1105, EXFOR-40306.

[18] D.L. Smith, Report ANL - NDM - 20 (1976), EXFOR-10613.

[19] C.G. Hoot, V.J. Orphan, J. John, R., GULF-RT-A-10743 (1971), EXFOR-10219.

[20] M.V. Savin, I.N. Paramonova,Yu.A. Khokhlov, Nejtronnaya Fizika, Part 1, pp 282-289, Naukova Dumka Kiev, 1972, Materialy Vsesoyuznogo Soveshchaniya Kiev, 24-28 May (1971).

[21] M.V. Savin, Yu.A. Khokhlov, I.N. Paramonova, et al., Yadernaya Fizika v. 23 (1976) N3, EXFOR-40346.

[22] F. Voss, S. Cierjacks, L. Kropp, Report KFK-1494, Karlsruhe (1971).

[23] J.K. Dickens, C.Y. Fu, D.M. Hetrick, D.C. Larson, J.H. Todd, Nuclear Data for Science and Technology, p. 307-309, Proceeding of an Jut. Conf., Jülich, Germany, 13-17 May (1991), Report - ORNL-TM-11671 (1990), EXFOR-13500.

00-30130 [8]
Translated from Russian

UDC 539.163

RESOLVED RESONANCE PARAMETERS FOR ^{232}Pa

L.A. Bakhanovich, G.B. Morogovskij
Radiation Physics and Chemistry Problems Institute, Minsk
Belarus National Academy of Sciences

RESOLVED RESONANCE PARAMETERS FOR ^{232}Pa. Multilevel Breit-Wigner parameters have been obtained for fission cross-section representation in the energy region 0.01-21 eV on the basis of an evaluation of the experimental fission cross-section for ^{232}Pa in the resolved resonance region.

The solution of transmutation problems requires a knowledge of the nuclear physics constants of the short-lived nucleus ^{232}Pa ($T_{1/2}$ = 1.31 d) in the thermal and resonance neutron range. As no measurements of the detailed behaviour of the cross-sections have been performed until recently, with the exception of insufficiently reliable thermal values (see below), there are no resonance parameters in the only existing file of evaluated nuclear data on ^{232}Pa (JENDL-3.2 [1]). This file gives the cross-sections up to 1 eV as a point curve with an energy dependence of $1/\sqrt{E}$ and based on values σ_f^{2200} = 700 b, σ_γ^{2200} = 464 b and I_γ = 300 b [2], where the value of σ_f^{2200} [2] is based on personal communications from as early as 1946 whilst the activation measurements of σ_γ^{2200} and I_γ have been taken from Ref. [3]. The cross-sections above 1 eV are based on theoretical calculations. The fission cross-section measurements for the energy range 0.01-100 eV performed by Danon et al. in their recent work [4] enabled the authors to calculate Breit-Wigner parameters up to 9 eV. In the present paper, we have used an analysis of the experimental data from Ref. [4] as a basis for obtaining multilevel Breit-Wigner parameters which adequately reproduce the fission cross-section curve over a wider energy range.

The curve for $\sigma_f(E)$ measured in Ref. [4] gives values of σ_f^{2200} =1506 ± 14 b and I_f = 1075 ± 11 b which are substantially higher than in Refs [1, 2]. It is quite possible that the $\sigma_f(E)$ curve in Ref. [4] is slightly overestimated, as may be concluded from an analysis of the fission cross-section measurements for ^{236}Np and ^{238}Np carried out in the same study; nevertheless, the data of Ref. [4] have been taken as a basis for the present paper because sufficiently detailed information exists as to how they have been obtained, which is not the case with Ref. [2]. The curve of $\sigma_f(E)$ for ^{232}Pa obtained in Ref. [4] is influenced considerably by the accuracy with which ^{232}U and ^{233}U impurities, whose levels are very high, are taken into account.

Analysis of the experimental values given in Ref. [4] for the ^{232}Pa fission cross-section in the energy range 1-21 eV leads to the conclusion that the aforementioned impurities were

not taken into account entirely correctly. The ^{232}U impurity content in the sample adopted by the authors of Ref. [4] was lower than the actual value, as indicated by the σ_f (E) curve in the 6 and 13 eV regions, where fairly strong resonances of this nucleus are located. As regards the ^{233}U impurity, the use of the ENDF/B-VI parameters [5] to take it into account is not altogether justified, since the energy scales of this evaluation and of the experiment in Ref. [4] differ somewhat, resulting in a distortion of the σ_f (E) curve in the energy range in question. Moreover, as with the ^{232}U impurity, the ^{233}U content in the sample was higher than suggested by the authors of Ref. [4]. All this renders it necessary to introduce corrections to the authors' values for σ_f (E). The experimental values for the ^{232}Pa fission cross-section in Ref. [4] over the energy range 0.01-21 eV were recalculated as follows:

1. The ^{232}U fission cross-section was calculated using the ENDF/B-VI parameters [5] and taking into account actual experimental conditions for all energy points of the ^{232}Pa fission cross-section from Ref. [4] and deducted from the latter using a coefficient of 0.023, which reduces practically to zero the contribution of the ^{232}U impurity to the ^{232}Pa fission cross-section;

2. The ^{233}U fission cross-section was calculated using the ENDF/B-VI parameters [5] and recalculated parameters from Ref. [6] to a greater accuracy than in Ref. [5], since the curve of the ^{233}U fission cross-section based on actual experimental conditions is reproduced for all energy points of Ref. [4]. Then the contribution of ^{233}U calculated using the parameters of Refs [5] and [6], respectively, was added to and deducted from the ^{232}Pa fission cross-section, applying appropriate coefficients, which made it possible to eliminate a number of anomalies in the σ_f (E) curve for ^{232}Pa given in Ref. [4].

The corrections applied give a more precise curve for the measured fission cross-section of Ref. [4], lowering it somewhat so that σ_f^{2200} is equal to 1480.16 b and I_f (0.5-21 eV) is 833.38 b rather than 866.59 b. Such a minor change nevertheless makes it possible to determine more accurately the number of resonances and the resonance parameters for levels up to 9 eV, as well as to identify the resonances with sufficient confidence and to calculate their parameters in the energy range 9-21 eV, by making the experimentally measured σ_f (E) curve more accurate.

In what follows, the experimentally measured fission cross-section for ^{232}Pa, used to carry out parametrization for the present study, will be taken to mean the ^{232}Pa fission cross-section from Ref. [4] recalculated as described above.

In Ref. [4] the authors identified 10 resonances for representing the fission cross-section in the energy range 0.01-9 eV and one background resonance with E_γ = -5.0 eV required to describe the curve of the fission cross-section in the thermal range. The calculations performed showed that the agreement between the experimentally measured and the calculated values for the fission cross-sections in the energy range in question can be improved considerably in the following way:

1. The resonance with an energy E_γ = 1.37 eV is replaced by two others: E_γ = 1.14 eV and E_γ = 1.42 eV;

2. Resonances with energies of 4.90, 5.35 and 5.82 eV are added;

3. The resonance energies are changed: 6.44 to 6.45 eV, 7.45 to 7.48 eV, and 8.41 to 8.44 eV;

4. New values of the parameters for all resonances in the range 0.01-9 eV are calculated.

In the energy range 9-21 eV, analysis of the experimentally measured fission cross-section makes it possible to identify 18 resonances with some confidence and to calculate their parameters, which permits good reproduction of the measured fission cross-section curve up to 21 eV.

Since the parameters of all resonances were calculated on the basis of the fission cross-section alone, and the resolution of the experiment was low, a large uncertainty arises in obtaining Γ_γ values for each resonance. Value $\langle\Gamma_\gamma\rangle$ = 40 meV was used as additional information in calculating the radiation widths.

The contribution to σ_f^{2200} from all resonances with $E_\gamma > 0$ is approximately 45% of the measured value; thus, to obtain the required value σ_f^{2200} = 1480.16 b we need at least one additional resonance with an energy under 0.3 eV. For the present paper, we used a resonance with E_γ = -5.0 eV and fully physical values of Γ_f and Γ_γ as the level for fitting in this way. However, the value of Γ_n^0 for this resonance proved to be greater by two orders of magnitude than the value of $\langle\Gamma_n^0\rangle$ for the remaining resonances, which was reflected in a value σ_n^{2200} = 17.66 b, whereas without including the negative resonance we have σ_n^{2200} = 9.45 b.

The calculated value of I_f(0.5-21 eV) = 824.33 b is 1.1% less than the value of I_f(0.5-21 eV) = 833.38 b (see above) used for parametrization.

The table gives resolved resonance parameters up to 21 eV obtained in the present study. Thermal constants derived from Table 1 using a value R = 9.89 fm are as follows:

σ_t^{2200} = 1667.47 b, σ_f^{2200} = 1480.16 b, g_f = 1.04197,

σ_n^{2200} = 17.66 b, σ_γ^{2200} = 169.65 b, g_γ = 1.07913.

Mean resonance parameters obtained for all resonances with $E_\gamma > 0$ are:

$\langle\Gamma_n^0\rangle$ = 0.16377 meV, $\langle D\rangle$ = 0.6548 eV,

$\langle\Gamma_f\rangle$ = 374.529 meV, $S_0 = 1.2505 \times 10^{-4}$,

$\langle\Gamma_\gamma\rangle$ = 40.142 meV.

An evaluation of the possible transmission of resonances gives the values:

$$\langle D \rangle = 0.5971 \pm 0.527 \text{ eV}, \qquad S_0 = (1.1142 \pm 0.0428) \times 10^{-4}.$$

Figure 1 gives a comparison, in the energy range 0.01-21 eV, of the fission cross-section values used for parametrization with those calculated using the parameters set out in the table and taking into account the experimental conditions of Ref. [4]. It is clear that the parameters in the table provide an adequate description of the fission cross-section curve over the entire energy range under consideration.

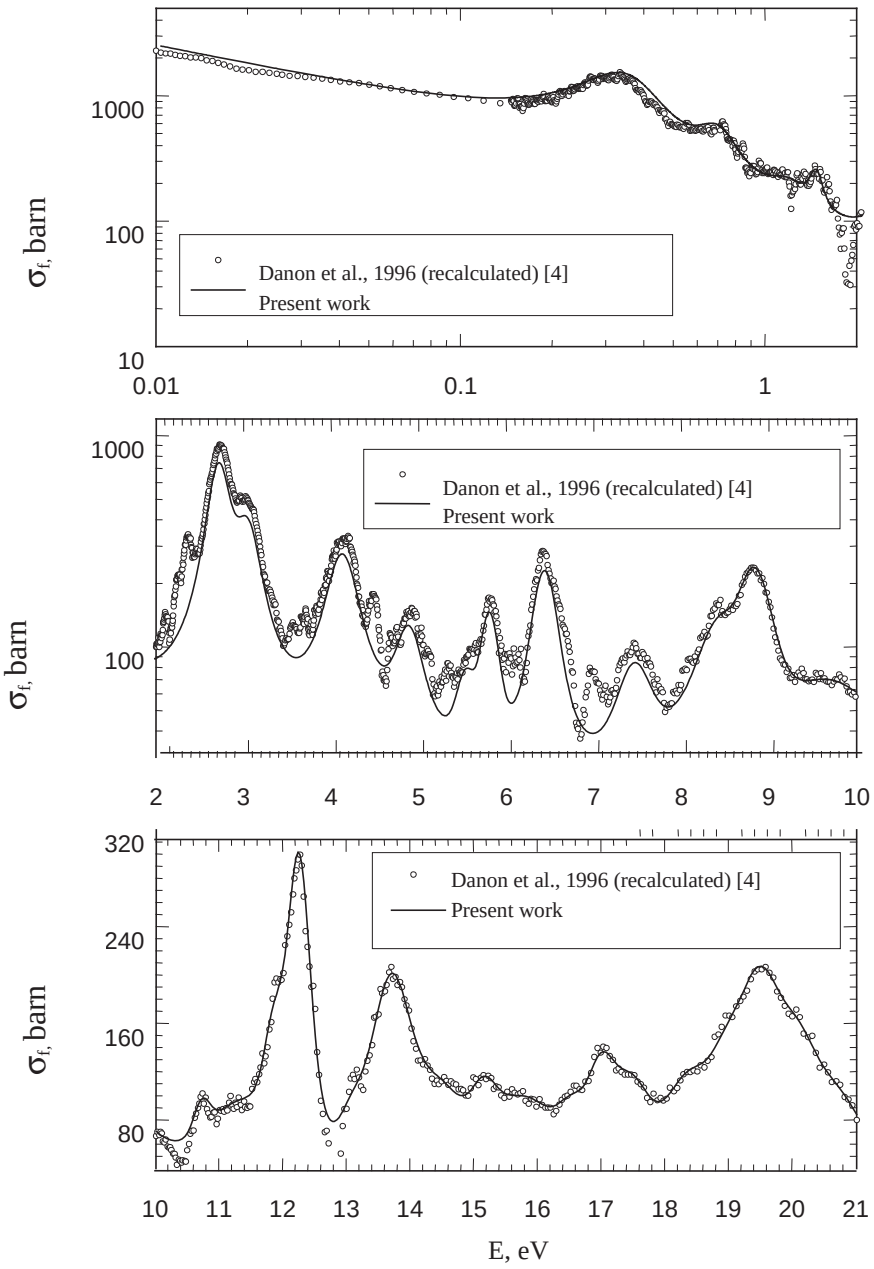

Fig. 1. Comparison of experimental fission cross-sections for ^{232}Pa with cross-sections calculated using the parameters in the table for the energy range 0.01-21 Ev.

Table 1

Resonance parameters for ^{232}Pa

E_r, eV	J	Γ_n, meV	Γ_γ, meV	Γ_f, meV
-5.000	1.5	32.5600	35.46	860.410
0.330	2.5	0.06759	41.97	194.280
0.670	2.5	0.03707	37.83	203.460
1.140	1.5	0.03482	43.99	363.070
1.420	2.5	0.02234	41.02	99.800
2.730	2.5	0.45673	43.68	214.060
3.060	1.5	0.34400	41.53	243.330
4.140	1.5	0.48403	36.12	327.930
4.900	1.5	0.17894	37.67	249.250
5.550	2.5	0.04618	40.75	99.950
5.820	2.5	0.13762	38.52	62.501
6.450	1.5	0.50520	41.48	157.960
7.480	2.5	0.14410	43.84	300.870
8.440	2.5	0.33788	44.11	437.140
8.850	2.5	0.50652	42.50	215.270
9.700	1.5	0.43338	34.76	946.770
10.720	2.5	0.17967	39.95	11.435
11.300	1.5	1.16292	30.83	1468.000
11.860	2.5	0.24457	38.94	118.960
12.250	2.5	0.84017	42.93	142.520
13.070	2.5	0.06627	39.37	100.600
13.700	1.5	1.84963	35.86	672.380
14.500	2.5	0.39400	44.72	725.240
15.150	2.5	0.15567	36.29	91.006
15.800	1.5	1.87330	50.33	1447.700
16.550	2.5	0.18503	39.72	90.172
17.000	1.5	0.76042	36.67	40.160
17.470	1.5	0.71170	43.80	308.890
18.370	2.5	0.88950	33.66	731.950
18.950	2.5	0.28400	40.52	90.381
19.500	2.5	1.73933	35.30	594.840
20.100	1.5	0.93190	40.22	17.947
20.630	2.5	1.64015	45.67	1217.100

References

[1] Japanese Evaluated Data Library, Version 3, JAERI 1319 (1990).

[2] S.F. Mughabghab, BNL-325, Neutron Cross Sections (1984) V. 1.

[3] E. Gryntakis, D.E. Cullen, G. Mundy, Handbook on nuclear activation data, STI/DOC/10/273, IAEA, Vienna (1987) p. 199.

[4] Y. Danon, M.S. Moore, P.E. Koehler, et al., Nucl. Sci. Eng. (1996) V.124, p. 482.

[5] C.L. Dunford, Nuclear Data for Science and Technology (Proc. Int. Conf. Jülich, 1991) p. 788. Springer-Verlag (1992) Berlin.

[6] G.B. Morogovskij, Voprosy atomnoj nauki i tekhniki, Ser. Yadernye konstanty (1999) No. 1, p. 9.

CONSTANTS AND PARAMETERS OF NUCLEAR STRUCTURE AND NUCLEAR REACTIONS

UDC 539.17:6813.016

BOFOD-99: PRESENT STATUS OF THE EVALUATED PHOTONUCLEAR DATA FILE

A.I. Blokhin, N.N. Buleeva, V.V. Vozyakov, M.V. Mikhailyukova, S.M. Nasyrova
State Scientific Centre of Russian Federation "Institute of Physics and Power Engineering", Obninsk, Russia

BOFOD-99: PRESENT STATUS OF THE EVALUATED PHOTONUCLEAR DATA FILE. The activity on the creation of evaluated photonuclear data library for 63 isotopes and elements is described briefly. The photonuclear data library BOFOD-99 includes in mainly the photoneutron and photofission cross sections in the gamma ray energy range up to 20 MeV and is constructed in the ENDF-6 format.

The BOFOD-99 library is one of various kinds of BROND special purpose files. Prepared in previous years the BOFOD library included in mainly the photonuclear data up to 20 MeV for 27 elements and was described in Ref. [1].

In this article the present status and content of the BOFOD-99 library is described briefly. The main efforts in 1994-1999 were aimed to prepare the complete sets of evaluated photonuclear data for the more number of the elements and their isotopes. The present BOFOD-99 library consists from two parts and is aimed for transport calculations and radioisotope production cross sections. The first part of the BOFOD library includes the sets of photoneutron and photofission data (cross sections and angular-energy distributions of secondary neutrons) in the gamma-ray energy range up to 20 MeV. The second part of the BOFOD library includes data for calculations of production of radioisotopes in photonuclear reactions. For that the complete evaluated photneutron data files for two materials (Be, Ta-181) were prepared in the gamma-ray energy range up to 70 MeV. Cross sections for production of radioisotopes in the gamma-ray energy range up to 70 MeV needed for the Positron Emitter Tracer task were produced using the combination of fitting of experimental data and theoretical calculations. The list of those 11 elements is: ^{12}C(γ, n), ^{14}N(γ, n), ^{16}O(γ, n), ^{19}F(γ, n), ^{nat}Ne(γ, 2n+p), ^{32}S(γ, np), ^{54}Fe(γ, np), ^{63}Cu(γ, n), ^{65}Cu(γ, n), ^{nat}Ga(γ, n), ^{141}Pr(γ, n).

For a presentation of the evaluated photonuclear we used MT's numbers which differ slightly from MT's numbers recommended by the 1-st Research Co-ordination Meeting on "Compilation and Evaluation of Photonuclear Data for Applications" [2]. Table 1 presents the types of photonuclear processes included in the evaluated photonuclear data files.

The BOFOD-99 library is in "ENDF-6" format and has N-LIB=42 for identifying the library. As in the case of the neutron data, we used the following scheme to present the photonuclear data:

MF=1: Descriptive data and dictionary;
MF=2: Resonance parameters (in our case we give only the scattering radius);
MF=3: Photonuclear cross sections for the various photonuclear processes presented with the help of MT identifiers defined in the Table 1;
MF=4,5: Data for angular and energy distributions of photoneutrons, respectively.

In Table 2 we give a present content of the first part of the BOFOD-99 library. The following notations are used:

σ - integral cross sections (MF=3);
$\nu(E_\gamma)$, $\nu_p(E_\gamma)$, $\nu_d(E_\gamma)$ – Total, Prompt and Delayed Number of Neutrons per Fission, respectively;
$d\sigma/d\Omega$ - angular distribution of photoneutrons (MF=4);
$d\sigma/dE$ – energy distribution of photoneutrons (MF=5);
$d\nu_p/dE_n$, $d\nu_d/dE_n$ – energy distributions of Prompt and Delayed Photofission Neutrons, respectively.

Table 1

Definition of MT's numbers for presentation of photonuclear data in BOFOD-99 library

MT= 1 for $\sigma(\gamma,tot) = \sigma(\gamma,abs) + \sigma(\gamma,\gamma)$ - total photo-interaction cross-section;
MT= 2 for $\sigma(\gamma,\gamma)$ - photo-elastic cross-section;
MT= 3 for $\sigma(\gamma,abs)$ - photo-absorption cross-section;
MT= 4 for $\sigma(\gamma,n+np)$ - single neutron emission cross-section;
MT= 5 for $\sigma(\gamma, Sn) = \sigma(\gamma,n+np) + \sigma(\gamma, 2n+2np) + \sigma(\gamma, fis)$ - total photoneutron cross section;
MT=16 for $\sigma(\gamma,2n+2np)$ - double neutron emission cross-section;
MT=18 for $\sigma(\gamma,fis)$ - photo-fission cross-section;
MT= 28 for $\sigma(\gamma,np)$ - cross-section;
MT= 41 for $\sigma(\gamma,2n+p)$ - cross-section;
MT= 201 for $\sigma(\gamma, Xn) = \sigma(\gamma,n+np) + 2*\sigma(\gamma, 2n+2np) + \nu*\sigma(\gamma, fis)$ - photoneutron yield cross section;
MT=451 - Descriptive Data and Directory;
MT=452 - Total Number of Neutrons per Fission;
MT=455 - Number of Delayed Neutrons per Fission;
MT=456 - Number of Prompt Neutrons per Fission;
MT=458 - Components of Energy Release Due to Fission.

Table 2

Content of Evaluated Photonuclear Data Files from BOFOD-99 Library

Element or Isotope	MAT	Reaction	Quantity
Be-009	409	(γ, n)	σ
Na-023	1123	(γ, n)	σ
Cr-050	2450	(γ, abs), (γ, Sn) (γ, n), (γ, 2n)	σ, dσ/dE, dσ/dΩ
Cr-052	2452	(γ, abs), (γ, Sn) (γ, n), (γ, 2n)	σ, dσ/dE, dσ/dΩ
Cr-053	2453	(γ, abs), (γ, Sn) (γ, n), (γ, 2n)	σ, dσ/dE, dσ/dΩ
Cr-054	2454	(γ, abs), (γ, Sn) (γ, n), (γ, 2n)	σ, dσ/dE, dσ/dΩ
Mn-055	2555	(γ, n)	
Fe-054	2654	(γ, abs), (γ, Sn) (γ, n), (γ, 2n)	σ, dσ/dE, dσ/dΩ
Fe-056	2656	(γ, abs), (γ, Sn) (γ, n), (γ, 2n)	σ, dσ/dE, dσ/dΩ
Fe-057	2657	(γ, abs), (γ, Sn) (γ, n), (γ, 2n)	σ, dσ/dE, dσ/dΩ
Fe-058	2658	(γ, abs), (γ, Sn) (γ, n), (γ, 2n)	σ, dσ/dE, dσ/dΩ
Ni-nat	2800	(γ, abs), (γ, Sn) (γ, n), (γ, 2n)	σ, dσ/dE, dσ/dΩ
Ni-058	2858	(γ, abs), (γ, Sn) (γ, n), (γ, 2n)	σ, dσ/dE, dσ/dΩ
Ni-060	2860	(γ, abs), (γ, Sn) (γ, n), (γ, 2n)	σ, dσ/dE, dσ/dΩ
Ni-061	2861	(γ, abs), (γ, Sn) (γ, n), (γ, 2n)	σ, dσ/dE, dσ/dΩ
Ni-062	2862	(γ, abs), (γ, Sn) (γ, n), (γ, 2n)	σ, dσ/dE, dσ/dΩ
Ni-064	2864	(γ, abs), (γ, Sn) (γ, n), (γ, 2n)	σ, dσ/dE, dσ/dΩ
Sr-088	3888	(γ, abs), (γ, n), (γ, 2n)	σ, dσ/dE, dσ/dΩ
Zr-nat	4000	(γ, abs), (γ, Sn) (γ, n), (γ, 2n)	σ, dσ/dE, dσ/dΩ
Zr-090	4090	(γ, abs), (γ, Sn) (γ, n), (γ, 2n)	σ, dσ/dE, dσ/dΩ
Zr-091	4091	(γ, abs), (γ, Sn) (γ, n), (γ, 2n)	σ, dσ/dE, dσ/dΩ
Zr-092	4092	(γ, abs), (γ, Sn) (γ, n), (γ, 2n)	σ, dσ/dE, dσ/dΩ
Zr-094	4094	(γ, abs), (γ, Sn) (γ, n), (γ, 2n)	σ, dσ/dE, dσ/dΩ
Zr-096	4096	(γ, abs), (γ, Sn) (γ, n), (γ, 2n)	σ, dσ/dE, dσ/dΩ
Mo-092	4292	(γ, abs)	σ
Mo-094	4294	(γ, abs)	σ

Element or Isotope	MAT	Reaction	Quantity
Mo-096	4296	(γ, abs)	σ
Mo-098	4298	(γ, abs)	σ
Mo-100	4299	(γ, abs)	σ
Sn-114	5014	(γ, abs)	σ
Sn-116	5016	(γ, abs)	σ
Sn-117	5017	(γ, abs)	σ
Sn-118	5018	(γ, abs)	σ
Sn-119	5019	(γ, abs)	σ
Sn-120	5020	(γ, abs)	σ
Sn-122	5022	(γ, abs)	σ
Sn-124	5024	(γ, abs)	σ
Te-120	5220	(γ, abs)	σ
Te-122	5222	(γ, abs)	σ
Te-124	5224	(γ, abs)	σ
Te-126	5226	(γ, abs)	σ
Te-128	5228	(γ, abs)	σ
Te-130	5230	(γ, abs)	σ
W-182	7482	(γ, abs)	σ
W-184	7484	(γ, abs)	σ
W-186	7486	(γ, abs)	σ
Pb-nat	8200	(γ, abs), (γ, Sn) (γ, n), (γ, 2n)	σ
Bi-209	8309	(γ, abs), (γ, Sn) (γ, n), (γ, 2n)	σ
Th-232	9032	(γ,tot), (γ,γ), (γ, abs), (γ, Sn), (γ, Xn), (γ, n), (γ, 2n), (γ, fis)	σ, ν(E), ν_p(E), ν_d(E), dσ/dE, dσ/dΩ, $d\nu_p/dE$, $d\nu_d/dE$
U-233	9233	(γ,tot), (γ,γ), (γ, abs), (γ, Sn), (γ, Xn), (γ, n), (γ, 2n), (γ, fis)	σ, ν(E), ν_p(E), ν_d(E), dσ/dE, dσ/dΩ, $d\nu_p/dE$, $d\nu_d/dE$
U-234	9234	(γ,tot), (γ,γ), (γ, abs), (γ, Sn), (γ, Xn), (γ, n), (γ, 2n), (γ, fis)	σ, ν(E), ν_p(E), ν_d(E), dσ/dE, dσ/dΩ, $d\nu_p/dE$, $d\nu_d/dE$
U-235	9235	(γ,tot), (γ,γ), (γ, abs), (γ, Sn), (γ, Xn), (γ, n), (γ, 2n), (γ, fis)	σ, ν(E), ν_p(E), ν_d(E), dσ/dE, dσ/dΩ, $d\nu_p/dE$, $d\nu_d/dE$
U-236	9236	(γ,tot), (γ,γ), (γ, abs), (γ, Sn), (γ, Xn), (γ, n), (γ, 2n), (γ, fis)	σ, ν(E), ν_p(E), ν_d(E), dσ/dE, dσ/dΩ, $d\nu_p/dE$, $d\nu_d/dE$
U-238	9238	(γ,tot), (γ,γ), (γ, abs), (γ, Sn), (γ, Xn), (γ, n), (γ, 2n), (γ, fis)	σ, ν(E), ν_p(E), ν_d(E), dσ/dE, dσ/dΩ, $d\nu_p/dE$, $d\nu_d/dE$
Np-237	9237	(γ,tot), (γ,γ), (γ, abs), (γ, Sn), (γ, Xn), (γ, n), (γ, 2n), (γ, fis)	σ, ν(E), ν_p(E), ν_d(E), dσ/dE, dσ/dΩ, $d\nu_p/dE$, $d\nu_d/dE$
Pu-238	9438	(γ,tot), (γ,γ), (γ, abs), (γ, Sn), (γ, Xn), (γ, n), (γ, 2n), (γ, fis)	σ, ν(E), ν_p(E), ν_d(E), dσ/dE, dσ/dΩ, $d\nu_p/dE$, $d\nu_d/dE$

Element or Isotope	MAT	Reaction	Quantity
Pu-239	9439	(γ,tot), (γ,γ), (γ, abs), (γ, Sn), (γ, Xn), (γ, n), (γ, 2n), (γ, fis)	σ, ν(E), ν_p(E), ν_d(E), dσ/dE, dσ/dΩ, $d\nu_p/dE$, $d\nu_d/dE$
Pu-241	9441	(γ,tot), (γ,γ), (γ, abs), (γ, Sn), (γ, Xn), (γ, n), (γ, 2n), (γ, fis)	σ, ν(E), ν_p(E), ν_d(E), dσ/dE, dσ/dΩ, $d\nu_p/dE$, $d\nu_d/dE$
Am-241	9541	(γ,tot), (γ,γ), (γ, abs), (γ, Sn), (γ, Xn), (γ, n), (γ, 2n), (γ, fis)	σ, ν(E), ν_p(E), ν_d(E), dσ/dE, dσ/dΩ, $d\nu_p/dE$, $d\nu_d/dE$
Am-243	9543	(γ,tot), (γ,γ), (γ, abs), (γ, Sn), (γ, Xn), (γ, n), (γ, 2n), (γ, fis)	σ, ν(E), ν_p(E), ν_d(E), dσ/dE, dσ/dΩ, $d\nu_p/dE$, $d\nu_d/dE$
Cm-243	9643	(γ,tot), (γ,γ), (γ, abs), (γ, Sn), (γ, Xn), (γ, n), (γ, 2n), (γ, fis)	σ, ν(E), ν_p(E), ν_d(E), dσ/dE, dσ/dΩ, $d\nu_p/dE$, $d\nu_d/dE$
Cm-244	9644	(γ,tot), (γ,γ), (γ, abs), (γ, Sn), (γ, Xn), (γ, n), (γ, 2n), (γ, fis)	σ, ν(E), ν_p(E), ν_d(E), dσ/dE, dσ/dΩ, $d\nu_p/dE$, $d\nu_d/dE$
Cm-245	9645	(γ,tot), (γ,γ), (γ, abs), (γ, Sn), (γ, Xn), (γ, n), (γ, 2n), (γ, fis)	σ, ν(E), ν_p(E), ν_d(E), dσ/dE, dσ/dΩ, $d\nu_p/dE$, $d\nu_d/dE$

References

[1] A.I. Blokhin, N.N. Buleeva, S.M. Nasyrova et al. Preparation and use of “BOFOD” evaluated photoneutron data library. J., YK (1992), v.3-4, p.3-54.
See also: A.I. Blokhin, N.N. Buleeva, S.M. Nasyrova et al. Report INDC(CCP)-381, IAEA, Vienna, 1994.

[2] Summary Report of the 1-st Research Co-ordination Meeting on “Compilation and Evaluation of Photonuclear Data for Applications” by P. Oblozinsky. Report INDC(NDS)-364, IAEA, Vienna, 1997.

00-30130 (113) [10]
Translated from Russian

UDC 002.63: 539.17: 681.3

WEB SERVER OF THE CENTRE FOR PHOTONUCLEAR EXPERIMENTS DATA OF THE SCIENTIFIC RESEARCH INSTITUTE FOR NUCLEAR PHYSICS, MOSCOW STATE UNIVERSITY: HYPERTEXT VERSION OF THE NUCLEAR PHYSICS DATABASE

I.N. Boboshin, A.V. Varlamov, V.V. Varlamov, D.S. Rudenko, M.E. Stepanov
D.V. Skobel'tsyn Scientific Research Institute for Nuclear Physics,
M.V. Lomonosov Moscow State University,
Centre for Photonuclear Experiments Data

WEB SERVER OF THE CENTRE FOR PHOTONUCLEAR EXPERIMENTS DATA OF THE SCIENTIFIC RESEARCH INSTITUTE FOR NUCLEAR PHYSICS, MOSCOW STATE UNIVERSITY: HYPERTEXT VERSION OF THE NUCLEAR PHYSICS DATABASE. The nuclear databases which have been developed at the Centre for Photonuclear Experiments Data of the D.V. Skobel'tsyn Scientific Research Institute for Nuclear Physics, M.V. Lomonosov Moscow State University, and put on the Centre's web server, are presented. The possibilities for working with these databases on the Internet are described.

At the current stage of development in science, wide use is being made of computer technology and automated systems not only to carry out experiments and process the results, but also for subsequent analysis and evaluation of the data. On the one hand the experiments themselves are getting much more complex, and on the other hand much higher requirements are being imposed as regards the quality of the results. The problems of elaborating dependable and reliable methods for processing the data already available, and for evaluating the data both with and without using theoretical models, are becoming more and more acute. If we are to solve these problems, we need to create large databases and data banks, and effective software packages for working with them. Producing different types of data bank, database and electronic data library provides a good basis for achieving a new qualitative level in fundamental and applied research. The development and improvement of computerized data manipulation techniques facilitates not only the effective processing and analysis of the results of previous experiments, but also the planning of new experiments, and the modelling of experiments which - for one reason or another - cannot be carried out.

These trends in various fields of science and technology play a significant role in nuclear physics as well, where it is more often than not impossible to measure certain values directly; this means that indirect methods must be used to study them, as well as various combinations of the available data. This makes for significantly higher requirements as regards the accuracy and reliability of such data and means that effectiveness of scientific research is directly linked to progress in information technology. Moreover, using modern information technology [1] not only facilitates effective work with the currently available data; it also in many cases allows new physical results to be obtained [2, 3].

The Centre for Photonuclear Experiments Data of the Scientific Research Institute for Nuclear Physics, M.V. Lomonosov Moscow State University, and the International Nuclear Data Centres Network

Large volumes of nuclear physics information are generated and maintained by special organizations, the Nuclear Data Centres, which have been organized into a global system by the International Atomic Energy Agency (IAEA). In recent years this system has become a kind of network (Nuclear Data Centres Network) [4]. Nuclear data groups and centres from Austria, Hungary, China, Russia, the USA, Ukraine, France and Japan are participating in this collaborative effort. Russia is represented here by three organizations: the Nuclear Data Centre of the Institute for Physics and Power Engineering, Obninsk; the Centre for Nuclear Structure and Reaction Data of the Kurchatov Institute, Moscow; and the Centre for Photonuclear Experiments Data of the Scientific Research Institute for Nuclear Physics, M.V. Lomonosov Moscow State University. These centres prepare specific sections of the numerical nuclear data files in a co-ordinated manner, and they then combine them and organize work with the data within the framework of various databases or data banks which meet practically all data requirements for research into the physics of the nucleus and low- and intermediate-energy nuclear reactions.

Within the context of this international collaboration with the IAEA, the Centre for Photonuclear Experiments Data is responsible for photonuclear data, i.e. data on nuclear reactions induced by photons and electrons. In addition, the Centre processes data on reactions involving radiative capture of neutrons and various charged particles. To date, the Centre has prepared 80% of the photonuclear data included in the data collections produced by this international co-operation.

The Centre uses the various data banks, databases and data files which are generated or obtained through exchange arrangements, and which contain information on nuclear reactions induced by neutrons and charged particles and reference and bibliographical data on the structure of nuclei, to meet the requests of its users. The Centre carries out this work as part of the work programmes under an IAEA research contract, a similar State-level activity, the BAPHYS programme, and with a grant from the Russian Foundation for Fundamental Research.

Nuclear Data in the Internet

Recently, what one might call “on-line service” Internet-based information systems have become very common in the Nuclear Data Centre Network. Two main access routes to the data are used, depending mainly on the capabilities of the user’s PC:

- **Internet** (multifunctional search systems containing a large amount of additional visual information (graphs and diagrams); the most recent Internet browser versions have the greatest capabilities thanks to the use of the latest data presentation resources (frames, JavaScript, JScript, JAVA, CGI, ASP, etc.));

- **Telnet** (search systems where the user's options are significantly limited because the data is presented in text form; the advantages of this route are that it can be used with low-transmission-capacity connections and offers additional specialized real-time data processing facilities).

The Internet addresses of the various nuclear physics data collections of some of the Nuclear Data Centres are well known to the experts:

BNL NNDC Brookhaven National Laboratory, National Nuclear Data Center (USA):

telnet://bnlnd2.dne.bnl.gov
http://www.nndc.bnl.gov

IAEA NDS International Atomic Energy Agency, Nuclear Data Section (Austria):

telnet://iaeand.iaea.org
http://www-nds.iaea.org

LUND Lund University, Lund Nuclear Data Web Service (Sweden):

http://nucleardata.nuclear.lu.se/nucleardata/

NIST National Institute of Standards and Technology, Physics Laboratory (USA):

http://physics.nist.gov/

NEA-DB OECD Nuclear Energy Agency Data Bank (France):

http://www.nea.fr

A web server has been set up at the following address to provide permanent access for remote Internet users to the nuclear physics information available at the Centre for Photonuclear Experiments Data:

http://depni.npi.msu.su/cdfe;

the Centre's main photonuclear databases are available here [5-7].

Web Server of the Centre for Photonuclear Experiments Data

A hypertext version of the Centre's main database was developed so that the data could be placed on the Centre's web server. This hypertext version has advantages and disadvantages. Users who are not acquainted with the database format will find this presentation of the data more convenient. More experienced users will find that a search system based on - for example - the MySQL or Oracle DBMS, and specially adapted to the web environment, will offer them greater possibilities. We are currently developing this type of presentation of the data at the Centre.

The hypertext tables on the Centre's web server are being created with help of several software packages, chief among which is the Borland Paradox relational DBMS. A program has been written in Pascal to generate automatically the hypertext files from the source file, which is in Paradox DBMS format. All the documents in the databases are written only in HTML, without using such technologies as JavaScript, Java, CGI, ASP, etc.

Main web page of the server

The databases on the Centre's server are accessed through the *"On-line Services"* section of the server's main (home) page (see Fig. 1). The other sections of the main page contain the following information:

- **"About"**: information on the aims and main emphases of the Centre's activities;
- "**People**": list of the Centre's principal staff;
- "**Partners**": list of the Centre's main partners for international collaboration;
- "**Contact Us**": contact addresses for the Centre.

Main system menu

The main system menu is used to search for the required data. Data can be searched for by element (nucleus, isotope) and reaction.

For the purposes of searches by element, part of the main system menu is organized in the form of the familiar periodic table of the elements. Selecting a specific element calls up an intermediate system menu which can be used to select one of the main databases on the server (DB1, DB2 and DB3).

For the purposes of searches by reaction, the relevant part of the main system menu is organized in the form of a full list of the reactions for which data is available on the web server (see Fig. 2). Selecting a specific reaction also calls up an intermediate menu which allows the user to make a selection among the databases on the server (DB1, DB2 and DB3).

Intermediate system menus

The intermediate system menu for an element search comprises a table of the abundances of the stable isotopes of the selected element (see Fig. 3; in this case we are dealing with the isotopes of tin: ^{112,114,115,116,117,118,119,120,122,124}Sn) in their naturally occurring mixture, together with a list of the databases on the server which may be selected for the actual data search.

The intermediate system menu for a reaction search only includes a list of the databases on the server:

DB1 - database of giant dipole resonance parameters and photonuclear reaction cross-sections (Giant Dipole Resonance Data);
DB2 - database of the abundances of the stable isotopes of nuclei and the energy

thresholds of photonuclear reactions (Reaction Thresholds Data);

DB3 - bibliographical reference database of photonuclear reaction data published over the whole research history (as of the middle of 1999 - for 1955-1996) (Photonuclear Data Index).

Database of giant dipole resonance parameters and photonuclear reaction cross-sections (DB1)

DB1 [8, 9] (see Fig. 4) contains data on the following characteristics (a reference and the name of the primary author of the relevant publication is also given) of resonances observed in the cross-sections of a large number of the most important photonuclear reactions, which are listed below, for the majority of known nuclei:

EXFOR	sub-accession number (SUBENT) in the EXFOR international database;
NUCL	nucleus studied (symbol);
A	nucleus studied (mass number);
REACT	reaction studied;
E-MAX	energy (in MeV) of the resonance maximum in the reaction cross-section;
SIG	cross-section (in mb) at the resonance maximum in the reaction cross-section;
FWHM	full width (in MeV) at half maximum of the resonance in the reaction cross-section;
E-INT	energy (in MeV) of the upper integration limit;
SIG-INT	integrated cross-section (in MeV∗mb);
SIG-INT-1	first moment (in mb) of the integrated cross-section;
REFERENCE	reference;
AUTHOR	last name and initials of primary author ((+) indicates that there are other authors).

G,ABS	total photoabsorption	[(γ,n) + (γ,p) + (γ,np) + (γ,2n) + (γ, d) + (γ,t) +...+ (γ,F)]
G,XN	neutron yield	[(γ,n) + (γ,np) + 2(γ,2n) + 3(γ,3n) + ... + ν (γ,F)]
G,SN	total neutron production	[(γ,n) + (γ,np) + (γ,2n) + (γ,3n) + ... + (γ,F)]
G,N	single neutron	[(γ,n) +(γ,np)]
G,NP	neutron-proton	(γ,np)
G,1N	pure one-neutron	(γ,n)
G,2N	double neutron	[(γ,2n) + γ,2np)]
G,3N	triple neutron	[(γ,3n) + (γ,3np)]
G,P	single proton	[(γ,p) + (γ,np)]
G,1P	pure one-proton	(γ,p)
G,D	deutron	(γ,d)
G,T	triton	(γ,t)
G,HE-3	He-3 nucleus	(γ,^{3}He)
G,A	alpha-particle	(γ,α)
G,F	fission/neutron for actinides	[(γ,f) + ν(γ,nf) + ...]

Since the information for the various maxima, which may be clearly observed in the cross-sections is given in separate rows of the table, the data can also be used to obtain a general picture of the shape of the resonances in the reaction cross-sections.

As of the middle of 1999, the database contained information (1317 sections in total) on 82 elements (220 isotopes and their naturally occurring mixtures) with values of Z = 1 - 95. In addition, numerical and graphical information on the energy dependences of the cross-sections (excitation functions) of the various types of photonuclear reaction has been prepared for the majority of the sections of the database (846 as of the middle of 1999) based on the EXFOR international nuclear reactions database [10].

The DB1 pages (Giant Dipole Resonance Data) provide the option of looking at a graphical representation of the selected reaction cross-section. The column containing the numbers of the sections of the EXFOR system in which the relevant numerical data are contained are used for this (see Fig. 4).

The source data in the table for the selected reaction cross-section can be downloaded to the user's computer for further use. In addition, the user is given summarized information on the publication in which the data on the selected cross-section were published.

Database of the abundances of isotopes and the thresholds of photonuclear reactions (DB2)

DB2 (see Fig. 6) contains numerical data on the abundances of the majority of the known stable isotopes of nuclei in their naturally occurring mixture.

The database also includes data on the energy thresholds (the rounded values from Ref. [11] are used) of the main reactions involving interaction of photons with all stable isotopes of nuclei (in the case illustrated, the isotopes of tin (Sn)) where there is accompanying emission of nucleons, various charged particles and certain combinations thereof.

Bibliographical reference database on photonuclear reactions (DB3)

The database contains a bibliography of publications (reference, primary author) in scientific periodicals from 1955 to the present day on experimental research into reactions involving interaction of low- and intermediate-energy electrons and photons with atomic nuclei, and reactions involving radiative capture of neutrons and charged particles.

The database also includes short descriptions (coded abstracts) of the experimental conditions (target nucleus, incident and emitted particles, nucleus excitation energy region or incident particle energy region, emission angle region of the reaction products) and the main results.

The database is based on the data in a file containing textual and numerical information prepared at the Centre for the period 1976-1996 [8] and at JAERI (Japan Atomic Energy Research Institute) for the period 1955-1992 [12].

DB3 (Photonuclear Data Index) contains (see Fig. 7) bibliographical reference information on publications in the scientific press on electromagnetic interaction of nuclei (the reactions listed in Fig. 3) for the period 1955-1996.

The database also includes a description of the experimental conditions (nucleus excitation energy region or incident particle energy region (**EN-MIN**, **EN-MAX**)), particle emission angle region (**ANG-MIN**, **ANG-MAX**)) and a list (in the form of codes from the relevant dictionary) of the main results obtained (**QUANTITY**):

NUMBER	relevant numbers of the sections in the indexes of the Centre for Photonuclear Experiments Data [8] and JAERI [12];
E	code for numerical data in the EXFOR system;
NUCL	nucleus studied (symbol);
A	nucleus studied (mass number);
REACT	reaction studied;
QUANTITY	codes for main results obtained;
EN-MIN	minimum energy (in MeV);
EN-MAX	maximum energy (in MeV);
ANG-MIN	minimum angle (in degrees);
ANG-MAX	maximum angle (in degrees);
REFERENCE	reference;
AUTHOR	last name (and initials) of primary author ((+) indicates that there are other authors).

The required information can be extracted from DB3 by element and by reaction in a similar manner to DB1.

The Centre's web server provides options for moving around DB1 (Giant Dipole Resonance Data) and DB2 (Reaction Thresholds Data) and selecting information on other reactions or nuclei, and for transferring from DB1 to DB2 and vice-versa. At present, DB3 (Photonuclear Data Index) is independent.

Access statistics for data on the server and prospects for its development

The Centre's web server has two standard user access counters. As of the end of June 1999, these were giving the following figures:

- Rambler's Top 100 (since the beginning of 1998) - 1182;

- ALPHA COUNTER (after 1998-11-10) - 556.

At present at the Centre:

- **we are working on adding data on photonuclear reactions published in 1997-1998 to the bibliographical reference database (DB3);**

- we are working on placing on the server data on the structure of nuclei prepared

at the Centre [13] using the international ENSDF file, and data on the cross-sections of reactions induced by charged particles prepared at the Centre for Nuclear Structure and Reaction Data using the new version of the catalogue in Ref. [14];

- we are developing a search version with a single universal presentation of the data from the Centre's databases based on the MySQL DBMS (using CGI) and the Oracle DBMS (using JAVA).

This work is being done with the support of the Russian Foundation for Fundamental Research (RFFI)
RFFI grant 99-07-90015

Fig. 1.

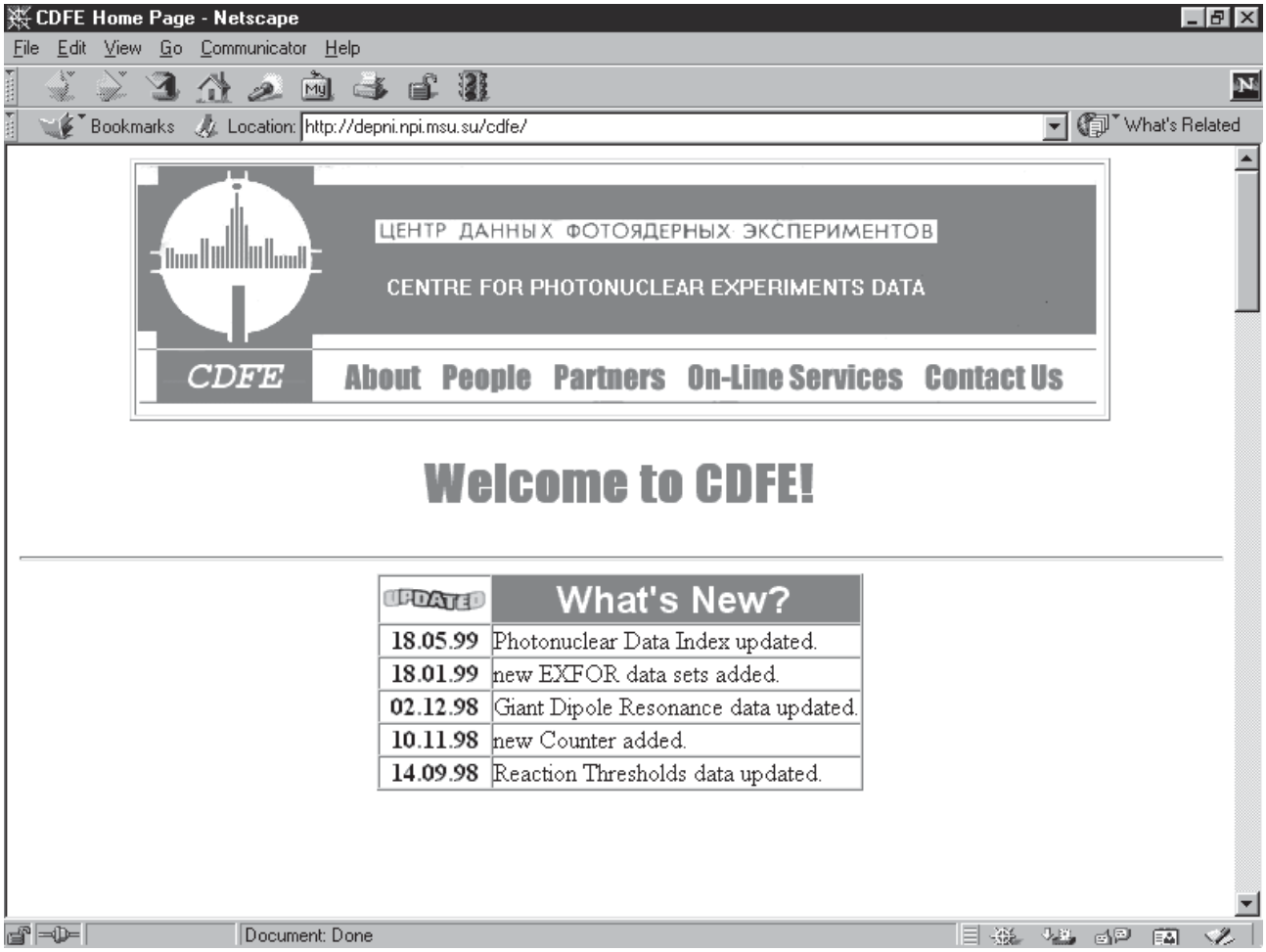
CDFE Home Page - Netscape
File Edit View Go Communicator Help
Bookmarks Location: http://depni.npi.msu.su/cdfe/ What's Related
ЦЕНТР ДАННЫХ ФОТОЯДЕРНЫХ ЭКСПЕРИМЕНТОВ
CENTRE FOR PHOTONUCLEAR EXPERIMENTS DATA
CDFE
About People Partners On-Line Services Contact Us
Welcome to CDFE!
UPDATED
What's New?
18.05.99 Photonuclear Data Index updated.
18.01.99 new EXFOR data sets added.
02.12.98 Giant Dipole Resonance data updated.
10.11.98 new Counter added.
14.09.98 Reaction Thresholds data updated.
Document: Done

Fig. 2.

Select the reaction to view:

(following abbreviations are in use:
GDRPRM - included into Giant Dipole Resonance data, **RTHR** - included into Reaction THResholds data, **PNI** - included into PhotoNuclear Data Index.) _

incident particle - G

G,E - (PNI only)
G,G - (PNI only)
G,G~ - (PNI only)
G,N
G,1N
G,NP
G,N2P
G,NA
G,NPA
G,N+X - (PNI only)
G,2N
G,2N+X - (PNI only)
G,3N
G,SN - (GDRPRM only)
G,SNF - (GDRPRM only)
G,XN
G,P
G,PA
G,PD
G,PT
G,P+X - (PNI only)
G,2P
G,2PN
G,2P+X - (PNI only)
G,XP
G,D
G,D+X - (PNI only)
G,2D
G,T
G,T+X - (PNI only)
G,HE - (PNI only)
G,HE3
G,XHE - (PNI only)
G,ION - (PNI only)
G,F
G,X - (PNI only)
G,ABS
G,MESON - (PNI only)
G,A
G,3A
G,4A

incident particle - E

(PNI only)

E,E
E,E~
E,E~N
E,E~NP
E,E~2N
E,E~3N
E,E~P
E,E~2P
E,E~D
E,E~T
E,E~HE
E,E~F
E,XN
E,XP
E,X
E,ION
E,ABS
E,MESON

incident particles - N, P, D, T, HE, IONS

(PNI only)

N,E
N,G
N,2G
N,ABS
P,G
D,G
T,G
HE,G
ION,G

Fig. 3.

Return to the CDFE On-Line Services Main Menu

	A	ABUNDANCE(%)
50-SN	112	1.00
	114	0.70
	115	0.40
	116	14.70
	117	7.70
	118	24.30
	119	8.60
	120	32.40
	122	4.60
	124	5.60

[Photonuclear Data Index]

[Giant Dipole Resonance Data | Reaction Thresholds Data]

RETURN TO CDFE

If you have questions, comments, and suggestions - please contact Webmaster

Fig. 4.

Data for *50-SN*

Return to the CDFE On-line Services Main Menu

[Reaction Thresholds Data]

Press here to view legend

EXFOR	NUCL	A	REACT	E-MAX MEV	SIG MB	FWHM MEV	E-INT MEV	SIG-INT MEV*MB	SIG-INT-1 MB	REFERENCE	AUTHOR
	50-SN		G,XN	16.	300.	5.	40.00	1640.	134.	PHYS.REV.,112,554(1958)	E.G.FULLER+
	50-SN	112	G,XN	15.8	295.	5.5	27.00	2230.		YAD.FIZ.,20,233(1974)	YU.I.SOROKIN+
	50-SN	112	G,SN	15.8	295.	5.5	27.00	1900.		YAD.FIZ.,20,233(1974)	YU.I.SOROKIN+
	50-SN	112	G,N	16.	340.	5.	21.00	1820.	152.	ZHETF,40,85(1961)	KU0 CHI-DI+
	50-SN	114	G,XN	15.7	265.	7.5	27.00	2260.		IZV.AN SSSR,39,114(1975)	YU.I.SOROKIN+
	50-SN	114	G,SN	15.7	265.	7.	27.00	1860.	108.	IZV.AN SSSR,39,114(1975)	JU.I.SOROKIN+
	50-SN	116	G,XN	15.6	260.	9.	27.00	2400.		IZV.AN SSSR,39,114(1975)	YU.I.SOROKIN+
I0035017	50-SN	116	G,XN	15.44	277.3	7.5	22.10	1823.		NUCL.PHYS.,A219,39(1974)	A.LEPRETRE+
I0017006	50-SN	116	G,XN	15.362	272.	6.	29.60	2083.		PHYS.REV.,186,1255(1969)	S.C.FULTZ+
I0017006	50-SN		G,XN	18.769	168.9						
I0017006	50-SN		G,XN	27.131	76.						
	50-SN	116	G,SN	15.6	260.	6.	27.00	2850.	110.	IZV.AN SSSR,39,114(1975)	YU.I.SOROKIN+
I0035046	50-SN	116	G,SN	15.44	277.3	7.5	29.50	1630.	104.	NUCL.PHYS.,A219,39(1974)	A.LEPRETRE+
I0017030	50-SN	116	G,SN	15.982	262.	4.	29.60	1669.	99.	PHYS.REV.,186,1255(1969)	S.C.FULTZ+
I0017030	50-SN		G,SN	27.131	55.						
I0035018	50-SN	116	G,N	15.44	277.3	7.5	22.10	1437.		NUCL.PHYS.,A219,39(1974)	A.LEPRETRE+

Fig. 5.

SUBENT	**L0017006 970129**
TITLE	**Photoneutron cross sections for Sn116, Sn117, Sn118,**
	Sn119, Sn120, Sn-124, and indium.
AUTHOR	**(S.C.FULTZ,B.L.BERMAN,J.T.CALDWELL,R.L.BRAMBLETT,**
	M.A.KELLY)
REFERENCE	**(J,PR,186,1255,6910)**
INC-SOURCE	**Positron annihilation**
REACTION	**(50-SN-116(G,X)0-NN-1,,SIG)**
	The sum: (G,N)+(G,N+P)+2(G,2N).

If you need the source data, you may download the
the source data file

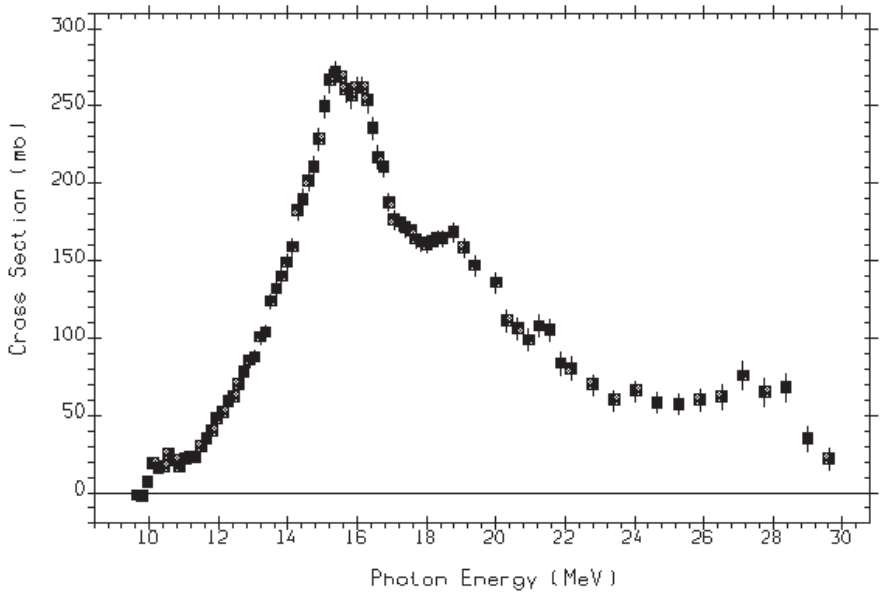

Contacts: Vladimir V.Varlamov, Webmaster

Fig. 6.

Reaction Thresholds for *50-SN*

Return to the CDFE On-Line Services Main Menu
Return to the main index of Reaction Thresholds

NUCL	A	ABUNDANCE(%)	G,N	G,P	G,T	G,HE3	G,A	G,2N	G,NP	G,2P
50-SN	112	1.00	10.8	7.6	17.1	15.0	1.8	19.0	17.6	12.9
50-SN	114	0.70	10.3	8.5	17.1	16.2	2.6	18.0	17.9	14.6
50-SN	115	0.40	7.5	8.8	17.0	14.4	3.2	17.9	16.0	15.6
50-SN	116	14.70	9.6	9.3	17.1	17.4	3.4	17.1	18.3	16.1
50-SN	117	7.70	6.9	9.4	16.8	15.3	3.8	16.5	16.2	16.9
50-SN	118	24.30	9.3	10.0	17.1	18.5	4.1	16.3	18.8	17.5
50-SN	119	8.60	6.5	10.1	16.8	16.3	4.4	15.8	16.5	18.2
50-SN	120	32.40	9.1	10.7	17.1	19.6	4.8	15.6	19.0	19.0
50-SN	122	4.60	8.8	11.4	17.2	20.7	5.7	15.0	19.8	20.6
50-SN	124	5.60	8.5	12.1	17.4	21.5	6.7	14.4	20.0	22.2

RETURN TO CDFE

[Giant Dipole Resonance Data | Reaction Thresholds Data]

Fig. 7.

Data for *50-SN*

Return to the CDFE On-line Services Main Menu

Click here to view legend

RETURN TO CDFE

NUMBER	E	NUCL	A	REACT	QUANTITY	EN-MIN MEV	EN-MAX MEV	ANG-MIN DEG	ANG-MAX DEG	REFERENCE	AUTHOR
87097		50-SN	0	G-MON,G	DST,SIG	.272	.662	10.5	59	J,NIM/A,255,59,87	D.A.BRADLEY+
89070		50-SN	0	G-BRST,G	DST,SIG,FMF	60.	662	5.	140	J,NIM/A,280,375,89	O.D.GONCALVES+
89079		50-SN	0	N,G	SIG,STFUN	20.	450			J,YF,50,609,89	V.M.TIMOKHOV+
92049		50-SN	0	G-BRST,G	DST,SIG	.122	245	50.	100	J,NIM/B,71,361,92	L.P.GUY+
94035		50-SN	0	G-BRST,ABS	SIG	300.	1200			J,PL/B,325,333,94	N.BIANCHI+
95062		50-SN	0	G-BRST,X	SIG	.0139	.0595			J,ARI,46,113,95	A.A.TAJUDDIN+
96021		50-SN	0	G-MON,ABS	SIG	300.	1200	9.	171	J,PR/C,54,1688,96	N.BIANCHI+
94084		50-SN	110	TI48,G	SPC,ABY,SIG	50.	90			J,ZP/A,349,213,94	A.BRACCO+
70027j		50-SN	112	E,E	DST	230.00				J,NP/A,146,15,70	KHVASTUNOV+
70027j		50-SN	112	E,E'	DST	230.00				J,NP/A,146,15,70	KHVASTUNOV+

Click here to view legend

RETURN TO CDFE

89079		50-SN	113	N,G	SIG,STFUN	20.	450			J,YF,50,609,89	V.M.TIMOKHOV+
74144j		50-SN	114	G,P	T:DST					J,SNP,18,21,74	TERTYCHNYI+
88027j		50-SN	114	G,X	ABY	4500.00				J,SNP,48,395,88	ARAKELYAN+
88090		50-SN	114	G-BRST,X	ABY,SIG,MDIS	0.	4500			J,YF,48,618,88	A.A.ARAKELJAN+
88091		50-SN	114	A,G	SPC,MULT,ISY ,DNG,COINC,E, J-PI	24.	24			J,PL/B,200,13,88	A.STOLK+
89078		50-SN	114	G-BRST,N	SIG-M	0.	4500			J,YF,50,1226,89	A.A.ARAKELJAN+
92069		50-SN	114	G-BRST,XN+YP	ABY,SIG	0.	4500			J,YF,55,2593,92	A.A.ARAKELJAN+

References

[1] V.V. Varlamov, B.S. Ishkhanov, Advanced Informational Technologies in Nuclear Physics Research, International School - Seminar on Automation and Computing in Science, Engineering and Industry (ACS' 98), Moscow (1998) p. 85.

[2] V.V. Varlamov, N.G. Efimkin, B.S. Ishkanov, V.V. Sapunenko, M.E. Stepanov, Evaluation of the cross-sections of the ^{63,65}Cu(γ,np) and ^{63,65}Cu(γ,p) reactions in the giant dipole resonance region and isospin splitting of the giant dipole resonance in nuclei of copper, Izvestiya RAN, seriya fizicheskaya 59 N5 (1995) p. 223.

[3] I.N. Boboshin, V.V. Varlamov, B.S. Ishkhanov, I.M. Kapitonov, New Information on Nuclear Subshells of Medium Nuclei on the Basis of ENSDF Data, Book of Abstracts of International Conference on Nuclear Data for Science and Technology, Juelich, Germany (1991) p. B 44.

[4] Ed. by H.D. Lemmel, The Nuclear Data Centres Network, IAEA Nuclear Data Section, INDC(NDS)-359, IAEA, Vienna, Austria (1997).

[5] I.N. Boboshin, A.V. Varlamov, V.V. Varlamov, M.E. Stepanov, The MSU INP CDFE Nuclear Data Files and Bases. Coordination of the Nuclear Reaction Data Centers, Report on an IAEA Advisory Group Meeting on the (11-15 May 1998, Vienna, Austria), INDC(NDS)-383, IAEA Nuclear Data Section (1998) p. 59.

[6] V.V. Varlamov, B.S. Ishkhanov, Advanced Informational Technologies in Nuclear Physics Research, International School-Seminar on Automation and Computing in Science, Engineering and Industry (ACS' 98), Moscow, Publishing Division of the Nuclear Research Institute of the Russian Academy of Sciences (1998) p. 85.

[7] I.N. Boboshin, A.V. Varlamov, V.V. Varlamov, D.S. Rudenko, M.E. Stepanov, Nuclear Physics Databases of the Centre for Photonuclear Experiments Data of the Scientific Research Institute for Nuclear Physics, M.V. Lomonosov Moscow State University: Hypertext Presentation in the WWW, Preprint NIIYaF MGU-99-26/584, Moscow (1999).

[8] V.V. Varlamov, V.V. Sapunenko, M.E. Stepanov, Photonuclear Data for 1976-1995: An Index, Moscow University Press, Moscow (1996).

[9] A.V. Varlamov, V.V. Varlamov, D.S. Rudenko, M.E. Stepanov, Atlas of Giant Dipole Resonances: Parameters and Graphs of Photonuclear Reaction Cross Sections, INDC(NDS)-394, IAEA NDS (1999).

[10] Ed. By V. McLane, EXFOR Systems Manual. Nuclear Reaction Data Exchange Format, BNL-NCS-63330, BNL, NNDC, USA (1996).

[11] G. Audi, A.H. Wapstra, The 1995 Update to the Atomic Mass Evaluation, Nucl.Phys. A595 (1995) p. 409.

[12] T. Asami, T. Nakagawa, Bibliographic Index to Photonuclear Reaction Data (1955-1992), JAERI-M-93-195, INDC(JPN) - 167L, JAERI, Japan (1993).

[13] I.N. Boboshin, V.V. Varlamov, The New ENSDF Search System NESSY: IBM/PC Nuclear Spectroscopy Data Base, Nucl.Instr. and Meth. A369 (1996) pp 113-119.

[14] V.V. Varlamov, G.M. Zhuravlev, V.V. Surgutanov, F.E. Chukreev, Nuclear Reactions Induced by Charged Particles and Photons in the EXFOR System (Reference Data). TsNIIAtominform, Moscow (1987).

NUCLEAR REACTOR DATA

00-30130 (113) [11]
Translated from Russian

UDC.539.17

LIBRARY OF NEUTRON REACTION CROSS-SECTIONS IN THE ABBN-93 CONSTANT SYSTEM

S.V. Zabrodskaya, Zh.A. Korchagina, V.N. Koshcheev, M.N. Nikolaev, A.M. Tsibulya
State Scientific Centre of the Russian Federation
A.I. Leipunsky Institute for Physics and Power Engineering, Obninsk

LIBRARY OF NEUTRON REACTION CROSS-SECTIONS IN THE ABBN-93 CONSTANT SYSTEM. The library of neutron reaction group cross-sections in the ABBN-93 constant set is described. The format used for data representation, the content and purpose of the sub-libraries and their practical application in the SCALE criticality safety estimation system are discussed.

Individual neutron reaction cross-sections were not determined in the ABBN-64 constant system [1]. In the ABBN-78 constant system [2], group cross-sections of the most important neutron reactions were determined, although their use in practical calculations was limited. This was because the ABBN-78 constant system was not intended to be used, nor indeed has it been used, for calculating the radiation characteristics of irradiated materials, where a knowledge of the reaction cross-sections is highly important. The ABBN-93 constant system [3] had greater applicability from the outset. In particular, the intention was to gradually introduce it, *inter alia*, into calculations of the radiation characteristics of irradiated fuel, reactor designs and technological environments. Consequently, from the beginning it was envisaged that the ABBN-93 constant system contain libraries of all the data required to carry out these calculations: fission product yields, decay characteristics of radionuclides and group neutron reaction cross-sections. Although actually these libraries were all set up, in practical terms their application did not, of course, involve the use of ABBN constants in the traditional areas, namely in calculating neutron and photon fields in reactors and in shielding. Instead of using these ABBN constants in the calculations, appropriate constants were used that had previously been included in the data libraries of programs for calculating isotope kinetics and radiation characteristics: CARE [4], ORIGEN [5] and FISPACT [6]. Recently the situation has begun to change. The Standardized Computer Analyses for Licensing Evaluation of nuclear power facilities system (SCALE) [7] allows for certain data used by the CARE and ORIGEN programs to be replaced with data from the ABBN libraries. This relates primarily to data on neutron cross-sections since it is clear that the cross-sections used to calculate isotope kinetics should not differ (not substantially, at any rate) from those used to calculate neutron fields in a reactor. The initial application of the library of group neutron reaction cross-sections also prompted the appearance of the present publication since it became necessary to record the stage of development that had been reached at this point.

A general-purpose library of reaction cross-sections

The first task when setting up the library of neutron reaction cross-sections was to ensure the completeness of the data. It was decided that the library should contain data on:

(a) All stable nuclides;

(b) All actinides with half-lives of more than one day, ranging from Ac-225 to Es-255;

(c) All fission products with half-lives of more than one day;

(d) All radionuclides with half-lives of more than one day that can be formed as a result of two to three sequential neutron reactions from the nuclides listed in the previous points;

(e) Some of the main, shorter-lived nuclides (for example, Xe-135).

In the case of all the above nuclides (including isomers with a half-life of more than one day) the library had to contain group neutron cross-sections for each reaction where the threshold was lower than the upper boundary of the (-1)th ABBN group (13.98 MeV). As far as possible, the contents of the library had to correspond with the evaluated neutron data files in the FOND-2 library, on which the ABBN-93 constant system was based. If the FOND-2 library contained a data file relating to a particular nuclide and, in addition, that file provided information on a particular reaction, then the library of group reaction cross-sections included cross-sections obtained using that file. In the case of reactions for which the FOND-2 library files contained no information (as a rule, reactions with high thresholds and very low cross-sections), the data were taken from other libraries, in particular from the EAF-3 library [8]. During the initial stage, data for all the nuclides for which there were no files in the FOND-2 library were also taken from this library. The second stage involved establishing a more complete correspondence between the library of group reaction cross-sections and the FOND-2 data. In particular, isomer production cross-sections, which, as a rule, were missing from the FOND-2 library, were obtained from the total reaction cross-sections, calculated from data in this library by means of multiplication by the probabilities of isomer production (or of the ground state) used in EAF-3. Moreover, additional MF=9 and (or) MF=10 files, containing data on the branching ratios that had been used, began to be included in FOND-2. As a rule, missing data on the cross-sections of improbable reactions with high thresholds were also included (with compensation on account of cross-sections of the most probable reactions). In this way, a more complete correspondence was achieved between the cross-sections library and the files library.

The most undesirable disparity lay in the divergence between data on reactions in a natural isotopic mixture of basic reactor materials, in those cases where the FOND library contained data only for the natural mixture. This disparity was gradually eliminated by the introduction into the FOND-2 library of data on all the stable isotopes and by obtaining, on the basis of these data, a file for the natural mixture. This was carried out in the case of the files on iron, chromium, nickel, zirconium and others. Differences have now been eliminated

between data in the modified version of the FOND-2 - FOND-2.2 [9] - library and the library of neutron cross-sections for the basic reactor materials.

The contents of the library of group cross-sections are given in Table 1. All data in this library are given in 28-group representation. The data format is the standard for tables of ABBN tables of group constants [3]. Each table contains cross-sections of all reactions for all the relatively long-lived isotopes of the element, determined by the NAM identifier. The tables have the identification numbers MF=9 and MT=0. By way of example, a table is given of the group reaction cross-sections for aluminium isotopes (Table 2).

Rows that begin with an asterisk contain a commentary and are not processed by the computer. The first two rows are standard ABBN table heading rows. The first of these contains: the NAM material designation (in this example, NAM=Al - aluminium); numbers that identify the data type (MF=9 and MT=0 for tables of group neutron reaction cross-sections); and the material parameter which characterizes the data given in the table as a whole. In tables of the type under consideration, this is the atomic number, Z. The second heading row contains: LT - the number of rows in the table of data (in tables of the MF=9, MT=0 type, invariably LT=33); LC - the total number of columns in the table (in this example LC=20); LS - the number of columns in one part of the table (in tables of the type under consideration, invariably LS=8); and the read-out format of the data from the row containing LT columns. In tables of group neutron reaction cross-sections, as a rule, LC > LS, i.e. the table is divided up into a number of parts (in the example under consideration - three). Column one is repeated in every part. The first columns of the second and subsequent parts, are not included in the total number of columns, LC.

The contents of the data in the table are determined by the parameters MF and MT. In tables of the type under consideration, column one contains the ABBN group number (from the 1st to the 26th) whilst the remaining columns contain group cross-sections of the appropriate reactions. Reactions are identified by the data contained in the first five rows of each column (i.e. in the third, fourth, fifth, sixth and seventh rows, allowance being made for the table heading rows). The first of these rows contains the identification number of the isotope on which the reaction occurs. This is in numerical form with the part in front of the decimal point having the structure ZZAAAM. Here, ZZ is the atomic number (in this example - 13), AAA is the mass number (in this example - 026 or 027) and M is the number of the metastable state (M=0 for ground states).

The second heading row of the column contains the identification number of the evaluated data library, on the basis of which the cross-sections given in the column have been derived. In this identifier the figure in front of the decimal point signifies the following:

1. FOND library;
2. ENDF/B library;
3. JENDL library;
4. JEF library;
5. BROND library;
8. ADL library;
9. EAF library;

0. Group cross-sections evaluated directly and do not correspond to any library.

The part of the identifier after the decimal point, provided that it is less than 0.7, refers to the version number: 2.06 signifies ENDF/B-6; 3.32 signifies JENDL-3.2, and so on. If this part exceeds 0.9, it refers to the year in which the data evaluation or re-evaluation took place. For example, 0.95 means that the group cross-sections were evaluated directly in 1995.

The third row contains the reaction identification number. The three lowest-order digits of this number in front of the decimal point have precisely the same meaning as the ENDF/B reaction identifier MT. The highest-order digit (number of thousands) indicates the isomeric state in which the product-nucleus is formed. For example, 1016 represents the (n,2n) reaction which results in the formation of a product-nucleus in the first isomeric state, and 0016 represents the same reaction which results in the formation of a product-nucleus in the ground state. Number 6 refers to an (n,2n) reaction which results in the formation of a product-nucleus in any state. This identifier value is only used in cases where no individual isomer production cross-sections are given.

The fourth row contains the product-nucleus identifier. This information is superfluous since the product-nucleus is clearly determined by the target-nucleus and the reaction type identifiers.

The fifth heading row of the column indicates the reaction energy, Q, and is expressed in MeV.

In the columns, these heading rows are followed by the cross-sections, given in barns, for the energy groups whose numbers are indicated in the first column of each part. Any gaps in these columns mean that in energy terms reactions in these groups are impossible. 0.000000 indicates that the reaction cross-section is less than a microbarn.

One of the library annexes is a tolerably accurate evaluation of the activity of materials and structures that are being dismantled, transported, stored or sent for recycling. The library is sufficiently reliable and provides considerable scope for calculating activation channels. On the basis of this library and in conjunction with the UK FISPACT program, calculations were made of the radiation characteristics of materials irradiated in the core of the BN-350 [10] and BN-600 [11] fast reactors. Similar calculations are being carried out for BR-10 reactor designs [12] that are being decommissioned. Studies have also been carried out of the radioecological properties of sodium, lead-bismuth and lead coolants in fast neutron reactors [13].

Libraries of fission product and actinide cross-sections

As has already been mentioned, the first area in which the library of neutron reaction cross-sections could be applied was in calculating the nuclide composition of spent fuel in the SCALE system. For this, it was necessary to extract from the general library data on cross-sections of the fission products and actinides accumulating in the fuel. During the calculation process, the appropriate data drawn from the libraries of nuclide composition calculation programs, and in particular from the ORIGEN program, had to be substituted with these cross-sections. For fission products the main point is to substitute their radiative capture cross-sections: the (n,p), (n,α) and (n,2n) reactions have a far weaker impact on the nuclide composition of fuel and calculating the difference between the cross-sections of these reactions taken in the ORIGEN library and the more up-to-date data from our library is of secondary importance. As regards actinides, there was a need for calculation of the latest data on fission and radiative capture cross-sections and also on (n,2n) and (n,3n) reaction cross-sections.

To make this task easier, two sub-libraries were set up on the basis of the general library, one for fission products and the other for actinides. Each sub-library was presented in the form of a single ABBN table, the first with the parameters NAM=FP, MF=309 and MT=102 and the second with the parameters NAM=ACT, MF=309 and MT=18. The format of the tables was exactly the same as that described above. The first table contained data on the radiative capture cross-sections of 169 fission products and the second contained data on capture, fission and (n,2n) and (n,3n) reaction cross-sections, as well as data on the value of $\bar{\nu}$ for all 60 actinides, for which cross-section data were available in the general library. These sub-libraries started to be used in calculations of the nuclide composition of fast reactor spent fuel. To enable them to be used in thermal reactor nuclide fuel calculations, account had to be taken of the extent to which the thermal group cross-sections depended on the neutron gas temperature. It was proposed that Westcott g-factor be used to this end. Consequently, for all fission products and actinides, whose cross-section behaviour in the thermal region diverged substantially from 1/v, the Westcott g-factors were calculated and presented in the form of standard ABBN tables with MF=7. Putting this into practice showed that, when calculating the nuclide composition of thermal reactor fuel, it was expedient not to use the 28-group constants of fission products and actinides with Westcott g-factors, but instead to set up 299-group libraries of cross-sections of the required reactions and to use these. The reason for this approach was that the neutron field calculations in the SCALE system are carried out in ABBN 299-grouping, and the multigroup (299-group) neutron spectra in fuel, required for convolution of the cross-sections, are available in the system. Thus, 299-group tables were created of fission product capture cross-sections and cross-sections of the main reactions on actinides, differing only in terms of group number from the aforementioned 28-group tables. The 28-group and 299-group cross-sections were derived from exactly the same evaluated data files.

The data from the 299-group libraries of fission product and actinide cross-sections are used in the SCALE system as follows. Using reactor calculation programs, the 299-group integral neutron fluxes are calculated for all fuel-filled areas for which the change in nuclide composition needs to be calculated. In this calculation, the ABBN-93 299-group constants prepared for the CONSYST program are used. When preparing the constants, the resonance

self-shielding (blocking) of the cross-sections is calculated. The microconstants of each nuclide, blocked with respect to the composition of each area, are stored in the CONSYST program's GMF output format and are also accessible to the system after the macroscopic 299-group constants for the reactor calculation have been worked out on their basis. Once the reactor calculation is complete and the integral neutron spectra in the fuel areas have been calculated, the single group cross-sections of all the fission products and actinides are worked out for each area (using the standard method of averaging out the cross-sections across the spectrum). Account is taken of the fact that part of the actinides, and at times also part of the fission products, are included in the irradiated fuel composition and in the relevant blocked microconstants obtained by the CONSYST program. The shielded cross-sections, recorded in the aforementioned GMF file are used for all these materials. Data from the 299-group cross-section libraries are used for the remaining fission products and actinides.

Then the integral neutron fluxes are normalized to the given power of the reactor (or of a specific fuel area). To this end, data are used on the original fuel composition (taken from the job prepared for CONSYST), the capture and fission reaction rates on the nuclides in this composition, as well as data on the energy release during these reactions, which are given in the column header rows of the neutron reaction cross-section table (for convenience sake, these data are collected in separate ABBN tables).

The next stage involves substituting the capture and fission cross-sections (as well as the (n,2n) and (n,3n) reaction cross-sections on actinides), taken from the ORIGEN program libraries, with the cross-sections calculated using the ABBN constants. Then, the program is run and, using the neutron fluxes that have been normalized to the power and the given irradiation time regime, the composition of the irradiated fuel is calculated (and if necessary its radiation characteristics).

The composition obtained is used by the SCALE system to formulate reactor calculation tasks at the next burnup step. In the process, the fission poison capture cross-sections may be made more accurate. The term poison means the build-up of fission products, whose concentrations are not explicitly taken into account in the calculation. At the very least, explicit allowance needs to be made for poison-products in thermal reactor calculation. Usually, explicit allowance is made for several additional products with large yields and capture cross-sections. The remaining fission products are "lumped together" in the fission poison. As the fission poison contains a large number of fission products, the cross-sections, averaged out with respect to fission poison composition, are comparatively weakly dependent on that composition, thus allowing "standard" fission poison constants, calculated when its composition has been determined once and for all, to be included in the ABBN constant system. The SCALE system allows for recalculation of the fission poison cross-section at each step, taking its real composition into account. To this end, the fission product concentrations in the fuel burned during the previous steps and the 299-group capture cross-sections are used. The 299-group fission poison capture cross-sections obtained in the subsequent step replace the fission poison radiative capture cross-sections taken from the standard ABBN tables. The cross-sections for all the remaining fission poison neutron constants (aside from the total cross-section, which is calculated as the sum of the partial cross-sections) are left as before.

The SCALE system's method of calculation, as described here, can also be used in conjunction with the Russian CARE program instead of ORIGEN.

Alongside the libraries of group neutron reaction cross-sections in the ABBN 28-group and 299-group, similar tables were created of WIMS 69-group cross-sections. These tables are actively used in the WIMS-ABBN constant system [14], which differs from the original version of the WIMS-D4 program [15] in that it reviews the entire library of constants based on the FOND-2 file library, expands the list of resonance nuclides and includes a number of other improvements that have increased the program's applicability to calculations for thermal reactors with any type of MOX-fuel.

Table 1

Contents of the ABBN-93 activation library

№	Element	Number of isotopes	Number of reactions	№	Element	Number of isotopes	Number of reactions
1	H	3	4	35	Sn	18	320
2	He	1	3	36	Sb	9	201
3	Li	2	13	37	Te	21	373
4	Be	2	9	38	I	8	151
5	B	5	32	39	Xe	15	231
6	N	2	17	40	Cs	8	149
7	O	3	23	41	Ba	15	236
8	F	1	10	42	La	5	83
9	Ne	3	21	43	Ce	9	129
10	Na	2	18	44	Pr	3	44
11	Mo	3	24	45	Nd	11	157
12	Al	2	18	46	Pm	10	142
13	Si	5	35	47	Sm	11	150
14	P	3	26	48	Eu	15	213
15	S	5	45	49	Gd	15	204
16	C	3	32	50	Tb	10	153
17	Ar	7	69	51	Dy	13	186
18	K	5	53	52	Ho	4	59
19	Ca	9	80	53	Er	10	152
20	Sc	5	58	54	Tm	8	114
21	Ti	7	74	55	Yb	10	127
22	V	4	49	56	Lu	11	167
23	Cr	5	49	57	Hf	12	223
24	Mn	4	44	58	Ta	7	146
25	Fe	7	68	59	W	11	178
26	Co	6	71	60	Re	7	116
27	Ni	11	111	61	Os	11	170
28	Cu	5	49	62	Ir	11	224
29	Zn	7	79	63	Pt	13	226
30	Ga	3	38	64	Au	8	148
31	Ge	8	94	65	Hg	14	216
32	As	7	88	66	Pb	9	116
33	Se	10	118	67	Bi	7	105
34	Br	4	56	68	Po	5	79

Table 2

Neutron cross-sections for Al

```
NAM=Al       BIB= ACT  MF=  9  MT=  0   Z = 13.
             LT =  33  LC= 20  LS=  8  LF = (I4,7E9.0)
      130260.  130260.  130260.  130260.  130260.  130260.  130260.
         9.03     9.03     9.03     9.03     9.03     9.03     9.03
          16.      22.      28.      32.     102.     103.     107.
      130250.  110220.  120250.  120240.  130270.  120260.  110230.
     -11.3630  -9.4456  -6.3037 -11.4090  13.0540   4.7858   2.9675
  -1    .0161    .1042    .3993   8.62-3   3.70-4    .1779    .0763
   0   1.01-3    .0216    .2193   1.42-3   3.79-4    .2218    .0791
   1            2.37-4    .0643            2.03-4    .2499    .0773
   2                                       1.00-4    .2499    .0631
   3                                       3.84-5    .2476    .0368
   4                                       1.19-6    .2438    .0207
   5                                       1.00-5    .2319    .0130
   6                                       1.03-5    .1084   5.62-3
   7                                       1.84-5
   8                                       4.90-5
   9                                       9.29-5
  10                                       1.38-4
  11                                       2.06-4
  12                                       3.04-4
  13                                       4.40-4
  14                                       6.49-4
  15                                       9.57-4
  16                                       1.40-3
  17                                       2.06-3
  18                                       3.02-3
  19                                       4.44-3
  20                                       6.51-3
  21                                       9.56-3
  22                                        .0140
  23                                        .0206
  24                                        .0302
  25                                        .0444
  26                                        .1558
*
      130260.  130260.  130270.  130270.  130270.  130270.   130270
         9.03     9.03     1.97     1.97     1.22     1.22     1.22
         111.    1004.    0016.    1016.      22.      28.     102.
      110250.  130261.  130260.  130261.  110230.  120260.  130280.
      -9.3538  -0.2280 -13.0540 -13.2820 -10.0860  -8.2681   7.7229
  -1    .0271   2.67-3 2.972-2    9.57-4 8.1783-3  .080    2.5958-4
   0    .0187   5.51-3 6.877-5    1.63-6 6.5786-5  .040    2.4232-4
   1   2.61-4   5.72-3                             .0006   2.8115-4
   2            5.69-3                                     3.2790-4
   3            4.50-3                                     4.246- 4
   4            6.12-4                                     5.6921-4
   5                                                       7.0219-4
   6                                                       8.4671-4
   7                                                       1.2228-3
   8                                                       2.2116-3
   9                                                       1.1429-3
  10                                                       4.5385-3
  11                                                         3.04-3
  12                                                       2.8717-2
  13                                                       6.5655-4
  14                                                       8.2197-4
```

Table 2 (cont.)

```
  15                                                                1.1575-3
  16                                                                1.7047-3
  17                                                                2.5273-3
  18                                                                3.7540-3
  19                                                                5.5940-3
  20                                                                8.3420-3
  21                                                                1.2430-2
  22                                                                1.8563-2
  23                                                                2.7728-2
  24                                                                4.1377-2
  25                                                                6.1873-2
  26                                                                2.3104-1
*
      130270.  130270.  130270.  130270.  130270.
         1.22     9.03     9.03     1.97     1.97
         103.     104.     105.    0107.    1107.
      120270.  120260.  120250.  110240.  110241.
      -1.8260  -6.0441 -10.8780  -3.1293  -3.6013
   -1 7.3790-2    .0189   6.13-3  .0815    .0359
    0 9.4496-2   6.56-3   3.16-5  .0759    .0346
    1 7.9561-2   8.84-5           .0296    .010
    2 2.4491-2                    .000213  .000135
    3 2.413- 3                    .000000  .000000
    4 1.6391-6
    5
    6
    7
    8
    9
   10
   11
   12
   13
   14
   15
   16
   17
   18
   19
   20
   21
   22
   23
   24
   25
   26
*
```

References

[1] L.P. Abagyan, N.O. Bazazyants, I.I. Bondarenko, M.N. Nikolaev, Group constants for nuclear reactor calculations, Atomizdat, Moscow (1964).

[2] L.P. Abagyan, N.O. Bazazyants, M.N. Nikolaev, A.M. Tsibulya, Group constants for reactor and shielding calculations, Handbook, Ehnergoizdat, Moscow (1981).

[3] G.N. Manturov, M.N. Nikolaev, A.M. Tsibulya, ABBN-93 Group Constants System, Verification Report, TsNIIAI (Atominform), Moscow (1995).

[4] A.L. Kochetkov, CARE program - calculation of the isotope kinetics, and the radiation and ecological character of nuclear fuel during irradiation and hold-up, Preprint IPPE-2431, (1995).

[5] O.W. Hermann, R.M. Westfall, ORIGEN-S: SCALE system module to calculate fuel depletion, actinide transmutation, fission product build-up and decay, and association source terms, NUREG/CR-0200, Revision 4, Vol.2, Section F7, (1995).

[6] R.A. Forrest, D.A. Encacott, J.A. Khursheed, FISPACT - Program Manual, Nuclear Physics Division, Harwell Laboratory, AERE-M3634, (1988).

[7] V. Vnukov, et al., Burnup Credit Calculational Estimations and Possibilities of their Experimental Validation, 7th International Conference on Nuclear Criticality Safety, Versailles, France (September 1999).

[8] Ju. Kopecky, D. Nierop, Contents of EAF-3, ECN-1-92-023, (1992).

[9] Current Status of the ABBN-93 Library of Constants, IPPE Report No. 9866, (1998). Compiled by M.N. Nikolaev, S.V. Zabrodskaya, V.N. Koshcheev, A.M. Tsibulya.

[10] Eh.P. Popov, A.G. Tsikunov, S.V. Zabrodskaya, V.A. Grabezhnoj, Evaluation of the activity and volumes of solid radwaste from a BN-350 reactor that is being shut down, Paper presented at the 7th Russian scientific conference “Protection of Nuclear Engineering Facilities from Ionizing Radiation”, Obninsk, 22-24 September 1998, Obninsk (1999).

[11] Eh.P. Popov, S.V. Zabrodskaya, A.G. Tsikunov, V.I. Usanov, Evaluation of the admissible alloy content in low-activated fast reactor shielding materials, Paper presented at the 7th Russian scientific conference “Protection of Nuclear Engineering Facilities from Ionizing Radiation”, Obninsk, 22-24 September 1998, Obninsk (1999).

[12] L.A. Kochetkov, A.G. Tsikunov, L.I. Mamaev, Eh.P. Popov, S.V. Zabrodskaya, A.G. Khokhlov, Investigation of induced activity in the structure of a decommissioned BR (fast reactor)-5, Proc. of an international seminar on nuclear safety, Cadarache, 1997.

[13] V.I. Usanov, D.V. Pankratov, Eh.P. Popov, P.I. Markelov, L.D. Ryabaya, S.V. Zabrodskaya, Radioecological properties of sodium, lead-bismuth and lead coolants in fast neutron reactors, Yadernaya Ehnergetika, (1999), №. 2.

[14] M.J. Halsall, A Summary of WIMSD4 Input Options, AEEW- M 1327, (1980).

[15] Current status of the WIMS/ABBN 69-group system of constants, IPPE Report No. 9861, (1998). Compiled by G.N. Zherdev, V.N. Koshcheev.

00-30130 (117) [12]
Translated from Russian

UDC.539.17

A LIBRARY OF PRODUCTION CROSS-SECTIONS FOR DISPLACEMENTS AND HYDROGEN, HELIUM AND TRITIUM IN THE ABBN-93 CONSTANT SYSTEM

S.V. Zabrodskaya, M.N. Nikolaev, A.M. Tsibulya
Russian Federation National Research Centre
A.I. Leipunsky Institute for Physics and Power Engineering, Obninsk

A LIBRARY OF PRODUCTION CROSS-SECTIONS FOR DISPLACEMENTS AND HYDROGEN, HELIUM AND TRITIUM IN THE ABBN-93 CONSTANT SYSTEM. A new library of 28-group production cross-sections for displacements and hydrogen, helium and tritium is described. The library is part of the ABBN-93 constant system. The FOND-2.2 evaluated neutron data library is the original source. The group displacement production cross-sections were calculated using the NJOY-91 code.

The irradiation of materials with neutrons alters many of the physical and mechanical properties of those materials and thus has a significant impact on the durability of nuclear reactor structures. The main factors involved in these changes are, firstly, disruption of the crystal lattice, characterized by the number of displacements of lattice atoms during irradiation (i.e. by the number of displacements per atom - DPA), secondly, accumulation of hydrogen, and thirdly, accumulation of helium.

In the mid-1980s, under the leadership of Yu.V. Konobeev, libraries of group displacement production cross-sections were collected for the main groupings used in this country [1]. The initial data for this exercise came mainly from the American library DAMSIG-81, which has a 620-group representation [2]. Until recently it was this evaluation by Yu.V. Konobeev et al. that was used for calculations in the ABBN constant system. However, the DAMSIG-81 data upon which this library is based were obtained using ENDF/B-3 neutron data that are now obsolete. Consequently, it was decided to create, for the ABBN-93 constant system, a new version of the displacement, hydrogen and helium production cross-section library taking into account recent data and programmes. In this process, as also when obtaining the main ABBN-93 neutron constants for the calculation of neutron fields, the evaluated neutron data file library FOND-2.2 [3] was used as the initial data, since it comprises the most reliable evaluated neutron interaction data from all the well-known libraries in the world, namely BROND-2, ENDF/B-6, JENDL-3.2 and JEF-2.2. The group displacement production cross-sections were calculated using NJOY-91 [4], an internationally recognized and widely used program for processing files of evaluated neutron data. The method employed by NJOY-91.4 to calculate DPA is based on the Robinson cascade function. Details of this are given in Ref. [4]. Here we will look at just one important

aspect: the minimum values adopted for the energy E_d needed to produce a stable Frenkel pair in different materials.

Values for E_d recommended by specialists vary considerably. Thus, for example, in the previous version of the displacement production cross-section library, E_d = 40 eV was adopted for all materials. We have used the values for E_d recommended in Ref. [4] (except for Re and Ir). These are set out in Table 1. Clearly, for a number of materials these values differ significantly from 40 eV. With the help of this information, experienced users holding their own views as to the value of E_d to take for one material or another can easily recalculate the appropriate cross-sections, since their value is simply inversely proportional to E_d.

On account of the appreciable uncertainties in the values of E_d, we felt the use of the detailed 299-group representation adopted in ABBN-93 for the main constants of the most important reactor materials to be unnecessary; the displacement, hydrogen and helium production cross-sections are given in the coarser 28-group representation of ABBN. Besides these cross-sections, this library also contains tritium production cross-sections, which are needed for the purposes of environmental analysis. The production cross-sections for hydrogen, helium and tritium are based upon the 28-group neutron reaction cross-section library of ABBN-93 [5]. Calculations were made by simple summation with a weight multiplicity n. For example, the hydrogen production cross-section is:

$$\sigma^{g}_{Hydr} = \sum_{MT} \sigma^{g}_{MT} \times n_{MT} \ .$$

The summation is performed over all reactions which produce hydrogen (any of its isotopes). n_{MT} is the number of hydrogen atoms produced. The production cross-sections for helium and tritium are calculated in a similar way. Table 2 lists reactions in which hydrogen, deuterium and tritium are produced with the respective multiplicities. Clearly only those reactions that have a threshold lower than 13.98 MeV (the upper limit of the energy range covered by the 28-group representation) make a real contribution to the production cross-sections.

The displacement, hydrogen, helium and tritium production cross-section are presented in standard ABBN tables [5] along with the identification number MT = 13. The format of these tables is the same as that of the tables of neutron reaction cross-sections with MT = 9. Data for aluminium are given as an example in Table 3.

Lines beginning with an asterisk contain a commentary and are not processed by the computer. The first two lines are the standard ABBN table subheadings. The first of these contains the name of the material, the data source and the MF and MT numbers identifying the data type. In this case MF = 13; MT = 0 in all cases. Then, one or two real parameters may follow that characterize the data as a whole. One such parameter, ED, is given in the MF = 13 type tables. The second subheading line gives the number of lines, LT, as well as the number of columns in the table as a whole, LC, and in the particular part of the table, LS. MF = 13 type tables always have LT = 28 and LC = LS = 6. Additionally, the second line gives the format for extracting the data from the line.

The columns contain the following data: column one - number of the ABBN neutron group; column two - displacement cross-section; columns three, four and five - production cross-sections for hydrogen, helium and tritium, respectively. All cross-sections are expressed in barns.

Data like those in Table 3 have been obtained for all the materials listed in Table 1.

The data obtained were verified by comparing them with data collected on a completely independent basis in the 175-group library RLF-1 [6]. Figure 1 compares the data for aluminium. Clearly, the agreement in this case is entirely satisfactory. The same is true of the data for beryllium, graphite, silicon, vanadium, copper, zirconium, niobium and tantalum. Figure 2 compares the data for nickel. Although the same values have been adopted for E_d in both libraries, there are appreciable discrepancies in this case. Similar discrepancies are found in the data for other components of stainless steel (iron, chromium, manganese and titanium), as well as for molybdenum. The discrepancies arise because different evaluated neutron data files have been used. In those cases where both libraries are based on the same file (carbon and niobium, for example), the agreement is excellent. This further confirms the accuracy of data processing by the NJOY-91.4 program: the RLF-1 library was obtained using the independently developed KERMA module of the TERMIS program.

The new library of group cross-sections for the production of displacements, hydrogen, helium and tritium is now linked to the program for three-dimensional engineering calculations for TRIGEX fast reactors [7], where this library can be used alongside earlier data.

To obtain data from the library, contact the Constant Laboratory of the Institute of Physics and Power Engineering at the following e-mail address: abbn@ippe.rssi.ru.

Table 1

Energy required to produce displacements

	Material	E_d, eV		Material	E_d, eV
1	Be	31	12	Co	40
2	C	31	13	Ni	40
3	Mg	25	14	Cu	40
4	Al	27	15	Zr	40
5	Si	25	16	Nb	40
6	Ca	40	17	Mo	60
7	Ti	40	18	Ta	90
8	V	40	19	W	90
9	Cr	40	20	Re	90
10	Mn	40	21	Ir	90
11	Fe	40			

Table 2

Reactions producing hydrogen, helium and tritium

Production								
Hydrogen			Helium			Tritium		
MT	Reaction	n	MT	Reaction	n	MT	Reaction	n
28	(n,np)	1	22	(n,nα)	1	33	(n,nt)	1
32	(n,nd)	1	23	(n,n3α)	3	36	(n,nt2α)	1
33	(n,nt)	1	24	(n,2nα)	1	105	(n,t)	1
35	(n,nd2α)	1	25	(n,3nα)	1	113	(n,t2α)	1
36	(n,nt2α)	1	29	(n,n2α)	2	116	(n,pt)	1
41	(n,2np)	1	30	(n,2n2α)	2			
42	(n,3np)	1	34	(n,n^3He)	1			
103	(n,p)	1	35	(n,nd2α)	2			
104	(n,d)	1	36	(n,nt2α)	2			
105	(n,t)	1	107	(n,α)	1			
111	(n,2p)	2	108	(n,2α)	2			
112	(n,pα)	1	109	(n,3α)	3			
113	(n,t2α)	1	112	(n,pα)	1			
114	(n,d2α)	1	113	(n,t2α)	2			
115	(n,pd)	2	114	(n,d2α)	2			
116	(n,pt)	2						

Table 3

Example of a table in ABBN format containing data on displacement, hydrogen and tritium production

```
NAM=AL    BIB=L103  MF=13     MT=0 ED = 27
            LT =    28   LC=6 LS=6 LF = (I4,3E9.0)
*                   13-AL- 27
*
*    G    DPA            Hydrogen       Helium         Tritium
*         product.       product.       product
     -1   3074.07        0.1788         0.0897         0.0061
    0     2916.67        0.1411         0.0760
    1     2605.56        0.0802         0.0296
    2     2427.78        0.0245         0.0002
    3     2266.67        0.0024
    4     1944.44
*
    5     1609.44
    6     1380.19
    7     874.63
    8     807.04
*
    9     351.85
    10    207.96
    11    14.24
*
    12    13.21
    13    4.56
    14    2.21
*
    15    1.01
    16    0.35
    17    0.04
*
    18    0.04
    19    0.06
    20    0.10
*
    21    0.14
    22    0.21
    23    0.32
*
    24    0.48
    25    0.71
    26    2.66
*
```

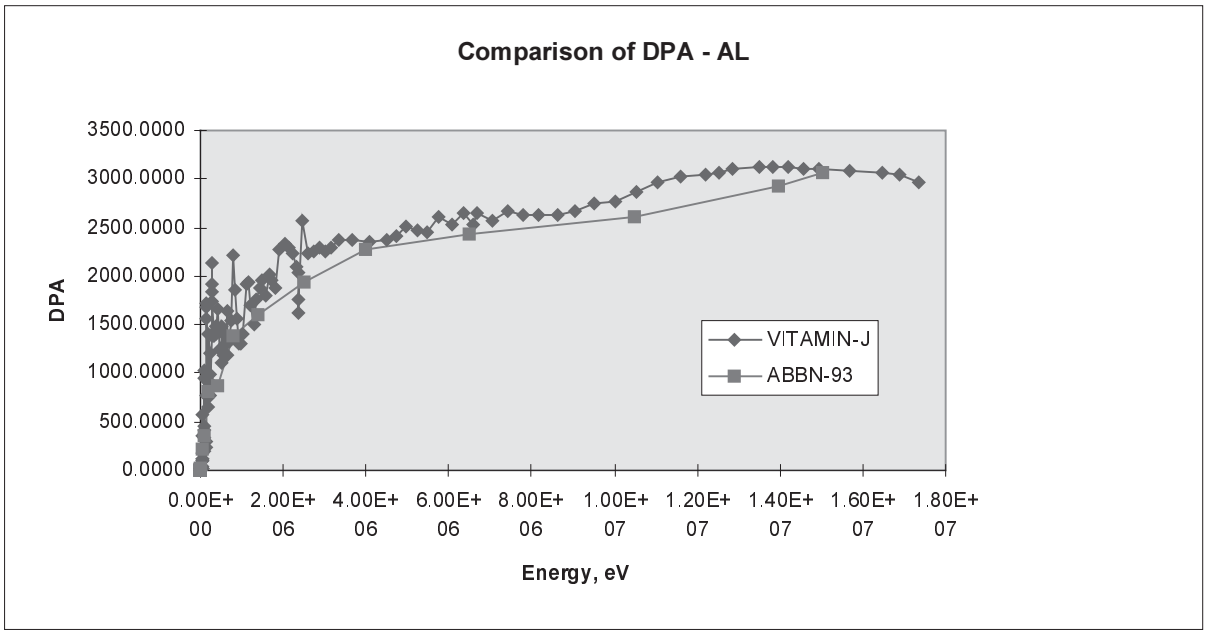

Fig. 1. Comparison of DPA data for aluminium.

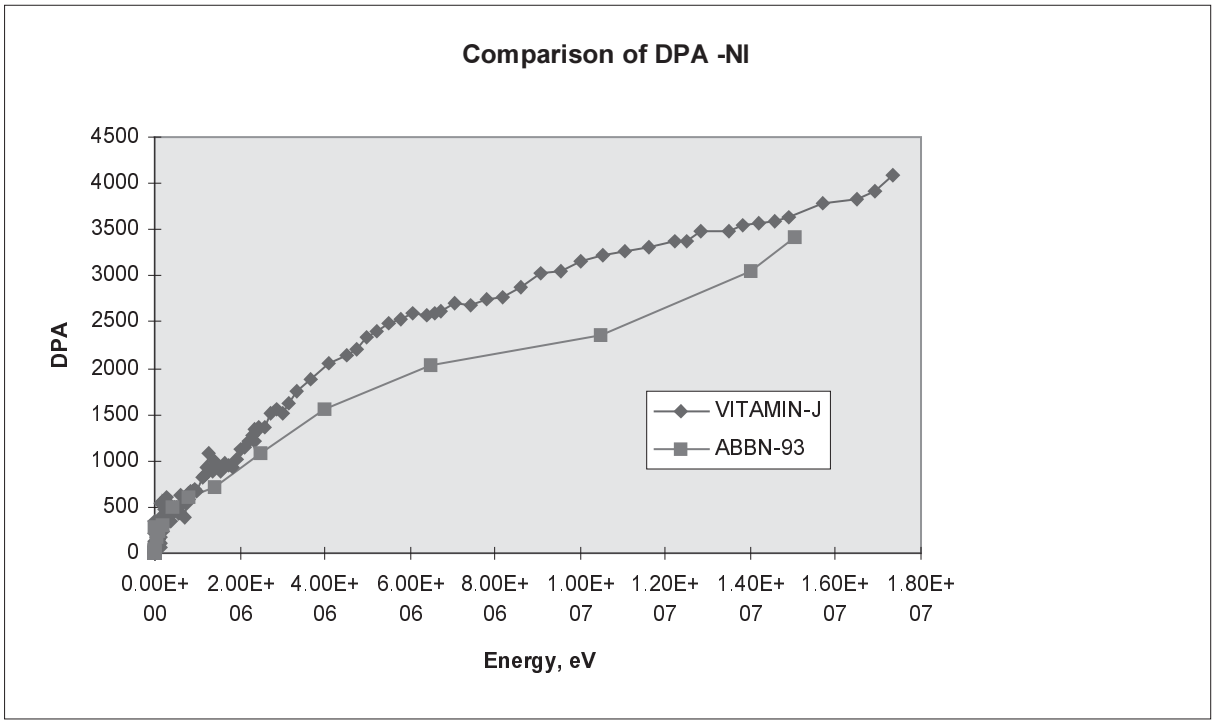

Fig. 2. Comparison of DPA data for nickel.

References

[1] V.I. Avramenko, Yu.V. Konobeev, A.M. Strokova; Neutron cross-sections for the calculation of damaging doses for reactor materials [in Russian], Atomnaya Ehnergiya, Vol. 56, No. 3 (1984).

[2] W. Zijp, et al., Damage Cross-Sections Library DAMSIG-81, Netherlands, ECN-104 (1980).

[3] Current status of the ABBN-93 library of constants, Institute of Physics and Power Engineering Report No. 9866 (1998) compiled by M.N. Nikolaev, S.V. Zabrodskaya, V.N. Koshcheev, A.M. Tsibulya.

[4] RSIC Peripheral Shielding Routine Collection, Los Alamos National Laboratory, PSR-355 (1995).

[5] G.N. Manturov, M.N. Nikolaev, A.M. Tsibulya; The ABBN-93 group constant system. Verification report [in Russian], Moscow, TSNIIAI (1995).

[6] M. Frisoni, G.C. Panini, P. Peerani; Status report on the computation of kerma and photon production data for RFL-2, EFF-DOC-177 (1992).

[7] A.S. Seregin, T.S. Kislitsyna; Notes on the program package TRIGEX-CONSYST-ABBN-90, Preprint FEhI-2655 (1997).

UDC 621.039:539.141

DISCRETE PROCESSES MODELLING AND GEOMETRY DESCRIPTION IN RTS&T CODE

I.I. Degtyarev, O.A. Liashenko, A.E. Lokhovitskii, I.A. Yazynin
SRC Institute for High Energy Physics, 142284 Protvino, Moscow region, Russian Federation
V.I. Belyakov-Bodin
SRC Institute of Theoretical and Experimental Physics, Moscow, Russian Federation
A.I. Blokhin
SSC Institute of Physics and Power Engineering (Nuclear Data Center of Russian Federation),
249020 Obninsk, Russian Federation

DISCRETE PROCESSES MODELLING AND GEOMETRY DESCRIPTION IN RTS&T CODE**.** This paper describes the recent version of the RTS&T code system. RTS&T performs detailed simulations of many types of particles transport in complex 3D geometries in the energy range from a part of eV up to 20 TeV. A description of the main processes is given.

The RTS&T [1] code (Radiation Transport Simulation and Isotopes Transmutation Calculation) was assigned for detailed Monte Carlo simulation of many particle types transport in a complex 3D geometry's with composite materials and calculation of particle fluxes and functionals of radiation fields and isotopes transmutation problem as well. A direct using of evaluated nuclear data libraries (ENDF/B-VI, JENDL, FENDL, BROND, EAF and so on) to particle transport simulation and isotopes transmutation in low and intermediate energy regions is the general idea of RTS&T code. The code can be successfully used for verification of non-grouping constant systems recorded in ENDF format. It is possible to use the RTS&T code to criticality calculation and nuclear safety analysis. The main changes compared to the previous code version concern the hadron- and photo-production model in intermediate and high energy regions, hadron- and photon-nucleus cross sections compilations, improved data for charged particle energy losses in composite materials.

I. Elementary processes simulation

PEF99 (Pre-equilibrium-Equilibrium-Fission): cascade-exciton model of intermediate energy hadron and photon interactions

In the RTS&T calculations the hadron-induced nuclear reaction process in energy region about 20 MeV to 5 GeV is assumed to be a three-step process of spallation (intra-nuclear cascade stage), pre-equilibrium decay of residual nucleus and the compound nucleus decay process (evaporation/high-energy fission competition). To calculate the intra-nuclear cascade stage the Dubna-version of intra-nuclear cascade model [2] coupled with the Lindenbaum-Sternheimer isobar model for single- and double-pion production in nucleon-nucleon collisions and single-pion production in pion-nucleon collisions was provided. Recently the addition of multiple-pion channels includes in code package to simulate up to 5 pions emission. The pre-equilibrium stage of nuclear reaction simulation is based on the exciton model. As proposed in [3] the initial exciton configuration for pre-equilibrium decay is formed in cascade stage of reaction or postulated in general input. The equilibrium stage of

reaction (evaporation/fission processes competition) is performed according to the Weisskopf-Ewing statistical theory of particle emission and Bohr and Wheeler or Fong theories of fission. To calculate the quantities determining the total fission width, Atchison prescriptions are used. Double-humped fission barrier parameters for *Z≥90* were taken from data set obtained in Obninsk and recommended for RIPL [4]. Experimental single-humped fission barrier heights are incorporated in RTS&T as proposed in Refs. [5,6] or according to many models: Barashenkov et al. phenomenological approach [7]; Barashenkov and Gereghi semi-phenomenological approach [8]; liquid drop model with Myers and Swiatecki's parameters [9]; liquid drop model with Pauli and Ledergerber's parameters [10]; Krappe and Nix's single-Yukawa modified liquid drop model [11]; Krappe, Nix and Sierk's Yukawa-plus-exponential modified liquid drop model [12]; Yukawa-plus-exponential modified liquid drop model to calculate the macroscopic barriers as proposed in [13]. Approximation for Coulomb barrier transmission probability is taken from [14]. In the current version of RTS&T code the Fermi breakup model for disintegrating of light nuclei has replaced the evaporation model for nuclei with a mass number between 2 to 16. The evaporation of fragments with a mass number > 4 is not included in the current version RTS&T. The RIPL recommended Audi and Wapstra experimental compilation [15] of atomic masses and binding energies is used in RTS&T model. Level density parameter values are chosen according to RIPL recommended systematics for any level density models: Gilbert-Cameron (Beijing group data set); backed-shifted Fermi-gas (Beijing group data set) or Ignatyuk form of Fermi-gas model; generalized superfluid model (Obninsk group data set); microscopic generalized superfluid model; shell dependent model proposed by S.K. Kataria and V.S. Ramamurthy [17] or according to the set of Malyshev's empirical systematic for 24≤A≤247 [18]. To estimate of the averaged squared matrix element 3 different models can be used:

1) estimation in approximation of quasi-free scattering of a nucleon above the Fermi level on a nucleon of the target nucleus [3];
2) parameterization taken from [19];
3) a set of empirical parameterizations.

PEF99 has three different models to simulate the gamma-ray emission in pre-equilibrium and equilibrium stages: the Weisskopf single-particle model, the Brink-Axel giant dipole resonance model, and the Kopecky-Uhl generalized Lorentzian model. To calculate the partial level densities for preequilibrium emission simulation the Avrigeanu systematic [16] is used. Composite (recommended) formulas include the advanced pairing and shell correction in addition to the Pauli effect, and average energy-depended single-particle level densities for the excited particles and holes. The PEF99 routine allows to calculate mean multiplicities of emmited particles, production, elastic and fission cross sections, energy- and angular-integrated and double-differential cross sections for each stage of the reaction. Residual nuclide distributions are available too.

To calculate the distance to the interaction point and simulation of the hadronic process type, the Barashenkov's experimental cross sections compilation [20] (coupled with the EXFOR [21] database information for any channels of proton- and neutron-induced reactions) or modified parameterizations of [20] was used. A proton and ion nonelastic cross section was obtained from parameterization in [22-24] as an alternative case. The elastic angular distribution in the energy region 50-400 MeV was taken from [25-29]. At the higher

energies other equations can be used for the parameterization of the hadron angular distributions in elastic collisions (only diffractive scattering is considered).

At E_{kin}>20 MeV and up to 5 GeV a cascade stage of hadron-nucleus inelastic collisions is simulated according to the approximation model based on a set of modified semi-empirical formulas [30] as alternative approach. This approximation of the double-differential cross sections was modified to calculate the emitted particle parameters in photon-induced reactions. Initial exciton configuration for aftercascade stage taken from parameterization of calculation results based on the intranuclear cascade model. Recently, another approach to simulate the nucleon transport in the energy region up to 150 MeV has been developed and tested. This method is based on the *direct* using of evaluated data containing in ENDF-VI high-energy data file [31].

High energy hadronic interactions

Simulation of hadron-nucleus inelastic collisions at E≥5 GeV is based on a set of the inclusive semi-empirical formulas for a one-particle production in *pp*-interactions coupled with the additive quark model of hadron-nucleus interactions for fast secondaries and a phenomenological model for slow particles. To calculate correctly the secondary particles production correlations in inelastic nucleon-nucleus interactions the modified FRITIOF 7.02 [32] code can be used. FRITIOF is a Monte Carlo code that implements the Lund string dynamics model for hadron-hadron, hadron-nucleus and nucleus-nucleus collisions. This code has been completed [33] with a simulation of the nuclear spallation at the fast stage of the interaction, with a calculation of the excitation energy of the nuclear residual nuclei and with a simulation of the nuclear relaxation stage in the framework of the statistical evaporation model. All of these allow one to calculate the characteristics of the inelastic hadron-nucleus and nucleus-nucleus interactions at the energies higher 3 GeV per nucleon. More than 20 decay channels are available in the current code version. Residual nucleus yields due high-energy hadron interactions are available too.

Neutron transport below 20 MeV

Neutron transport in the energy region 10^{-5} eV≤E_n≤20 MeV in the RTS&T code is based on the *direct* (without the interim library compilation) use of ENDF/B-VI [34] evaluated data library for detailed low-energy neutron interactions simulation. Universal data reading and preparation procedures allow to use another database written in ENDF format (for example JENDL, FENDL, EAF, BROND, etc.). During the execution of the linearization (fastest method of cross sections interpolation between adjacent data points), restoration of the cross sections in the resolved resonance region, temperature dependent Doppler broadening of the neutron cross sections and checking/correcting of angular distributions and Legendre coefficients for negative cross-section values are produced automatically with a help of standard ENDF preprocessing codes LINEAR, RECENT/RECENT-DD, SIGMA1 and LEGEND [35]. For the data storage in the memory and their further use the dynamically allocated tree of objects is organized. These objects have the standard types of ENDF-6 records (CONT, LIST, TAB1, TAB2, etc.). All types of reactions provided by the ENDF-6 format are taken into account in the neutron transport modeling: elastic scattering and reactions with production of one neutron in the exit channel, absorption with production of other type particles (with division on excited states of the residual nucleus), the fission with

separate yields of prompt and delayed neutrons and residual nucleus simulation by MF=8 data, etc. The energies and angles of emitted particles are simulated according to the distributions from MF=4, 5, 6, 12, 13, 14 and 15 files. The properties of residual nucleus are defined too. Data reading and constants preparation procedure was written in the ANSI C language to obtain the fast execution of data preprocessing and generation of secondary particle parameters due to the neutron transport simulation.

Photonic processes

In the current version of the RTS&T code following photonic processes are simulated:

1. *Photoelectric effect from K, $L_{I\text{-}III}$ atomic shells (fluorescence x-ray yield and tracking is simulated too);*
2. *Rayleigh scattering;*
3. *Compton scattering;*
4. *Pair production by photons;*
5. *Interactions of photons with nuclei.*

Photonuclear reactions are simulated in giant dipole resonance, quasi-deuteron, isobar production and high energy regions. Photoneutrons are generated isotropically and with Maxwellian energy distribution in the photon energy range 10-40 MeV. The GDR parameters of total photoneutron production cross section parameterization are taken into atlas by Dietrich and Berman [36] or RIPL-recommended systematics. As an alternative, the photonuclear part of EXFOR database (for selected isotopes only) can be used for partial channel simulation. At E>40 MeV and up to 1.2 GeV the intranuclear cascade-exciton model is used. The angular distribution of pre-equilibrium particles can be determined with the RIPL recommended Kalbach systematic or Chadwick-Oblozinsky theory for pre-equilibrium angular distributions, as implemented in the **kalbach_systematics** and **losalamos_analitical** codes. A high-energy photo-fission of heavy elements is simulated too. To simulate the photo-fission process two different approaches can be used: (a) using the approximation from [37], (b) with cascade-exciton model of photonuclear reactions (at E>100 MeV).

The EPDL evaluated data library [38] of total cross sections for photon-interactions, coherent and incoherent scattering form-factors are used in photon transport simulation for the energy range from about 10 eV to 100 GeV.

Charged particles ionization processes

To simulate the ionization processes induced by the charged particles two different models are provided: continuous energy losses model with δ-electron generation; continuous energy losses model without δ-electron production and full fluctuations (below δ-electron production threshold). The mean energy loss of the heavy charged particle can be described by the Bethe-Bloch formula or formula from [39] or the restricted energy loss formula if the incoming velocity is larger than the velocity of orbital electrons. In the low-energy region where this approach is not valid, the parameterization [40] was used. The density effect correction and shell correction terms in the stopping power formulas have been taken into account. For calculation the mean or restricted energy loss of electrons and positrons formulae [41] are used. Recently, the ICRU recommended data for collision stopping power for

electrons, positrons, protons and alpha particles in composite materials was included in the current code version. A multiple scattering of charged particles was simulated in the Moliere approximation. The particle path correction due to the multiple Coulomb scattering and direct pair production by charged hadrons at high energies is included in the calculations as well.

$e^{\pm}$ discrete bremsstrahlung process

The discrete bremsstrahlung photon energy is sampled from a Seltzer and Berger [42] differential cross section for electron kinetic energy below 10 GeV and Bethe-Heitler [43] cross section above this value. The angular distribution of the emitted photon is sampled according to the facilitated form of the double differential cross section. The differences between the radiative stopping power of positrons and electrons are taken into account. At very high energies the Landau-Pomeranchuk-Migdal effect is taken into account too.

Discrete interactions of muons

The double differential cross section for the discrete bremsstrahlung process was implemented in Ref. [44] using the formulae of Petrukhin and Shestakov [45] which were obtained by a comprehensive treatment of atomic and nuclear form factors. The double differential cross section for direct pair production was taken from [44]. The total cross section parameterization and Monte Carlo sampling scheme to simulate the discrete bremsstrahlung and direct pair production by muons was taken from [46]. To simulate the nonelastic muon-nucleus interaction, two different approaches can be provided in RTS&T code:

1) discrete process simulation (deep inelastic muon-hadron scattering) according to Lohmann et al. approach;
2) to use a continuous energy loss from nuclear interactions contribution to average energy loss of muon.

II. RTS&T Geometry Module

The RTS&T code has an effective geometry definition system provided with a combinatorial method. Universal geometry module GEOMETRY basically was intended for the performing of two functions:

1) detailed description of the spatial geometry and material composition of the considered system;
2) localizations of the site of transported particle in this system.

In the framework of the combinatorial approach the geometry of any physical object is extremely precisely described through definition of a set of geometrical regions, limited by closed surfaces and filled by homogeneous material, and rules of their mutual arrangement. The surface form of each region must correspond to one of the primitive shapes from a fixed set.

Shape definition

The recursivial coordinate surface method is used in effective algorithms for analysis whether the considered point is into the region limited by the given form of the surface. 30 primitive shapes are defined in the current code version; some of them are shown in Fig.1.

Each of the shapes is characterized in size parameters and has an own local coordinate system. The beginning of a local coordinate system serves a point of binding.

Hierarchical enclosure tree

The complex 3D geometry can be constructed with Boolean algebra operations on the primitive shapes with arbitrary displacements and rotations. The considered object will be broken into the set of regions, which can be enclosed but cannot be crossed. Let us consider a system defined by a set of the geometrical regions $\{S_n\}$, n=1, 2,..., N. The region S_{n1} will be enclosed in S_{n2}: $S_{n1} \subset S_{n2}$, if S_{n1} is wholly in S_{n2} and these regions do not coincide: $S_{n1} \subset S_{n2} = \bar{r}/\forall\ r: (r \in S_{n1} \Rightarrow r \in S_{n2}) \wedge (\exists\ r: (r \in S_{n2}) \wedge (r \notin S_{n1}))$, where $\bar{r}=(x,y,z)$ - point in a cartesian coordinate system. Regions $\{S_n\}$, n=1, 2,..., N must not be crossed: $\exists\ r: (r \in S_{n2}) \wedge (r \in S_{n1}) \Rightarrow (S_{n1} \subset S_{n2}) \vee (S_{n2} \subset S_{n1})$. We shall name the enclosed region S_{n1} as a daughter in relation to the mother region S_{n2}. Thus in addition, it is supposed, that the transitivity property is not saved: if S_{n1} is enclosed in S_{n2}, and S_{n2} is enclosed in S_{n3}, S_{n1} will not be considered to be enclosed in S_{n3}, no less than S_{n3} will not be mother in relation to S_{n1}: $S_{n1} \subset S_{n2} \subset S_{n3} \Rightarrow S_{n1} \not\subset S_{n3}$. All geometrical regions are numbered in any order by numbers from 1 to N, where N is the general number of regions, and the mother region number of each region is specified in an explicit form. For the most external region, containing all others, the mother region number is zero.

If it is necessary to consider some regions, to which object is divided, as one region, these regions can be united and get a common number.

The positioning of the region in the space is defined by means of displacement and rotation of its local coordinate system in relation to a coordinate system of the mother region. Displacement and rotation of a coordinate system of the most external region are set in relation to some global coordinate system. The optimization algorithms are used for hierarchical enclosure tree analysis.

A set of service routines was created for automatic forming of geometry input files for often used configurations, such as a standard WWER-440 core cell shown in Fig. 2. The geometry of a WWER-440 core cell is considered as a set of 506 regions, two of which are hexagonal prisms and others are cylinders. The regions, which present covers, air clearances and central channels of fuel elements, can be united.

III. RTS&T-CAD-interface

The problem of a visual presentation of the investigated object's geometry was solved with transformation of the RTS&T input data format to the ASCII DXF® (Drawing Interchange) format, designed by the Autodesk company as a standard for exchange by graphic information between AutoCAD® and other applications. The format transformation is performed using a set of special routines forming DXF-images of each shape. Thus the powerful capabilities of CAD-systems make not only possible the visualization of three-dimensional objects with an arbitrary rotation in the screen space and with hidden lines removed from the drawing but they are also preparing the designer documentation.

RTS&T output files in DXF format will be used for visualization of 3D geometry and material composition of the considered system (Fig. 2) and also for showing particle trajectories and output functionals.

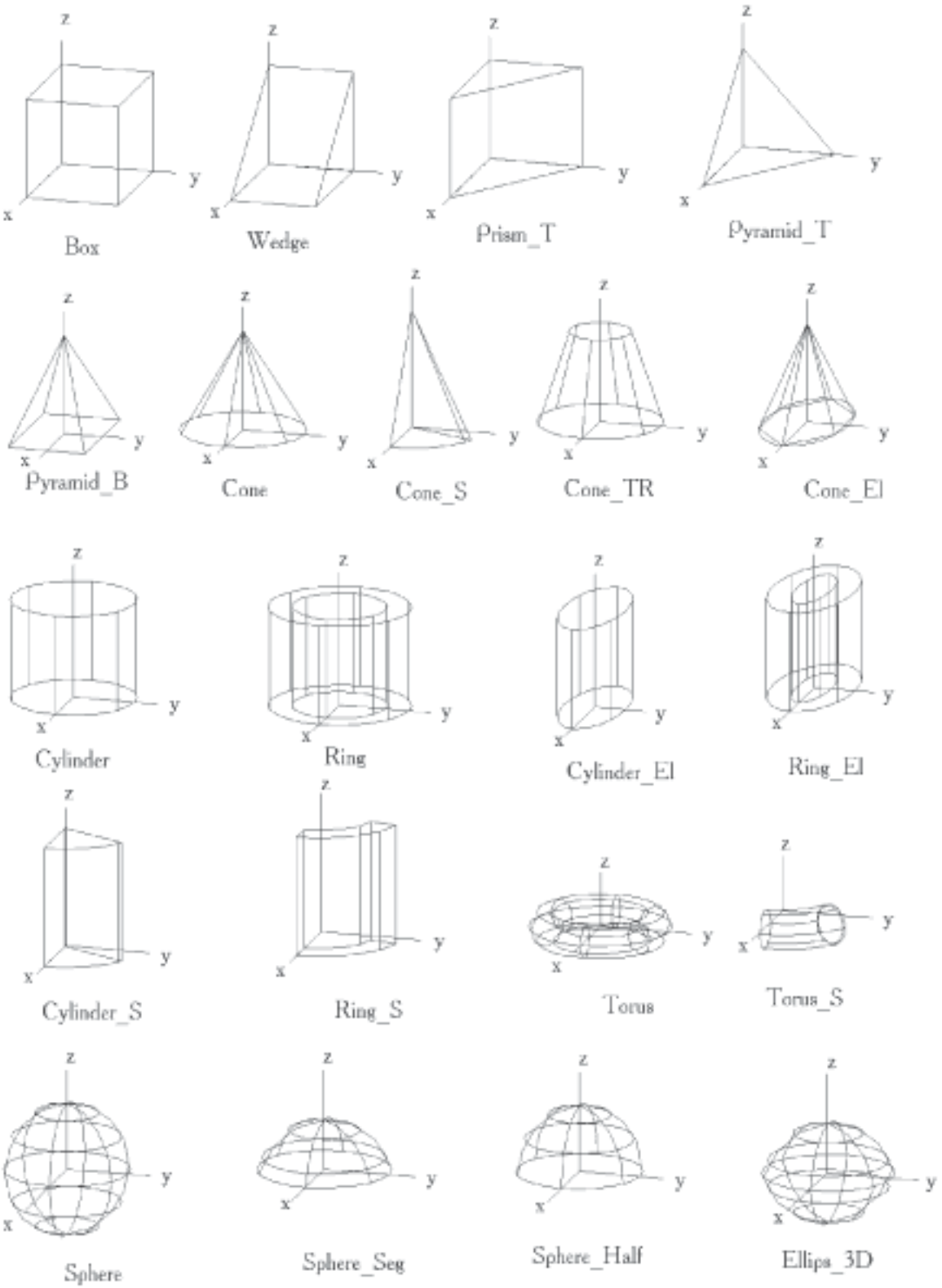

Fig. 1. RTS&T Standard set of shapes.

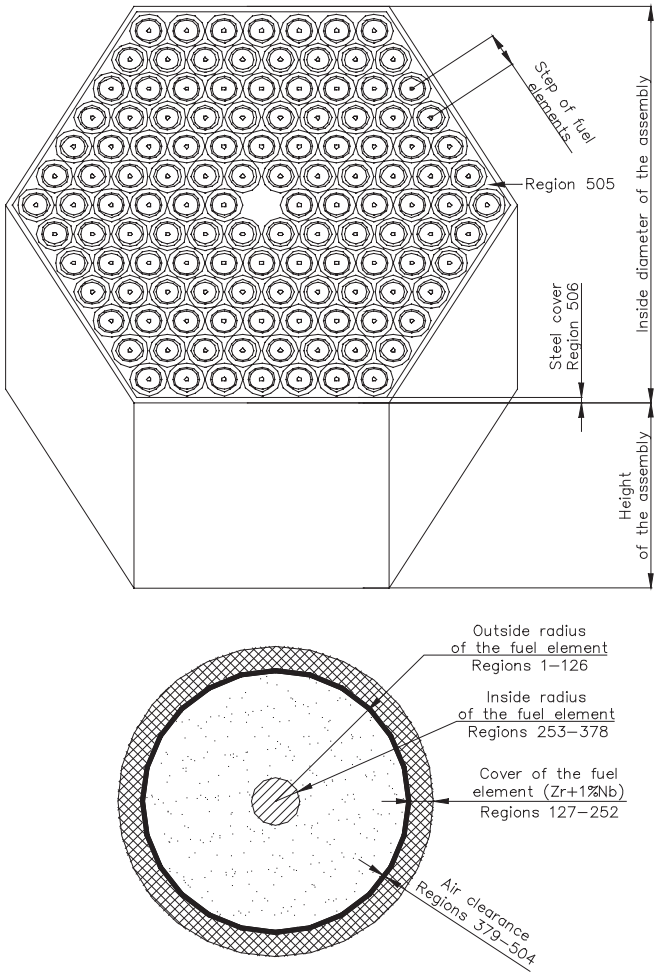

Fig. 2. Example of geometry input.

References

[1] A.I. Blokhin, I.I. Degtyarev, A.E. Lokhovitskii, M.A. Maslov, and I.A. Yazynin: "RTS&T Monte Carlo Code (Facilities and Computation methods)", in Proceedings of the SARE-3 Workshop, KEK, Tsukuba, Japan, May 1997.

[2] V.S. Barashenkov and V.D. Toneev: "Interaction of high energy particles and atomic nuclei with nuclei", Moscow, Atomizdat, 1972.

[3] K.K. Gudima, S.G. Mashnik and V.D. Toneev, Nucl. Phys. A401 (1983) 329.

[4] Handbook for calculations of nuclear reaction data, IAEA-TECDOC-1034, IAEA, Vienna, August 1998.

[5] W.D. Myers and W.J. Swatecki: Lawrence Berkeley Lab. Report CA 94720, Berkeley, 1995.

[6] P. Moller and J.R. Nix: LANL Report NM 87545, Los Alamos, 1995.

[7] V.S. Barashenkov et al., Nucl. Phys. A206 (1973) 131.

[8] V.S. Barashenkov and F.G. Gereghi: JINR Communications, P4-10781, Dubna, 1977.

[9] W.D. Myers and W.J. Swiatecki: Ark. Physik 36 (1967) 343.

[10] H.C. Pauli and T. Ledergerber: Nucl Phys. A175 (1971) 545.

[11] H.J. Krapp and A.J. Sierk: IAEA-SM-174/12, Vienna (1974).

[12] H.J. Krapp, J.R. Nix and A.J. Sierk: Phys. Rev. C20 (1979) 992.

[13] A.J. Sierk: Phys. Rev. C33 (1986) 2039.

[14] R.E. Prael: "Approximations for Coulomb Barrier Transmission Probability in HETC and Related Codes", LANL Report NM-87544, Los Alamos (1988).

[15] G. Audi and A.H. Wapstra: Nucl. Phys. A595 (1995) 409.

[16] S.K. Kataria and V.S. Ramamurthy: "Macroscopic systematics of nuclear level density", Nucl. Phys., A349 (1980).

[17] A.V. Malyshev: "Level density and structure of atomicnuclei", Atomizdat, Moscow, 1969.

[18] P.G. Young, E.D. Arthur, M.B. Chadwick: "Comprehensive nuclear model calculations: introduction to the theory and use of the GNASH code", LA-12343-MS.

[19] M. Avrigeanu and V. Avrigeanu, Comp. Phys. Comm., 112 (1998) 191.

[20] V.S. Barashenkov: "Cross Section of Interaction of Particle and Nuclei with Nuclei", Dubna, JINR (1993).

[21] NEA report DBG-006.2, EXFOR network service (1989).

[22] R.E. Prael and M.B. Chadwick, "Addendum to: Applications of evaluated nuclear data in the LAHET^{TM} code", LANL report NM 87545, Los Alamos National Laboratory, Los Alamos (1997).

[23] J.R. Letaw, R. Silberberg and C.H. Tsao, *Astrophysical J. Suppl.s*, 51, (1983) 271.

[24] S. Pearlstein, Astrophys. J. 346, (1989) 1049.

[25] D.A. Hutcheon et al., Phys. Rev. Let. 47 (1981) 315.

[26] R.E. Prael, "A Review of Physics Models in LAHET^{TM} Code", LA-UR-94-1817 (1994).

[27] D.G. Madland, R.E. Prael, "A nucleon-nucleus elastic scattering model for LAHET^{TM}", Proceedings of the 1996 ANS Topical Meeting Radiation Protection and Shielding, No. Falmouth, Massachusetts, April 21-25 1996, (1996) 251.

[28] J. Ranft, "Estimation of radiation problems around high-energy accelerators using calculations of the hadronic cascade in matter", Part. Accel. 3 (1972) 129.

[29] H. Weitzig et al., “Monte Carlo simulation of elastic hadron-nucleus reactions with the computer code NUCREL”, Leipzig report KMU-HEP 81-07, 1981.
[30] B.S. Sychev, A.Ya. Serov and B.V. Man'ko, Preprint of Radiotechnical Institute of USSR Academy of Sciences N799 (1979) (in Russian).
[31] P.G. Young et al.: “Transport data libraries for incident proton and neutron energies to 100 MeV”, LANL report LA-11753, Los Alamos (1990).
[32] B. Andersson et al. Nucl. Phys. 281B (1987) 289.
[33] V.V. Uzhinskii: “Modified code FRITIOF”. User's Guide. JINR preprint E2-96-192, Dubna (1996).
[34] ENDF-102 Data formats and procedures for the evaluated nuclear data file ENDF-6. BNL-NCS 44945 (1990).
[35] D.E. Cullen: “The 1996 ENDF Pre-processing Codes”, IAEA-NDS-39, Rev. 9 (1996).
[36] S.S. Dietrich and B.L. Berman, Atomic Data and Nucl. Data Tables 38 (1988) 199.
[37] H.C. Fesefeldt: “Simulation of hadronic showers, physics and applications”, Technical Report PITHA 85-02, III Physikalisches Institut, RWTH Aachen Physikzentrum, 5100 Aachen, Germany, September 1985.
[38] D.E. Cullen et al.: “Tables and Graphs of Photon-Interaction Cross Section from 10 eV to 100 GeV Derived from the LLNL Evaluated Photon Data Library (EPDL)”. UCRL-50400 vol.6, Lawrence Livermore National Laboratory (1989).
[39] N.N. Pucherov and T.D. Chesnokova: Atomic Energy (in Russian), 62 (1) (1987) 51.
[40] H.H. Andersen and J.F. Ziegler: “Hydrogen stopping powers and ranges in all elements”, Vol. 3 of “The Stopping and Ranges of Ions in Matter”, Pergamon Press, New York (1977).
[41] S.M. Seltzer and M.J. Berger, NASA Publ. SP-3012, Washington.
[42] S.M. Seltzer and M.J. Berger, NIM B12 (1985) 95.
[43] Y.S. Tsai, Rev. Mod. Phys. 46 (1974) 815; Erratum: Rev. Mod. Phys. 49 (1977).
[44] W. Lohmann et al., “Energy loss of muons in the energy range 1-10000 GeV, CERN Report 85-03 (1985).
[45] A.A. Petrukhin and V.V. Shestakov, Can. J. Phys. 46 (1968) 377.
[46] GEANT3.2, CERN Program Library entry W5013, CERN, Geneva, Switzerland (1994).

UDC 621.039:539.141

VERIFICATION BENCHMARK CALCULATIONS IN LOW AND MEDIUM ENERGY REGIONS USING RTS&T CODE

I.I. Degtyarev, A.E. Lokhovitskii, O.A. Liashenko, I.A. Yazynin
SRC Institute for High Energy Physics, 142284 Protvino, Moscow region, Russian Federation
V.I. Belyakov-Bodin
SRC Institute of Theoretical and Experimental Physics, Moscow, Russian Federation
A.I. Blokhin
SSC Institute of Physics and Power Engineering (Nuclear Data Center of Russian Federation), 249020 Obninsk, Russian Federation

VERIFICATION BENCHMARK CALCULATIONS IN LOW AND MEDIUM ENERGY REGIONS USING RTS&T CODE. The main changes compared to the previous RTS&T [1] code version, concern the hadron- and photo-production model in intermediate and low energy regions, hadron- and photon-nucleus cross sections compilations, improved data for charged particle energy losses in composite materials, low energy neutron transport. The analysis of the neutron and gamma-ray transmission benchmarks problem in the low- and energy deposition in the intermediate energy region were done for the verification of the new code version and the nuclear data used in the code. The comparison between calculation and measurement data is presented.

The RTS&T [1] code (Radiation Transport Simulation and Isotopes Transmutation Calculation) was assigned for detailed Monte Carlo simulation of many particle types transport in a complex 3D geometry's with composite materials. Comparisons between experimental and simulated data are presented for 4 different benchmark problems connected to a secondary neutron and γ-rays production from non-elastic hadron-nucleus collisions in low energy region and energy deposition of medium energy protons.

I. Intermediate energy protons benchmark

The experimental data set of the heat deposition inside any material targets has been compared with results obtained by Monte Carlo simulation of three-dimensional hadronic and electromagnetic cascades by LAHET^{TM} [2] and/or RTS&T codes. Calorimeter measurements of the heat deposition inside beryllium, carbon, aluminum, iron, copper, tungsten, bismuth, lead, and uranium targets have been described in Refs. [3-7]. The results of the theoretical and experimental data comparison for longitudinal distribution of energy deposition in cylindrical targets (d=20 cm and L=60 cm) of various materials under 1.21 GeV proton point-like beam irradiation are shown in Figs 2-10. In LAHET^{TM} calculations [3] the value of incident proton energy was taken as 1.2 GeV.

II. Neutron Leakage Spectra from Beryllium Sphere and Beryllium-Lithium sphere [8]

The spectrum of the initial isotropic point source of neutron is shown in Fig. 11. The computational and experimental spectra comparison for 6 various shell configurations are shown in Figs 12-17. The shell configurations for 6 considered cases are shown in Fig. 1.

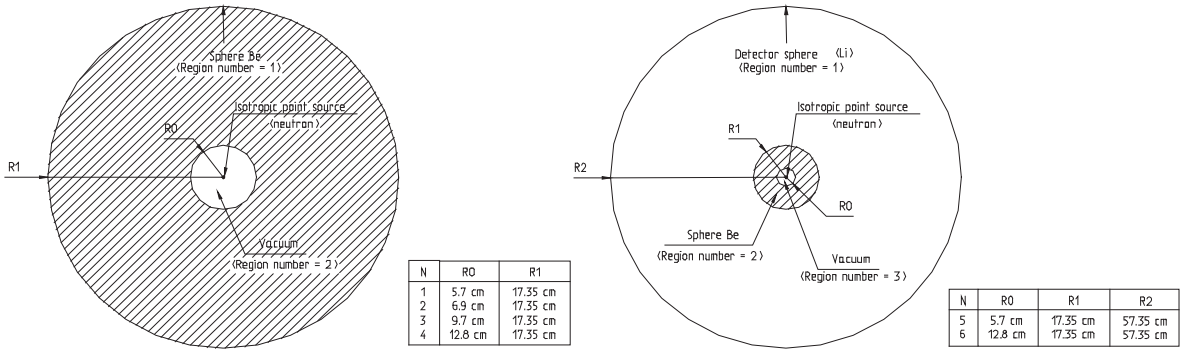

N	R0	R1
1	5.7 cm	17.35 cm
2	6.9 cm	17.35 cm
3	9.7 cm	17.35 cm
4	12.8 cm	17.35 cm

N	R0	R1	R2
5	5.7 cm	17.35 cm	57.35 cm
6	12.8 cm	17.35 cm	57.35 cm

1. Shell (1) inner radius 57 mm, outer radius 173.5 mm.
2. Shell (2) inner radius 69 mm, outer radius 173.5mm.
3. Shell (3) inner radius 97 mm, outer radius 173.5 mm.
4. Shell (4) inner radius 128 mm, outer radius 173.5 mm.
5. Shell (5) Beryllium (1) + Lithium (400 mm thickness).
6. Shell (6) Beryllium (4) + Lithium (400 mm thickness).

Fig. 1. Benchmark geometry.

III. Gamma-ray energy spectra emitted from spheres with 14 MeV neutron source [9]

The γ-rays were produced from *(n,xγ)* reactions in spheres and emitted from the spherical piles. The measured and calculated quantity was a leakage spectrum. The spectrum of the initial isotropic point source of neutron is shown in Fig. 18. Piles characteristic parameters are shown in Table 1. The calculational and experimental spectra comparison for 4 various piles configurations are shown in Figs 19-22.

Table 1

List of piles parameters

Material	Diameter (cm)	Density (g/cm^3)	Thickness (cm)
Al	40	1.22	9.8
Cr	40	3.72	9.8
Cu	61	6.23	27.5
Nb	28	4.39	11.2

IV. Neutron leakage spectra from the surface of the iron spherical shell with Cf-252 neutron source

The comparison of the RTS&T (ENDF/B-VI) calculations has been performed through the analyses of the neutron leakage spectrum from spherical assemblies measured in integral experiments with Cf-252 fission neutron sources and analogous calculational results with ANISN (BROND-2, ENDF/B-VI, JENDL-3) and MCNP4A (FENDL-1, EFF-3) codes [10]. The energy spectrum of the initial isotropic point source is taken from Ref. [11]. The experiment was performed with the time-of-flight technique using the initial source intensity measured as 5×10^{5} neutrons/sec. Leakage neutrons were registrated by the paraphenile detector (D=5×5 cm). A detailed description of the experimental method is given in Refs [12-14]. Figs 23-26 show the results of comparison C/E ratio for iron spherical shell of 4.5, 9.5, 12.0, 20.1, and 32 cm in diameter with a central hole of 2 cm in diameter.

Acknowledgements

The authors are grateful to T. Fukahori (JAERI, Japan) for sending the CD-disk release with the JENDL 3.2 library.

Experimental data for energy depositions of medium energy proton in tungsten were offered in the framework of the Project No. 157 supported by the International Science and Technological Center.

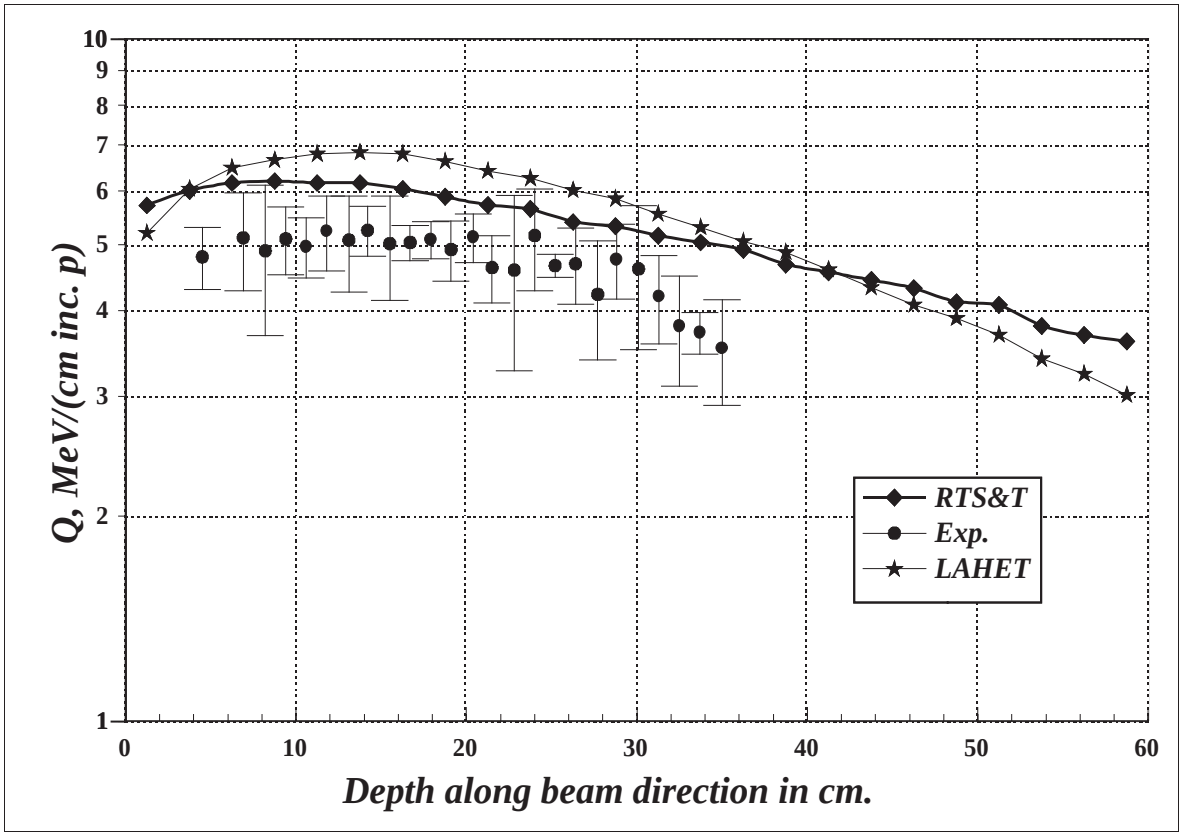

Fig. 2. Proton beam on beryllium.

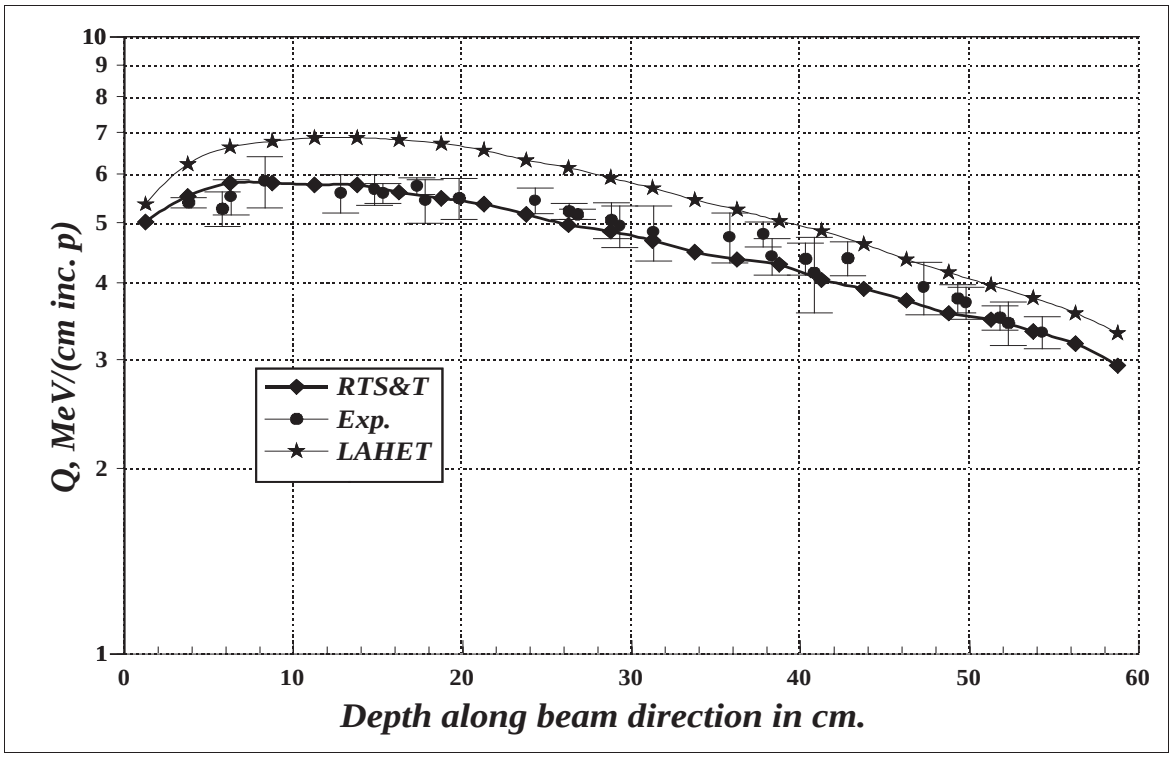

Fig. 3. Proton beam on carbon.

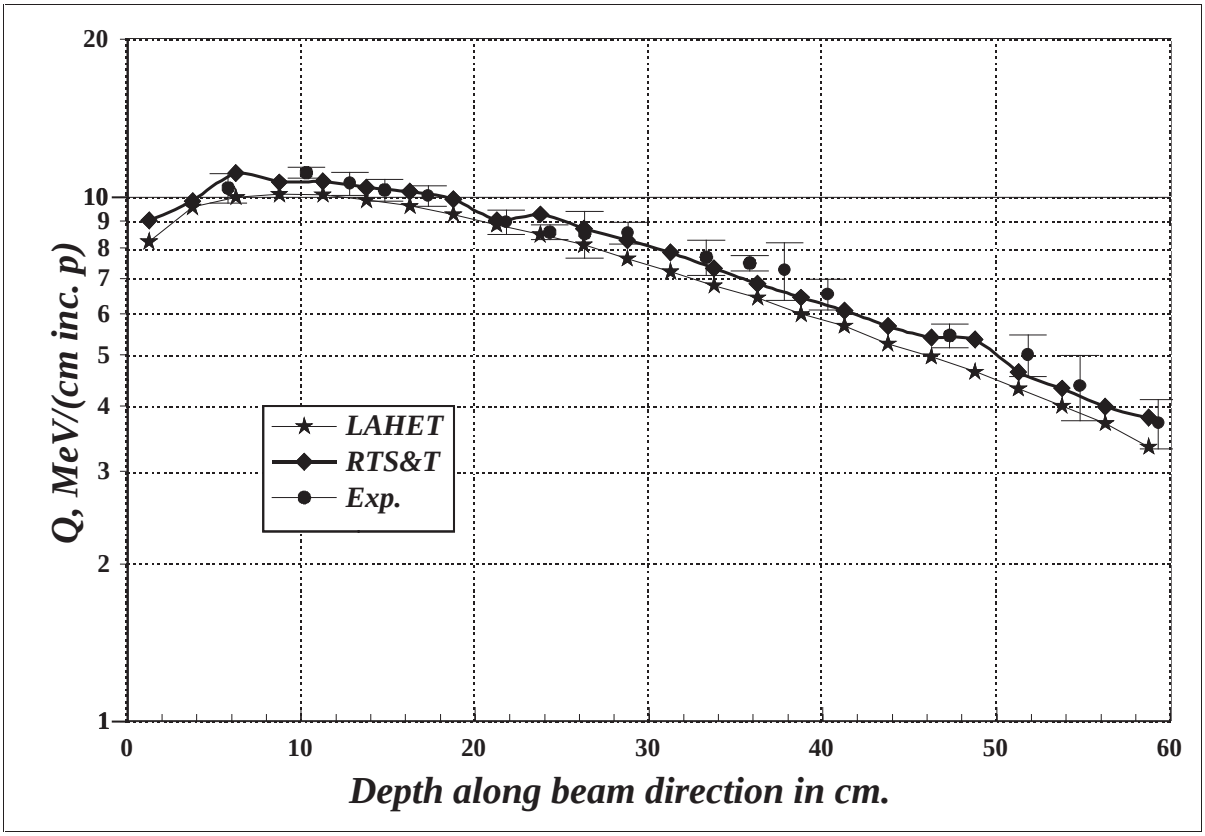

Fig. 4. Proton beam on aluminum.

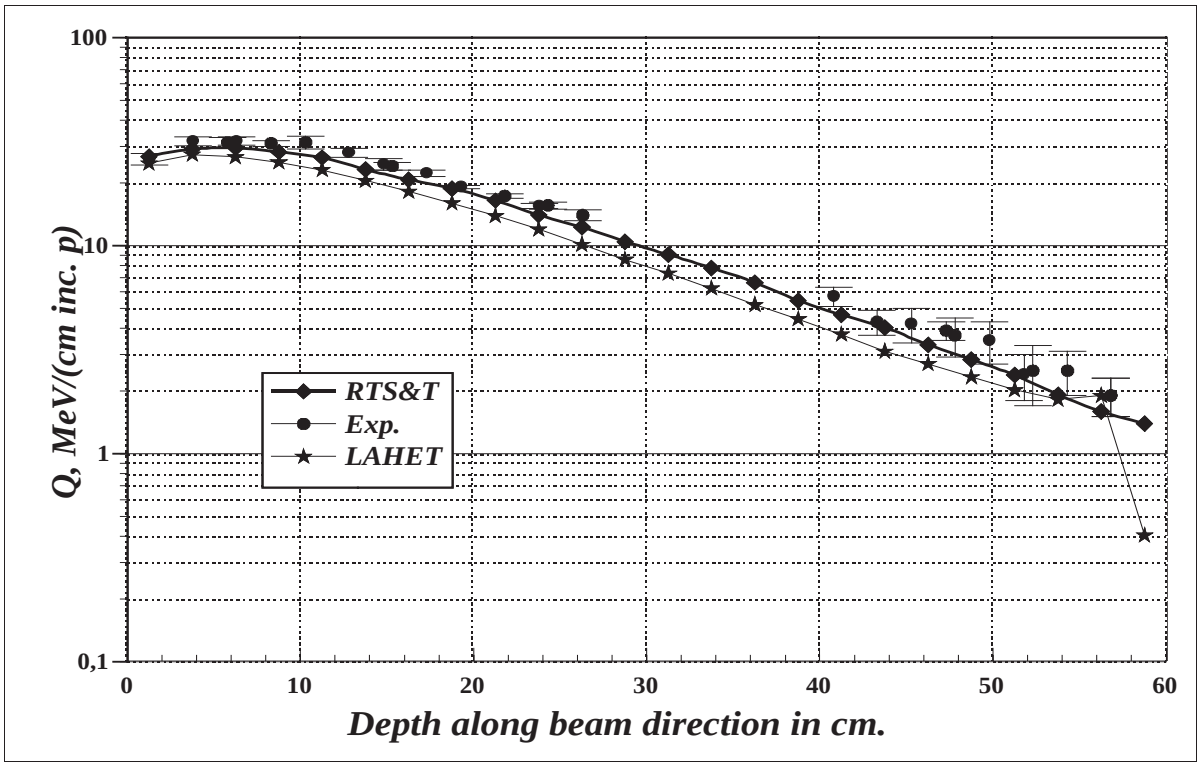

Fig. 5. Proton beam on iron.

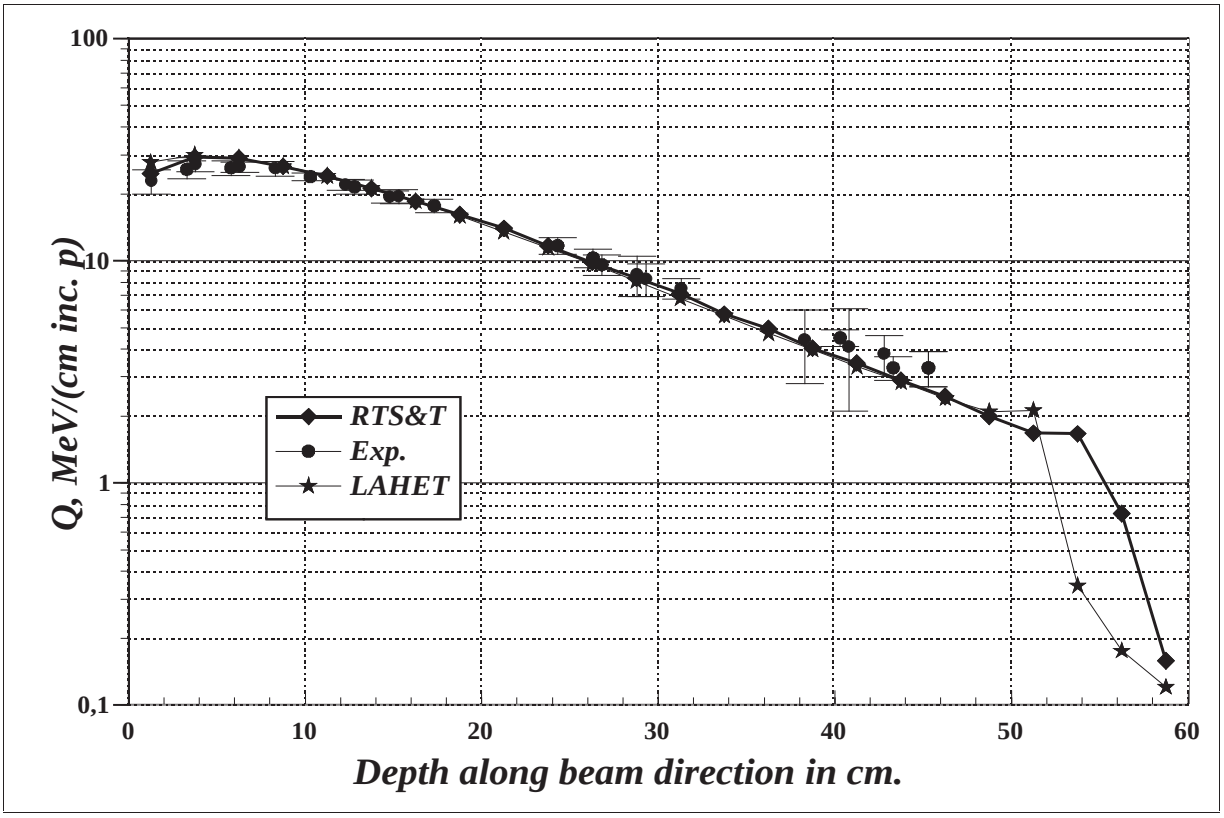

Fig. 6. Proton beam on copper.

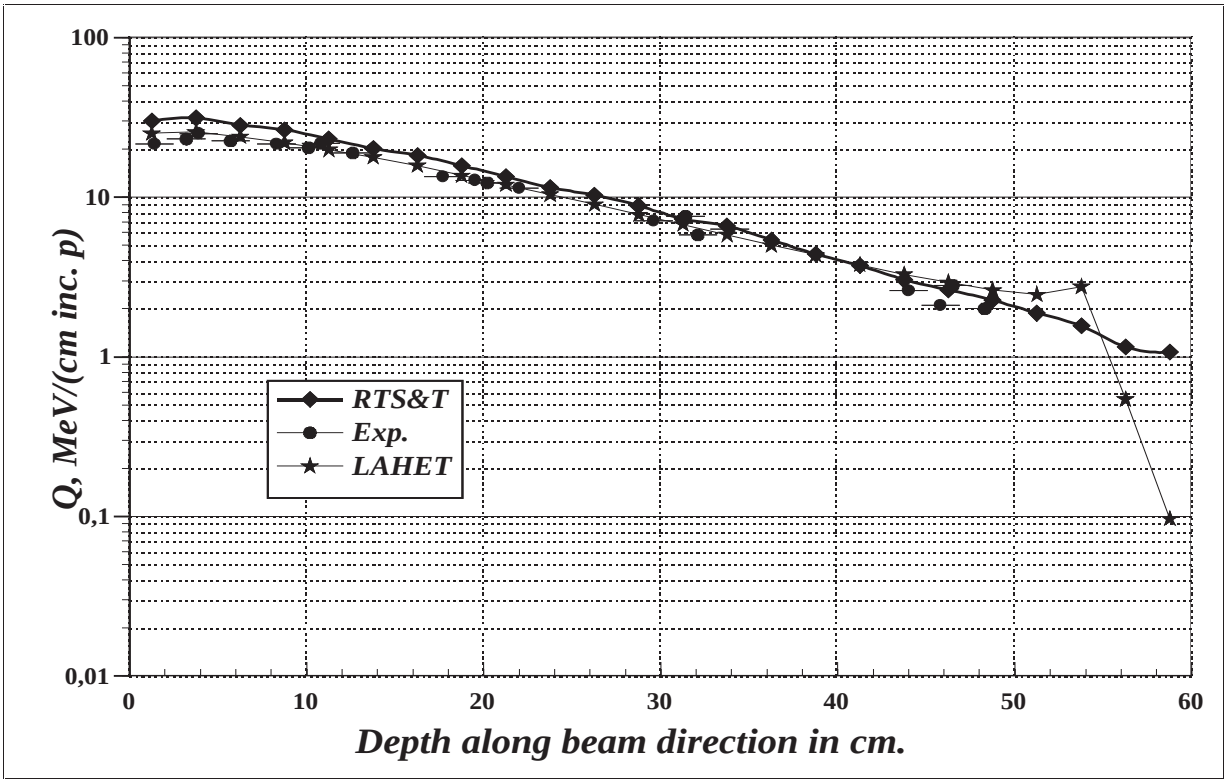

Fig. 7. Proton beam on lead.

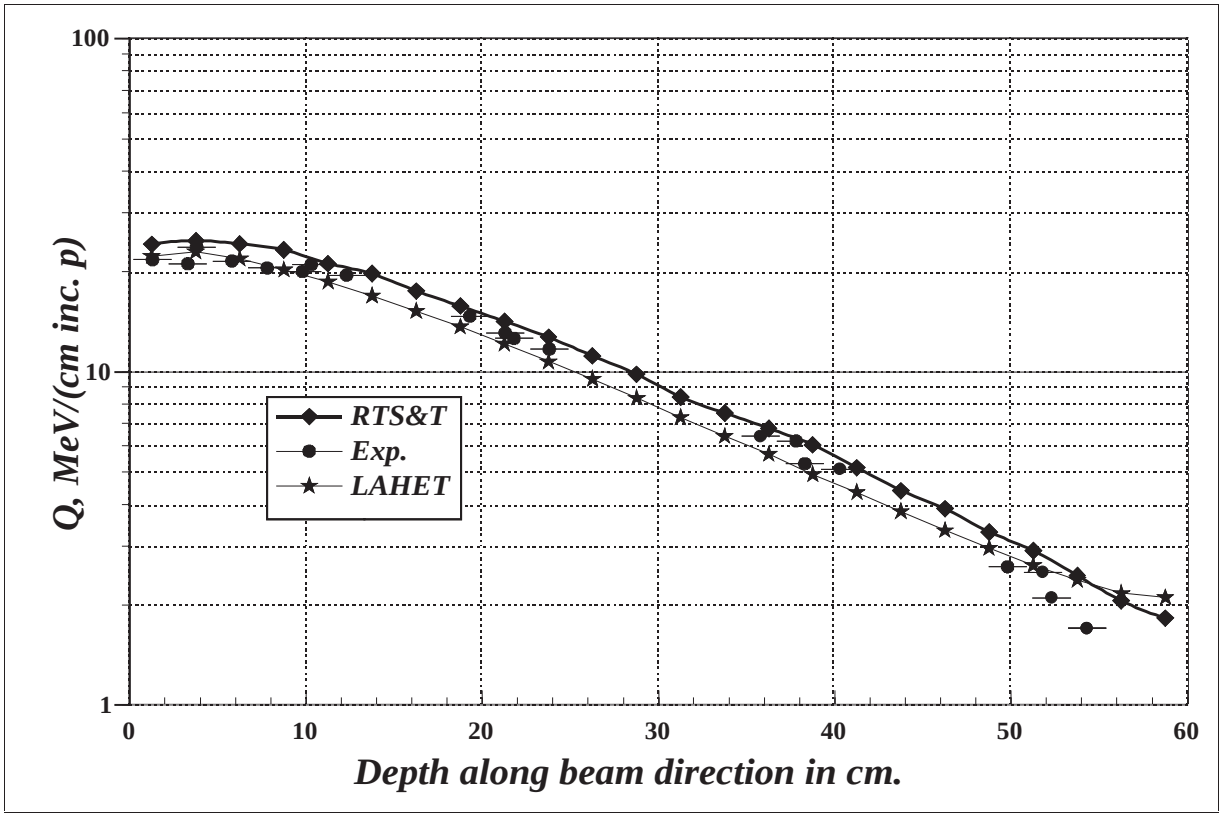

Fig. 8. Proton beam on bismuth.

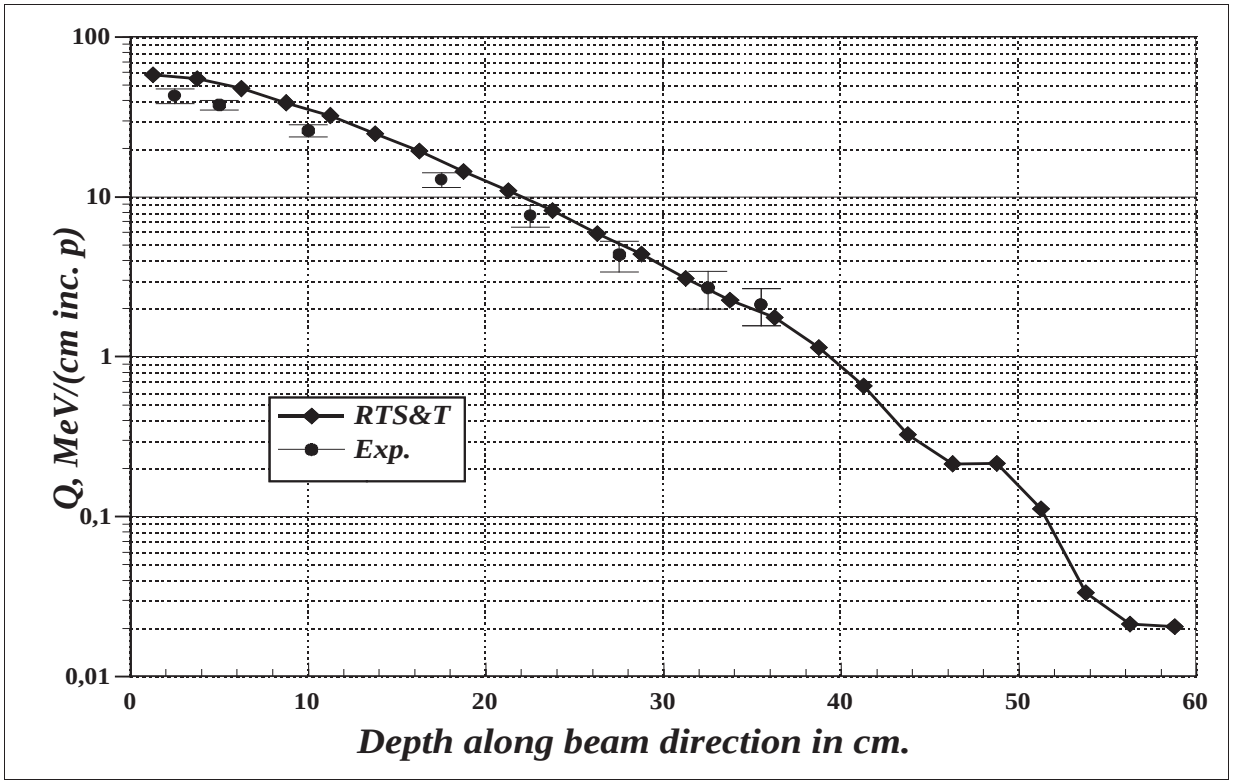

Fig. 9. Proton beam on tungsten.

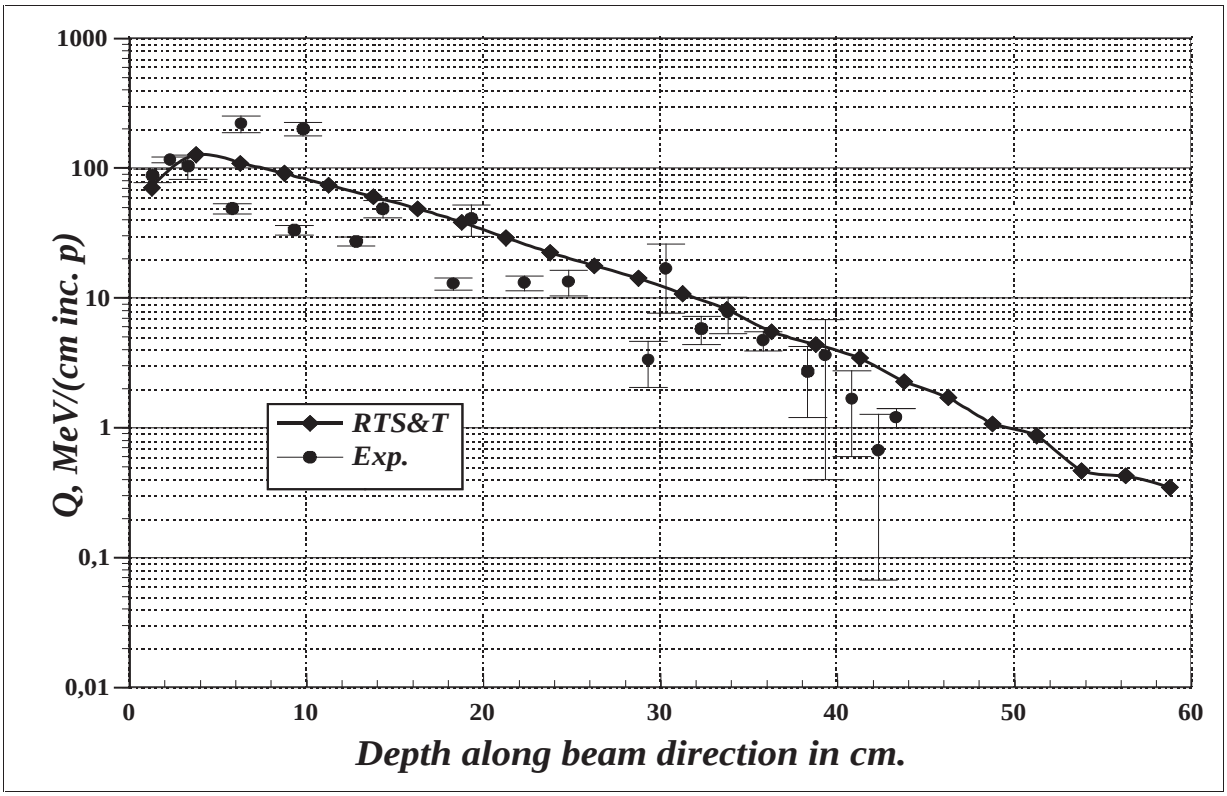

Fig. 10. Proton beam on uranium.

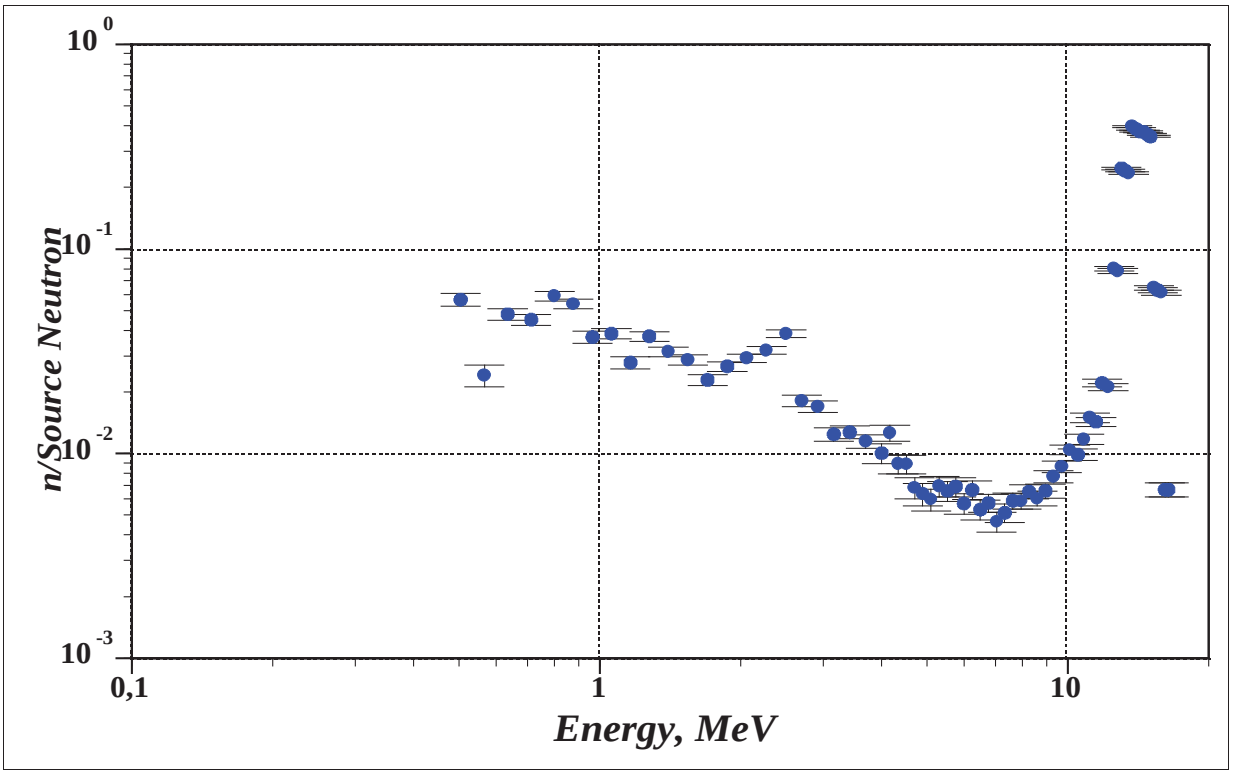

Fig. 11. Spectrum of D-T neutron source.

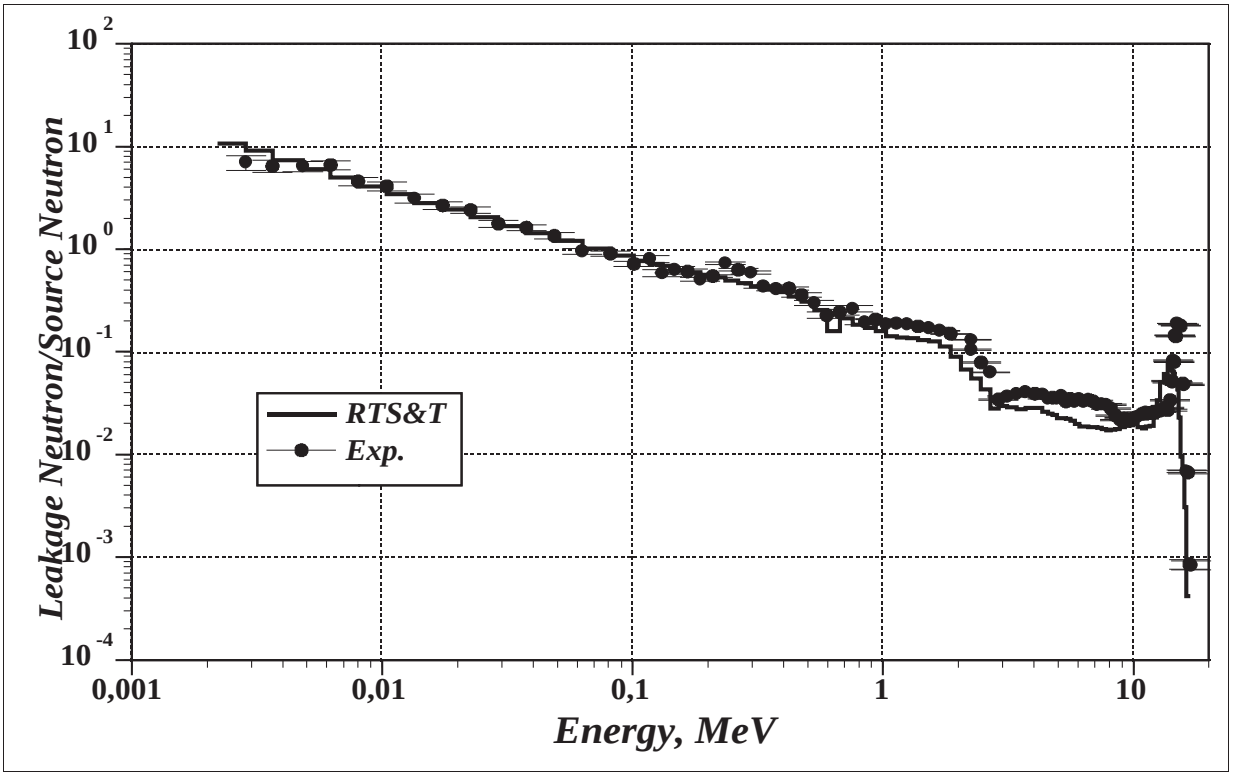

Fig. 12. Leakage spectra of low energy neutrons from beryllium sphere (internal radius is 57 mm, external radius is 173.5 mm).

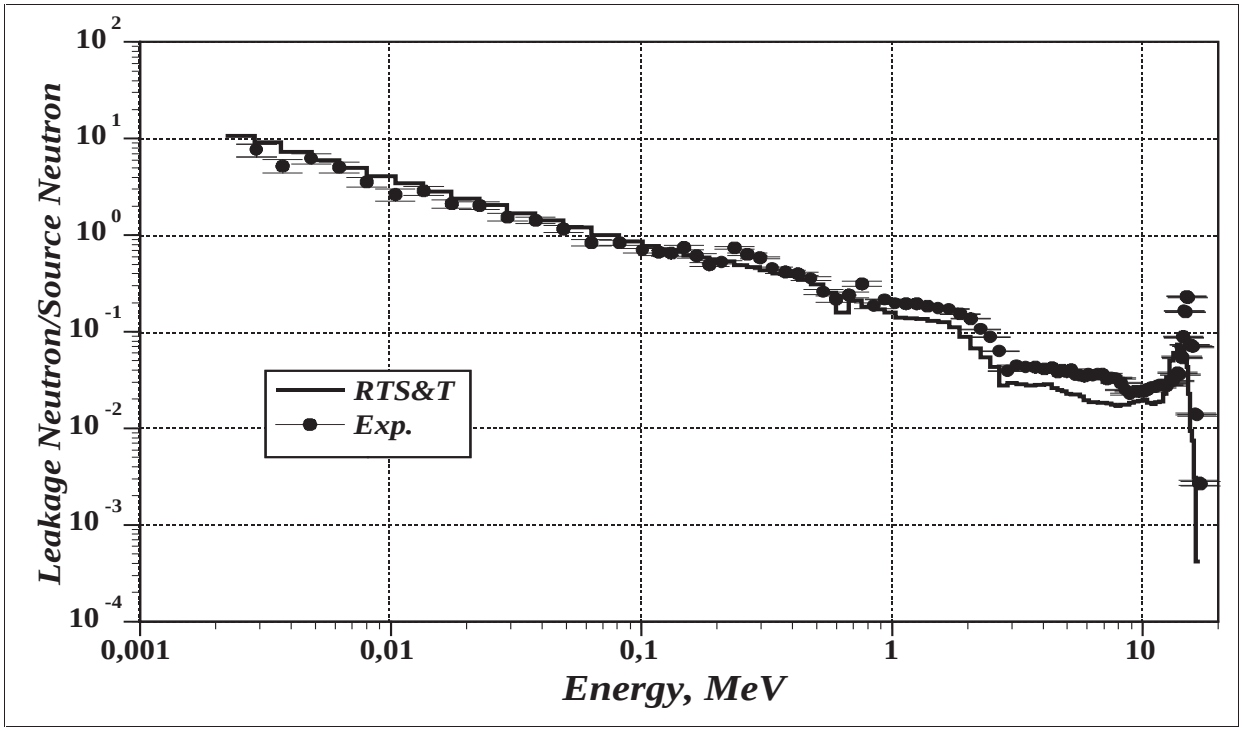

Fig. 13. Leakage spectra of low energy neutrons from beryllium sphere (internal radius is 69 mm, external radius is 173.5 mm).

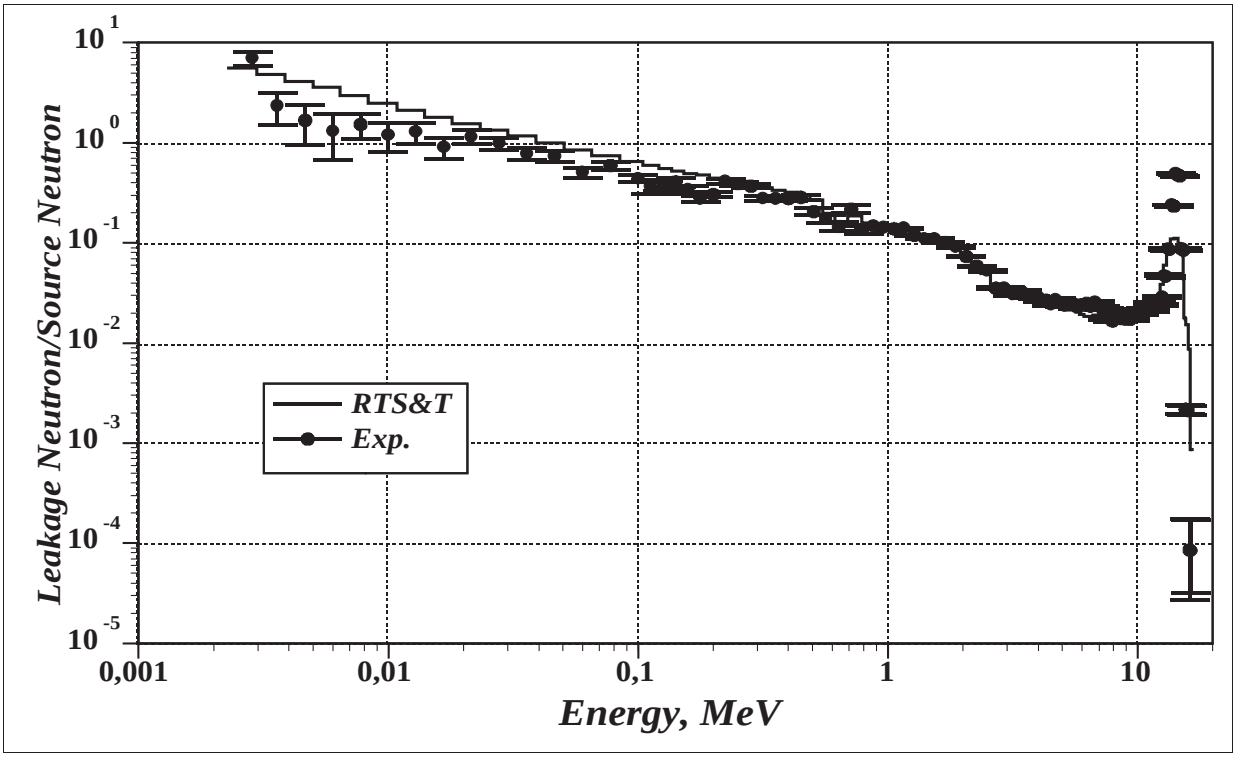

Fig. 14. Leakage spectra of low energy neutrons from beryllium sphere (internal radius is 97 mm, external radius is 173.5 mm).

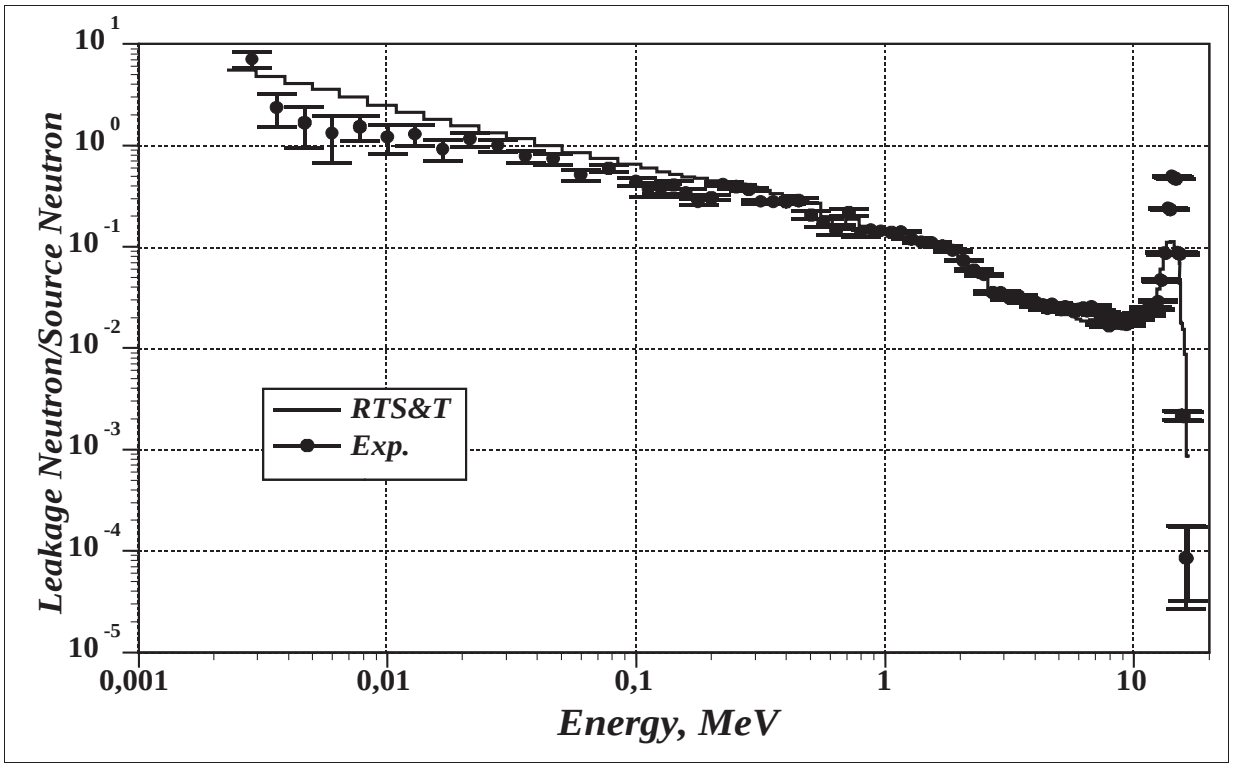

Fig. 15. Leakage spectra of low energy neutrons from beryllium sphere (internal radius is 128 mm, external radius is 173.5 mm).

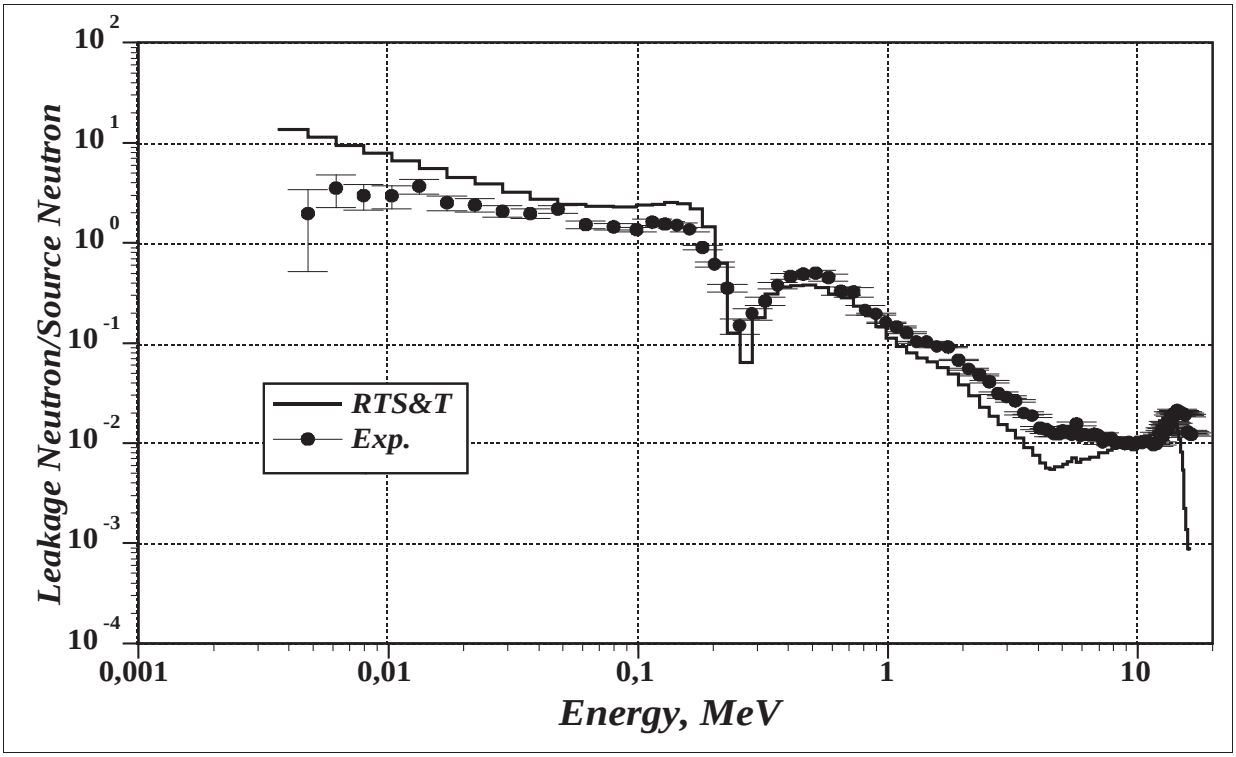

Fig. 16. Leakage spectra of low energy neutrons from beryllium-lithium sphere (Be radius is 116.5 mm, Li radius is 400 mm).

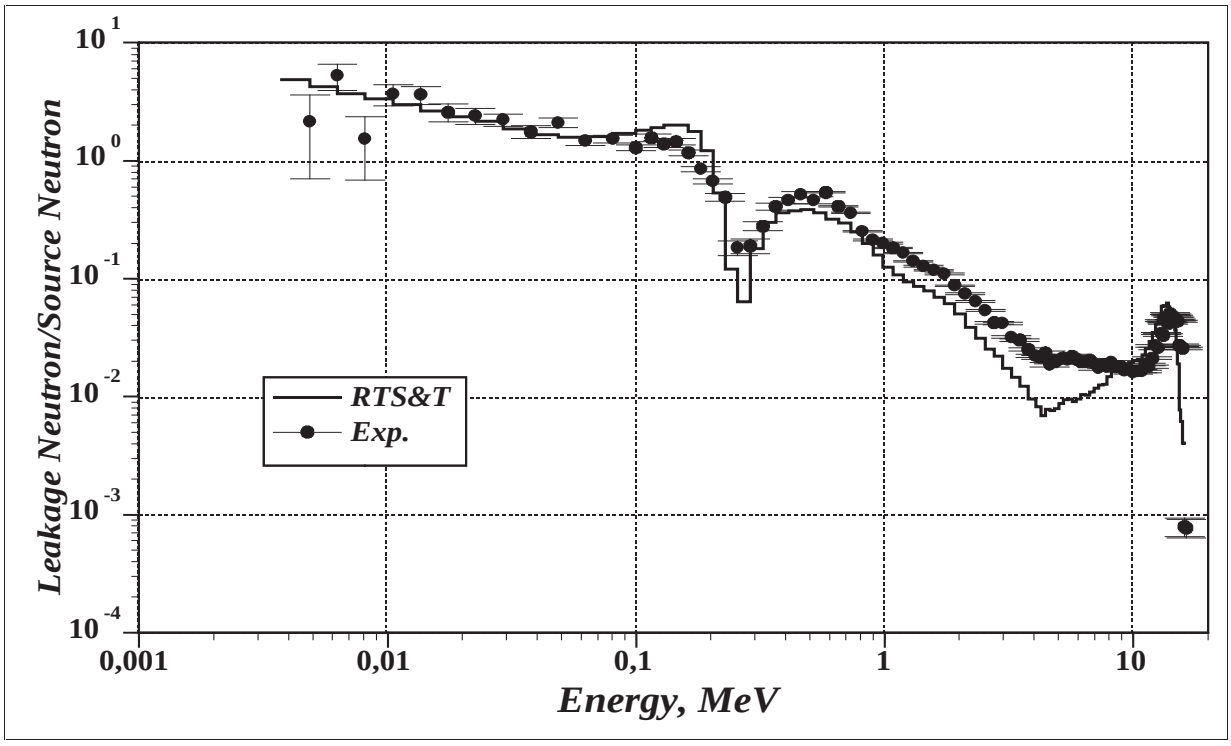

Fig. 17. Leakage spectra of low energy neutrons from beryllium-lithium sphere (Be radius is 45.5 mm, Li radius is 400 mm).

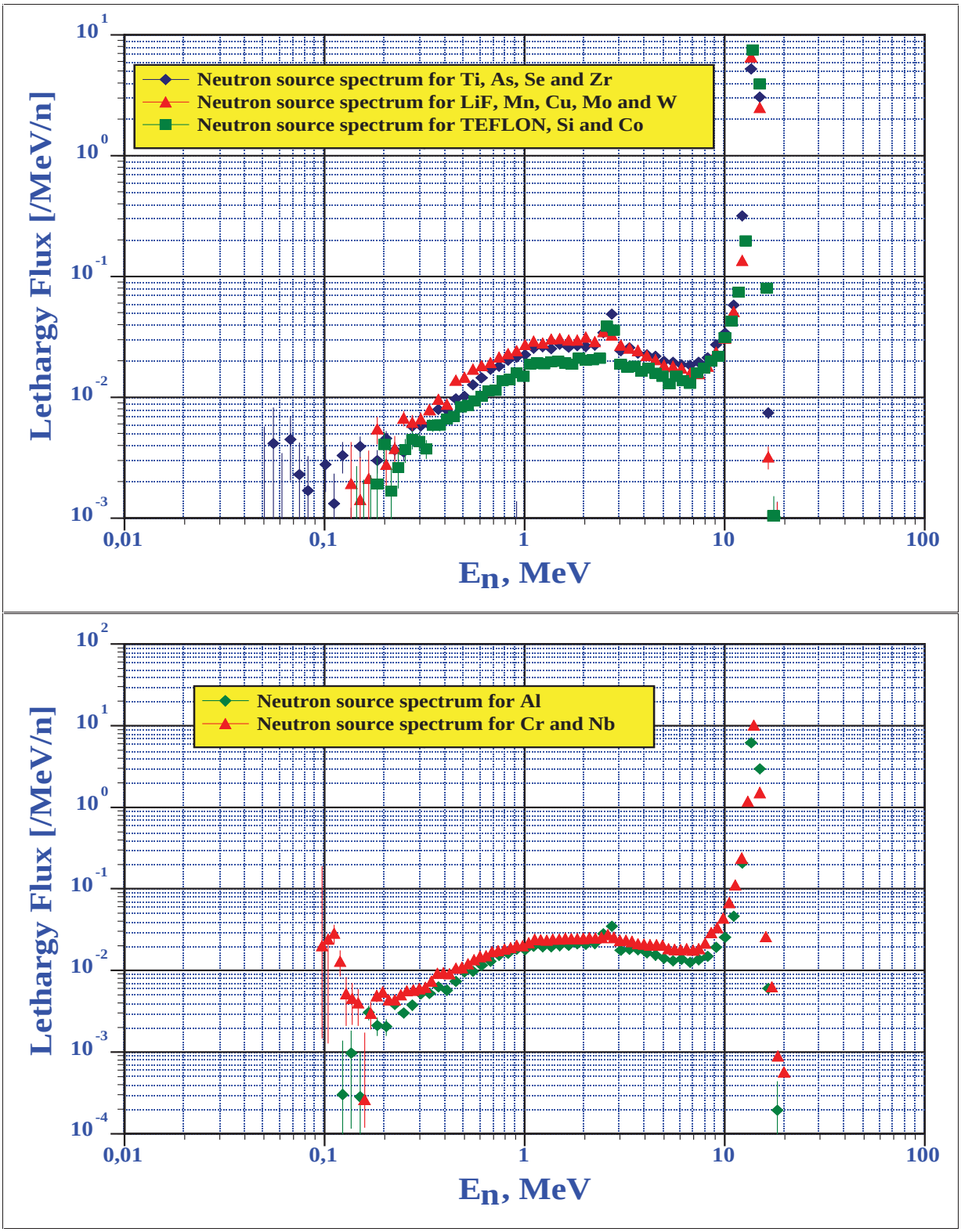

Fig. 18. Initial neutron spectra.

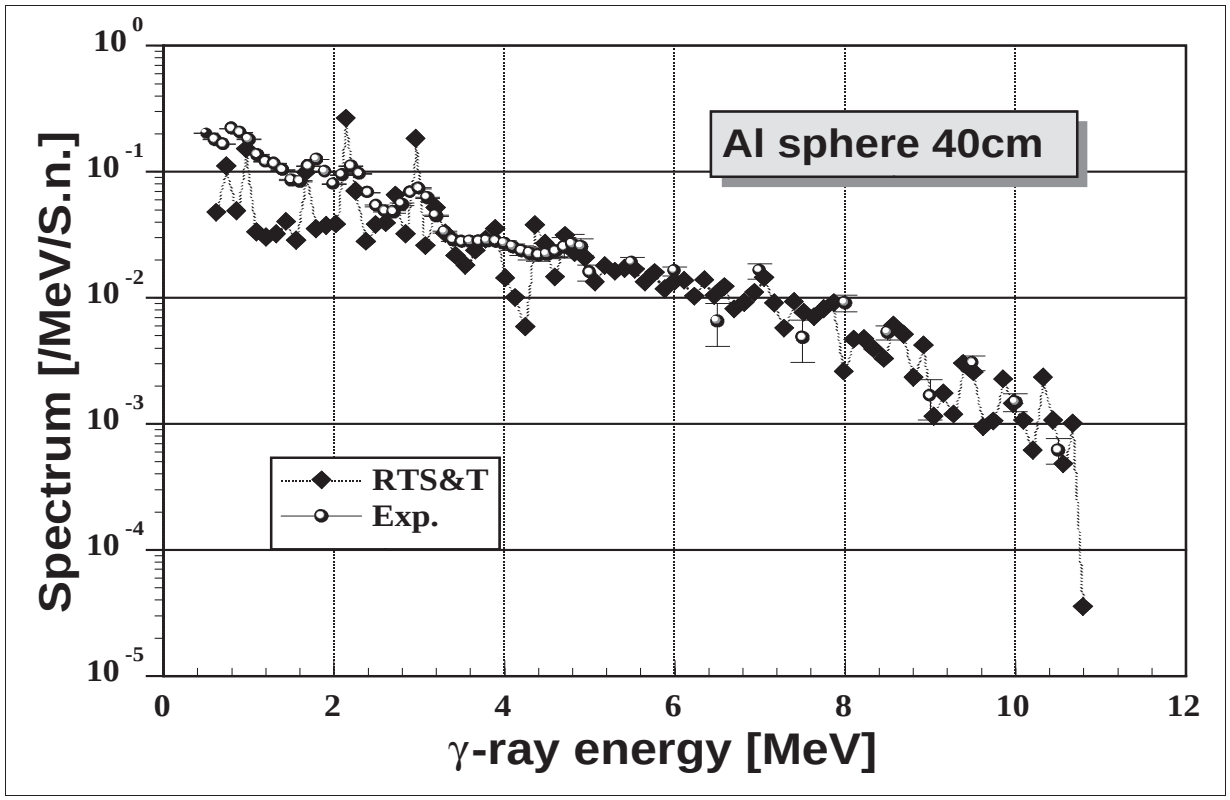

Fig. 19. γ-ray leakage spectra from aluminum sphere.

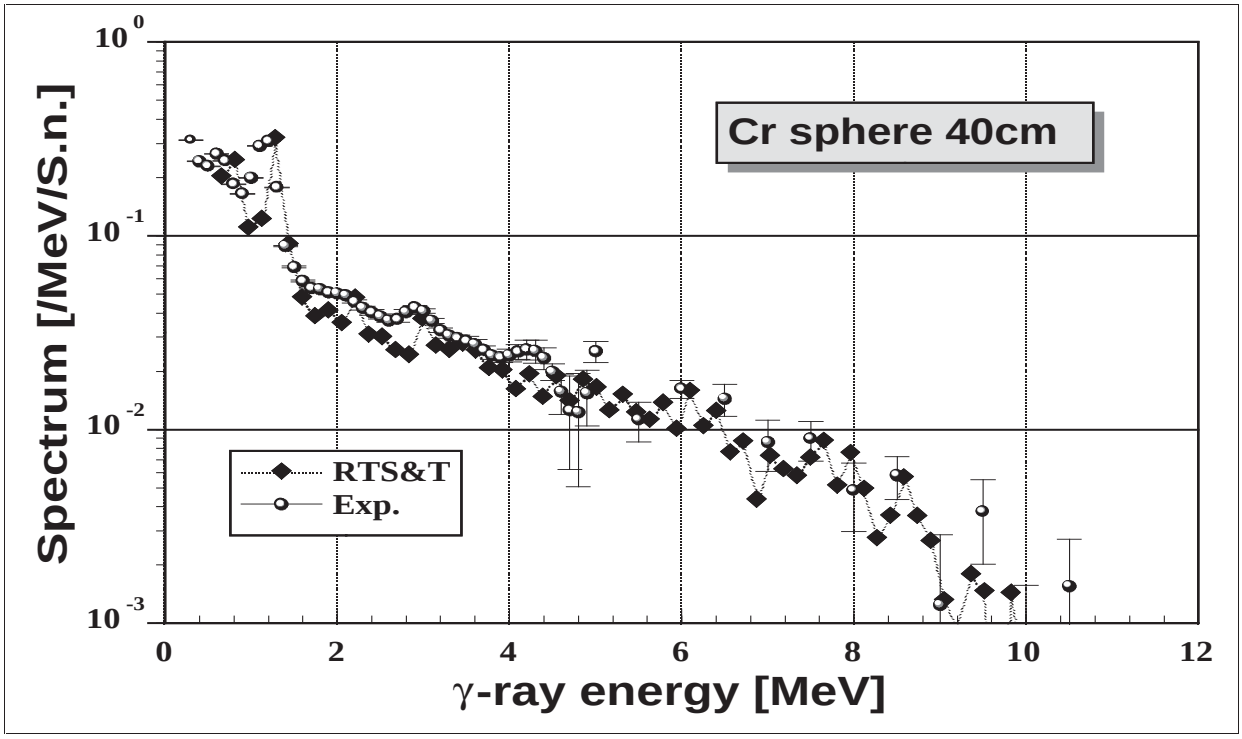

Fig. 20. γ-ray leakage spectra from chromium sphere.

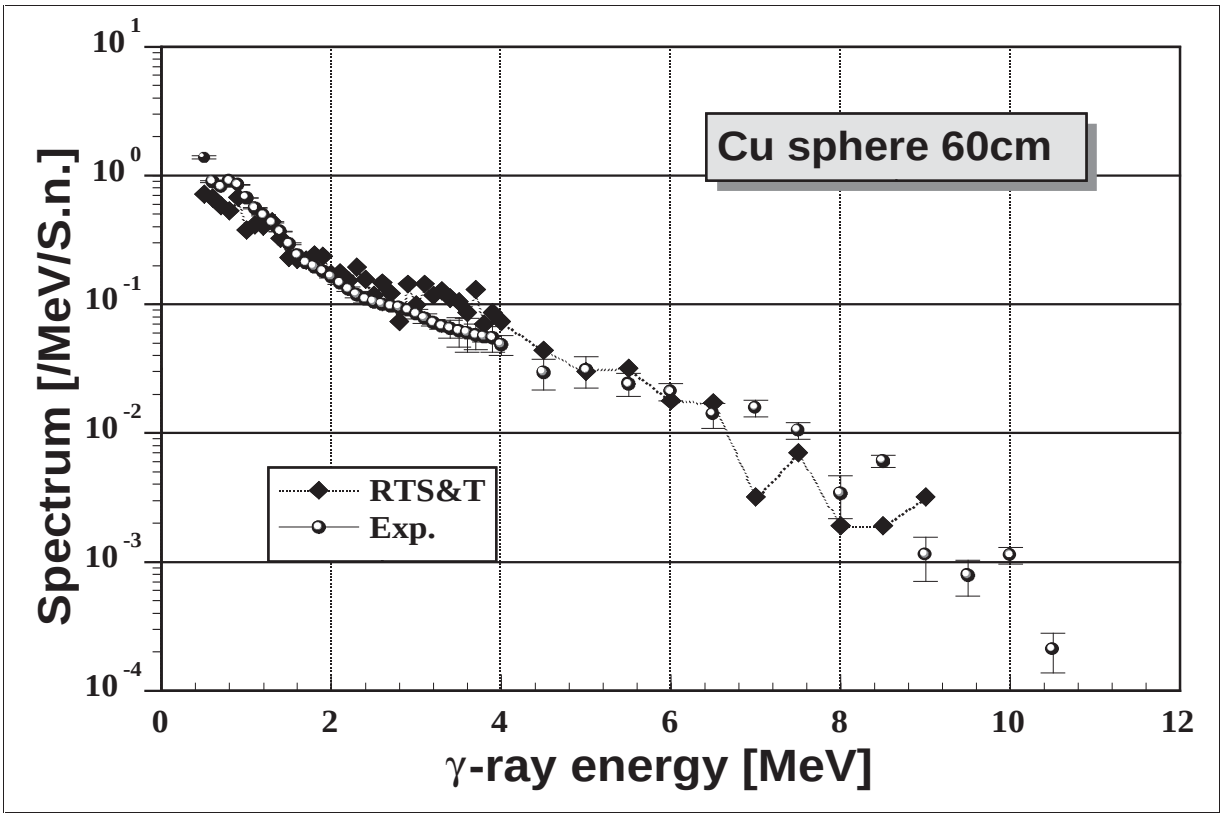

Fig. 21. γ-ray leakage spectra from copper sphere.

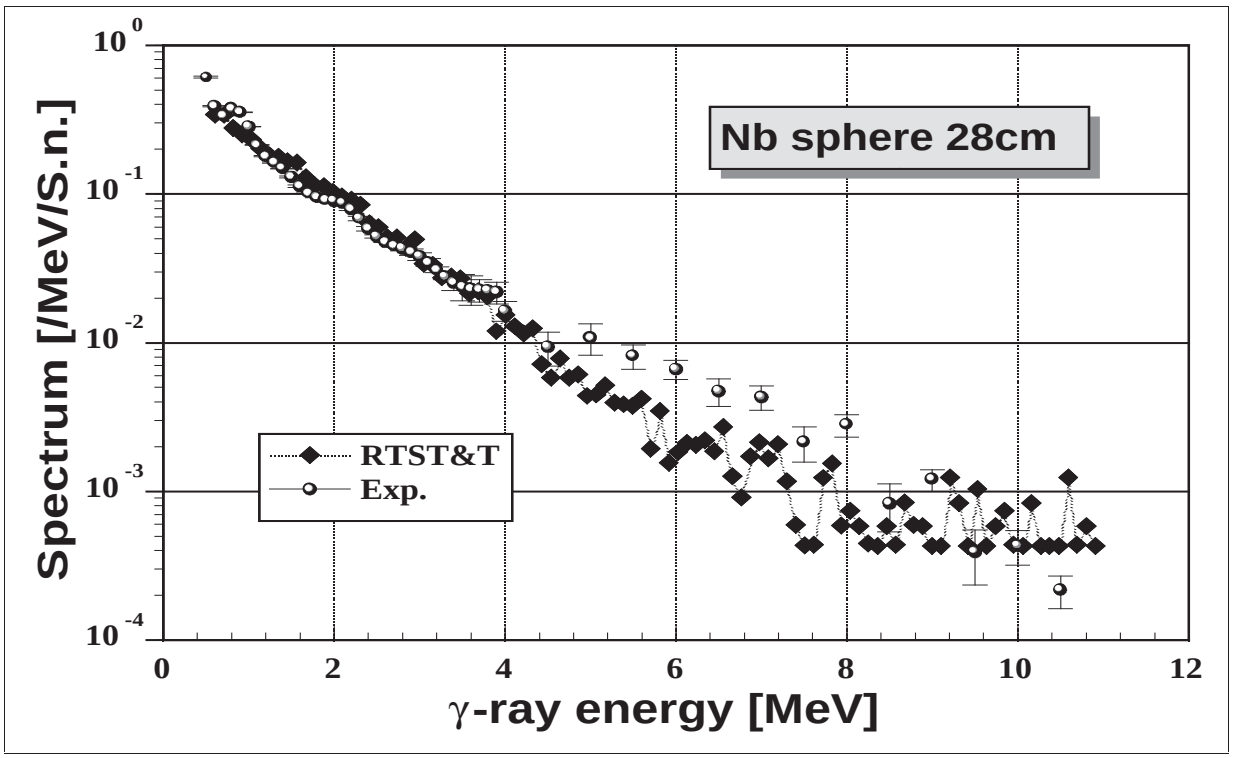

Fig. 22. γ-ray leakage spectra from niobium sphere.

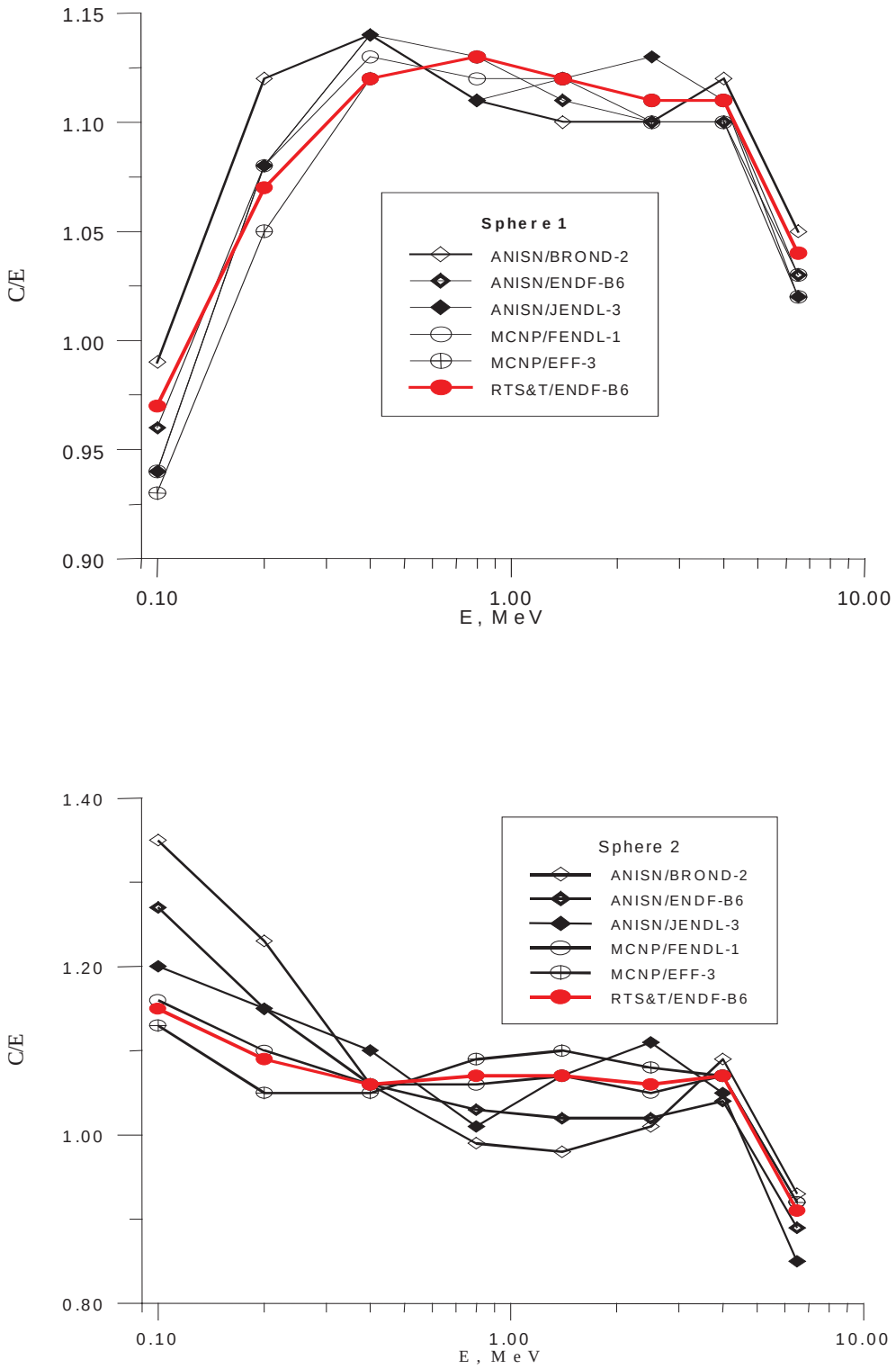

Fig. 23. C/E ratio for iron spherical shells of 4.5 and 9.5 cm in diameter with a central hole of 2 cm in diameter.

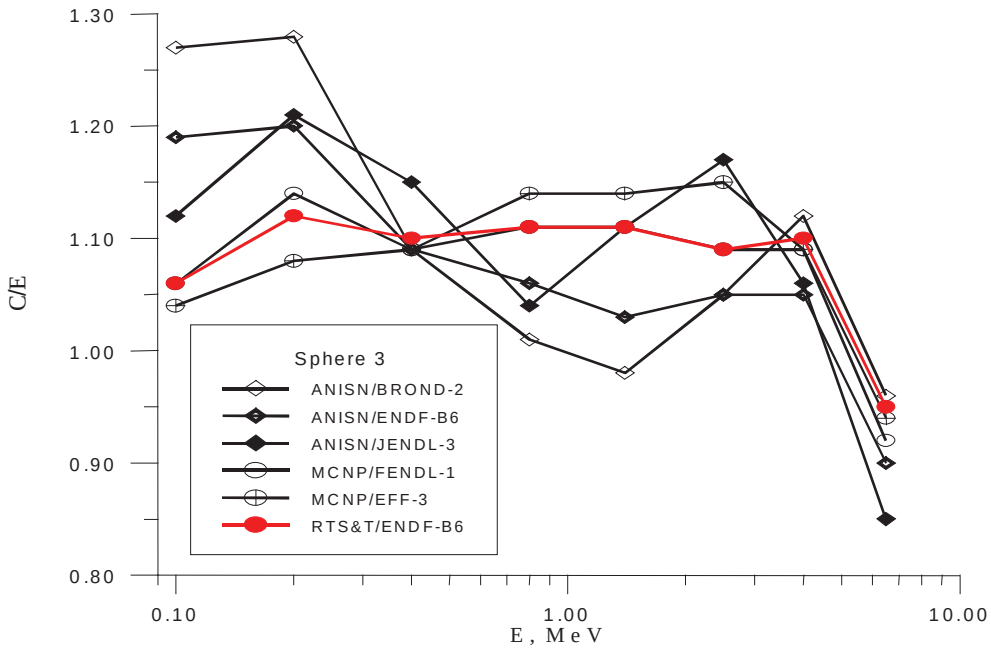

Fig. 24. C/E ratio for iron spherical shell of 12.0 cm in diameter with a central hole of 2 cm in diameter.

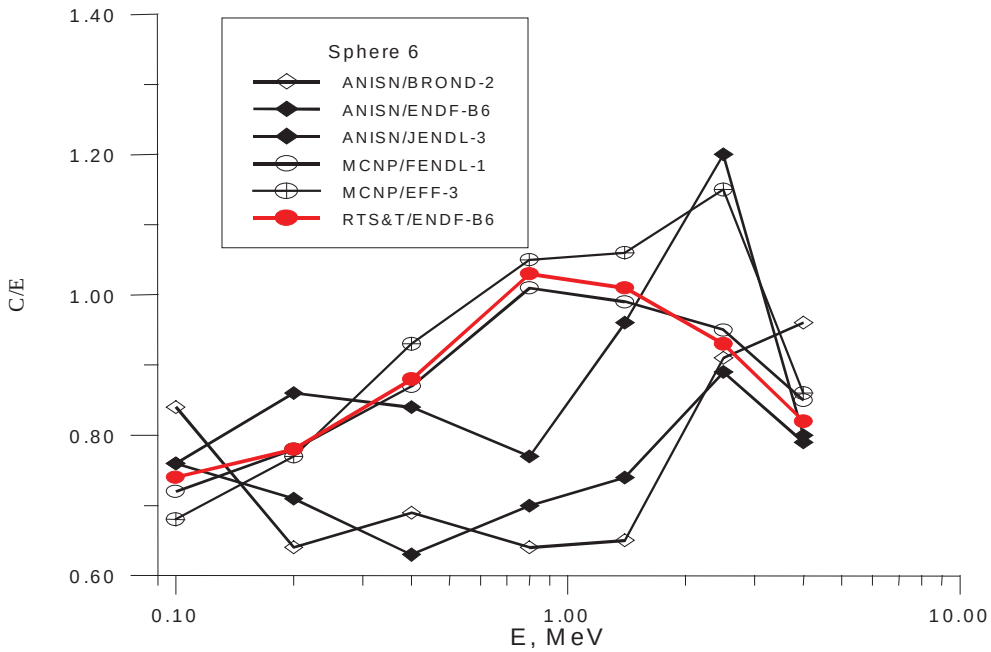

Fig. 25. C/E ratio for iron spherical shell of 20.1 cm in diameter with a central hole of 2 cm in diameter.

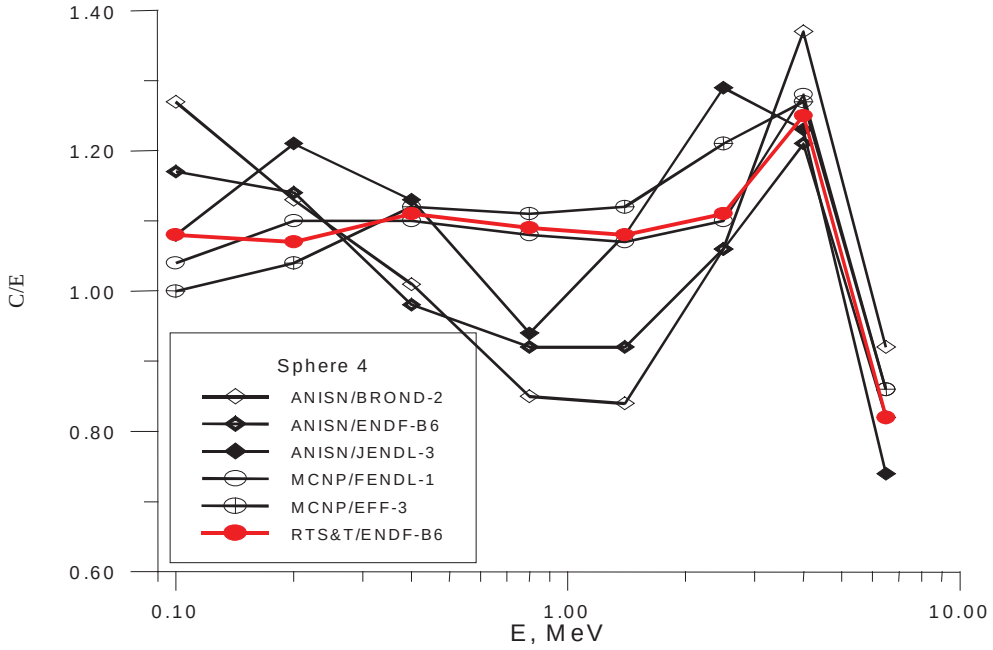

Fig. 26. C/E ratio for iron spherical shell of 32 cm in diameter with a central hole of 2 cm in diameter.

References

[1] A.I. Blokhin, I.I. Degtyarev, A.E. Lokhovitskii, M.A. Maslov and I.A. Yazynin: "RTS&T Monte Carlo Code (Facilities and Computation methods)", in Proceedings of the SARE-3 Workshop, KEK, Tsukuba, Japan (1997).

[2] R.E. Prael and H. Lichtenstein, User Guide to LCS: "The LAHET Code System", LANL Report LA-UR-89-3014, Los Alamos National Laboratory (1989).

[3] C. Beard and V.I. Belyakov-Bodin: "Comparison of Energy Deposition Calculation by the LAHET™ Code System with Experimental Results", Nuclear Science and Engineering, 119, (1995) 87.

[4] V.I. Belyakov-Bodin et al., "Calorimetric Measurements and Monte Carlo Analysis of Medium-Energy Protons Bombarding Lead and Bismuth Targets", Nucl. Instr. Meth., A295, (1990) 140.

[5] V.I. Belyakov-Bodin et al.: "Calorimetric Measurements and Monte Carlo Analysis of Medium-Energy Protons Bombarding Uranium Target, Atomic. Energy", 70, (1991) 339.

[6] V.I. Belyakov-Bodin et al.: "Heat Deposition in Targets Bombarded by Medium Energy Protons", Nucl. Instr. Meth., A335, (1993) 30.

[7] V.I. Belyakov-Bodin et al.: "Calorimetric Measurements of the Spatial Component of Heat Deposition in Targets from Lead and Bismuth Bombarded by Medium-Energy Protons", Nucl. Instr. Meth., A373, (1996) 3.

[8] Y. Murakami, K. Yoshioka, K. Yamanaka, A. Takahashi and K. Sumita, Leakage Spectra from Beryllium and Beryllium-lithium Sphere, Report JAERI-M, 94-014, Japan Atomic Energy Research Institute (JAERI), Japan, 1994.

[9] J. Yamamoto, T. Kanaoka, I. Murata, A. Takahashi and K. Sumita: “Gamma-ray energy Spectra Emitted from Spheres with 14 MeV Neutron Source”, JAERI-M, 94-014, (1994) 32.
[10] L.A. Trykov, Yu.I. Kolevatov et al., Report IPPI-1730, Obninsk, 1985.
[11] W. Manhart, Report IAEA-TECDOC-410. IAEA Vienna, 1987, p. 158.
[12] B.V. Devkin et al.: “Neutron leakage spectra from the iron spherical shell with Cf-252 neutron source”, the Proc. of the VII Russian scientific conference on radiation shielding of nuclear installations, Obninsk (1998).
[13] S.P. Simakov: Report ZFK-646, Dresden, (1988) 111.
[14] V.A. Talalaev, S.P. Simakov et al.: Acta Universitates Debreceniensis, Debrecen (1991) 13.

00-30130 (113) [15]
Translated from Russian

NOTES ON THE CONSYST CODE

G.N. Manturov, M.N. Nikolaev, A.Ju. Poljakov, A.M. Tsibulya
Russian Federation National Research Centre
A.I. Leipunsky Institute for Physics and Power Engineering, Obninsk

A description of the CONSYST code is given. The code is used to prepare ABBN-93 299-group neutron and 15-group photon constants for calculation of radiation fields and their functionals.

1. Name of the code

CONSYST constants package for calculations of neutron and gamma fields in various types of reactor and spectra in blankets in thermonuclear and electronuclear facilities and in radiation shielding.

2. Computer for which the program is designed

IBM PC

3. Underlying physics

The CONSYST/ABBN system provides constants for neutron physics calculations for reactors and radiation shielding. The CONSYST/ABBN constants package prepares macroscopic environment constants for neutron physics calculations in any number of energy groups from 26 to 299. This is achieved via a detailed, 299-group representation of the cross-sections in the source ABBN-93 constants library for the main reactor and shielding materials (uranium and plutonium isotopes, steel components, sodium, oxygen). For secondary materials, 299-group calculations are performed using 28-group constants. The option exists for preparing homogenized environment constants with regular heterogeneity and a correction for resonance absorption. When convolving these constants into a small number of groups, a weighting is applied to the current and flow neutron spectra, which may be calculated both within the CONSYST/ABBN system itself and introduced into the system from outside, having been calculated in advance using a program module.

The CONSYST/ABBN system provides the option of preparing data for calculating photon sources produced by neutron reactions. Constants for calculating photon fields may also be prepared. Fifteen energy groups are used for the photon field description.

The source constants in the CONSYST/ABBN system are the ABBN-93 group constant libraries which give constants for approximately 140 materials (isotopes and their mixtures), describing various neutron interaction processes with matter in a 28-group energy

representation and, for the most important materials, in a more detailed 299-group representation.

4. Solution method

Resonance shielding of isotope cross-sections is taken into account using resonance self-shielding factors (or Bondarenko f-factors) which are given in the ABBN-93 constants relative to the neutron energy, the temperature of the environment and the dilution cross-section for other materials.

Several options are available for calculating constants in the thermal region:

1) Use of the library of 73-group thermal P_0 and P_1 scattering matrices, given relative to environment temperature, to calculate inter-group transitions in groups with an energy of less than 4.64 eV;

2) Use of Westcott factors - data on these are also given in the ABBN-93 system relative to neutron gas temperature; the neutron gas temperature may be evaluated by the system or inputted from outside;

3) Introduction of external correction factors for the capture and fission cross-sections in the thermal region, which may be calculated in advance using a separate program module.

The following options are available to take account of heterogeneity when calculating homogenized environment constants:

1) The impact of heterogeneity may be taken into account in the equivalence theorem approximation by introducing a so-called delta scatterer in an appropriate concentration (material called “D-SC”);

2) Inputting of information on the real cell structure of the environment; using the equivalence theorem, the system then recalculates the resonance isotope dilution cross-sections taking account of the cell geometry, after which the standard algorithms are applied to take account of self-shielding of the cross-sections employing Bondarenko f-factors;

3) Calculation of homogenized constants using a program specially developed for that purpose (FFCP) in which the convolution of constants for the cell takes account of heterogeneous group neutron spectra calculated using the VPS method; here, the resonance structure of the cross-sections of individual isotopes is taken into account using the subgroup parameters for which data are contained in ABBN-93.

The CONSYST/ABBN constants package provides the option of preparing constants for neutron and gamma radiation transport calculations:

- in a diffusion approximation;
- in a P_1 approximation;
- in several transport approximation variants (not taking into account scattering anisotropy);
- taking into account elastic scattering anisotropy - up to a P_5 approximation, and inelastic scattering anisotropy - in a P_1 approximation.

In all cases, anisotropy of the total cross-section due to resonance self-shielding is taken into account in the transport approximation.

When preparing constants for neutron field calculations, shielded microscopic group constants are also prepared for the nuclides in the reactor for which calculations are to be carried out or the shielding; these are needed to calculate the majority of the most important functionals of these fields, in particular those which are dependent on the neutron reaction rates.

5. Limitations on the complexity of the problem

Number of neutron energy groups **NGN**: $1 \leq \mathbf{NGN} \leq 299$

Number of photon energy groups **NGG** = 0/15

Total number of isotopes in materials **INZ**: $1 \leq \mathbf{INZ} \leq 100$

These are the maximum parameter values for the current version, not taking into account limitations imposed by the RAM of the computer used.

6. Time required to solve a typical problem

The calculation time depends on the number of energy groups, the number of physical zones and nuclides, and the calculation mode. The calculation time is not an important criterion since it is always significantly less than the time required for a basic neutron physics calculation, even a one-dimensional diffusion problem.

7. Features of the program

At least the basic ABBN-93 28-group constants library is required for work with the CONSYST/ABBN system.

The CONSYST/ABBN program modules use dynamic memory allocation; the amount of memory is set by the main program in the unnamed COMMON block and depends on the problem to be solved and the capacity of the computer used.

The results of constants calculations using the CONSYST code may come from the latter's internal GMF exchange file or from external files in the ARAMAKO [1], ANISN [2] or AMPX [3] formats.

The CONSYST program can work both independently to prepare constants for a single calculation, or as part of a package where it will be called several times to perform different types of job.

8. Auxiliary and secondary programs

The CONFIG.DRV configuration file, which contains a description of all available data files, is used to control exchange of information with external files. A CONSYST job file is also required, the name and location of which on the disk is specified in the CONFIG.DRV file.

9. Status of the program

At present, the CONSYST program package is used to provide constants for such programs as KENO [4], MMKKENO [5], TWODANT [2], TRIGEX [6], JAR [7], SYNTES [8], etc.

10. References

[1] N.O. Bazazyants, M.Yu. Vyrskij, et al., “The ARAMAKO-2F Neutron Constants System for Reactors and Shielding Radiation Transport Calculations”, Moscow (1976).

[2] R.E. Alcouffe, F.W. Brinkley, Jr., D.R. Marr and R.D. O’Dell, "User's Guide for TWODANT: A Code Package for Two-Dimensional, Diffusion-Accelerated, Neutral-Particle Transport", Los Alamos National Laboratory report LA-10049-M (February 1990).

[3] RSIC PERIPHERAL SHIELDING ROUTINE COLLECTION, AMPX-77, PSR-315.

[4] L.M. Petrie, N.F. Landers, “KENO V.a: An Improved Monte Carlo Criticality Program with Supergrouping”, NUREG/CR-0200, Revision 5, Volume 2, Section F11 of SCALE: A Modular Code System for Performing Standardized Computer Analyses for Licensing Evaluation, ORNL/NUREG/CSD-2/R5.

[5] A.A. Blyskavka, A.M. Tsibulya, G.N. Manturov, M.N. Nikolaev, “The CONSYST/MMKKENO Program Package for Nuclear Reactor Calculations Using the Monte-Carlo Method in a Multigroup Approximation with Scattering Indicatrices in a P_n Approximation”, (Interim) Report of the Institute for Physics and Power Engineering, Inv. No. 9860, Obninsk (1998).

[6] A.S. Seregin, T.S. Kislitsyna, Notes on the TRIGEX-CONSYST-ABBN-90 Program Package, Preprint of the Institute for Physics and Power Engineering (1997).

[7] L.N. Yaroslavtseva, The JAR program package for calculating the neutron physics characteristics of nuclear reactors, Voprosy atomnoj nauki i tekhniki, Ser. Fizika i tekhnika yadernykh reaktorov 8(37) (1983) pp 41-43.

[8] E.F. Seleznev, Notes on the SYNTES program package, Voprosy atomnoj nauki i tekhniki, Ser. Fizika i tekhnika yadernykh reaktorov 6(43) (1984) pp 56-58.

11. Computer requirements

Standard hardware. Minimum 8 MB RAM, around 500 kB disk space for the calculation module, 1-25 MB for outputted data, minimum 5 MB to store the libraries.

12. Programming languages

FOTRAN-77, Lahey FORTRAN F77-EM/32.

13. Operating system

MS DOS 3.3 and above, Lahey/ERGO OS/386.

14. Authors of program

G.N. Manturov, M.N.Nikolaev, A.Yu. Polyakov, A.M.Tsibulya.

15. Available materials

Texts of the programs, object module libraries, constants libraries and installation module on two 3.5″ diskettes.

Nuclear Data Section
International Atomic Energy Agency
Vienna International Centre, P.O. Box 100
A-1400 Vienna
Austria

e-mail: services@iaeand.iaea.org
fax: (43-1) 26007
telephone: (43-1) 2600-21710
Web: http://www-nds.iaea.org